

The Kinetics and Thermodynamics
of Human Erythrocyte Freeze-Thaw
Damage at Sub-Optimal Cooling Rates

by

John Joseph McGrath

B.S.M.E. Stanford University (1971)

S.M.M.E. Massachusetts Institute of Technology (1974)

Submitted in Partial Fulfillment

of the Requirements for the

Degree of Doctor of

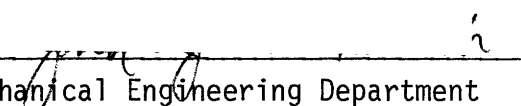
Philosophy

at the

Massachusetts Institute of Technology

January, 1977


Signature of Author


Mechanical Engineering Department
January 20, 1977

Certified by


Thesis Supervisor

Accepted by


Chairman, Departmental Committee
on Graduate Students



THE KINETICS AND THERMODYNAMICS OF HUMAN ERYTHROCYTE
FREEZE-THAW DAMAGE AT SUB-OPTIMAL COOLING RATES

by John J. McGrath

Submitted to the Department of Mechanical Engineering on January 20, 1977
in partial fulfillment of the requirements for the degree of Doctor of
Philosophy.

ABSTRACT

Sub-optimal cooling rate freeze-thaw injury has been studied using the human erythrocyte as a model biological system. The erythrocyte experiences simultaneous temporal variations of solute concentration and temperature during the general freeze-thaw process, hence the sensitivity of the damage rate to alterations in concentration and temperature has been examined experimentally and theoretically. A modified stop-flow apparatus in communication with a thermally controlled environment has been designed and developed to obtain human erythrocyte damage kinetic data induced by osmotic perturbation and/or thermal perturbation. The experimental technique developed provides real-time analog hemolysis data without centrifugation methods, thereby avoiding centrifugation artifacts and providing previously inaccessible short-time kinetic data. Hemolysis kinetics induced by osmotic perturbation for cells suspended in a binary sodium chloride-water solution are characterized by an initial rapid rate, followed by transition to a slow rate. The transition time is a function of temperature, with the longer transition times associated with lower temperatures. The rapid kinetics are a strong function of concentration as exemplified by the fact that the rate is proportional to the fifth power of sodium chloride molality at 298°K. These kinetics can be suppressed by temperature reduction, with an apparent activation energy of 7.3Kcal/mole measured for a concentration of 2.45 m NaCl between 273°K and 298°K. Temperature changes cease to affect the hemolysis rate for lower temperatures as measured between 262°K and 273°K. Preliminary experimental results for hemolysis kinetics induced by thermal perturbation are characterized by a slow reaction rate, followed by a rapid rate with a strong time dependency ($t^{3.6}$) and transition back to slower rates. Absolute rate theory has been applied in the development of a kinetic model describing the loss of membrane components. The rate of the hemolysis process is linked to this kinetic model by the assumption of a critical loss of membrane surface components. Hemolysis is modelled as a two step process. The first step requires activation of the membrane components in the form of a desorption step followed by a diffusion step which governs the characteristic time of the entire hemolysis process. A thermodynamic system is defined at the cell membrane surface and a Gibbs-Duhem relation is derived which couples changes in the surface free energy to temperature and concentration changes. Alterations of the surface free energy are directly translated to a change of desorption activation energy and rate of hemolysis. This model has identified the thermodynamic driving force for thermal shock damage and has produced an expression for the hemolysis reaction rate explicitly demonstrating the manner in which osmotic and thermal perturbation damage are related. Qualitative agreement is realized for a comparison of the theoretical consequences of this model and experimental data for both osmotic and thermal perturbation modes of damage. This model and the experimental rate data have been used to make preliminary predictions of post freeze-thaw erythrocyte recoveries for various computer simulated cryopreservation protocols.

THESIS SUPERVISOR: Ernest G. Cravalho
Matsushita Professor of
Mechanical Engineering
in Medicine

Table of Contents

	<u>Page</u>
Title	1
Abstract	2
Table of Contents	3
List of Figures	5
Nomenclature	9
Chapter 1 Introduction	12
A. Background	13
B. Scope of the Present Work	20
Chapter 2 Experimental Apparatus	26
A. Rationale for Development	27
B. The Optical System	28
1. Theory of Operation	28
2. Major Components	30
C. The Mixing System	32
1. Theory of Operation	32
2. Major Components	33
D. The Thermal System	33
1. Theory of Operation	33
2. Major Components	35
E. Calibration of the Optical System	35
F. Operational Characteristics of the System	44
Chapter 3 Experimental Procedures and Control Experiments	55
A. Experimental Procedure for the Isothermal, Hypertonic Osmotic Perturbation Mode	56
B. Experimental Procedure for the Hypertonic, Iso-osmotic, Temperature Perturbation Mode	59
C. Control Experiments	61
Chapter 4 Experimental Results for Hemolysis Kinetics Produced by Isothermal, Osmotic Perturbation and by Iso-osmotic, Thermal Perturbation	65
A. Hemolysis Induced by Isothermal, Osmotic Perturbation	66
B. Hemolysis Induced by Iso-osmotic, Thermal Perturbation	85
Chapter 5 A Thermodynamic and Kinetic Model for a Membrane Dissolution Theory of Hemolysis	96
A. Evidence for the Membrane Dissolution Theory of Hemolysis	97
B. A Review of Basic Membrane Theory	105
C. Derivation of the Gibbs-Duhem Equation for a Simplified Model of the Human Erythrocyte	109

	<u>Page</u>
Chapter 5 (continued)	
D. The Postulated Kinetic Theory of Hemolysis	119
E. Discussion and Conclusions	143
Chapter 6 A Comparison of the Theoretical Consequences of the Thermodynamic and Kinetic Model with Experimental Data	147
A. The Isothermal, Osmotic Perturbation Mode	148
B. The Iso-osmotic, Thermal Perturbation Mode	150
1. Dependence of Thermal Shock Hemolysis on Exposure Concentration	151
2. Dependence of Thermal Shock Hemolysis on Initial Temperature and the Magnitude of the Temperature Drop	154
Chapter 7 A Technique for Computer Simulation of Freeze-Thaw Damage	168
A. Introduction	169
B. Predicted "Limited Damage" Recovery for Various Cooling Rates and Warming Rates	173
C. A Comparison of the "Limited Damage" Simulation with Experimental Freeze-Thaw Data for Erythrocytes	179
Chapter 8 Discussion and Conclusions	186
Chapter 9 Suggestions for Future Research	204
Appendices	
A. Increase in Optical Signal Due to Erythrocyte Sedimentation in the Finite Length Optical Chamber	212
B. Optical Band Pass Filter Spectrum	215
C. Circuitry	216
1. Photocell Amplifier-Filter	216
2. Temperature Set-Point Proportional Controller	217
D. Mixer Schematic	218
E. Sensitivity of Optically Measured Percent Hemolysis to Variations in Delivered Hematocrit	219
F. Red Cell Velocity Damping Estimate	222
G. Hemolysis Rate Curve-fits for Hypertonic Sodium Chloride Exposure Times Greater than Three Minutes at 298°K.	224
H. Typical Resolution Capability of the Photocell for Percent Hemolysis Detection	225
I. Tabulation of Typical Activation Energies in Biological Systems	226
J. Computer Programs for Freeze-Thaw Simulations	227
K. General Phase Diagram Information	233
References	237
Acknowledgements	246
Biographical Sketch	248

List of Figures

	<u>Page</u>	
1.1	Survival signatures for various cell types	17
1.2	Osmotic perturbation and thermal perturbation effects on the hemolysis rate as depicted on the sodium chloride-water phase diagram	23
2.1	Experimental apparatus schematic including the optical, mixing, and thermal subsystems	31
2.2	Intracellular water mass as a function of sodium chloride osmolality	37
2.3	Normalized photocell voltage for erythrocytes at 4% hematocrit as a function of sodium chloride molality	39
2.4	Hemolysis as a function of exposure time at several hypertonic sodium chloride concentrations	41
2.5	Calibration data and curve-fit for the determination of percent hemolysis as a function of normalized photocell voltage	42
2.6	Linear nature of the photocell voltage as a function of lamp voltage for cases in which the optical chamber contains only normal saline or cells at 4% hematocrit in 1.0m NaCl	45
2.7	Normalized photocell voltage as a function of hematocrit	47
2.8	Normalized photocell voltage for cell-free suspensions as a function of suspension molality at various reference voltage levels	51
2.9	Quasi-steady state percent hemolysis as a function of suspension sodium chloride molality	53
3.1	Normalized photocell voltage as a function of time, demonstrating stability of the optical system for erythrocytes in normal saline	62
3.2	Strip chart recording demonstrating stability of the optical output for erythrocytes in normal saline during and after a temperature reduction	64
4.1	Strip chart recording for an isothermal, osmotic perturbation at 27°C for erythrocytes in 2.94m NaCl	67

List of Figures (continued)

Page

4.2	Hemolysis as a function of exposure time for the isothermal, osmotic perturbation experiments at 298°K and various concentrations	69
4.3	Hemolysis Rate A as a function of sodium chloride molality at 298°K and exposure times \leq 1.0 minute	71
4.4	Hemolysis Rate A as a function of water activity at 298°K and exposure times \leq 1.0 minute	73
4.5	Hemolysis Rate A as a function of sodium chloride activity at 298°K and exposure times \leq 1.0 minute	74
4.6	Hemolysis as a function of exposure time at 2.45m NaCl for isothermal, osmotic perturbation experiments at 273°K, 283°K and 298°K.	76
4.7	A composite view of hemolysis as a function of exposure time demonstrating the effects of sodium chloride concentration and temperature	77
4.8	The effect of the isothermal temperature set point on the hemolysis rate at 2.45m NaCl	79
4.9	Collapse of the hemolysis rate to a single value for a change in the isothermal set point temperature from 271°K to 262°K at 2.94m NaCl	80
4.10	Non-variant hemolysis percentages for five minute storage at various sub-zero temperatures	82
4.11	Hemolysis Rate A as a function of $-\text{Log}_e(a_w)$ at high temperature (298°K) and low temperature (273°K, 271°K, 262°K)	84
4.12	Percent erythrocyte recovery for thermal shock experiments as a function of hypertonic exposure time prior to the temperature drop	87
4.13	Percent hemolysis for thermal shock experiments demonstrating the effects of initial hypertonic exposure temperature and magnitude of the temperature drop	89
4.14	Percent erythrocyte recovery for thermal shock experiments demonstrating the effect of cooling rate	90
4.15	Strip chart recording of a thermal shock experiment for erythrocytes exposed to 1.0m NaCl for 5 minutes at 300°K prior to cooling at 9°K/min to 273°K.	92
4.16	Hemolysis as a function of time after initiating cooling for erythrocytes exposed to 1.0m NaCl for five minutes prior to cooling at 9°K/min from 300°K to 273°K.	93

<u>List of Figures (continued)</u>		<u>Page</u>
5.1	Removal of cell membrane components by repeated washings in normal saline	99
5.2	Electron micrograph of the erythrocyte "shaggy coat", 8000X	101
5.3	Removal of cell membrane components as a function of time as a result of exposure to alumina	102
5.4	Removal of cell membrane components as a function of time as a result of exposure to hypertonic sodium chloride	104
5.5	Schematic of the fluid mosaic model of the biological membrane	106
5.6	Chemical structures and orientations relative to the membrane surface for the four most abundant lipid types found in the human erythrocyte membrane	108
5.7	Schematic defining the thermodynamic system at the erythrocyte membrane surface	110
5.8	Free energy of a membrane lipid molecule as a function of distance from the membrane surface	120
5.9	Absolute rate theory interpretation of molecular free energy as a function of reaction coordinate	125
5.10	Absolute rate theory interpretation of membrane dissolution model	128
5.11	Schematic of the hemolysis process	136
5.12	Schematic transformation from the rate of loss of lipid from an individual cell to the percent hemolysis for the entire cell population	140
6.1	Water chemical potential, temperature, and hemolysis histories for an iso-osmotic, thermal perturbation experiment	155
6.2	Thermal shock hemolysis as a function of initial temperature and magnitude of the temperature drop, replotted and curve-fitted	160
7.1	Examples of freeze-thaw protocols simulated on the computer	174

List of Figures (continued)

Page

7.2	Predicted "limited damage" percent recovery for erythrocytes as a function of cooling rate for various constant warming rates	176
7.3	Predicted "limited damage" percent hemolysis as a function of temperature during freezing, storage, and warming for several cooling and warming rates	178
7.4	A comparison of predicted "limited damage" percent recovery and experimentally determined percent recovery as functions of cooling rate	181
7.5	A comparison of predicted "limited damage" percent hemolysis and experimentally determined percent hemolysis as functions of storage temperature	183
8.1	Two process paths for altering the state of the erythrocyte suspending medium from high temperature and low concentration to low temperature and high concentration	195
8.2	Phase contrast, 35 mm photograph of HeLa cells as seen post freeze-thaw on the cryomicroscope with lack of contrast for damaged cells (300X)	197
8.3	Rate of hemolysis as a function of $-\text{Log}_e(a_w)$ for isothermal, osmotic perturbation experiments: derived kinetics from Lovelock data (reference [27]) compared with present data	201
Table 4.1	Master chart of hemolysis rate curve-fit parameters for all of the isothermal, osmotic perturbation experiments cross-tabulated for temperature and concentration.	83

Nomenclature

A	membrane surface area
A	Hemolysis rate (percent/min)
a	activity
B	cooling rate
C	concentration
D	diffusion coefficient
E_a	activation energy
G	Gibbs free energy
g	gravitational field or constant
Hb	hemoglobin molecule
%H	percent hemolysis
HCT	hematocrit
I	light intensity
J	mass flux
K	equilibrium constant
K	Boltzmann constant
k	reaction rate constant
L	characteristic diffusion length
M	molarity
m	molality
mOsm	milliosmoles
N.D.	neutral density
N	number of experimental tests
n	number of molecules
P	product of reaction
P	pressure

Nomenclature, continued

R	universal gas constant
r	correlation coefficient
S	entropy
s	entropy per unit volume
T	temperature (°K)
t	temperature (°C)
t	time
V	volume
V	voltage
W	warming rate
x	mole fraction

Greek

α	thermal shock hemolysis parameter
β	thermal shock hemolysis parameter
γ	surface tension (surface energy per unit area)
ϵ	thermal shock data curve-fit parameter
η	thermal shock data curve-fit parameter
μ	chemical potential
ν	frequency
σ	surface entropy per unit area
τ	characteristic time
Γ	surface concentration
Δ	finite difference

Nomenclature, continued

θ	lipid loss to hemolysis transformation parameter
Ω	instantaneous standard Gibbs free energy

Subscripts

i	ith species or constant
LPS	hypothetical lipoprotein species
N.S.	normal saline (0.154M)
o	initial state
0%	no hemolysis present
P	product
R	reactant
s	salt
s	surface
T	at temperature T
w	water

Superscript

o	standard state
'	per molecule
*	activated state

To Connie

Chapter 1

Introduction

Background

Although the prospect of successful suspended animation for human beings remains very much within the realm of science fiction, the reversible storage of biomaterial at low temperature is a scientific reality. Since 1949 when the first successful cryopreservation techniques were discovered [1], several classes of biomaterials have received sufficient research effort to allow clinical scale preservation. These biomaterials include blood, spermatozoa, cornea and skin [2,3,4,5]. The object, of course, for all such cryopreservation techniques is to make use of the fact that the rates at which life processes proceed are strongly dependent on absolute temperature. Reversible cryopreservation offers the opportunity to arrest physiochemical processes, most notably those processes associated with deterioration, until such a time as the biomaterial is needed for revitalization by thawing and subsequent transfusion or transplantation.

Perhaps the most fully developed programs of modern cryopreservation technology are those within the field of red blood cell freezing. Certainly the potential of this remarkable concept is clearly demonstrated by the present blood banking endeavors. Prior to the development of successful red cell freezing methods, the maximum acceptable storage time for donated blood (stored at 4°C in citrate-phosphate-dextrose (CPD) or acid-citrate-dextrose (ACD) anticoagulants) was twenty-eight and twenty-one days respectively. This limit is primarily due to progressive loss of cell ATP and 2,3 DPG concentrations. Maintenance of red cell oxygen transport function depends principally on the 2,3 DPG level, and the

ATP is necessary to guarantee red cell post-transfusion survival [6]. Glycerolized packed red cells frozen at the Massachusetts General Hospital to -85°C have been stored for as long as 13 years with post-thaw ATP and 2,3 DPG levels that are within normal limits. Recovery of in vitro processing averaged $85 \pm 5\%$ with a large scale program processing approximately 12,000 units per year [7].

The most obvious advantage to an extension of shelf life is inventory control. Blood banking provides the opportunity to decouple the amount and type of blood available at any given time from the large seasonal and shorter term fluctuations in blood donating patterns. Storage of rare blood types is definitely of interest as one might imagine. In addition to these advantages, there have been several unexpected benefits resulting from the use of frozen cells. The reader is referred to reference [8] for a complete discussion, but several factors might be mentioned including: a reduced likelihood of hepatitis and salvage of outdated blood, which may make frozen blood programs even more attractive than they first appeared.

The principle of reversible low temperature storage for maximizing the use of available donations (whenever they happen to occur) is applied to tissues and organs as well as to single cells. However, as the biological subsystems are integrated up in size and complexity, one observes a marked diminution of cryopreservation success stories, as might be expected. On the other hand, there is reason to be optimistic in working for future successes since to date there appear to be no fundamental reasons why scale and complexity alone will rule out workable preservation protocols for a wide variety of these systems.

Finally, it should be pointed out that in addition to being a valuable clinical tool, cryobanking is also important as a research aid. Some examples cited below illustrate this premise nicely. It is standard practice in some biological laboratories to cryopreserve a sample of each cell line being cultured in case the cultured line becomes contaminated or otherwise lost. Cryopreservation can be used to great advantage in applications where a large or rare biological sample is to be used as a standard in small amounts over a long time period. Specific areas in which this situation arises include toxicology assays in which enzyme systems are preserved and tissue typing.

Having discussed the potential of successful cryopreservation techniques and having mentioned that the number of successful protocols is rather limited, one is immediately led to wonder what the difference is between a successful technique and an unsuccessful one. That is, what are the important factors involved in freeze-thaw damage and what is known about mechanism, if anything, for each case. Experimental evidence accumulated over the past twenty-five years has suggested that at least five major factors are responsible for determining whether or not a biological system will survive an attempt at cryopreservation: the rate at which the temperature of the system is reduced, the minimum temperature reached, the length of time at the reduced temperature, the rate at which the sample temperature is increased, and the presence or absence of protective chemicals (cryoprotective agents) as well as the characteristics of these chemicals. In an effort to reveal mechanistic detail, the effect of cooling rate (the rate of change of the sample temperature with respect to time) on cell survival has received quite intense attention. As a function of cooling rate, the cell survival curve

is generally an inverted U shape [9], which suggests that at least two competing phenomena are interacting to determine ultimate survival. Figure 1.1 shows this behavior for several cell types. Data on a number of cell types have led to the dual mechanism hypothesis for freezing damage which can be summarized as follows: at slow characteristic cooling rates (i.e., those below the optimum rate) the increased solute concentrations present during freezing and the longer exposure times are the dominant causes of cell damage. Survival can be improved by increasing the cooling rate but there is a limit to this enhancement since increasing the cooling rate will eventually cause intracellular ice formation and cell death [10]. There is considerable electron microscopic evidence to suggest that intracellular ice damage is actually produced mechanically by interaction of the internal ice crystals and the plasma membrane and internal organelles [11,12]. Recrystallization phenomena are of interest since manipulation of the warming rate can alter post-thaw survival for those cells which have frozen internally. Typically those cells which have been rapidly frozen should also be thawed rapidly [9,13]. Undoubtedly this fact is related to secondary growth of ice crystals upon warming and the minimization of damage on thawing is accomplished when substantial alteration of the crystals is prevented [11]. Curiously, the mere presence of extracellular ice does not seem to be a major contributor to the mechanical damage of cells (at least for slow cooling) since there are innumerable cases in which extracellular ice is present and no damage is observed [1,2,9]. On the other hand, this mode of damage has been observed directly on the cryomicroscope during freezing of mouse embryos [14] although it is indeed a very rare event.

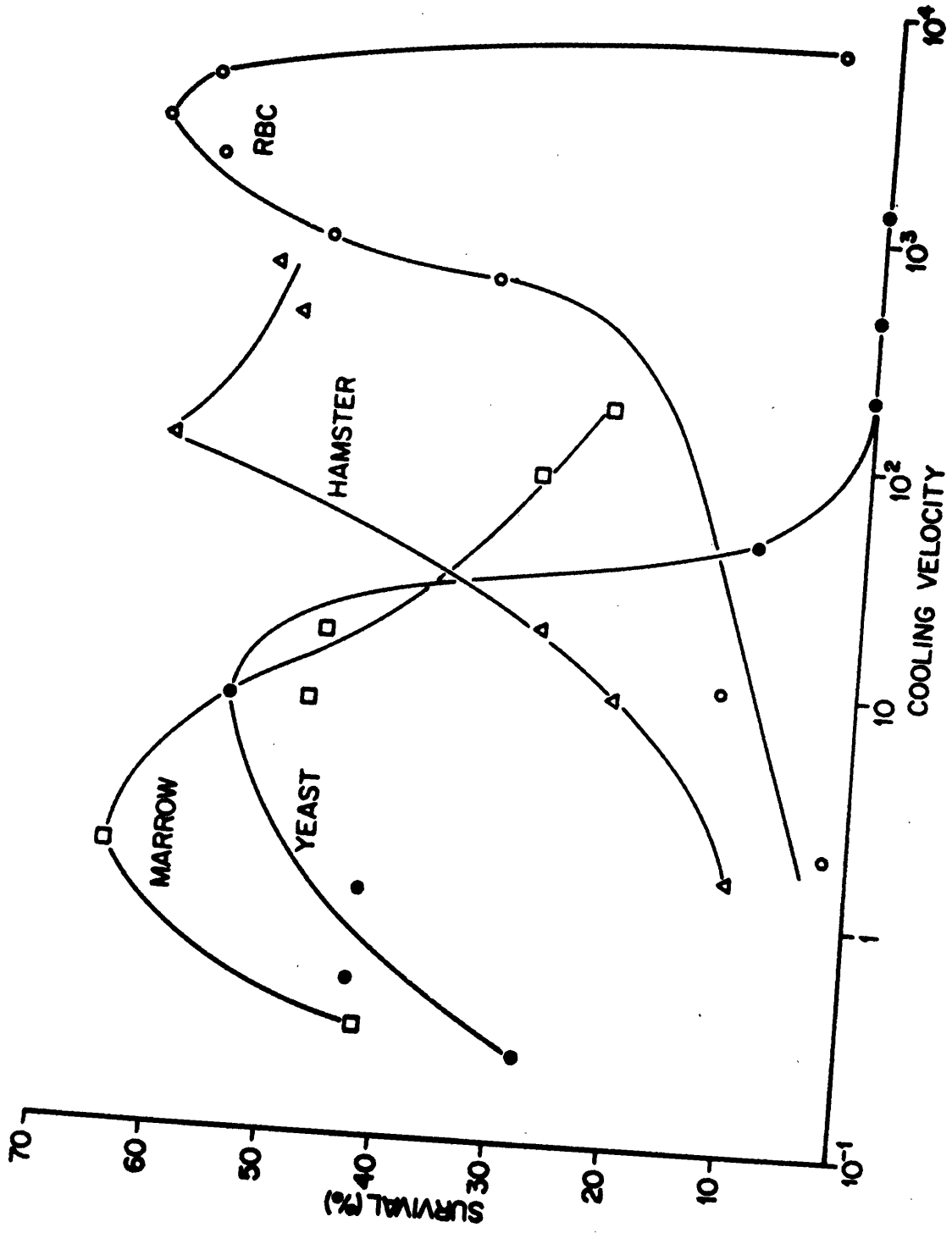


Figure 1.1 Survival Signatures For Various Cell Types (reproduced from Mazur et.al., reference [9]).

Studies of supraoptimal cooling show that for relatively constrained warming conditions, the formation of intracellular ice is to be avoided since for a number of cell types including mouse embryos, human red cells and human fibroblast [15,16,17,18] decreased survival has been indirectly or directly linked to increased intracellular ice formation. The conditions requisite for internal ice formation have been dealt with in several thermodynamic models [19,20,21,22] which demonstrate that in those cases in which heat transfer dominates over mass transfer, the intracellular liquid becomes supercooled, favoring transition to the solid state rather than continued dehydration by transmembrane mass transport. Several basic cell parameters such as surface area to volume ratio and plasma membrane permeability to water will determine the characteristic transition cooling rate at which mass transport becomes predominant rather than heat transfer. These parameters and such factors as the cellular sensitivity to solute damage will determine the unique survival signature (survival percentage as a function of cooling rate) for each cell type when the storage time and temperature are known, as well as the basic constituents of the suspending medium and the warming rate. The following general remarks can be made concerning storage time and temperature. Increasing the storage time at any temperature will normally result in additional damage [6]. Cell systems are most sensitive to storage temperatures in the range -5°C to -60°C and are less sensitive to temperatures below -60°C [11,23,24,25]. There appears to be no deleterious effect in placing red cells in an environment close to zero absolute temperature [26].

For any cell system in a given suspending medium and for a specified warming rate, so-called "solution effects" are responsible for low

survival at sub-optimal cooling conditions. In a classic paper, Lovelock was able to demonstrate that freeze-thaw hemolysis of red cells in normal saline could be duplicated by exposure to hypertonic saline solutions and redilution to isotonic concentrations [27]. In the course of this work Lovelock discovered that exposure of red cells to hypertonic sodium chloride produces hemolysis but that this is not in itself enough damage to simulate freezing damage. Two other critical details were unveiled. The first is that if the cells were exposed to hypertonic solutions for five minutes and the temperature of the cell suspension was lowered, the cells could be hemolyzed even if the solution did not freeze. Furthermore, the hemolysis was much more than expected from simply exposing the cells to the hypertonic media for five minutes. This phenomenon was called thermal shock. Thermal shock was found to be a function of the initial absolute temperature, the magnitude of the temperature drop, the concentration and time of exposure to hypertonicity before the temperature drop and the cooling rate. The second detail Lovelock found was that cells suspended in hypertonic media became susceptible to damage by redilution into isotonic media. This phenomenon has been termed posthypertonic hemolysis. If solute leakage occurs during hypertonic exposure, dilution to a less concentrated media can in some cases produce disruptive swelling by the osmotic influx of a volume of water exceeding that comparable to the isotonic case. In a freeze-thaw situation, solute leakage may occur during freezing (as it is known to in some cases) and upon subsequent thawing (dilution) the cells may burst as they exceed a maximum critical volume. Farrant and Morris present an overview of solution effect damage with the proposal that freezing injury at slow rates is primarily due to thermal shock and dilution shock [28]. In addition to Lovelock's work on posthypertonic hemolysis, the work

of Zade-Oppen has provided quantitative data demonstrating the tremendous amount of damage that can be imposed by this effect [29].

Scope of the Present Work

A review of the state of the art for solution effect freezing damage has shown that there are three modes of damage: exposure to hypertonic solutions, exposure to temperature reductions and solute leakage with subsequent dilution lysis upon thawing. It is clear from the various studies that the amount of damage produced is a rather complex function of absolute temperature, salt concentration and exposure time--the same variables that are changing simultaneously during the freeze-thaw protocol [27,30,31,32,33]. It is apparent that the first two modes in most cases are coupled and it is likely that all three are intimately related. Lovelock concluded from his experimental work that hypertonic solutions are capable of removing a sufficient amount of critical membrane components so that the cell becomes increasingly permeable to solutes, so much so that large molecules such as hemoglobin will eventually leave the cell [34]. Alteration of the membrane during hypertonic exposure renders the cell susceptible to temperature drops, but the manner by which the temperature reduction acts as a driving force for hemolysis remains unclear [30].

What has not been addressed to date is the problem of incorporating these important parameters into a unified model (even a very simple one)

by which one would be able to quantify the amount of damage to be expected from arbitrary but specified variations in any or all of the parameters: temperature, time and concentration. Conceivably this could be accomplished without detailed information as to the mechanisms involved if the kinetics of hemolysis were available as a function of temperature and concentration. Then for arbitrary freeze-thaw procedures the damage rate equation(s) could be integrated for a prediction of the total amount of damage to be expected. Since in most cases the cooling rates attainable clinically are slow enough to be classified as suboptimal for many cell types, the cells undergoing freezing are influenced primarily by solution effects. Although solute leakage may occur during freezing, the damage is not manifested until dilution occurs during thawing. It is known that extensive damage occurs during the freezing process alone, presumably due to thermal shock and hypertonic exposure [35] hence the focus of the present work is to quantify experimentally the kinetics for these two freezing damage modes and to incorporate the results into a form which can be used to predict recovery at suboptimal cooling rates. Therefore the goal of this work is to quantify hemolysis kinetics as a function of salt concentration and temperature and to formulate a damage function for use in predicting response to arbitrary cryopreservation protocols. Optimization of protocols is easily accomplished if accurate predictions are obtained from the model. Any modelling necessary for the formulation of the damage function and various conclusions derived from the kinetic studies may produce additional insight into the mechanisms of hypertonic and thermal shock damage.

Interpreting a cryopreservation protocol in thermodynamic terms is a very useful conceptual tool. It requires definition of the system and

environment. In view of the observations of Lovelock regarding loss of membrane components, the best model would seem to be that of choosing the membrane as an open thermodynamic system in communication with its suspending medium as the environment on one side of the membrane and the intracellular solution on the other. During the freezing process the phase change occurring within the suspending medium causes simultaneous changes in temperature and salt concentration, i.e., the thermodynamic state of the environment changes and the rate at which it does so is a strong function of the cooling rate. For suboptimal cooling rates used to freeze human red cells, the intracellular compartment is able to remain in equilibrium with the extracellular solution because transmembrane water transport is so rapid [20,22]. Figure 1.2, the phase diagram for a sodium chloride-water system, shows the freezing trajectory (locus of thermodynamic states) for red cell quasi-equilibrium freezing in normal saline. Also shown on the phase diagram are the two components of the damage rate function which will be called HR (for hemolysis rate). As the thermodynamic state of the environment is altered during the course of freezing, the system is perturbed and responds by approaching a new state of equilibrium with its environment. This new system state may or may not favor increased hemolysis but in any case the two modes of freezing damage previously discussed may be thought of in terms of the partial derivatives $(\partial HR/\partial X_s)_T$, osmotic shock and $(\partial HR/\partial T)_{X_s}$, thermal shock. In addition to revealing how the system may be sensitive to these two types of perturbations this interpretation points out the need for an experimental apparatus capable of decoupling the two perturbation modes so that the system sensitivity can be studied for each of the modes independently. Finally, the use of thermodynamics in this context

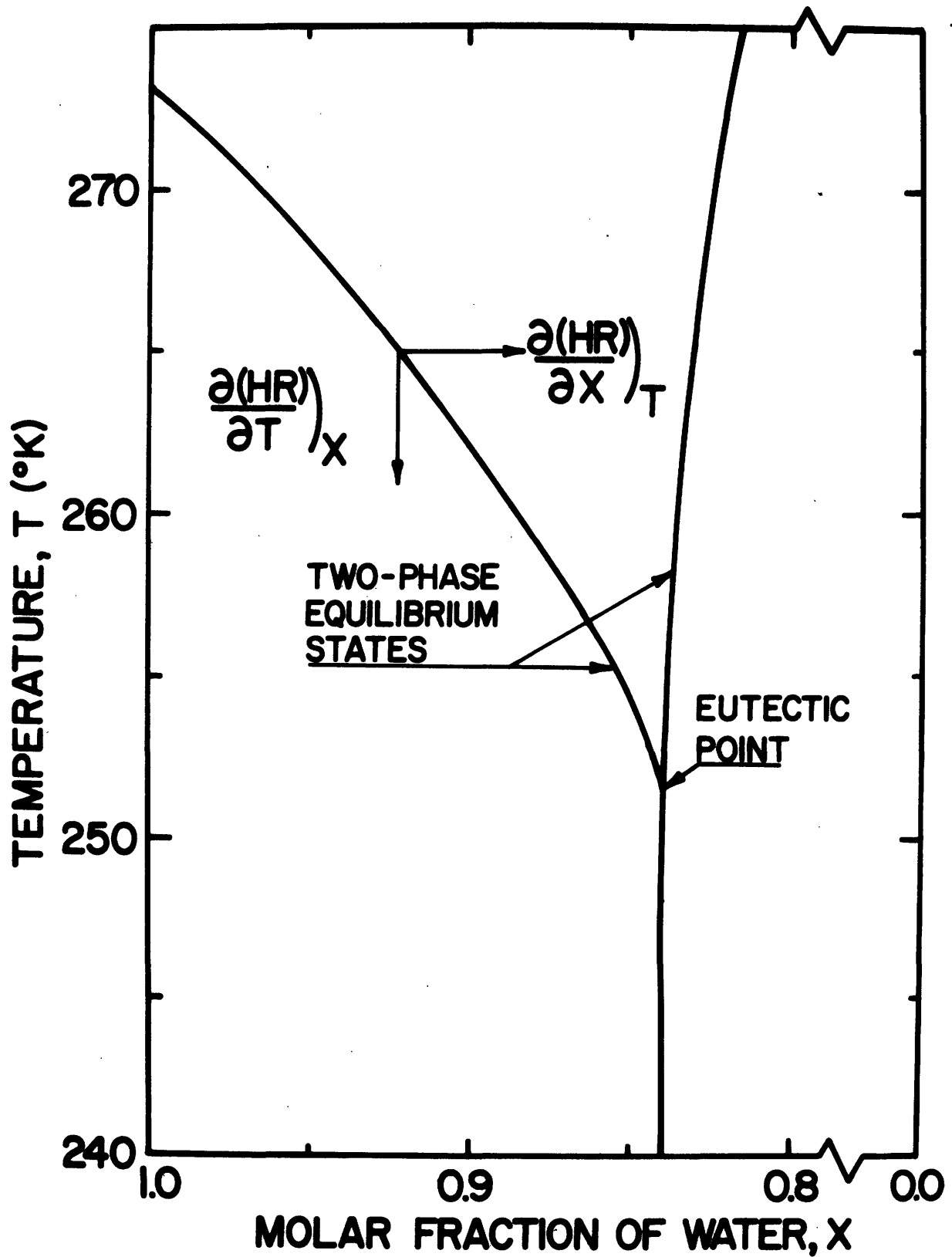


Figure 1.2 Osmotic Perturbation and Thermal Perturbation Effects on the Hemolysis Rate as Depicted on the Sodium Chloride-Water Phase Diagram.

gives meaning to the desired outcome of a successful cryopreservation technique, namely reversible freezing and thawing. The cryopreservation protocol is actually a thermodynamic cycle and it is essential that the state of the membrane and the environment be returned to their initial conditions after thawing, otherwise the irreversibilities are likely to result from what will be manifested as damage.

Thermodynamics alone is not sufficient information since it is well established that in general the rates of freezing produce pronounced effects in terms of total damage produced. Therefore kinetic information is vital, and in this respect it would not be unreasonable to assume that hemolysis would be consistent with Arrhenius rate theory. It is known both at elevated and reduced temperatures (relative to physiological temperature) that temperature induced changes in biological systems ranging from molecular constituents such as proteins, to complex cellular systems such as epidermal tissue [36,37,38,39,40,41] are consistent with the Arrhenius form.

The human erythrocyte was chosen as the model biological system for the work in this thesis for several reasons.

The red cell because of its medical importance has been studied very thoroughly as compared to other cell types. Of course this makes it attractive as a model because a wealth of biophysical and biochemical data is available, as well as general studies as to how various conditions affect cellular behavior. Compared with other mammalian cells, the mature red cell is a simple non-nucleated system whose function is to provide a

controlled environment for the oxygen binding protein hemoglobin. The release of hemoglobin (hemolysis) has been found to be an all or none phenomenon [29,42] and the detection of hemolysis (a well established technique) thereby provides a sensitive and meaningful experimental measure of damage kinetics. Lastly, the results of the thesis work on the red cell have potential significance by direct transfer of knowledge from the laboratory to the clinical practices in blood banking.

All experimental and theoretical work here will be for the simplest cellular environment--water and sodium chloride i.e., freezing for the unprotected cell in normal saline. This is done because the thermodynamic state of the intracellular and extracellular solutions can be specified at all temperatures, and because there are experimental data for post freeze-thaw survivals with which to compare predictions from the model.

Chapter 2

Experimental Apparatus

In this chapter the rationale for the development of a new experimental apparatus to measure red cell hemolysis is discussed. Each of the three subsystems comprising the apparatus: the optical system, the mixing system, and the thermal system are described in detail. In conclusion, the performance characteristics of the device are presented.

Rationale for Development

Hemolysis by definition is the release of the oxygen-binding protein hemoglobin from within the red cell to the extracellular medium. Since the release of the hemoglobin is considered to a good approximation to be an all or none event [29,42], i.e., a negligible amount of hemoglobin is retained internally, the extent of damage to a population of red cells can be determined by measuring the ratio of the hemoglobin present in the supernatant per unit volume divided by the total amount of hemoglobin (internal or external to the cell) per unit volume. The standard technique employed for hemolysis determination involves centrifugation, cell lysing, hemoglobin oxygenated state fixation, and measurement of hemoglobin absorption at 540nm. [30] Preliminary results for the hypertonic hemolysis kinetics using this standard technique revealed that the kinetics were quite rapid at the higher sodium chloride concentrations. Since the minimum time needed to obtain the first hemoglobin absorption data was approximately two to three minutes, an essential portion of the hemolysis dynamics close to time zero is inaccessible using this procedure. There are two other objections that can be made regarding the standard technique. As pointed out in the introduction, two modes of red cell perturbation are of interest, one involving concentration perturbations at various temperatures

and the other one involving temperature perturbations at various concentrations. Cold rooms or even refrigerated centrifuges simply do not offer the amount of flexibility in accurately setting and rapidly altering the thermal and osmotic conditions necessary to study both modes thoroughly. Also, in the case of the proposed study the red cells will be stressed either osmotically or thermally. Thus to centrifuge them subsequently is likely to induce mechanical damage [29]. It was therefore felt that the situation warranted development of a new apparatus and technique eliminating the need for centrifugation, providing access to "zero" time data and offering flexibility in the determination of a wide range of thermal and osmotic conditions. Observations from a modified stop-flow apparatus [43] demonstrated that the intensity of a light beam passing through a column of partially hemolyzed red cells could be calibrated as a function of hemolysis. Therefore, once calibrated, such a system has the potential of providing the desired hemolysis kinetics data as will be discussed in the next section.

The Optical System

Theory of operation:

The intensity of a light beam forward-scattered through a homogeneous mixture of erythrocytes and sodium chloride solution can be calibrated as a function of the extent of damage within the cell population and thereby provide the opportunity to follow damage reaction kinetics. Intact, healthy erythrocytes are very effective in scattering and absorbing light. As the cell hemolyzes (becoming what is called a "ghost") it is very much less effective in these capacities, which means a much

greater fraction of the incident beam passes through the cell solution and can be detected. The experimental outcome of this fact is that there will be a timewise-increasing, forward-scattered light intensity measured as hemolysis proceeds within the sample chamber. A tungsten light source powered by a regulated D.C. power supply provides a constant incident reference intensity to the cell suspension. If the oxygenation state of the hemoglobin molecule changes, so do its absorption characteristics [43,44]. This effect is experimentally eliminated by filtering the tungsten source with a band filter to block out those wavelengths where the shift occurs. For a given optical chamber geometry the amount of forward scattered light can be decreased by the addition of more red cells into the path of the light beam. This variable is held constant by the insertion of a fixed volume fraction (hematocrit) of red cells for all experiments. The measured light intensity is also a function of cell volume, making possible the measurement of trans-membrane transport properties of various permeable species by way of the stop-flow technique [43]. Cell volume changes are not a significant factor in the present work for several reasons. Firstly, all experiments are conducted in solutions hypertonic enough to produce minimum cell volume (i.e., greater than 1.0M NaCl) [29,33]. Secondly, the cell shrinkage from isotonic packed cell conditions to the minimum volume hypertonic conditions after mixing at time zero occurs on a time scale of approximately 100msec, whereas access to experimental times as long as several seconds after mixing are acceptable for the hypertonic kinetics. Finally, the forward-scattered light intensity is much less sensitive to volume changes than it is to the production of damage [43]. Erythrocytes have a density slightly greater than the sodium chloride

solutions which they are suspended in during the time in which hemolysis is measured. Unless the incident light beam is passing through a homogeneous mixture of cells and suspending medium, the measured light intensity may be a function of a parameter other than hemolysis. Specifically, the cells may sediment away from the light beam causing an increased intensity of transmitted light which could be erroneously interpreted as cell damage. This was observed during preliminary testing using an existing stop-flow device (see appendix A for details). Red cell sedimentation velocities are on the order of 0.5 cm/hr [45] which means that a sedimentation column of several centimeters height aligned with the gravitational field provides an "infinite" reservoir of a homogeneous mixture. Here the reaction kinetics are assumed uniform throughout the height of the column; thus if the sedimentation column has been designed to be long enough, the beam is no longer sensitive to sedimentation.

Major Components:

The major components of the optical system are shown in Figure 2.1, the schematic for the entire apparatus. The light source is a Zeiss 12 volt 60 watt tungsten microscope illuminator. This bulb is powered by a Hewlett-Packard Harrison 6428B D.C. power supply (voltage regulation to 0.15%). The incident light to the cell suspension is filtered by a band pass filter whose characteristics were measured on a Bausch and Lomb Spectronic 20 spectrophotometer and shown in appendix B. The test cell (or optical chamber) part of the system is optically isolated from the environment. The incident filtered beam from the tungsten source is transmitted by a 1/8" diameter bundle, 12" length fiber light guide. The forward-scattered light is incident upon a photocell sensitive to

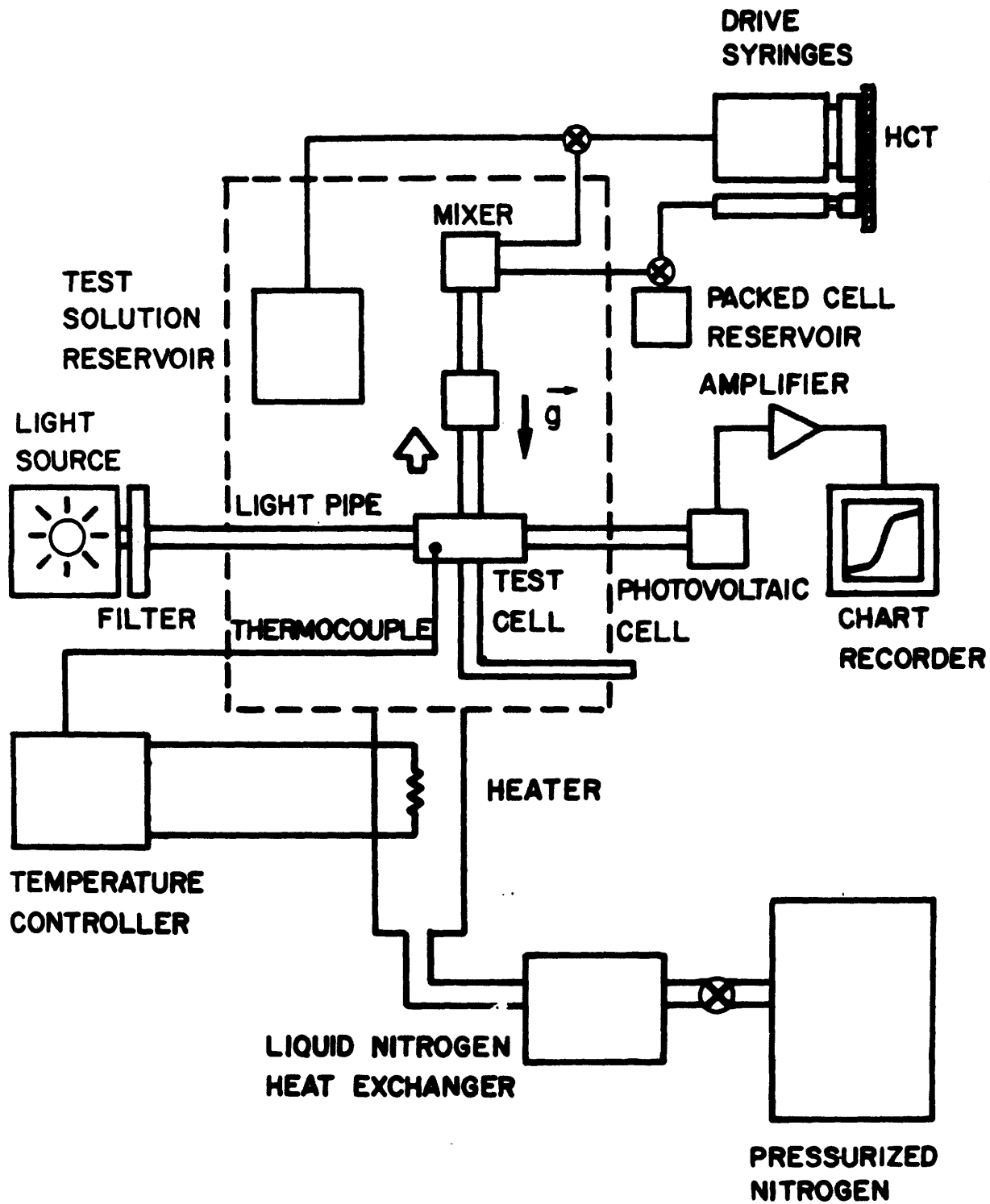


Figure 2.1 Experimental Apparatus Schematic Including the Optical, Mixing, and Thermal Subsystems.

near infrared wavelengths. The characteristics of this IRI photovoltaic silicon detector are given in Reference [86]. The detector voltage is amplified and high frequency noise is filtered by the circuit shown in appendix C. The amplified voltage characterizing hemolysis is displayed on a Hewlett-Packard 7100B strip chart recorder by means of a model 17501A multiple span (voltage) input module.

The Mixing System:

This subsystem consists of two drive syringes, a red cell reservoir, a test solution reservoir, a mixer and loop filter as well as the sedimentation column and assorted valving and tubing as shown schematically in Figure 2.1.

Theory of Operation:

This system serves several purposes. In the ideal case it instantaneously delivers to the test cell a homogeneous mixture of test solution and cells. The volume fraction of cells (the hematocrit) is precisely and reproducibly determined and the mixer itself produces no artifacts such as mechanical damage to the cells. The mixing can be assumed to expose the cells instantaneously to a step change in sodium chloride concentration and thus provide one of the perturbation modes of experimental interest. Once bulk flow is stopped at zero experimental time, no flow artifacts are present to introduce light intensity changes other than those due to hemolysis. All tubing and

valving is biologically inert to prevent cellular damage.

Major Components:

The drive syringes used are plastic Monoject 1cc and 35cc syringes. The diameters of the plungers are such that the area ratio is 1:23.73. For a coupled drive with equal stroke lengths for both plungers, the final volume fraction of cells (assuming the packed cell reservoir contains 100% cells by volume) is 4%. The red cell reservoir and the test solution reservoir are designed to provide convenient working volumes typical of those required in an experimental day. The mixer is basically a T-junction fashioned from acrylic plastic which by way of turbulence effectively mixes the test solution and packed red cells. (See appendix D for details.) Extremely small sizes are avoided since high Reynolds number flow can induce mechanical damage to erythrocytes [46]. The flow tube connecting the mixer and sedimentation column is bent into a 180° loop intended to trap any particulate or non-completely mixed cells from preferentially sedimenting into the test cell after flow is stopped following injection into the chamber. The sedimentation column as previously discussed consists of a 2 3/4" length section of tubing cut from a glass pipette (Roch Sci. Corp. 1ml in 1/10).

The Thermal System

Theory of Operation:

This subsystem provides for thermal control of the test chamber

where the cellular damage kinetics are monitored. It is not unlikely, from what has been reviewed in the literature, that the hemolysis reaction rate may be expressed in an Arrhenius form, suggesting that accurate control of temperature is essential since the rate would be exponentially related to $1/T$. In the case of the first type of experiment in which hemolysis is induced by a hypertonic concentration perturbation, the controller must be capable of producing an isothermal environment for the reaction chamber. A simple set point controller was designed to accomplish this. The controller compares an amplified, linearized thermocouple voltage proportional to the test chamber temperature with a selected voltage corresponding to the desired temperature. The difference is amplified by a one hundred fold gain and input to a power amplifier. The output of the power amplifier drives a resistive heater immersed in a refrigerant flow stream providing constant refrigeration. This flow stream is in direct contact with the test chamber which means that the energy dissipated in the heater appears as a temperature at the test chamber thermocouple and the feedback loop is complete. For the second type of perturbation mode in which hypertonic iso-osmotic condition hemolysis is induced by a temperature drop perturbation, the system should be capable of establishing accurate, reproducible initial and final temperatures as well as a range of constant rates of temperature reductions. An instantaneous step change in temperature for inducing damage is fortunately not necessary. The amount of damage induced by this perturbation mode appears to be more sensitive to the magnitude of the temperature drop rather than the cooling rate, although there is some cooling rate dependence [27,30]. Therefore a rate controller incorporating an integrator was not designed at this time. Reproducible cooling rates of $10^{\circ}\text{K}/\text{min}$ were achieved by manual control of the refrigerant

flow rate for the thermal perturbation mode experiments. (see appendix C for temperature controller circuit.)

Major Components:

The pressurized nitrogen supply and liquid nitrogen heat exchanger have been discussed elsewhere [47]. This refrigeration scheme is capable of delivering nitrogen gas to the optical system heat exchanger tube (shown as a dotted line in Figure 2.1) at approximately -150°C and 2.5 to $3.0\text{lb}_m/\text{hr}$ [47]. The immersion heater used consists of a length of 32 gauge chromel A wire measured at 9.93 ohms/ft for a total resistance of 22.7 ohms. The wire was sheathed with a number of 4 1/2" length $5\mu\text{l}$ micropipette glass tubes for electrical insulation, before insertion into the flow stream. The temperature of the brass section of the test chamber (see appendix D) was sensed by a 30 gauge Omega teflon-coated, copper-constantan thermocouple embedded with epoxy into intimate contact with the sedimentation column. The circuitry comprising the proportional set point controller including interfacing with the strip chart recorder retransmitting potentiometer is described in appendix C. The basic power amplifier circuit is discussed in references [47,48].

Calibration of the Optical System

For the purposes of reducing the raw kinetics data in the form of the photocell voltage trace to a hemolysis percentage history, a calibration of the optical system is necessary. The basic procedure employed involves the production of a partially hemolyzed solution of

cells at 4% hematocrit, spectrophotometric measurement of the amount of hemolysis and injection of this sample into the optical chamber for determining the photocell voltage output corresponding to that particular amount of hemolysis. The procedure is repeated for several levels of hemolysis so that an accurate basis for curve-fitting the hemolysis data as a function of the photocell voltage data is assured.

The final form of this calibration curve is actually in terms of a normalized photocell voltage and not the absolute voltages measured. A convenient reference for normalizing all other voltages is the photocell voltage corresponding to the minimum cell volume.

For the salt concentrations used in this work, minimum cell volumes are realized and since the transmembrane water transport is so rapid for red cells, the shrinkage to minimum volume occurs instantaneously as compared to the characteristic times associated with hemolysis kinetics even at the higher salt concentrations [33,43]. The concentrations used in the present work are in the range 1.0m to 4.0m and the fact that minimum volume should be reached for these concentrations is suggested by the results of Farrant et.al. [33] shown in Figure 2.2 for intracellular water mass. One notices that for solution concentrations exceeding 1500 - 2000 mOsm/Kg water there are no further changes in the intracellular water mass. A theoretical treatment of this effect in terms of a chemical potential driving force across the membrane for a hydrated intracellular solution is discussed in reference [22].

If there are no further changes in intracellular water mass and if cell volume is the major factor determining the magnitude of the light

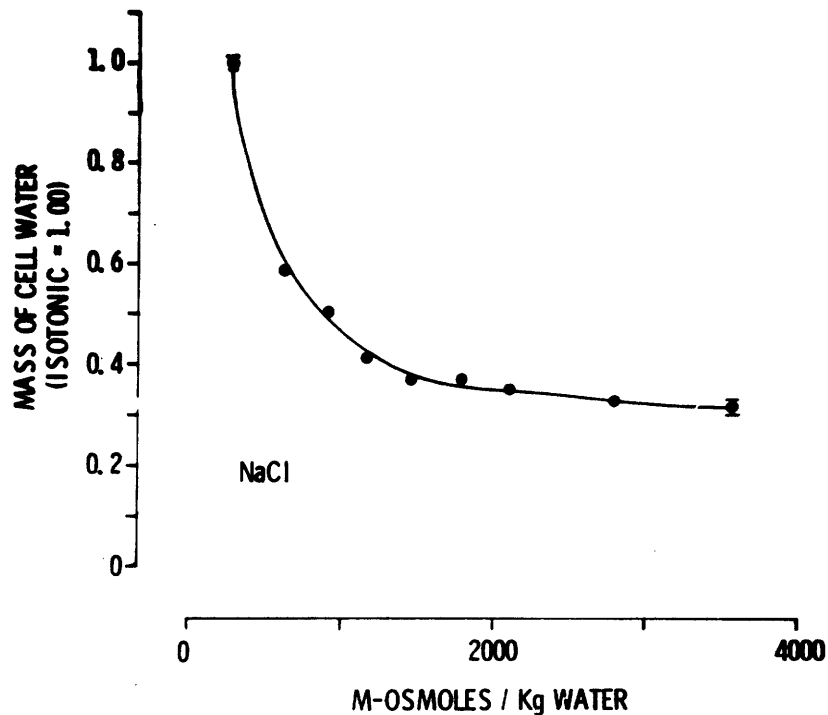


FIG. 3. Mass of intracellular water (in aliquots of packed cells) relative to that of cells in isotonic sodium chloride (= 1.00) as a function of the osmolality in hypertonic sodium chloride. The mass of cell water is increased at each point to allow for the cells lost by hemolysis and therefore represents a direct function of the mass of water in a single red cell. Cell water is lost as the osmolality increases and this process is almost complete by 1500–2000 mosmolal.

Figure 2.2 Intracellular Water Mass as a Function of Sodium Chloride Osmolality (reproduced from reference [33]).

intensity reaching the detector, one would expect negligible changes in the photocell output when the red cells are mixed with sodium chloride solutions of concentrations greater than 0.75 to 1.0m. This expected photocell response occurs as the results of Figure 2.3 show. The photocell voltage for cells at 4% hematocrit in a solution of a given NaCl concentration is divided by the photocell voltage for cells at 4% hematocrit in normal saline. This normalized voltage is plotted as a function of the given solution sodium chloride concentration. The close similarity of Figures 2.2 and 2.3 suggests that the photocell output is approximately linear with cell volume (or cell water mass) over a wide concentration range. This is known to be true for a similar system over a narrow range [43].

These results indicate that cells mixed into hypertonic NaCl solutions (fixed HCT) in the concentration range 1.0m - 2.0m will produce identical photocell outputs. The assumption is made that the results would be true from 2.0m to 4.0m as well since the chemical potential driving force for water transport will not change appreciably for the hydrated solution in the range 2.0m to 4.0m [22]. For these hypertonic concentrations, however, hemolysis occurs and the photodetector signal increases since the hemolyzed cells scatter and absorb less than healthy cells.

The instantaneous photocell voltage recorded during hemolysis (V_{test}) is normalized with respect to the minimum volume voltage ($V_0\%$). The quantity $V_0\%$ represents a condition in which the cells are at minimum volume and no hemolysis has occurred. This condition defines zero time experimentally and occurs immediately after bulk flow has ceased in the stop flow apparatus.

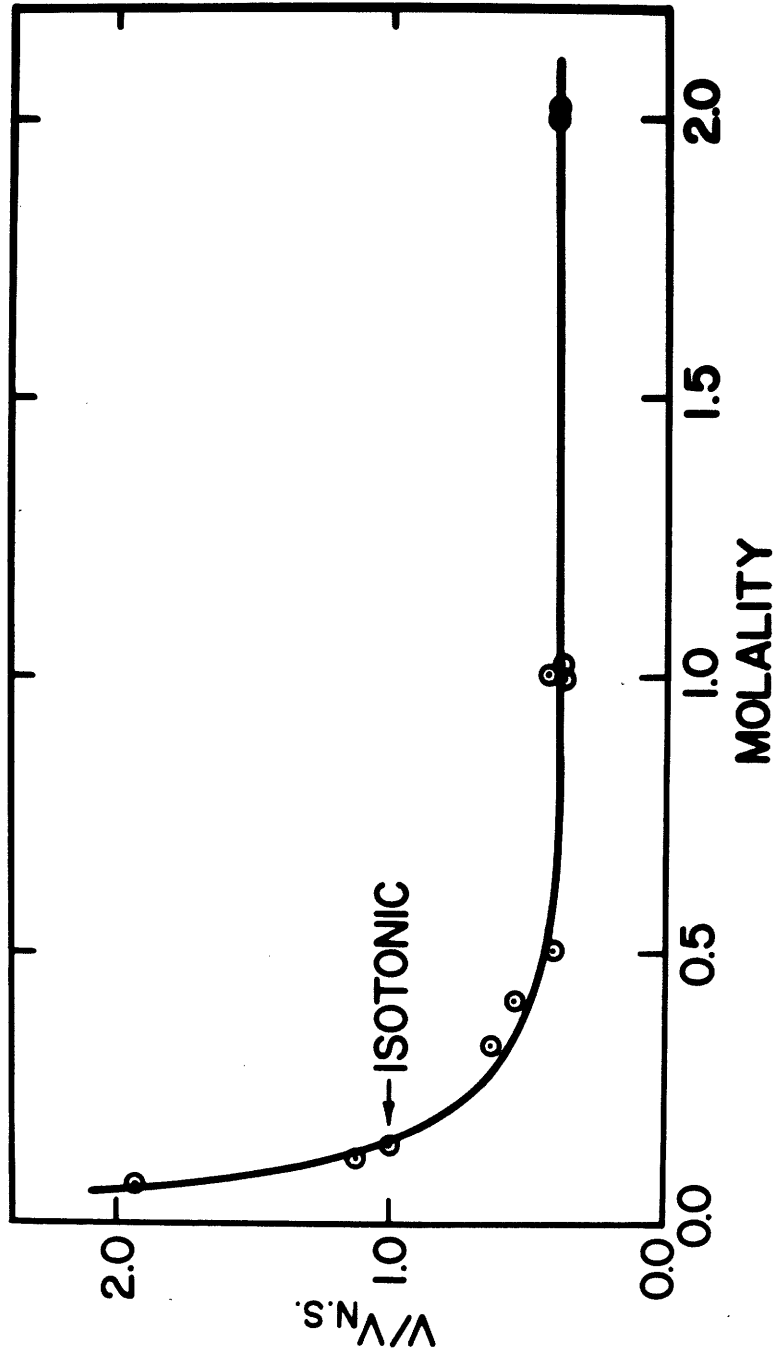


Figure 2.3 Normalized PhotoCell Voltage for Erythrocytes at 4% Hematocrit as a Function of Sodium Chloride Molality.

Red cells were placed in hypertonic sodium chloride solutions and the amount of hemolysis was monitored as a function of time by the use of the standard spectrophotometric technique. The results of these tests are shown in Figure 2.4. Two significant features of this figure should be noticed. At concentrations of 1.0m the hemolysis kinetics are indeed very slow. This means that the reference voltage $V_0\%$ for the minimum volume, zero percent hemolysis condition can be determined by mixing packed cells with 1.0m NaCl and injecting the homogeneous mixture into the optical chamber. The second significant feature is that a quasi-steady state in the hemolysis kinetics has been reached after three hours. (Note the agreement of the present results with those of Soderstrom and Zade-Oppen [29,50].)

This state of quasi-statics allows measurement of the amount of hemolysis for a sample of the hemolyzed cells on the spectrophotometer and subsequent insertion of another sample from the same hemolyzed cell suspension into the optical chamber. The time delay between the spectrophotometer reading and the determination of the photocell voltage corresponding to that particular level of hemolysis introduces an error on the order of 1-2% in the calibration curve of percent hemolysis as a function of the normalized voltage $\bar{V} = V_{\text{test}}/V_0\%$. Various levels of hemolysis are attained by mixing the cells into several different concentrations. The curve-fitted results for the calibration curve are shown in Figure 2.5. The best logarithmic fit for 32 such experimental data points shown as circles for a 4% nominal hematocrit appears as a solid line and can be expressed as

$$\% \text{ Hemolysis} = 24.313 \log_e(\bar{V})$$

with a correlation coefficient of $r = 0.96$. These tests were repeated at four hemolysis levels for a 10% nominal hematocrit and the results

QUASI-STEADY STATE HEMOLYSIS (8% HCT)
TYPICAL BEHAVIOR FOR PHOTOCCELL CALIBRATION

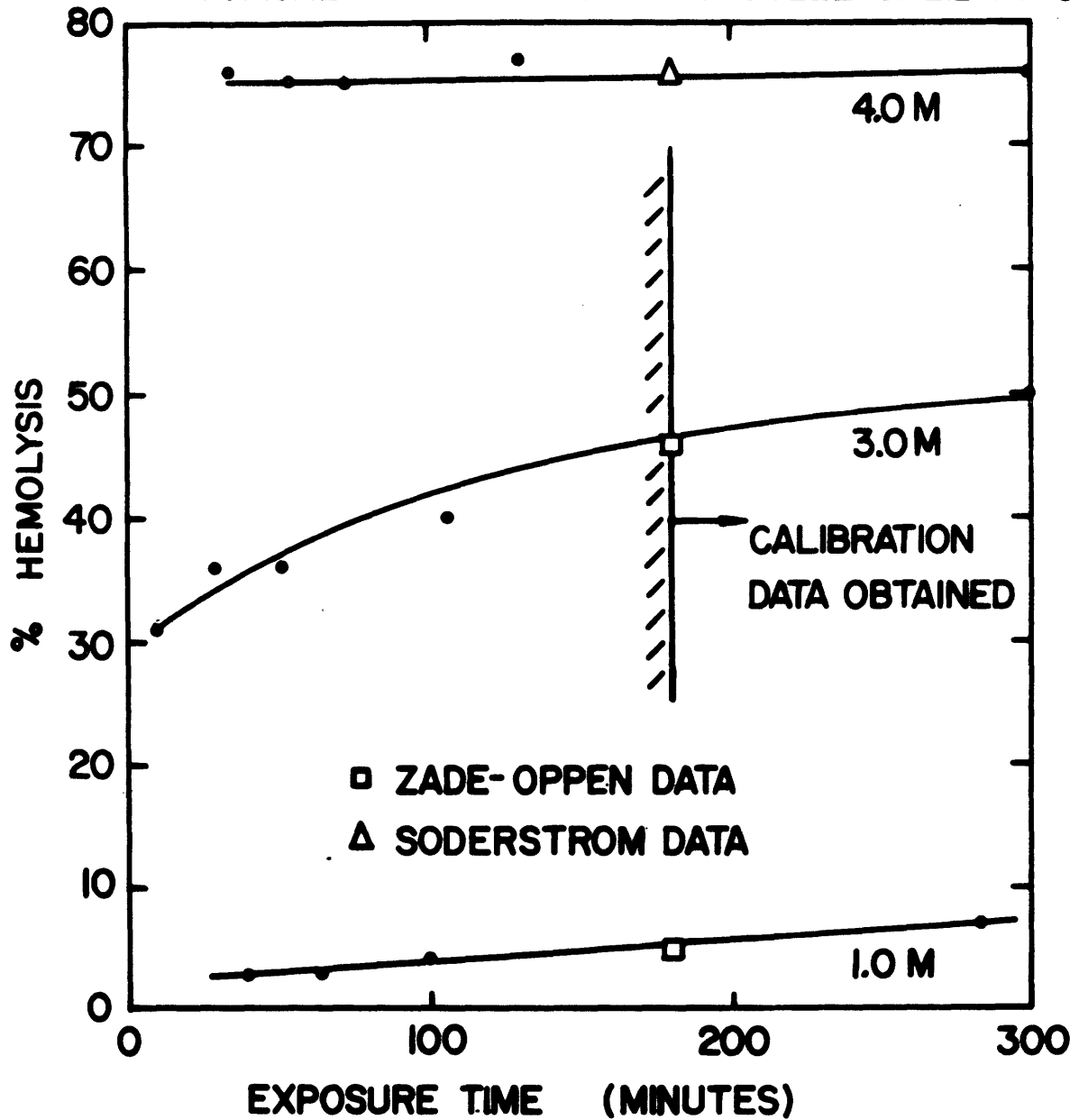


Figure 2.4 Hemolysis as a Function of Exposure Time at Several Hypertonic Sodium Chloride Concentrations.

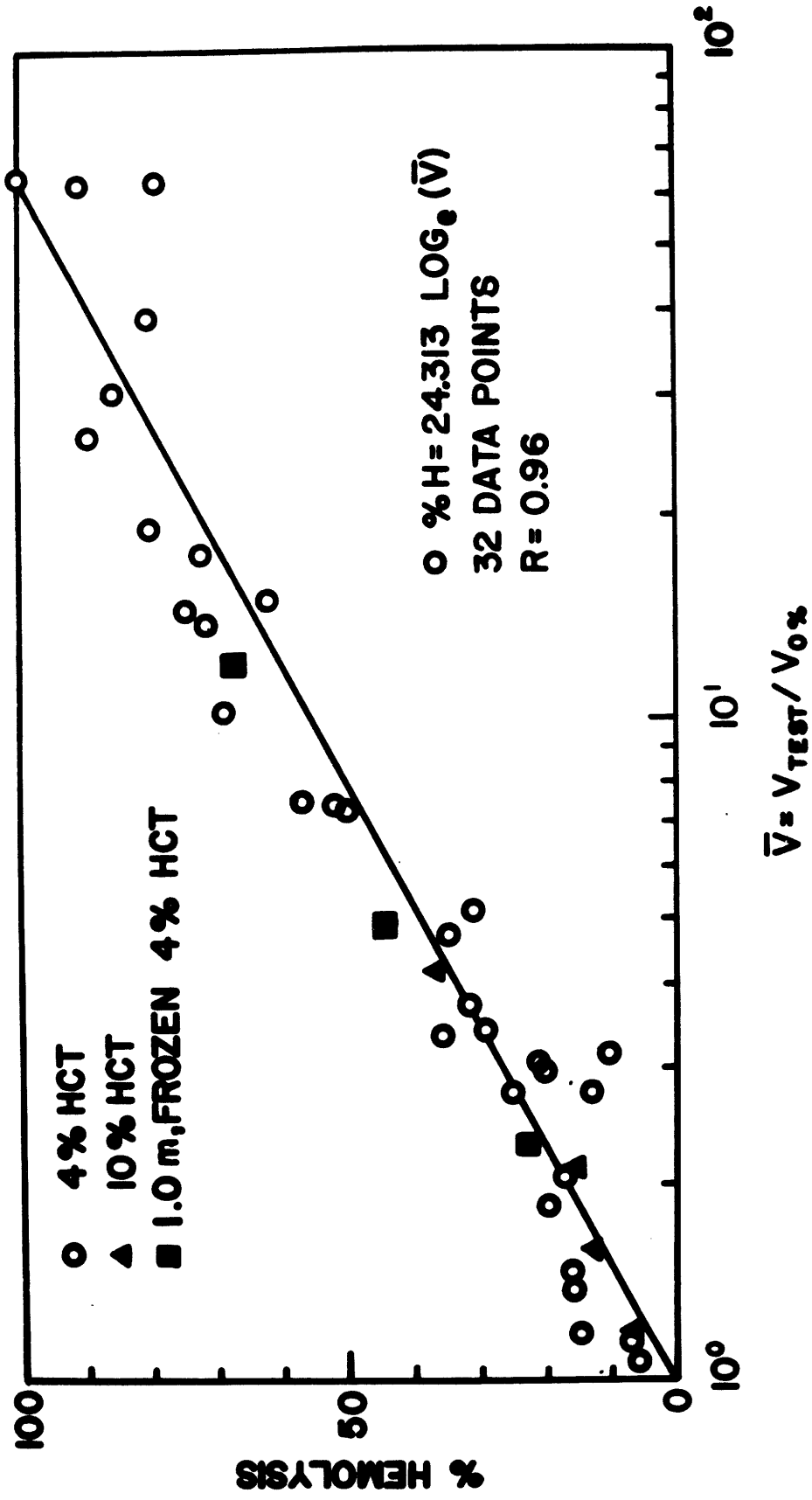


Figure 2.5 Calibration Data and Curve Fit for the Determination of Percent Hemolysis as a Function of Normalized Photocell Voltage

are shown as triangles on the same figure. These data suggest that \bar{V} is independent of the hematocrit chosen (for values between 4% and 10%). This behavior is undoubtedly a reflection of the fact that although the absolute values of V_{test} and $V_0\%$ change with hematocrit, the values of both parameters change in the same proportion. As a consequence, the ratio of the two is maintained at a constant level.

A second procedure was used as a check on the one just described. In this instance hemolysis was produced by freezing rather than solely hypertonic exposure. Red cells were mixed in 1.0M NaCl at a hematocrit of 4% and test tubes of this mixture were plunged into liquid nitrogen. The test tubes were thawed out after several minutes of residing in the liquid nitrogen bath and the amount of hemolysis produced was measured with the spectrophotometer. This procedure produced 90% hemolysis and also meant that the unhemolyzed cells were at minimum volume since they were in 1.0M NaCl still. Healthy packed cells were mixed in 1.0M NaCl at 4% hematocrit for a mixture of "0%" hemolyzed, minimum volume cells. Specified volume fractions of 90% hemolyzed and 0% hemolyzed cells were then mixed to yield total hemolysis values of 23%, 45% and 68%. The times associated with hypertonic exposure to 1.0M NaCl were short enough so that less than 2% error should be introduced in the 90% and 0% hemolysis levels, respectively. The \bar{V} data for these amounts of hemolysis are shown in Figure 2.5 as squares. The conclusion drawn from a comparison of the two sets of data is that there is no striking deviation from the previous results since these data appear to fall within the bounds defined by the scatter seen in the data from the former procedure.

Operational Characteristics of the System

The system warm-up time is approximately one half hour. This time is associated with the generation of a reference temperature within the strip chart recorder temperature module, and the approach to steady state behavior for the operational amplifiers, power supplies and tungsten lamp.

The stability of the system will be discussed in the section describing control experiments in Chapter 3. Suffice it to say at present that the photocell output is stable to better than $\pm 2\%$ for times exceeding six hours with normal saline in the test chamber and for over a twenty minute period for the case in which the test chamber contains red cells in normal saline.

The photocell output is a linear function of the regulated power supply voltage used to illuminate the tungsten lamp. This is true whether the optical chamber contains only normal saline or cells at 4% hematocrit and minimum volume (1.0m NaCl solution) conditions, see Figure 2.6. The only difference is that the absolute magnitudes of the photocell voltage output are different. The lower values occur, of course, when cells are present to scatter and absorb a larger portion of the incident beam.

Typical operating conditions are given to orient the reader as to the photocell voltage magnitudes involved for various situations. With a photocell voltage gain of one-hundred fold across the operational amplifier, the maximum amplified voltage is set at 8.0 volts for normal

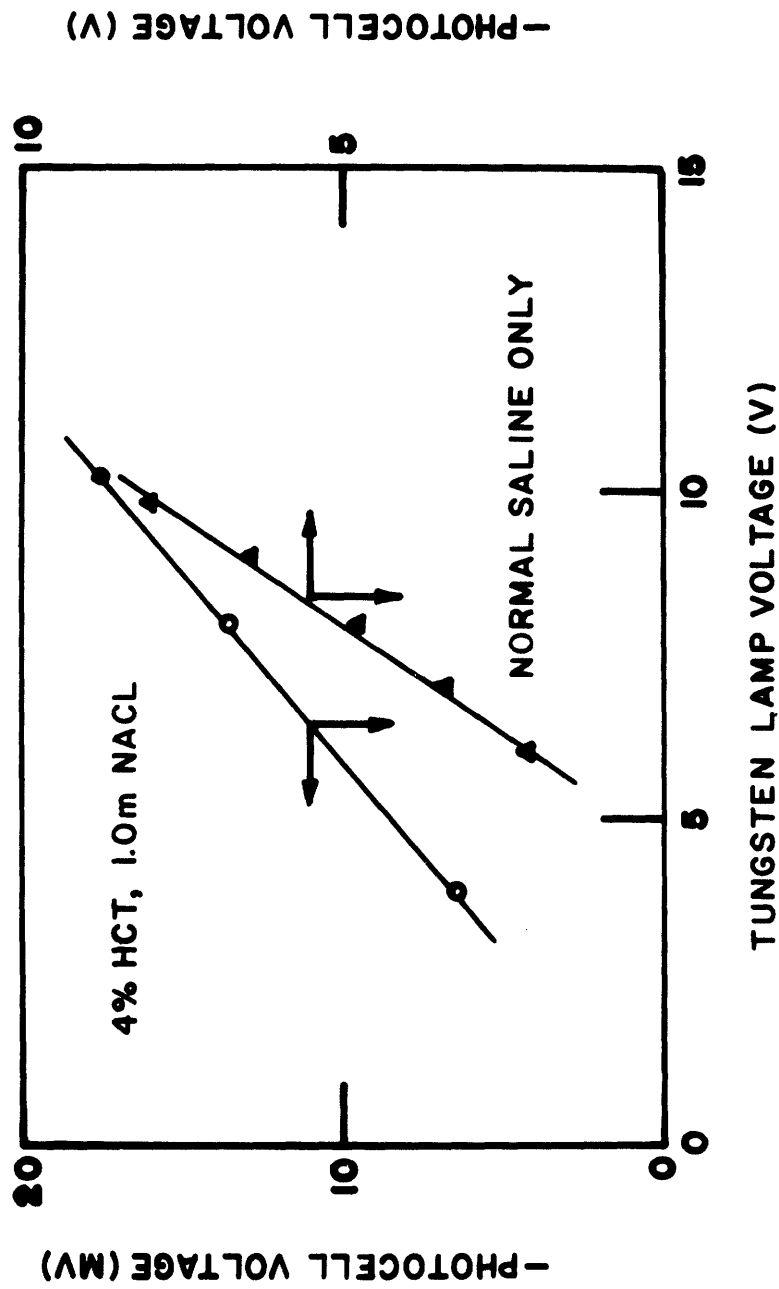


Figure 2.6 Linear Nature of the PhotoCell Voltage as a Function of Lamp Voltage for Cases in Which the Optical Chamber Contains Only Normal Saline or Cells at 4% Hematocrit in 1.0m NaCl.

saline in the optical chamber. For these conditions the minimum output would be approximately 13.5mv for zero hemolysis and minimum cell volume conditions for cells in 1.0m NaCl at a 4% nominal hematocrit.

The dynamic response of the optical system was experimentally determined by introducing normal saline into the sedimentation column, which produces a steady signal, and then switching off the power supply to the tungsten lamp. This does not produce a true step input to the photocell since there are transients associated with the power supply output capacitance and the thermal relaxation of the lamp filament. Nevertheless, the amplified and filtered output of the photocell responded with a characteristic time of two seconds to such a test. This dead time is negligible compared to the characteristic hemolysis kinetic transients.

This apparatus has been designed to monitor the transient extent of cellular destruction (hemolysis), and it is therefore necessary to identify and to control experimentally all other system variables that could cause variations in the detector output. The sensitivity of the detector output to cell volume has been discussed and quantified in the calibration section of this chapter. This factor should not alter results obtained from the apparatus because it has been demonstrated that minimum volume will be reached in all cases and this state is reached instantaneously with respect to the time scale for hemolysis.

Insertion of a greater cell density (hematocrit) decreases the total forward-scattered light intensity. This characteristic of the present device has been quantified and is shown in Figure 2.7. In this graph

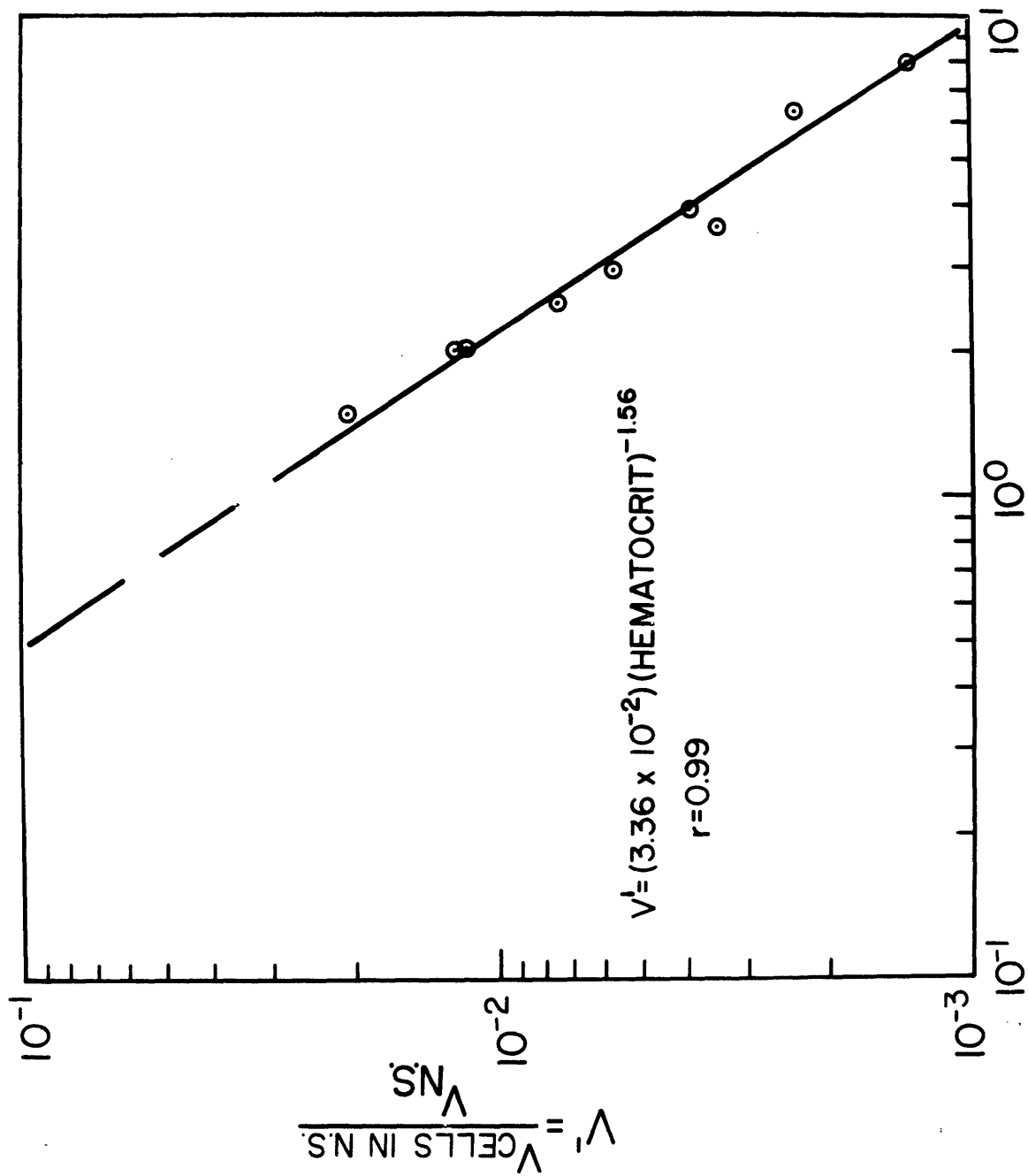


Figure 2.7 Normalized PhotoCell Voltage as a Function of Measured Hematocrit

V' is the photocell voltage normalized with respect to the 8.0 volt reference with only normal saline in the optical path. The parameter V' is plotted on log-log paper with measured hematocrit (not nominal hematocrit) on the abscissa. A best fit by least squares yields the expression for cells in normal saline;

$$V' = (3.36 \times 10^{-2}) (\text{Hematocrit})^{-1.56}$$

A distinction between measured and nominal hematocrits was observed experimentally. The drive syringes chosen for the mixing subsystem were designed to deliver a nominal hematocrit of 4%. However, the actual volume fraction of red cells delivered as a homogeneous mixture to the optical chamber has been measured at 2%. The reason for this is that the packed cell reservoir contains centrifuged red cells which are not 100% packed. The 50% degree of packedness experimentally measured is slightly lower than that observed by other investigators, probably due to short centrifugation times (3 minutes) at low force levels (900g) but the highest degree of packing attainable would appear to be 70% [49]. Since the system calibration curve parameter \bar{V} has been shown to be insensitive to hematocrit variations, this feature fortunately does not introduce errors into hemolysis detection measurements.

For any one reservoir full of packed cells, the packedness of the cell sample is invariant and the reproducibility of the syringe pair in delivering a constant hematocrit from test to test was checked. It was found that the system delivered a mean hematocrit of 2% with a standard deviation of $\pm 0.1\%$ absolute hematocrit. This represents a deviation of 5% about the mean value ($\frac{0.1}{2} = 0.05$), meaning that the delivery system is producing a constant hematocrit to within $\pm 5\%$ variability. The initial absolute value of the photocell voltage tends to shift

approximately 7% about a mean value for any one reservoir full of packed cells and this can be shown to be a direct result of the 5% variation in delivered hematocrit (appendix E). Deviations greater than 7% for the absolute photocell output are expected for tests conducted from different samples of packed cells if the centrifugation has produced differences in packedness that result in hematocrit variations greater than 5%. These variations do not effect the hemolysis derived since \bar{V} is not sensitive to hematocrit.

There are two features of the system characteristics that have rather undesirable consequences. These features represent weakness in this technique but arguments are given explaining why these weaknesses are probably not causing appreciable distortion of the hemolysis kinetic data derived from experiments performed on this device.

For the first 14 seconds after bulk flow is stopped, there is on the average a 7% decrease in absolute signal based on the minimum volume, 0% hemolysis signal level. This amounts to an absolute signal change of approximately 1.0mv. The cause of this artifact is unknown at the present time, but it appears to be related to the length of time cells have been stored (after donation) at 4°C in the refrigerator. Cells stored for longer than about 4 days show very little of this artifactual behavior [51]. This is particularly curious since water transport is occurring over a time span of less than 100-500msec and estimates of velocity damping for red cells in normal saline solution indicate very rapid characteristic times (see appendix F). Fortunately this effect should not introduce error in data retrieval for most situations. For example, at the higher sodium chloride concentrations

the kinetics are so rapid that the absolute signal level within several seconds after flow is stopped is large enough to make the 1.0mv drift insignificant. At the other extreme, for the lower concentrations, the kinetics are slow enough that the steady state for the drift has been reached well before any appreciable hemolysis has occurred. This means that the voltage level after 14 seconds have elapsed has not been altered by hemolysis, so the voltage at 14 seconds can be assumed to be the V_0 one would see at zero time. In between these limits the margin of error is worse, but as will be seen in the Chapter 4 presentation of the experimental results, the data obtained in the middle concentration ranges are consistent with those taken at both extremes where the error is negligible.

The other potential weakness of the apparatus and technique is a consequence of the system behavior described by the data summarized in Figure 2.8. This plot reveals that the photocell voltage output is a function of the concentration of the sodium chloride solution when no cells are present in the solution. A reference photocell voltage is selected when the optical chamber contains normal saline. The chamber is then sequentially filled with several increasingly concentrated solutions. The voltages observed for each of these solutions normalized by division using the normal saline reference voltage shows that the light intensity decreases linearly with increasing solution molality. This behavior is observed regardless of the absolute magnitude of the normal saline reference voltage. This voltage was altered by the introduction of neutral density filters (Kodak Wratten gelatin filters, No. 96 N.D. 2.00 and No. 96 N.D. 3.00) in the light path between the end of the light pipe and the beginning of the optical chamber housing.

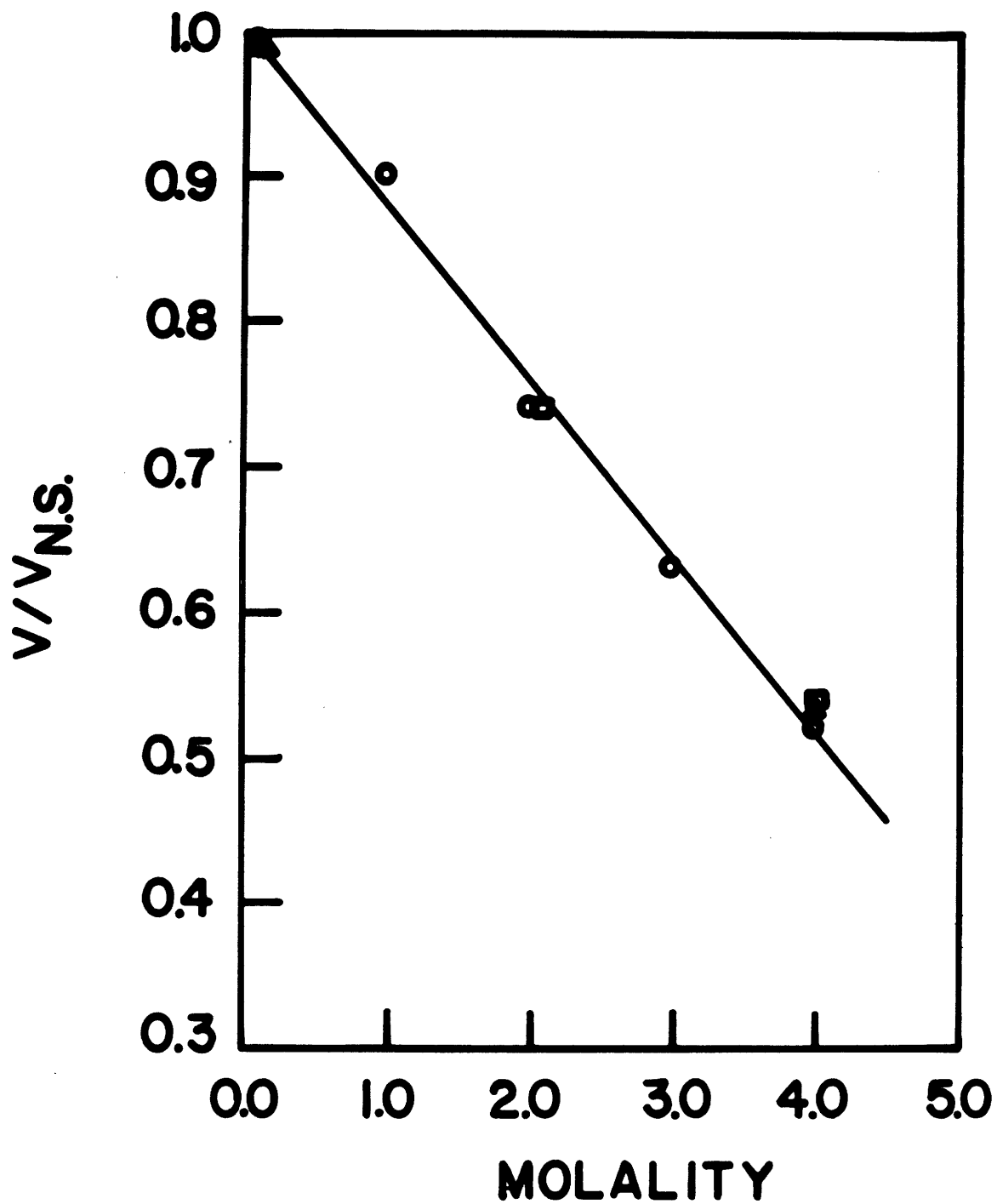


Figure 2.8 Normalized Photocell Voltage for Cell-Free Suspensions as a Function of Suspension Molality at Various Reference Voltage Levels.

The lamp supply voltage was not altered for these tests. Linearity was noted for normal saline voltages of 8.0 volts (circle data), 0.43 volts (triangle data) and 0.128 volts (square data).

The implications of this result can be appreciated with the aid of the data in Figure 2.9. This figure is a representation of the hemolysis percentages obtained in the quasi-steady state (for exposure times longer than 3 hours) at a given solution molality. These are the same hemolysis data points plotted in the calibration curve as Figure 2.5. The point is, that various solution molalities were necessary to produce the desired range of hemolysis percentages. If the measured photocell voltages are a function not only of the amount of hemolysis but also of the solution molality as indicated by Figure 2.8, then it is not correct to normalize all V_{test} data with respect to a 0% hemolysis, minimum volume $V_{0\%}$ obtained at 1.0m, unless the effect of the solution molality on V_{test} is small compared to the effect of hemolysis on V_{test} . If the absorbances of the two effects could be considered additive, then the overall intensity of light reaching the detector would directly include the results shown in Figure 2.8, namely that a cell solution at a given level of hemolysis in 4.0m NaCl would yield a signal only 58% ($0.525/0.90$) of that obtained for the same degree of hemolysis but in a solution of 1.0M NaCl. The actual system must be more complex than this and it must be the case that the effects of the solution concentration alone vis-a-vis the effects of the amount of hemolysis are negligible, at least for little hemolysis.

Evidence for this assertion comes from two separate types of experiments already described. When no hemolysis occurs and cells are forced to a

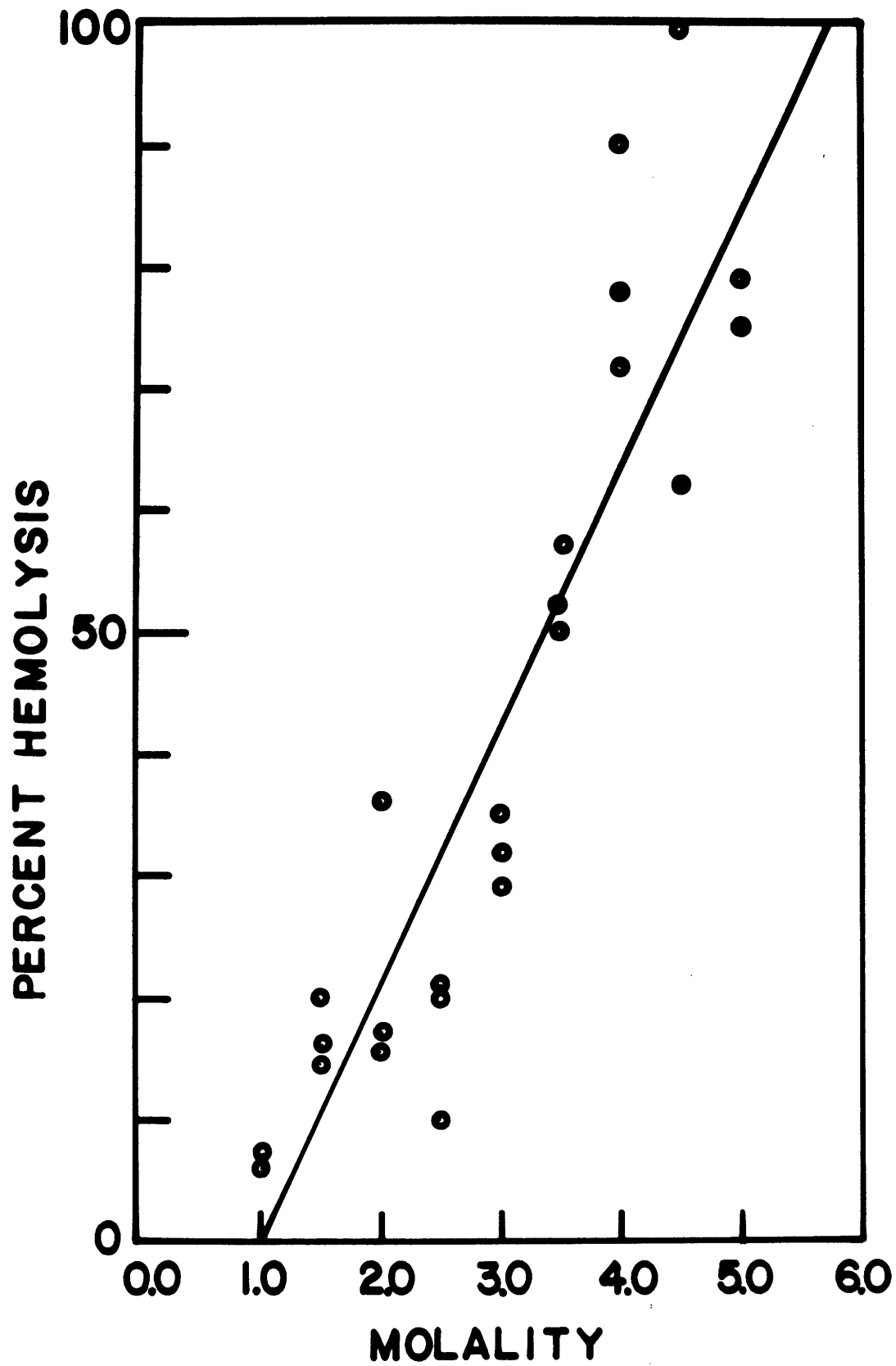


Figure 2.9 Quasi-Steady State Percent Hemolysis as a Function of Suspension Sodium Chloride Molality.

minimum volume state by increasing the solution concentration, the same voltage level is realized for both cells in 1.0m solution and cells in 2.0m solution (see Figure 2.30). If solution effects alone were to be directly reflected in the photocell output as expressed by Figure 2.8, then the expected difference between the 1.0m cell solution and the 2.0m cell solution would be of the order of 18% ($\frac{0.90 - 0.74}{0.90}$). This is not observed in Figure 2.3 which implies that the solution effect would not alter the calibration curve (% hemolysis vs \bar{V}). The second calibration procedure in which cells were frozen in 1.0m NaCl, mixed with unhemolyzed cells in 1.0m NaCl, and the measured V_{test} was normalized with respect to $V_0\%$ measured at 1.0m NaCl, yielded data in good agreement with the first calibration procedure. Thus the solution effect described in Figure 2.8 will not cause significant distortion of the calibration curve.

Chapter 3

Experimental Procedures and Control Experiments

Experimental Procedure for the Isothermal,
Hypertonic Osmotic Perturbation Mode

The electronics of the system are turned on and allowed to warm up for thirty minutes. The reference incident light intensity to the test chamber is set by filling the chamber with normal saline and adjusting the regulated power supply to the tungsten lamp such that the transmitted light intensity to the photocell yields an output of 8 volts. This can be done immediately after the rest of the electronics are turned on so that the entire system is ready for operation within thirty minutes.

Fresh whole blood collected in citrate phosphate dextrose (CPD) was obtained courtesy of Dr. C.E. Huggins, Director of the Blood Bank, Massachusetts General Hospital. All blood not used on the day of collection is sealed in the collection test tube and stored in its own plasma at +4°C. If not used within three days after collection, this blood is discarded. At the time of use, the whole blood collected in CPD is washed three times in normal saline by the standard technique. Specifically, the cells are centrifuged at 960g for three minutes, then the supernatant fluid is aspirated, including the white cells on the first aspiration. The fluid is replaced with normal saline and centrifuged. This cycle of aspiration, refilling with saline, and centrifugation is repeated three times. After the third centrifugation, all of the supernatant is removed and these "packed" cells are either placed into the system packed cell reservoir for immediate use or into the refrigerator for use later in the day.

The test solution reservoir is filled with the hypertonic sodium chloride solution of interest. There are five stock mixtures of sodium chloride and water chosen for experimental use. When mixed with packed cells in the syringe pair yielding the nominal 4% hematocrit, the post-mix equilibrium concentrations which the red cells are exposed to are 1.96m, 2.45m, 2.94m, 3.43m, and 3.94m which result from stock mixtures of 2.00m, 2.50m, 3.00m, 3.50m, and 4.00m respectively. These concentrations are chosen to cover a major portion of the region bounded by a minimum concentration of 0.8M, which according to Lovelock's estimates represents the minimum concentration required to produce initial damage [24], and bounded by a maximum concentration of 5.2m which is the eutectic concentration of a simple sodium chloride-water system [22]. At this point the mixing system is ready to use.

If temperatures other than ambient are desired, as they would be in the general case, the thermal system must be prepared for use before mixing begins. The liquid nitrogen heat exchanger is filled with liquid nitrogen and the temperature controller set point is selected for the desired temperature. The power amplifier output is applied to the immersion heater and nitrogen flow from the pressurized source is initialized. The strip chart recorder drive is turned on and the approach of the test cell to a thermal steady state is observed on the recorder. Full scale and zero settings are calibrated for the scale setting selected on the multiple span voltage input module, and the amplified photocell voltage is applied to this module for display on the second channel of the strip chart recorder. The appropriate scale can be chosen by use of the calibration curve for \bar{V} as a function of hemolysis and an estimate as to the amount of damage that will occur.

Once the thermal steady state is reached the blood and hypertonic solution are manually injected with a gentle sinusoidal motion through the mixer and filter loop into the test cell. Flow is stopped and the recorder now displays two simultaneous traces, one of the photocell voltage and one of the test cell temperature.

The photocell voltage data is then reduced as $\bar{V} (= V_{\text{instantaneous}}/V_{0\%})$ and plotted as a function of time. The calibration curve is then used to translate \bar{V} to percent hemolysis. The result is that the hemolysis kinetics at that particular temperature and concentration are determined. The test is then repeated for the same conditions to establish a reasonable statistical base for sampling the population behavior. Usually five to ten runs for each condition are done.

Once this data is complete either the temperature is changed to a new isothermal set point and a variety of hypertonic solutions are investigated or more concentrations are investigated at the same temperature. In this manner a complete sweep of the concentration range of interest and temperature range of interest can be pursued. The temperatures of primary concern are between physiological (+37°C) and the eutectic temperature of the sodium-chloride water system (-21.15°C) [22].

It is perhaps best before proceeding further to note and discuss a subtle but important point relating to this procedure. Although some information is gained about the kinetic process of damage and how it is related to temperature by these series of isothermal tests, these data are not necessarily representative of cellular behavior while experiencing temperature drops. Also note that the packed cells are maintained at

room temperature until injection, regardless of the chosen operating temperature of the system. This is necessary because otherwise the minimum operating temperature would have to be about -0.6°C where the packed cells in saline would begin to freeze out. Experimentally this means that the packed cells see a temperature drop as they are mixed with the precooled hypertonic solution. As the packed cell volume represents only 4% of the total volume, the temperature rise of the system associated with injection of the warm cells is negligible (maximum of 2°C at an operating temperature of -20°C) and occurs very rapidly due to the small packed cell volume and turbulent mixing. The result is that the red cells are in an environment which has equilibrated thermally and chemically within one to two seconds or less after injection. This means that the cells see essentially zero pre-exposure to hypertonic conditions before experiencing the temperature drop. Morris et.al. have demonstrated that for these conditions the thermal shock effect is negligible [30].

Experimental Procedure for the Hypertonic, Iso-osmotic Temperature Perturbation Mode

System preparation for this mode is identical to that of the previous section in all respects except the thermal protocol, since in this case the test cell experiences a temperature drop during part of the experiment. The typical procedure for these so-called thermal shock experiments is taken from the examples of Lovelock and Morris et.al. [27,30]. The red cells are mixed with the chosen hypertonic solution at a relatively high temperature (25°C) and are

exposed to this concentration and temperature for a given length of time. Without changing concentration, the temperature of the cell suspension is reduced at a known rate to a lower temperature. In most cases this temperature was 0°C, which is high enough to prevent solute concentration increases due to solution phase changes. The cells are sampled for hemolysis immediately after reaching the minimum temperature [30]. In the present set of experiments, the high temperature is ambient (26°C) and the minimum temperature is 0°C. The packed cells and hypertonic solution are injected into the test chamber and remain at ambient temperature for a chosen exposure time. Pressurized nitrogen is pumped through the liquid nitrogen heat exchanger cooling the refrigeration flow path upstream of the test chamber. Cooling for these experiments is accomplished manually. The refrigeration flow stream is directed away from the test chamber until cooling is initiated. At this time the refrigerant flow passes over the test chamber and the rate of temperature drop is controlled by adjusting the flow rate of refrigerant with a valve.

This method will reproducibly yield cooling rates of 10°K/min (\pm 1°K/min) from 26°C to 0°C and the 0°C value can be maintained within 1°C accuracy quite easily. The thermal diffusivity of the present test chamber limits the maximum cooling rate to approximately 10°K/min. The temperature and hemolysis histories are recorded on the dual channel strip chart recorder in the same manner used for the osmotic perturbation mode.

The photocell voltage data are reduced as before and the calibration curve is used to derive the hemolysis kinetics for this perturbation mode.

Again, there are five to ten experimental runs at each set of conditions to provide a statistically significant representation of the population behavior.

A complete investigation of the kinetics due to this mode would involve varying the following parameters: initial temperature, minimum temperature, cooling rate, hypertonic concentration and exposure time.

Control Experiments

The stability of the optical system is checked by inserting a solution of normal saline with no cells into the optical chamber after the system is warmed up. At the reference photocell voltage chosen for normal saline (8 volts), the output of the photocell remains constant to better than $\pm 1\%$ for periods exceeding six hours. This test establishes the stability of the basic optical components including the tungsten source and power supply, as well as the photocell detector and amplification circuit.

Packed red cells mixed with normal saline should produce a steady photocell signal because volume changes and hemolysis do not occur. If the 14 second artifact is neglected for the moment, the photocell output as a function of time (Figure 3.1) shows a maximum average deviation of 2% from the initial voltage for periods up to twenty minutes. This translates to approximately 1/2% uncertainty in the hemolysis derived and can be considered negligible. In addition to

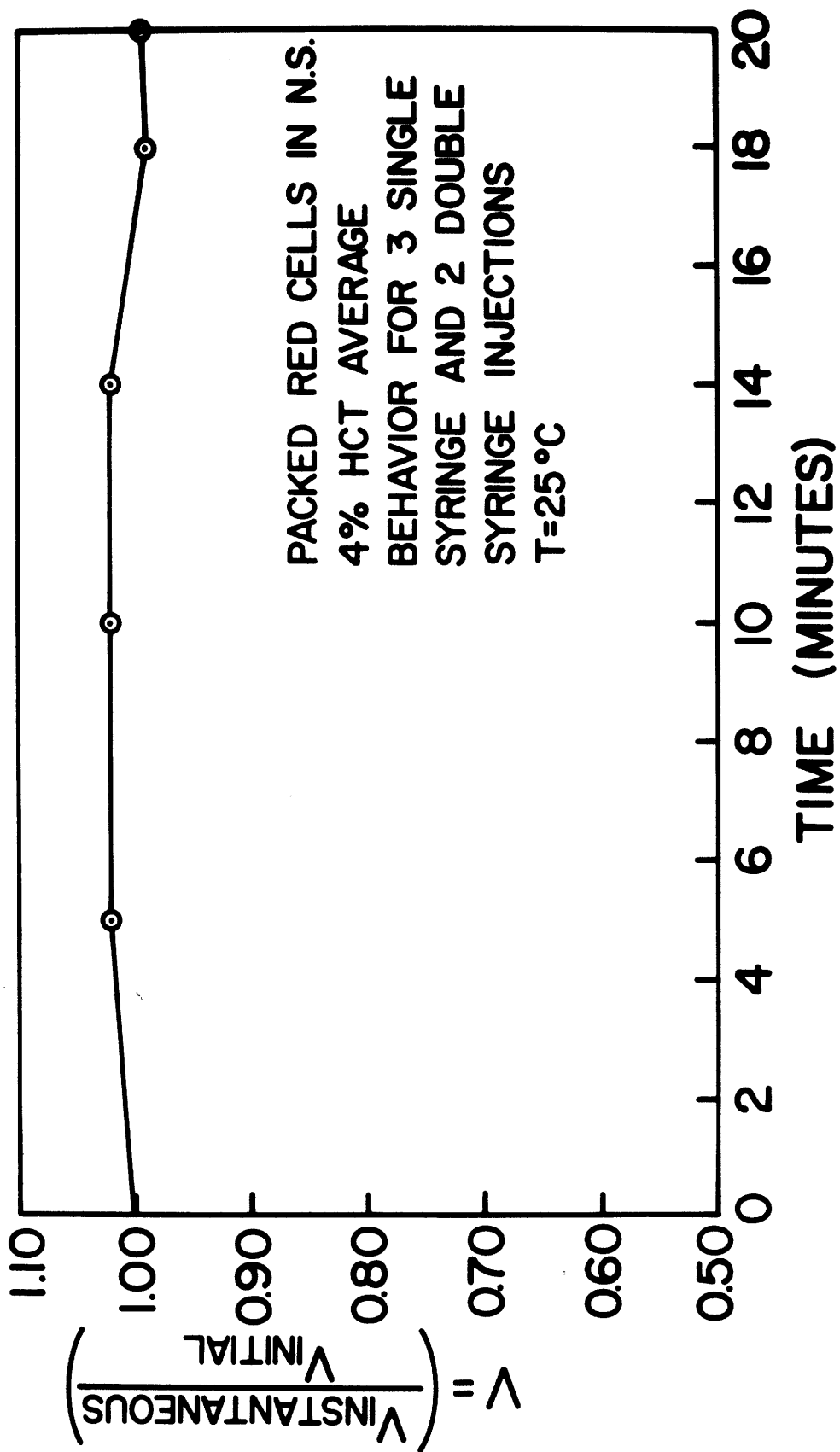


Figure 3.1 Normalized PhotoCell Voltage as a Function of Time, Demonstrating Stability of the Optical System for Erythrocytes in Normal Saline.

demonstrating that volume changes are not occurring, this test demonstrates that the device does not produce mechanical damage (at least for cells in normal saline at ambient temperature.)

If the photocell voltage output were a function of temperature, the method of data retrieval would be considerably more difficult than if it were not. Figure 3.2 which describes a control experiment for thermal shock (temperature perturbation mode of damage) reveals that the system is not sensitive to temperature. The top trace is the temperature history showing a two minute isothermal period at +24°C before cooling at about 9°K/min to 0°C. The bottom trace is the photocell output showing the typical 14 second artifact followed by a steady state after the packed red cells are mixed with normal saline for a final nominal hematocrit of 4%. One notices that with the exception of small fluctuations within the limits defined in the previous control, the output signal is uniform both while cooling and during the period at 0°C. This result means that the output is not a function of temperature within the temperature range +24°C to 0°C and further that red cells in normal saline are not affected by a 24°C temperature drop, in agreement with the results of Morris et.al. [30].

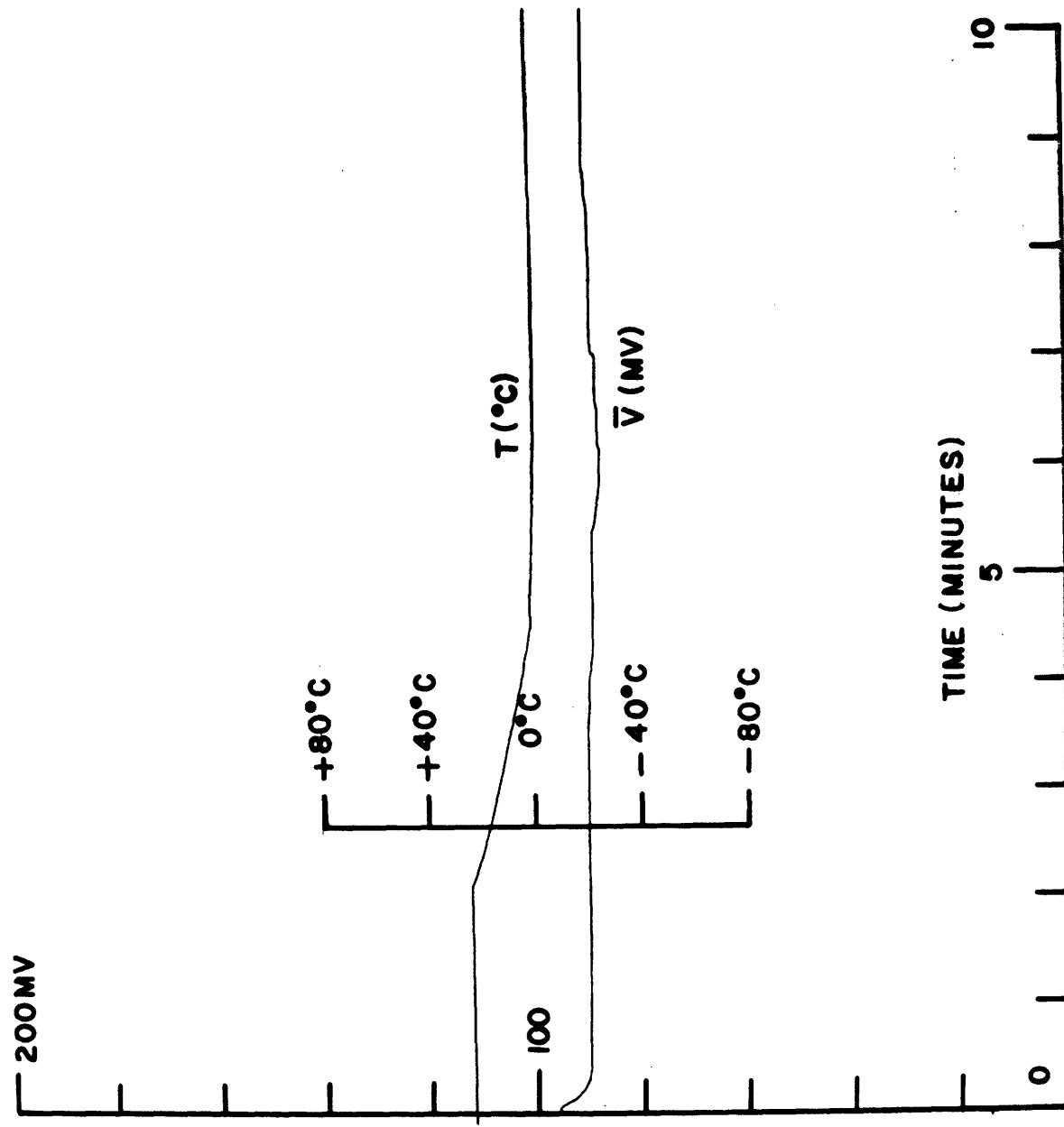


Figure 3.2 Strip Chart Recording Demonstrating Stability of the Optical Output for Erythrocytes in Normal Saline During and After a Temperature Reduction.

Chapter 4

Experimental Results for Hemolysis Kinetics
Produced by Isothermal, Osmotic Perturbation
and by Iso-osmotic, Thermal Perturbation

This chapter includes presentation of the experimental results for hemolysis kinetics due to hypertonic osmotic perturbations and subsequent manipulation of the data into forms most useful for the purposes of computer analysis of freeze-thaw simulations and thermodynamic modelling. It also contains data for hemolysis resulting from thermal perturbation. The complexity of the latter type of data is discussed and the rationale given for obtaining a limited amount of these data at the present time.

Hemolysis Induced by Isothermal, Osmotic Perturbation

All of the initial osmotic perturbation experiments were done at ambient temperature primarily for convenience and the fact that long exposure time hemolysis data for various NaCl concentrations were available in the literature; hence the validity of this technique and the accuracy of the apparatus could be checked. Figure 4.1 shows a representative example of photocell voltage output as a function of time for the case of mixing packed cells into a hypertonic solution of 3.0M NaCl. After the bulk flow is stopped, the cells have reached minimum volume instantaneously with respect to the characteristic times of minutes shown in this figure. At time zero the cells are at minimum volume and they are sedimenting down the length of the observation chamber at 0.5cm/hr, past the section of the chamber where the regulated light beam passes through the column. If the cells were not hemolyzing, the photocell output would remain constant as was shown in the control experiment for red cells in normal saline. In the present example,

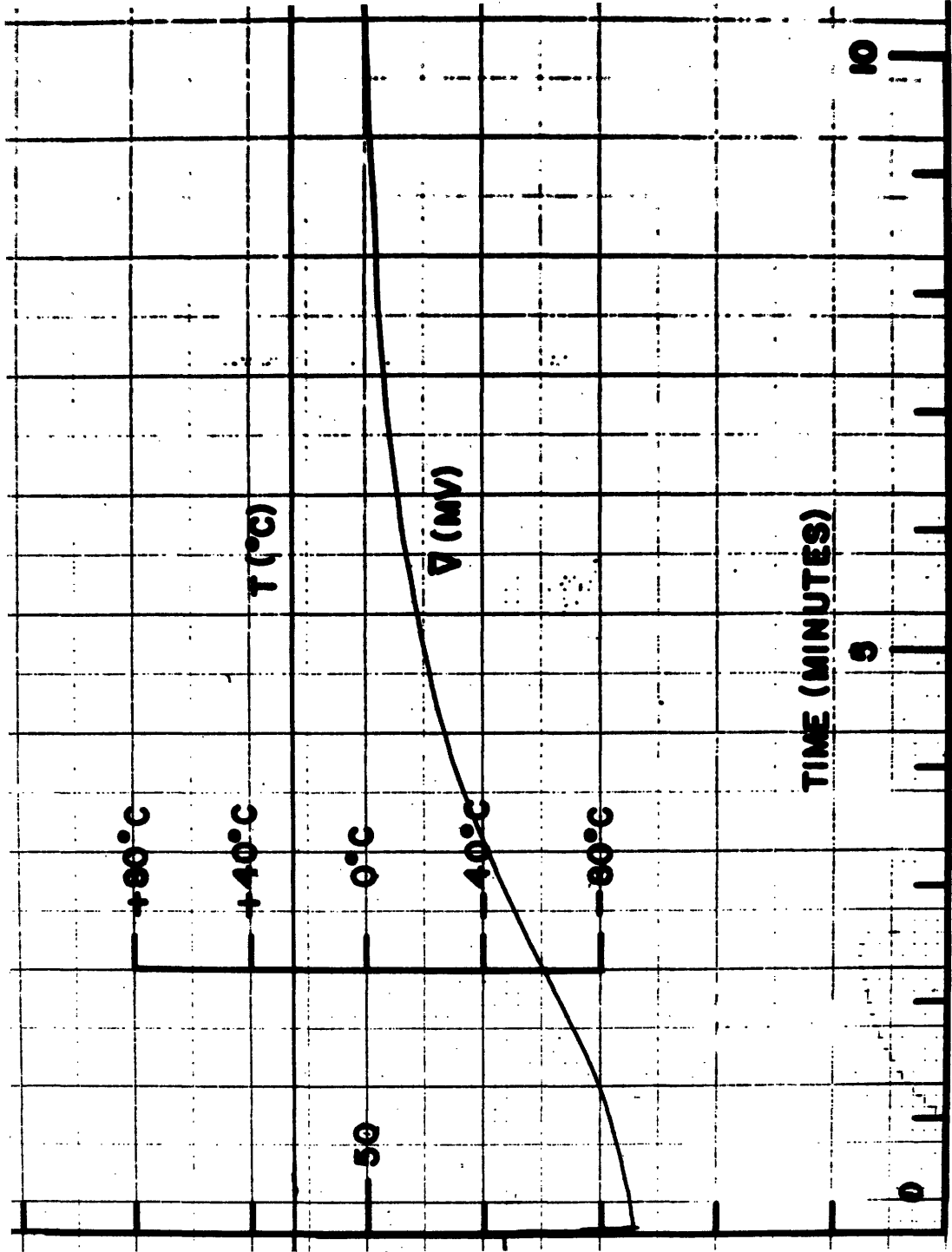


Figure 4.1 Strip Chart Recording for an Isothermal, Osmotic Perturbation at 27°C for

Erythrocytes in 2.94m NaCl.

the light intensity reaching the photocell increases with time. The reason for this is that as the cells are damaged they are no longer as effective in scattering the incident beam and more light is transmitted directly to the detector. As progressively more and more cells hemolyze, the signal continues to increase, and the result is as shown in the figure cited. One notices even in these raw data that the kinetics are a function of time, namely that the reaction proceeds in a relatively rapid manner at short times, followed by transition to a much slower rate. This tendency is found to be a general one as illustrated in Figure 4.2 which is the summary of osmotic perturbation data at 298°K. The curves shown represent the hemolysis histories for six different hypertonic exposure conditions and are plotted as $\log(\% \text{ hemolysis})$ as a function of $\log(\text{exposure time})$. Each number in parentheses to the left of the solid curves is the number of experimental tests run to determine the response corresponding to those particular conditions. The data to the right of the figure are from Soderstrom [50] for long exposure times (no kinetic data). Extrapolation from the present results by the dotted lines to the Soderstrom data indicates a very good correspondence between the two sets of data. Although the transition from a rapid rate to a slower one is less pronounced at concentrations of 2.45m and 2.94m, the average time dependence of hemolysis for exposure times less than or equal to one minute is $t^{0.97}$, whereas for times greater than three minutes the time dependence is as large as $t^{0.51}$ at 1.0m and as small as $t^{0.06}$ at 3.94m (see appendix G).

For the present, only simple freezing and thawing protocols will be considered; namely, only those situations are considered which result in the cell being exposed to any one concentration for one minute or less.

**HEMOLYSIS KINETICS AT 25°C
FOR VARIOUS EQUILIBRIUM NaCl CONCENTRATIONS**

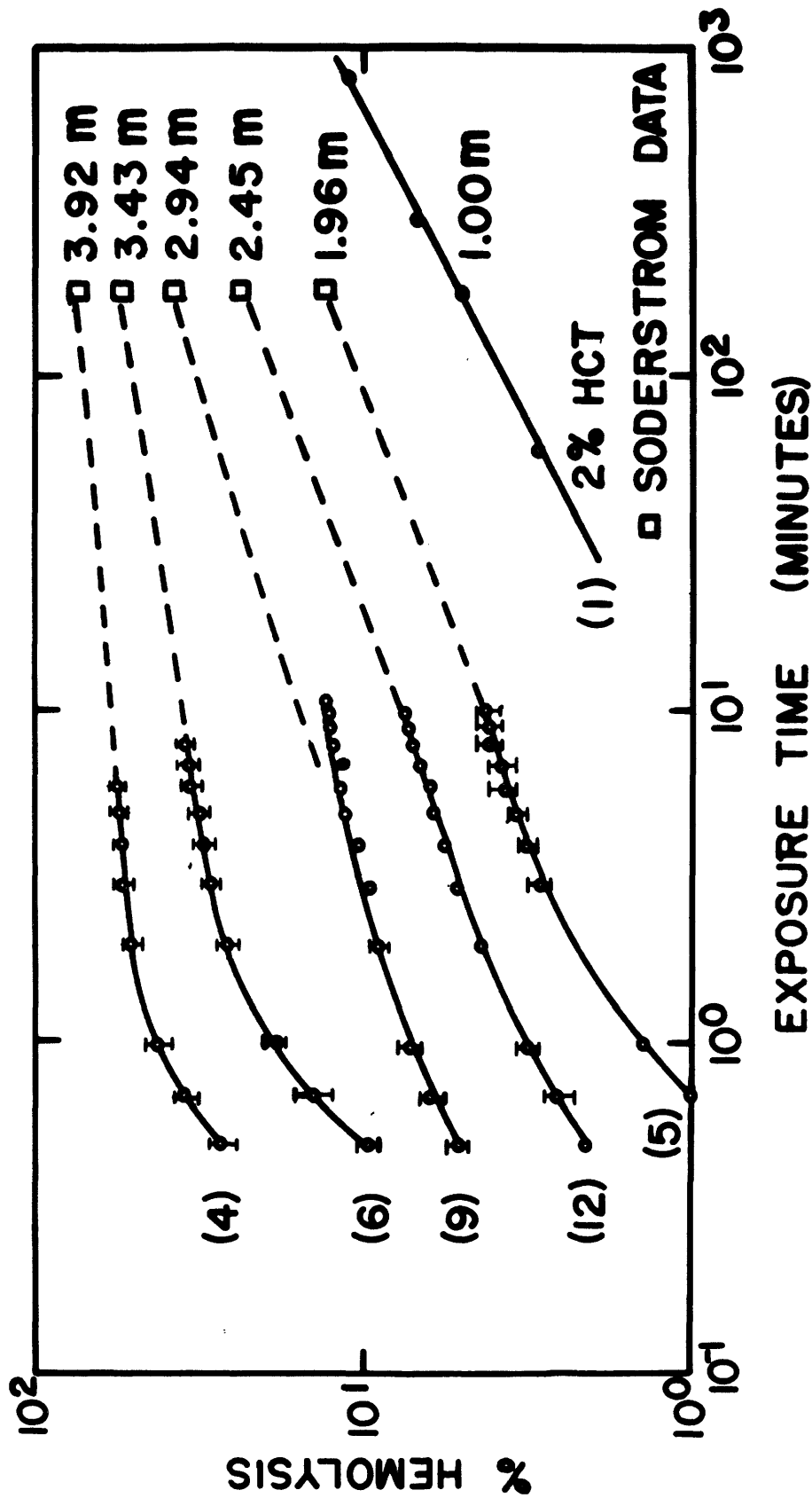


Figure 4.2 Hemolysis as a Function of Exposure Time for the Isothermal, Osmotic Perturbation Experiments at 298°K and Various Concentrations.

Working with only these short exposure time data helps considerably in simplifying the data and reducing it to a general form. Actually this restriction does not eliminate considering and simulating many of the cryopreservation protocols commonly encountered.

Focusing our attention on this type of short exposure time data and assuming for each case that the amount of hemolysis (%H) can be expressed as

$$(4.1) \quad \%H = a(\text{time})^b$$

where in the general case, a and b could be functions of temperature and concentration, all of the data were curve-fitted to the above form with an H-P 25 power curve-fit program. For a temperature of 298°K, the parameter b does not appear to be a function of concentration. The average value of b for the five concentrations was 0.97 and there is no discernable trend in the individual values scattered about this mean. The assumption is therefore made that during the initial stage of the hemolysis kinetics, the reaction is a linear function of time. As a result of this assumption, a simple expression is derived for the hemolysis reaction rate:

$$(4.2) \quad A = \frac{d(\%H)}{dt} = a$$

The values of a from the five curve-fits, in contrast to the b values, show marked dependence on the concentration. The hemolysis reaction rate (A) as a function of the molality of the sodium chloride solution is shown in Figure 4.3. These data are also curve-fitted to a power curve form and the result with a correlation coefficient $r = 0.99$

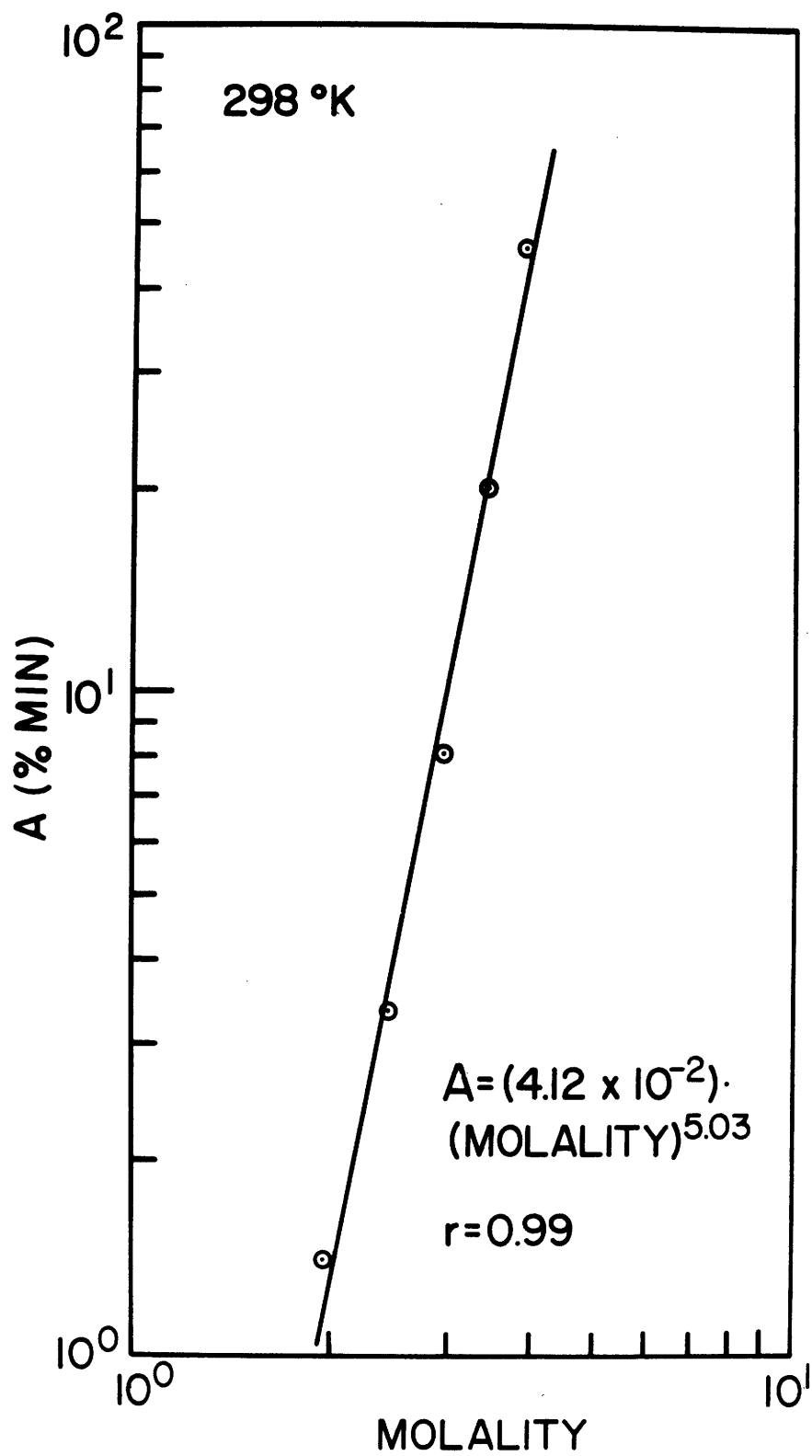


Figure 4.3 Hemolysis Rate A as a Function of Sodium Chloride Molality at 298°K and Exposure Times \leq 1.0 Minute.

is that the damage reaction rate is related to the solution molality by the fifth power. There is no a priori reason why the reaction rate data would be expressed best as a function of one measure of concentration rather than another. For this reason, alternate expressions for concentration were considered and the reaction rate data were replotted. Figure 4.4 suggests that an equally acceptable interpretation of the data ($r = 0.99$) is obtained when fitting the reaction rate as a function of the solution water activity. Incidentally, this water activity for the cell freezing situation would be both the intracellular value and the extracellular value since due to the large membrane water permeability for the red cell, rapid transmembrane equilibration occurs [44]. It is conceivable that when cells are frozen in solutions more complicated than the simple water-sodium chloride system chosen here, then a limited number of components of the solution (possibly just one) would be most responsible for damage. In such cases, following the kinetic behavior with respect to that component would yield the most information. A likely candidate for this component would be the salt present in the solution. Figure 4.4 predicts a substantial increase in the damage reaction rate when the solution water activity is reduced. This is true in the simple binary system because a reduction in the water activity is accompanied by an increase in salt activity. This figure would probably not be valid for the ternary system water-glycerol, sodium chloride. The addition of a glycerol and salt solution to a solution of water and salt (for equal salt concentrations in both solutions) would lower the water activity at a constant salt activity. If the reaction proceeded at the same rate as it did initially, then attention should be focused on the salt concentration and a curve fit like that of Figure 4.5 would be most useful. The correlation coefficient for this fit is as large as those for the other two fits, so for the

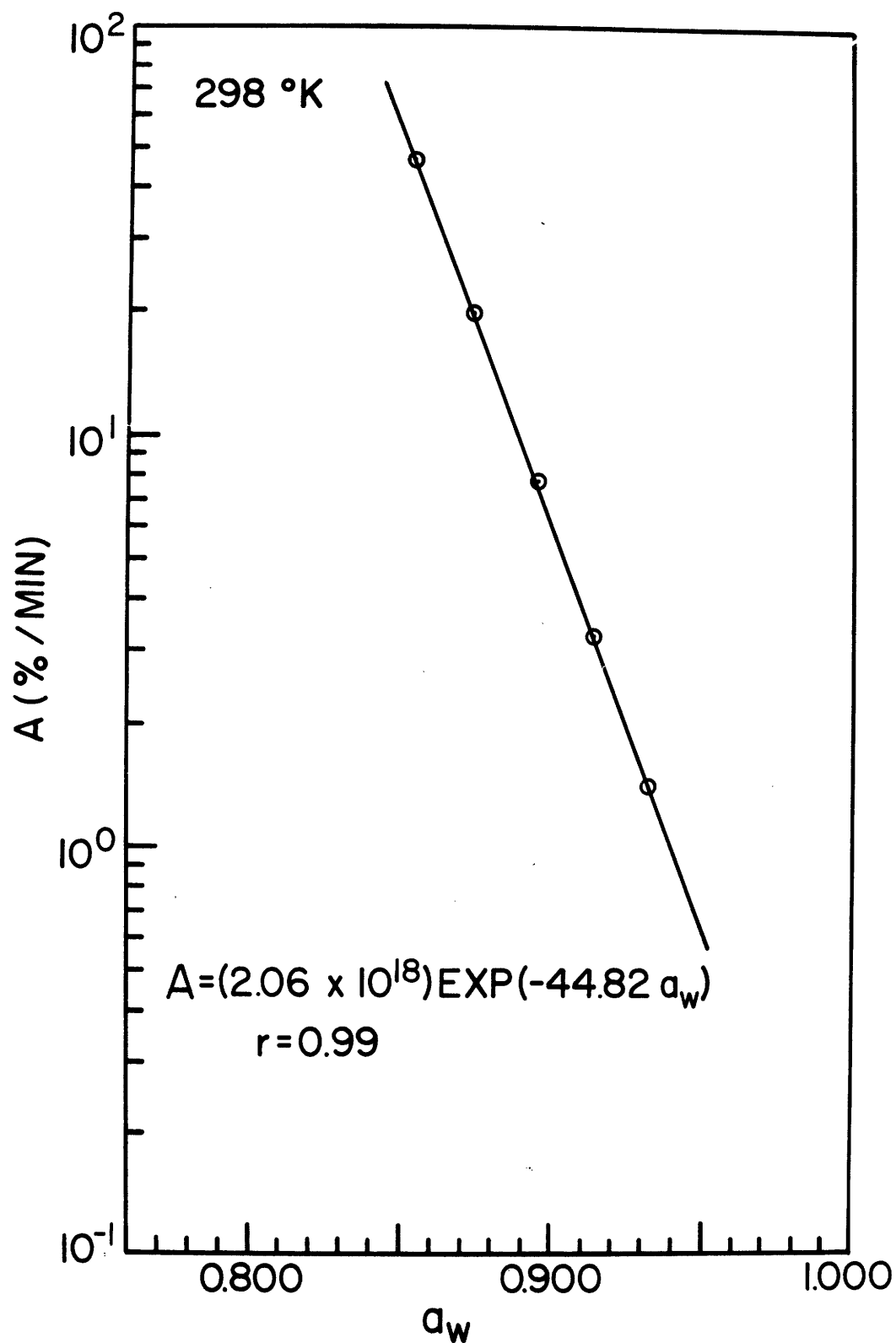


Figure 4.4 Hemolysis Rate A as a Function of Water Activity at 298°K and Exposure Times ≤ 1.0 Minute.

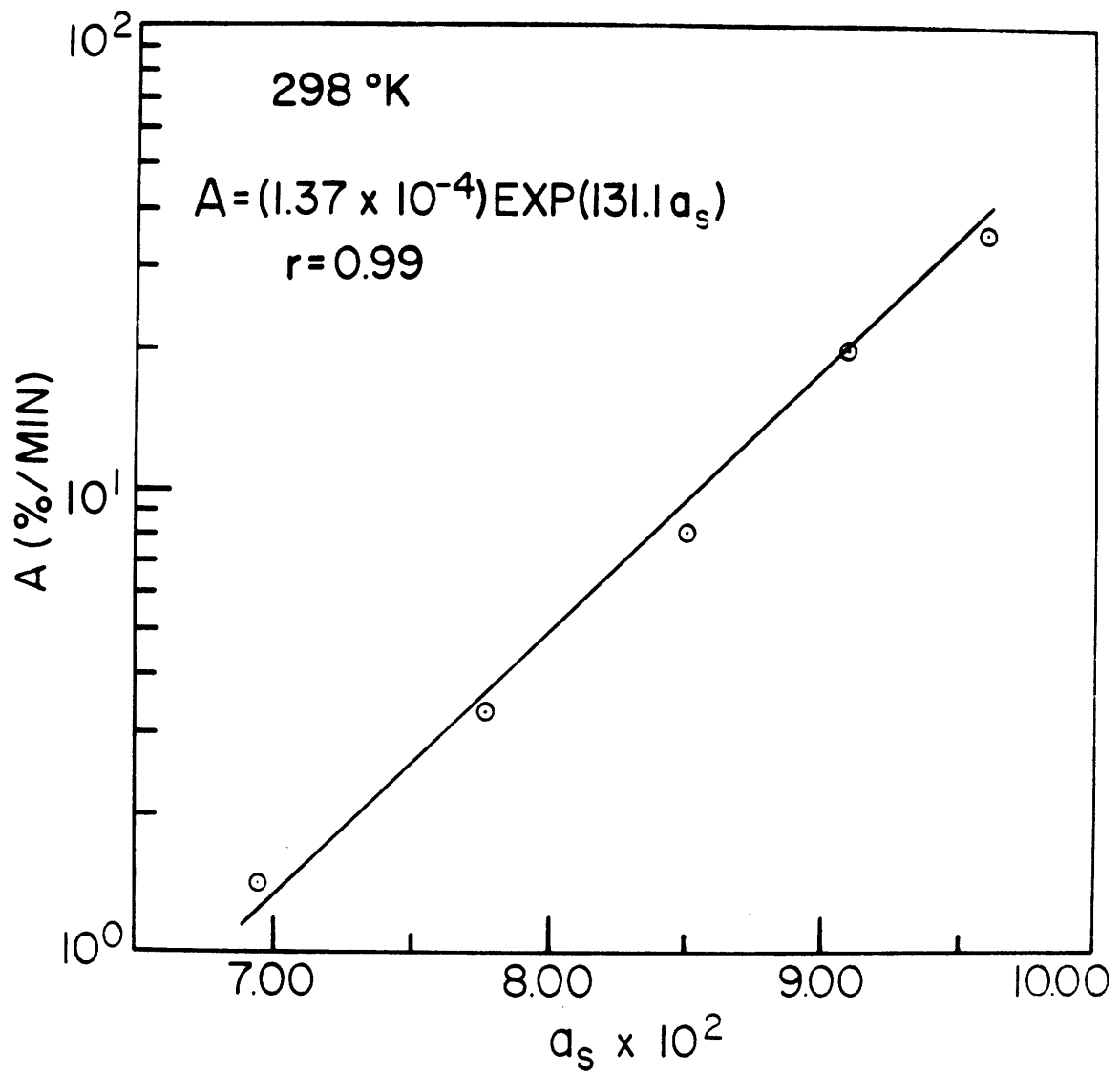


Figure 4.5 Hemolysis Rate A as a Function of Sodium Chloride Activity at 298°K and Exposure Times \leq 1.0 Minute.

binary system there is no preferential method of expressing concentration in terms of curve-fitting alone. The data are also nicely fit in one other form which is most interesting from the standpoint of thermodynamic modelling. This matter will not be fully discussed until a later chapter, but the form will be presented after the effects of temperature on the reaction rate are reviewed.

Red cells experiencing osmotic perturbation at 2.45m NaCl will have lower reaction rates if the isothermal temperature at which the reaction is proceeding is at a lower absolute level. Figure 4.6 is a summary of the results for the three temperatures 25°C, 10°C, and 0°C. For this temperature range, two effects are noticed. Firstly, the reduction in temperature causes the reaction to be slower for short exposure times even though the curves converge at longer times. Secondly, the transition from a fast reaction to a slower reaction which was apparent at the higher temperatures (298°K) is moved out to longer times (+10°C) and eventually disappears (0°C) within the exposure times investigated.

The composite effect of temperature and concentration on the reaction kinetics is seen in Figure 4.7. The same general trend is observed in both sets of concentration data. The difference is that at higher concentrations the data are displaced vertically, suggesting a more destructive condition. As before, with temperature changes there is lateral displacement of the time at which a transition is made between a rapid rate and a slower one. The fast portion of the damage kinetics at temperatures as high as 322°K would appear to be finished at quite short exposure times (30 seconds or less). Once again the data appear to converge at longer exposure times. It is apparent from these data

**HEMOLYSIS KINETICS AT A FIXED CONCENTRATION
WITH TEMPERATURE AS A VARIABLE**

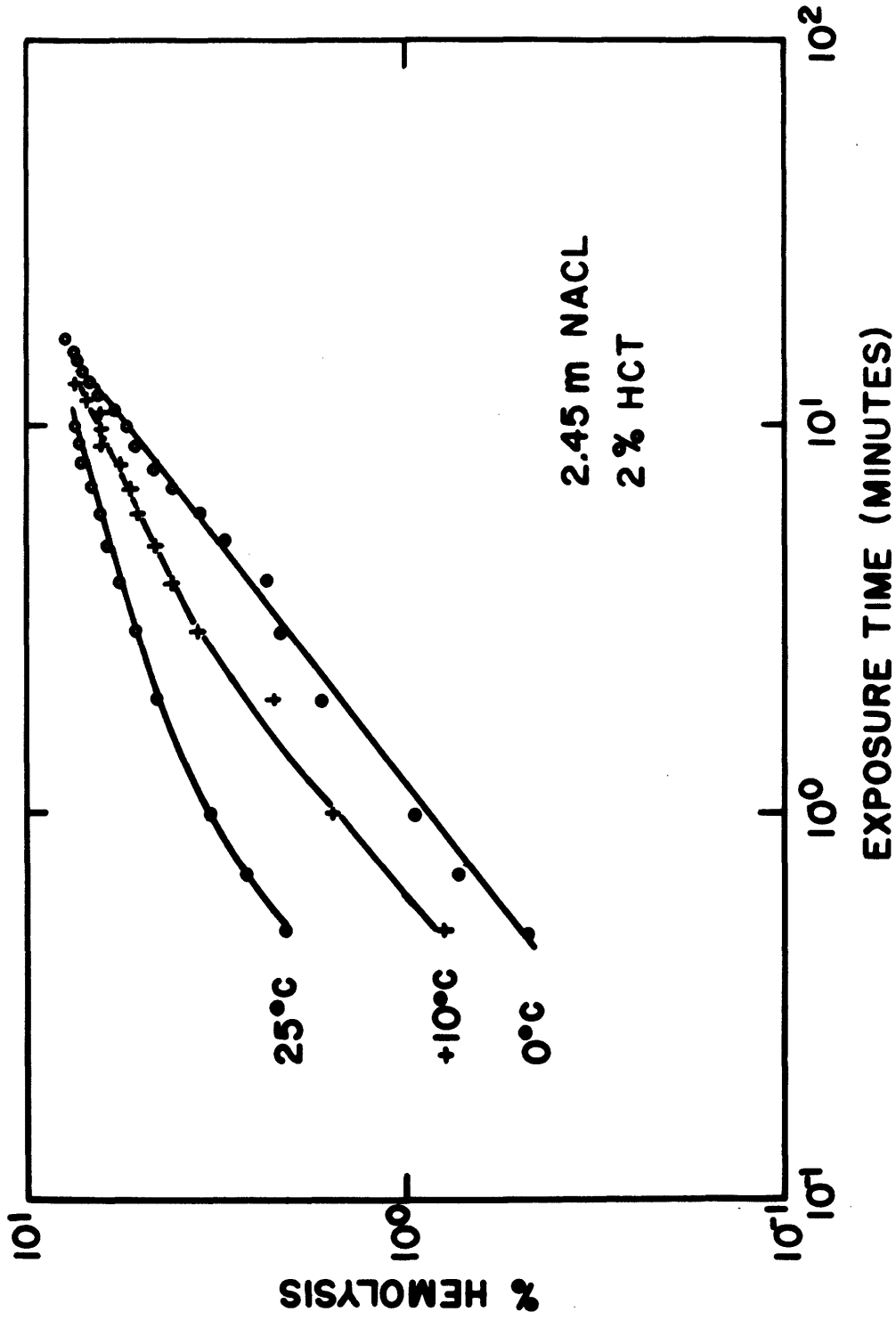


Figure 4.6 Hemolysis as a Function of Exposure Time at 2.45m NaCl for Isothermal, Osmotic Perturbation Experiments at 273°K, 283°K, and 298°K.

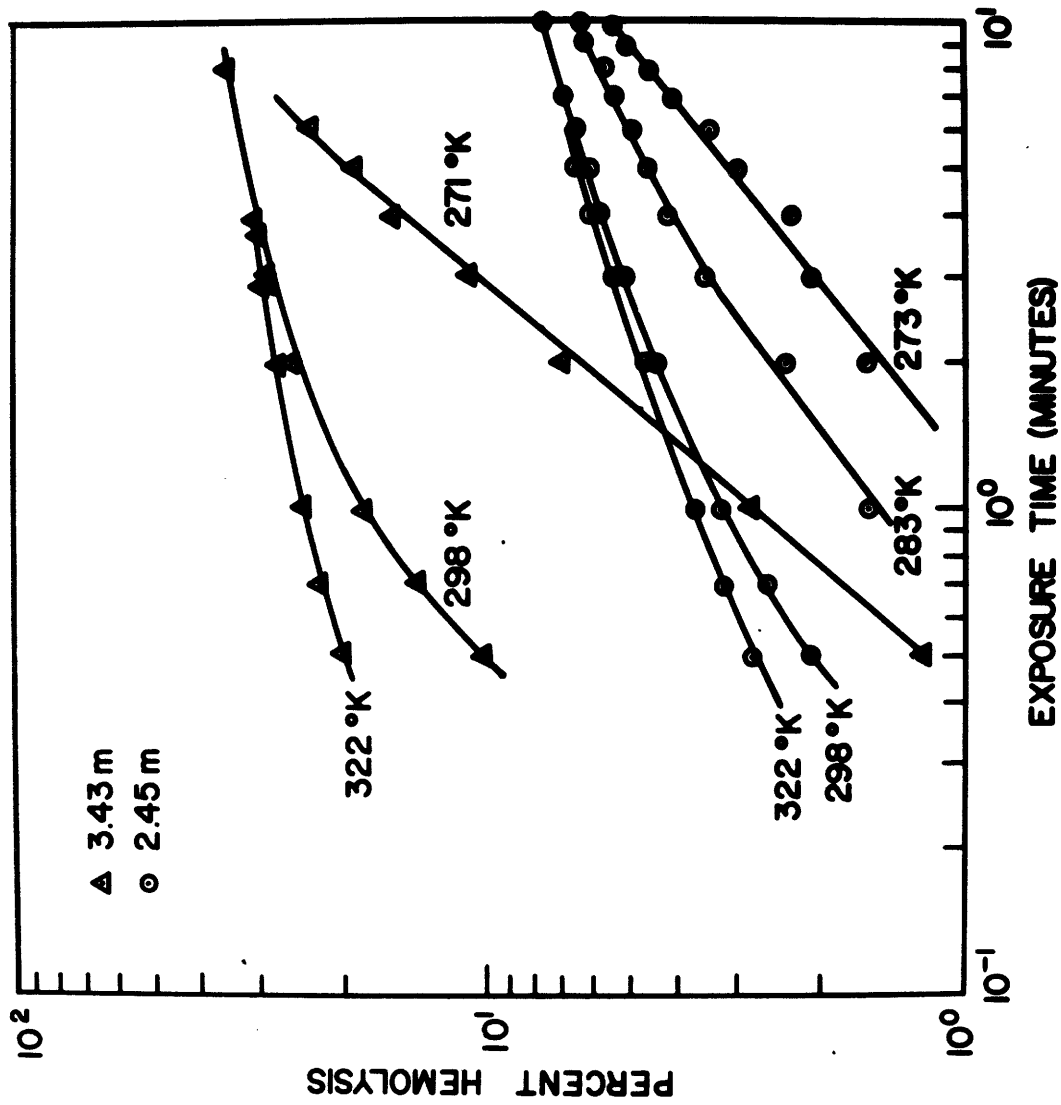


Figure 4.7 A Composite View of Hemolysis as a Function of Exposure Time Demonstrating the Effects of Sodium Chloride Concentration and Temperature.

that temperature reduction can reduce the damage kinetics. It is also obvious that a scheme involving temperature reduction and increased concentrations (analogous to the freezing situation) has some trade-offs. For example, red cells may be placed in the higher concentration (3.43m NaCl) and suffer less damage than those in a lower concentration (2.45m NaCl) if the temperatures of the respective solutions are 271°K and 298°K. However, this conclusion is only valid if the cells have been in the solutions for about 12 minutes or less. For storage times longer than this, the beneficial effect of the lower temperature is outweighed by the greater concentration and the cells in 3.43m NaCl continue to hemolyze at an appreciable rate.

An Arrhenius reaction rate temperature dependence is considered and the short exposure time reaction rates for the three temperatures shown in Figure 4.6 will be plotted. The ratio of the reaction rate at a given temperature A_T divided by the rate at 298°K, $A_{298^\circ K}$, is derived and plotted as a function of inverse absolute temperature in Figure 4.8. The apparent activation energy for the hemolysis process is 7.3Kcal/mole at a concentration of 2.45m. The implications of the magnitude of this energy will be discussed later when the thermodynamic model is developed. If one extrapolated these data to lower temperatures, the conclusion would be that the reaction rate can be very much depressed with further temperature reduction. Unfortunately this is not the case.

The osmotic perturbation induced hemolysis of red cells at a concentration level of 2.94m NaCl proceeds at the same rate whether the reaction occurs at 271°K or 262°K. The data from these two experiments with standard error bars are shown in Figure 4.9. Although unexpected,

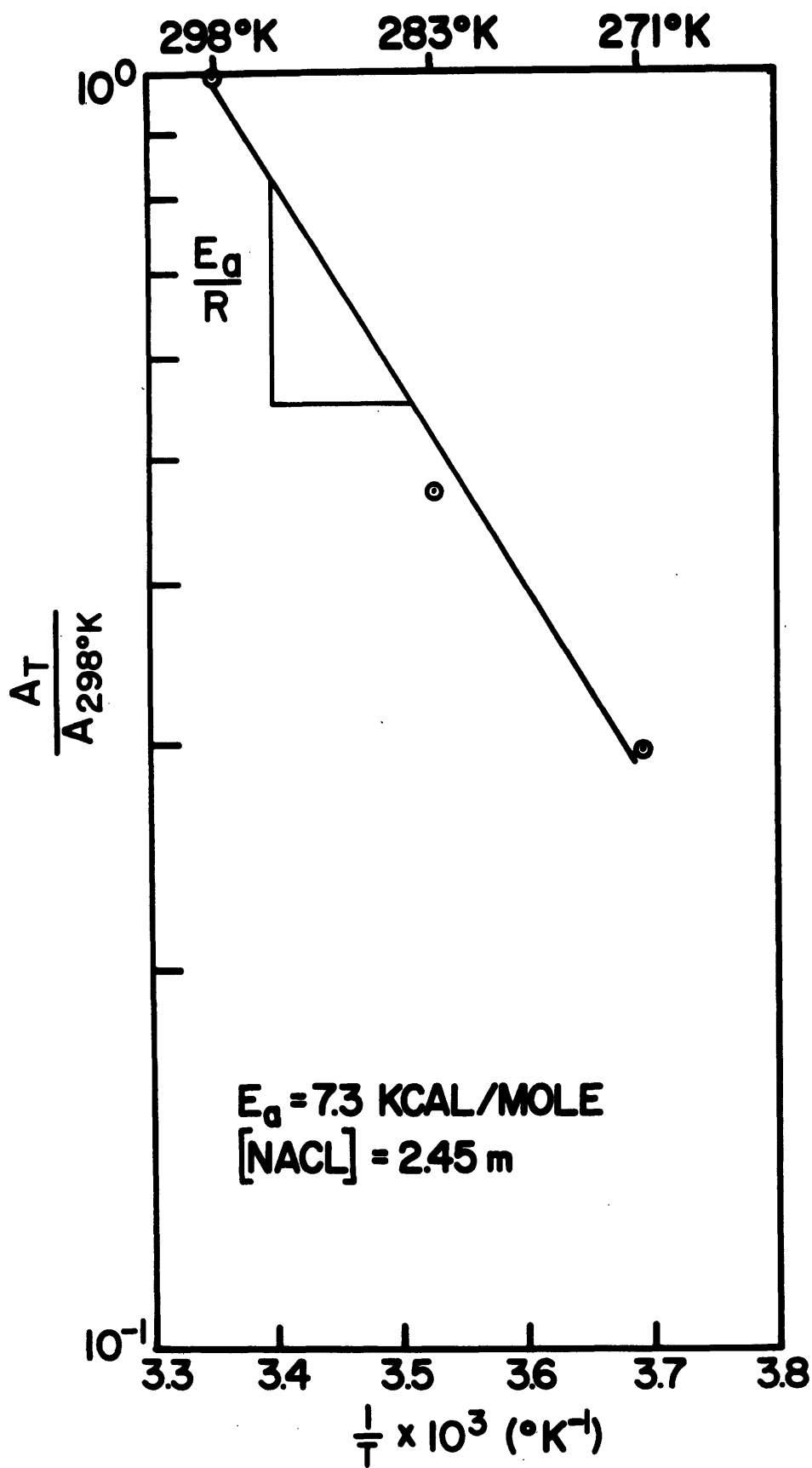


Figure 4.8 The Effect of the Isothermal Temperature Set Point on the Hemolysis Rate at 2.45m NaCl.

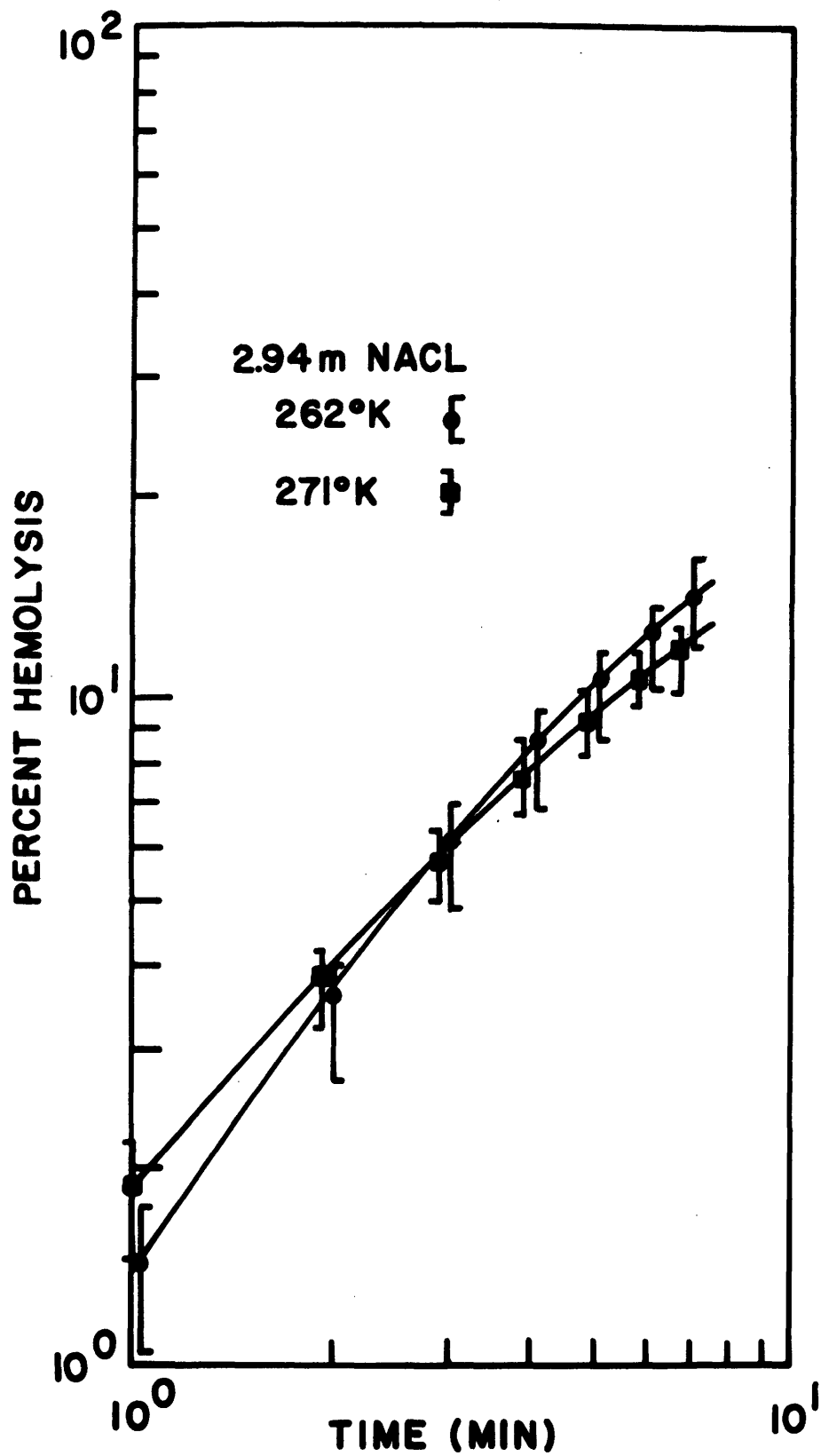


Figure 4.9 Collapse of the Hemolysis Rate to a Single Value for a Change in the Isothermal Set Point Temperature from 271°K to 262°K at 2.94m NaCl.

this effect is not unique to this system. Lovelock observed that cells in concentrations ranging from 1.0M to 4.0M NaCl were insensitive to differences in storage temperatures for five minute exposure times when temperatures between 0°C and -12°C were chosen [27] (Figure 4.10).

Table 4.1 contains the reduced form of all of the experimental data taken for the hypertonic osmotic perturbation mode for hemolysis production. The reaction rate data are given in terms of a and b as defined by equation 4.1. The number N is the number of experimental runs done to define the average values of a and b. The square of the correlation coefficient r^2 is given as well as the time range (in minutes) where the curve-fit defining a and b is valid. The information is cross-tabulated for temperature and concentration. Since the kinetic data were not found to be particularly well suited to curve fitting by any one concentration scale, four quantities at each concentration are given as a matter of convenient reference.

The form of the hypertonic kinetic data most useful for the thermodynamic modelling is obtained by graphing $\log_e A$ as a function of $-\log_e a_w$ (Figure 4.11). Curve-fitting yields the expression:

$$(4.3) \quad A = (9.078 \times 10^{-2}) \text{ EXP } (-39.98 \log_e a_w)$$

at 298°K and the expression:

$$(4.4) \quad A = (9.115 \times 10^{-2}) \text{ EXP } (-26.70 \log_e a_w)$$

at the low temperatures.

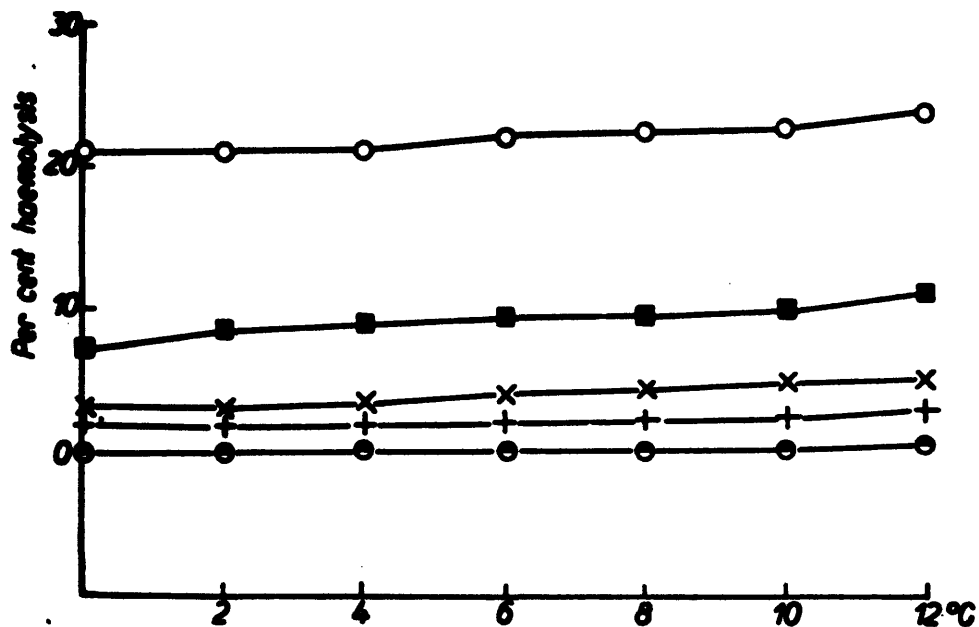


Fig. 6. The haemolysis which occurs when red blood-cells are suspended for 5 minutes in NaCl solutions of various strengths at different sub-zero temperatures. NaCl concentrations:
 ○ — 4 M; ■ — 3 M; × — 2 M;
 + — 1 M; ● — 0.15 M.

Figure 4.10 Non-Variant Hemolysis Percentages for 5-Minute Storage at Various Sub-zero Temperatures (reproduced from reference [27]).

TEMPERATURE (°K)

		262	271	273	283	298	322	
CONCENTRATION	$a_w = 0.854$ molality = 3.94m $\ln a_w = -1.578 \times 10^{-1}$ $x_s = 0.1237$	N=3 $a=6.21$ $b=0.97$ $r^2=0.99$ 0.5 to 3.0	N=5 $a=6.63$ $b=1.22$ $r^2=0.99$ 0.5 to 8.0			N=4 $a=45.75$ $b=0.90$ $r^2=0.97$ 0.3 to 1.0		
	$a_w = 0.875$ molality = 3.43m $\ln a_w = -1.335 \times 10^{-1}$ $x_s = 0.1099$		N=7 $a=2.85$ $b=1.20$ $r^2=0.99$ 0.6 to 6.0				N=6 $a=20.00$ $b=1.19$ $r^2=0.98$ 0.3 to 1.0	N=7 $a=22.81$ $b=0.27$ $r^2=0.96$ 0.3 to 2.0
	$a_w = 0.896$ molality = 2.94m $\ln a_w = -1.098 \times 10^{-1}$ $x_s = 0.0957$	N=9 $a=1.59$ $b=1.11$ $r^2=0.99$ 0.5 to 11.0	N=6 $a=1.96$ $b=0.96$ $r^2=0.99$ 1.0 to 6.0				N=9 $a=8.04$ $b=0.81$ $r^2=0.93$ 0.3 to 1.0	
	$a_w = 0.914$ molality = 2.45m $\ln a_w = 8.992 \times 10^{-2}$ $x_s = 0.0811$			N=5 $a=0.91$ $b=0.81$ $r^2=0.99$ 0.5 to 3.0	N=5 $a=1.47$ $b=0.80$ $r^2=0.99$ 0.5 to 4.0	N=12 $a=3.35$ $b=0.81$ $r^2=0.97$ 0.3 to 1.0	N=3 $a=3.55$ $b=0.40$ $r^2=0.99$ 0.3 to 5.0	
	$a_w = 0.932$ molality = 1.96m $\ln a_w = 7.042 \times 10^{-2}$ $x_s = 0.0659$		N=4 $a=0.82$ $b=0.80$ $r^2=0.99$ 0.5 to 7.0	N=3 $a=0.47$ $b=0.81$ $r^2=0.98$ 1.0 to 10.0			N=5 $a=1.403$ $b=1.16$ $r^2=0.99$ 0.3 to 1.0	

$b=0.97$ for 14 data points not including 322°K data

Table 4.1 Master Chart of Hemolysis Rate. Curve-fit Parameters for all of the Isothermal, Osmotic Perturbation Experiments Cross-Tabulated for Temperature and Concentration.

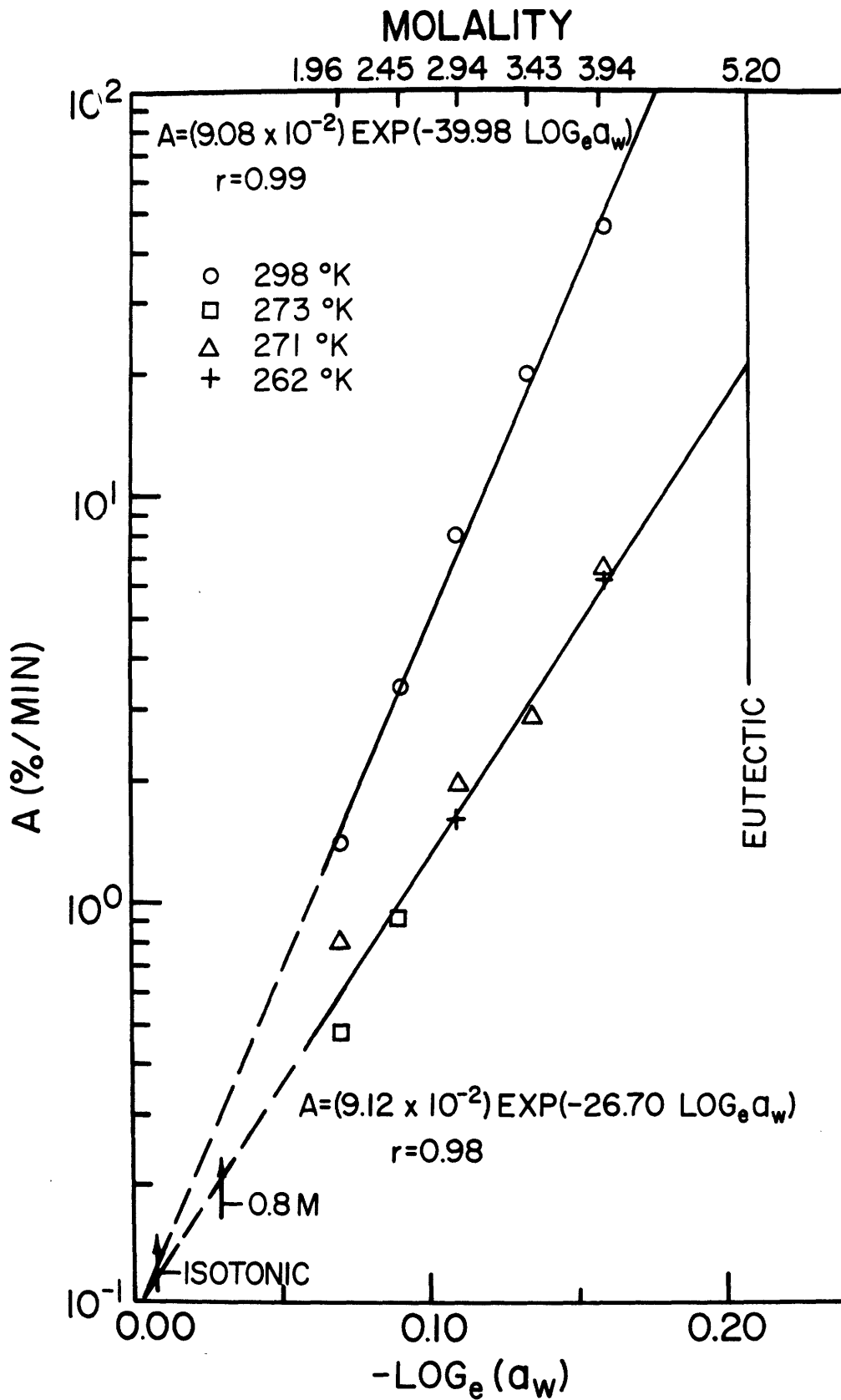


Figure 4.11 Hemolysis Rate A as a Function of $-\text{Log}_e(a_w)$ at High Temperature (298°K) and Low Temperature (273°K, 271°K, 262°K).

This representation contains all of the kinetic information given in Table 4.1 and shows the interactive nature of the temperature and concentration on the hemolysis kinetics. Three reference concentration levels have been superimposed on the figure: isotonic and the eutectic in addition to the 0.8M concentration where Lovelock first observed freezing damage [24]. The molality scale is given at the top of the graph for quick transformation from the $-\log_{e_w} a_w$ abscissa scale. It is clear from this plot that the low temperature kinetic data group together and that as a result nothing beneficial is gained by lowering the temperature from 273°K to 262°K. The red cells are more sensitive to temperature changes at the higher concentrations as revealed by the divergence of the two straight lines. The red cells are insensitive to temperature at isotonic conditions if the extrapolations made are valid (see Figure 4.11).

Hemolysis Induced by Iso-osmotic, Thermal Perturbation

In this section the so-called "thermal shock" mode of producing hemolysis is considered. Thermal shock or, what in this thesis is being termed iso-osmotic thermal perturbation, is one of the means by which hemolysis can be produced in red cells. This phenomenon occurs when red cells are rendered susceptible to temperature drops by a preliminary exposure to a hypertonic medium.

The data of Lovelock [27,34], Morris et.al. [30], and Daw et.al. [32] clearly demonstrate the complex nature of the thermally induced damage phenomenon. The amount of hemolysis produced in a sample of red

cells in a saline solution is a function of: the concentration of the solution, the initial temperature before cooling is begun, the exposure time to the hypertonic solution before the solution is cooled, the magnitude of the temperature drop, and the cooling rate used. To familiarize the reader with these effects, examples of each will be taken from the literature and discussed briefly.

The effect of the exposure time to the hypertonic solution prior to dropping the temperature is shown in Figure 4.12 which is reproduced from the work of Morris et.al. [30]. The plot is for the cell population recovery percentage as a function of the logarithm of the exposure time prior to the temperature drop (in minutes). The three sets of data shown are for different concentrations of sodium chloride (1.0m (o), 1.2m (●), and 1.5m (◻)). In each case the cells were exposed to the hypertonic solution at +25°C, and then after the chosen exposure time had elapsed, the cells were cooled from +25°C to 0°C at 75°C/min. Hemolysis measurements on these washed cells were made immediately after reaching 0°C. These data show that very short exposure times to the hypertonic solutions before cooling do not produce much damage. For times between 0.1 and 5.0 minutes, recovery decreases with increased exposure time and increases for times between 5.0 minutes and 60 minutes. The cell population response appears to differ in magnitude but not in the characteristic shape of the recovery versus time curve for the different concentrations. For example, maximal damage occurs at 5 minute exposure times for all three concentrations. The dependence of recovery on concentration is not explicit in this graph; however, it is apparent that increasing the tonicity of the salt increases damage.

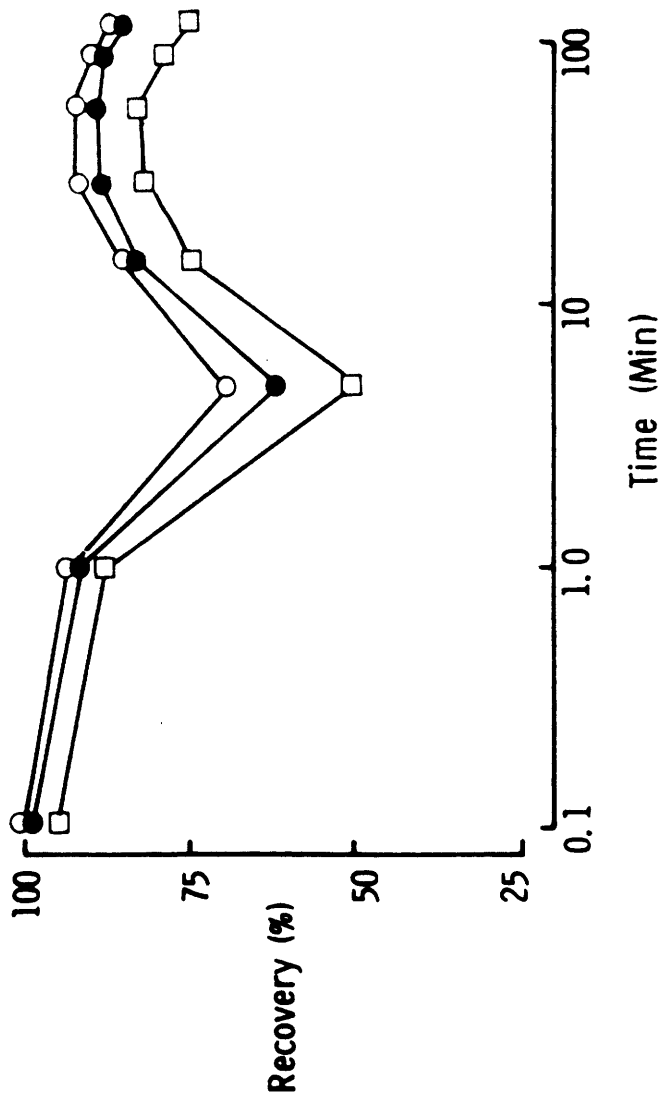


Figure 4.12 Percent Erythrocyte Recovery for Thermal Shock Experiments as a Function of Hypertonic Exposure Time Prior to the Temperature Drop (reproduced from reference [30]).

If the concentration of the solution, the exposure time, as well as the cooling rate are fixed, then the amount of hemolysis produced can be altered by changing the exposure temperature and the magnitude of the temperature drop. Lovelock studied this effect and the results are depicted in Figure 4.13 [27]. These data are for washed cells exposed to 1.0M NaCl for 5 minutes. In general, less hemolysis is produced for any given temperature drop (ΔT) if higher initial temperatures are chosen. It also appears that as the initial temperature is increased, quite a large drop is necessary before any significant hemolysis is produced.

The cooling rate also affects the recovery percentage with the faster rates producing more damage. Figure 4.14, reproduced from the work of Morris et.al. [30] shows this dependence for washed red cells cooled from +25°C to 0°C after a 5 minute exposure at +25°C to one of the three concentrations (1.0m (o), 1.2m (●), 1.5m (□)). Substantially different recoveries can be realized by varying the cooling rate, especially at the higher concentrations, but a change in the cooling rate of two to three orders of magnitude is necessary to accomplish this.

The apparatus developed in the present work was used to duplicate a set of thermal shock conditions chosen from the literature as a demonstration of the capability of this device for producing thermal perturbation data that is in agreement with literature data. Figure 4.14 predicts that approximately 17% of a red cell population would be hemolyzed if the cells were exposed to a solution of 1.0m NaCl for five minutes at +25°C before cooling at 9°C/min to 0°C.

Packed red cells were injected into the test chamber of the apparatus

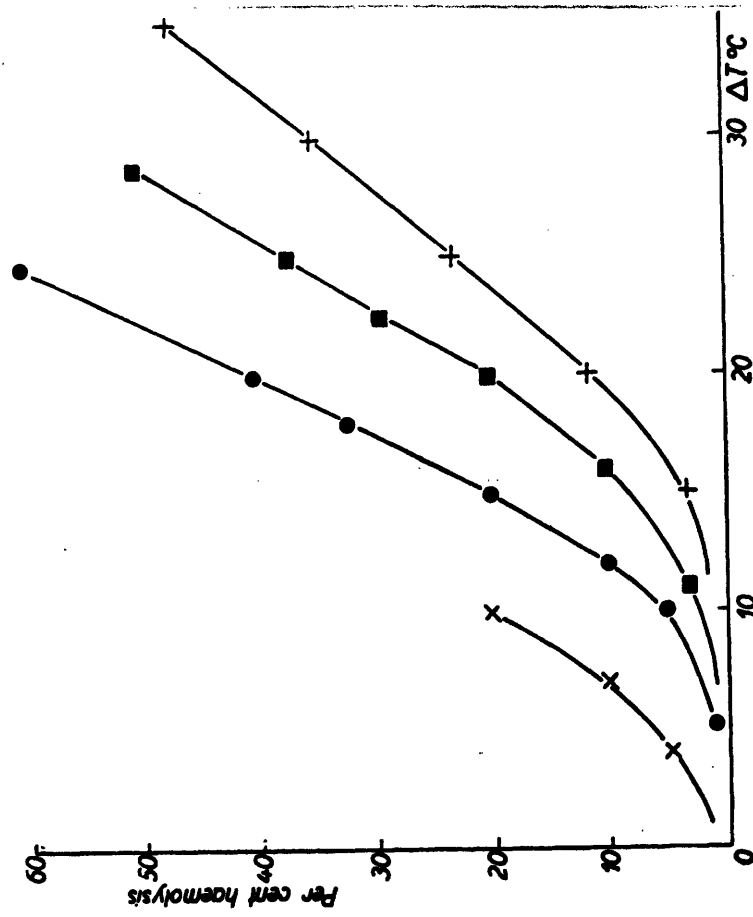


Fig. 8. The haemolysis which occurs when red blood-cells suspended in 1.0 M NaCl are suddenly cooled through various temperature intervals (ΔT), and from different initial temperatures.

Initial temperature:

- 0° X — X ;
- +20° ● — ● ;
- +30° ■ — ■ ;
- +45° + — + .

Figure 4.13 Percent Hemolysis for Thermal Shock Experiments Demonstrating the Effects of Initial Hypertonic Exposure Temperature and Magnitude of the Temperature Drop (reproduced from reference [27]).

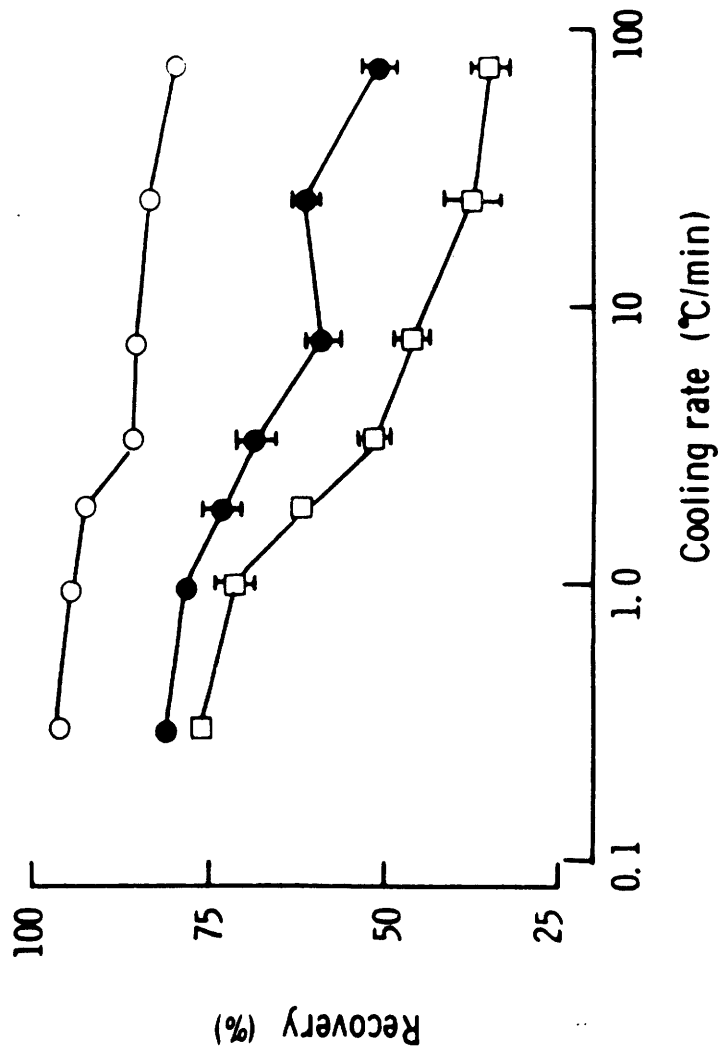


Figure 4.14 Percent Erythrocyte Recovery for Thermal Shock Experiments Demonstrating the Effect of Cooling Rate (reproduced from reference [30]).

at ambient temperature (27°C) and five minutes exposure time elapsed before initiating a cooling of the chamber. The cooling rate was 9°K/min to the minimum temperature of 0°C. Figure 4.15 shows the raw strip chart recorder data for a run of this type. The upper trace is for the temperature of the chamber and the lower one is the amplified voltage of the photocell. The photocell output clearly shows the initial artifact discussed in the operational characteristics section of Chapter 2, and also shows why it is not important. After the 14 second transient, the photocell steady state output is reached. For cells in 1.0m NaCl at 300°K, Figure 4.2 allows one to estimate damage at less than 2% for a five minute exposure. This is the reason the photocell output remains constant while the temperature is at 27°C. By the time a temperature of 0°C is reached, after cooling at 9°K/min, the photocell is obviously responding to the hemolysis taking place within the chamber. The calibration curve was used to reduce these data to percent hemolysis as a function of time, and the data averaged for five experiments are graphed in Figure 4.16.

The horizontal line on the graph is the 17% value of hemolysis found by Morris et.al. for these experimental conditions. The correspondence appears to be very good, for after eight minutes had elapsed once cooling was initiated the hemolysis percentage asymptotically approached the 17% level. The exact time when the Morris et.al. data was taken, relative to the initiation of cooling, is not specified in their procedure. Although the thermally shocked solutions were sampled immediately after reaching 0°C, the procedure used to measure hemolysis involves centrifugation, conversion of a sample supernatant volume of hemoglobin to cyanmethemoglobin by mixing with

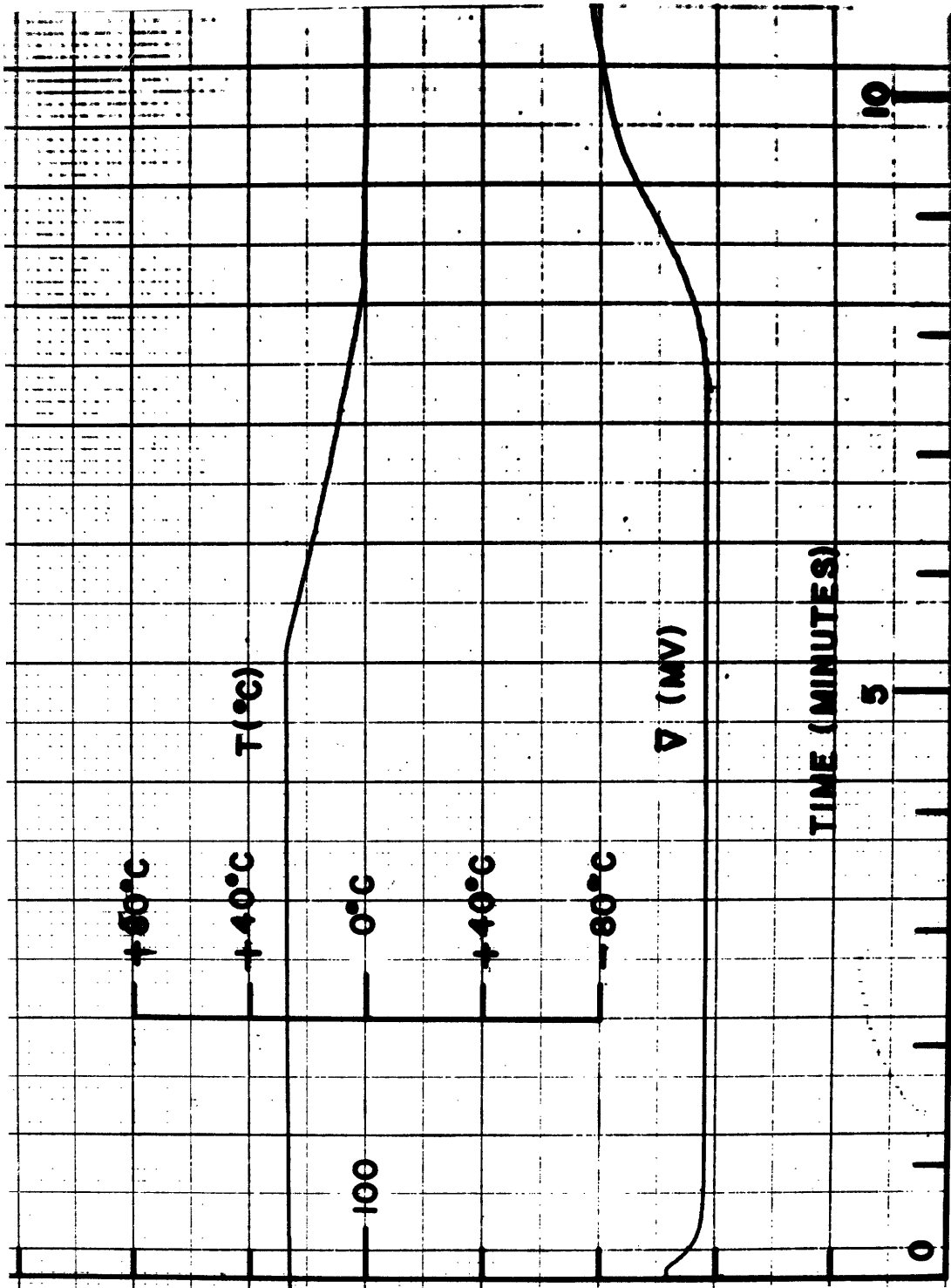


Figure 4.15 Strip Chart Recording of a Thermal Shock Experiment for Erythrocytes

Exposed to 1.0m NaCl for 5 minutes at 300°K Prior to Cooling at 9°K/min to 273°K.

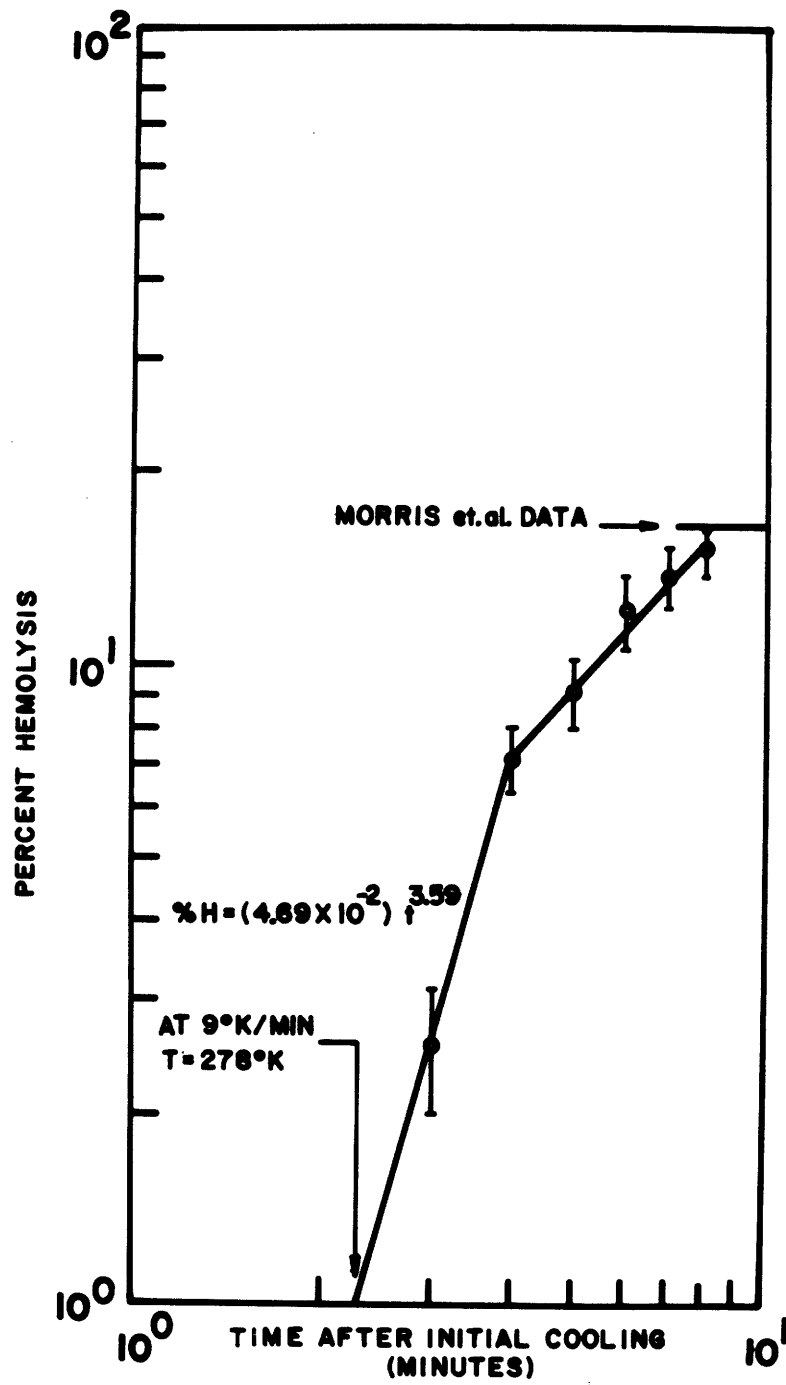


Figure 4.16 Hemolysis as a Function of Time After Initiating Cooling for Erythrocytes Exposed to 1.0m NaCl for 5 Minutes Prior to Cooling at 9°K/min From 300°K to 273°K.

Drabkin's reagent, and absorption measurements on a spectrophotometer [30]. This entire process is likely to take at least several minutes and probably more like five to ten minutes. In accounting for the cooling time from +25°C to 0°C at 9°C/min, which is 2.8 minutes, an estimate of the total elapsed time is between 5 and 13 minutes. If it is assumed that the quasi-steady state or asymptotic hemolysis value was the one measured by Morris et.al. (i.e., assuming that the 13 minute time is a more accurate estimate than 5 minutes), then a very reasonable agreement is attained.

To model a dynamic process such as freezing, the hemolysis kinetics are essential and the "asymptotic" values of thermal shock just discussed are less useful in comparison although they do indicate the relative effects to be expected from changing the various parameters such as ΔT , the cooling rate, etc. Therefore the new apparatus has added a dimension to the study of thermal shock experiments since kinetic data are accessible for the process and one is no longer limited to measurement of the quasi-steady state amount of hemolysis produced after the temperature drop has occurred.

Some interesting aspects of the thermal shock process are revealed as a result of this ability to access short-time data. For one thing, as the raw data in Figure 4.15 suggest, hemolysis does not occur for these experimental conditions until over two minutes have passed after cooling begins. Visual resolution of 1/2 of one small vertical division on the strip chart corresponds to a theoretical resolution of approximately 1% hemolysis at these photocell voltages (see appendix H). This sort of delay associated with exceeding the 1% hemolysis level was not apparent

in the isothermal, osmotically induced damage mode. Once hemolysis is evident for the thermal shock mode, the reaction rate is a much stronger function of time than it is for the case of the isothermal, osmotically perturbed damage. Using the three minute and four minute data points of Figure 4.16a curve-fit of the mean hemolysis values versus time gives the relation

$$(4.5) \quad \% \text{ Hemolysis} = (4.69 \times 10^{-2})t^{3.59}$$

whereas the osmotic perturbation mode was linear.

In conclusion, the kinetic data obtained for this mode of damage appear to be of a different form than those obtained for the isothermal, osmotically induced damage. There is, at present, no explanation for why the kinetic data should be different for the uncoupled perturbation modes presented in this chapter. Furthermore there is no known methodology by which to re-couple these two kinetic behaviors into a general kinetic interpretation that could be used for freeze-thaw simulations on the computer. Therefore, rather than pursuing an extensive experimental study of the thermal shock kinetics at this time, an effort has been made to model the general hemolysis process thermodynamically. The model developed provides a means by which to re-couple the two modes of damage and serves as a basis for understanding existing kinetics of both types. The model can also serve as a guideline for future experimental work particularly on thermal shock kinetics where so many parameters are known to be involved in determining the total amount of damage produced.

Chapter 5

A Thermodynamic and Kinetic Model for a Membrane Dissolution Theory of Hemolysis

In this chapter the hypothesis that hemolysis occurs by partial membrane dissolution is presented and a thermodynamic and kinetic model of this process is developed. The theory that hemolysis is a result of membrane dissolution is supported by the observations of Lovelock and Morris; thus their evidence is used as a starting point for the construction of a thermodynamic and kinetic model of the hemolytic process. The data of Lovelock and Morris suggest that mass transport of vital membrane components away from the membrane can proceed to the point that the membrane becomes increasingly permeable to intracellular molecules, even large molecules such as hemoglobin, thereby providing the means for hemolysis.

Evidence for Membrane Dissolution Theory of Hemolysis

Lovelock studied the relative stability of red cells with respect to several forms of stress, including exposure to concentrated salt, thermal shock, neutral absorbent, thermal gradients, etc. [27,34,52]. The quotes given below summarizing some of his conclusions are especially relevant to the problem of interpreting the kinetic data presented in the previous chapter. For example, he concludes: "The exposure to concentrated salt solutions causes first an increase in permeability of the cell membrane and finally complete dissolution of the cell. This appears to be due to the dispersion of lipids and lipoprotein from the cell membrane under the influence of the solvent action of concentrated salts." [34] The results of his studies also "... suggest that the dissolution takes place in two steps. First there is a rapid loss of superficial or surplus material which is not

immediately harmful. Thereafter the rate of loss of membrane components is closely proportional to the rate of hemolysis. This suggests that any further loss of material from individual cells leads to their rapid and complete destruction." [53] One way to remove membrane components is to repeatedly wash the cells in fresh normal saline. Lovelock found that after washing the red cells in normal saline five times, the concentration of lipids in the suspending medium was normally: cholesterol 22 μ gm/ml, phospholipid 20 μ gm/ml, lipoprotein 18 μ gm/ml. Regarding the transient nature of this process, he found "... that lipids and lipoprotein rapidly diffuse from red blood-cells suspended in fresh 0.16M sodium chloride. After about 3 minutes, an equilibrium level of these components is reached and the loss from the cell falls to a low value. The equilibrium concentration of lipids and of lipoprotein in the suspending medium did not appear to represent a simple saturation of the medium with these substances." [53] If these levels represent concentrations which are in chemical potential equilibrium with each respective component in the cell membrane, then each time the cells are washed and placed in fresh saline, additional membrane components must diffuse away to restore equilibrium concentrations of these species in the medium. This effect does occur as Lovelock's results shown in Figure 5.1 demonstrate. The percentage loss plotted for each component is based on the percentage of the composition of the test cells before treatment. The species considered are lipoprotein (+), volume (■), cholesterol (●), phospholipid (x), and hemoglobin (o). It is apparent that as washing is continued, more material is lost, although most of this loss is seen in the first few washes. This response would be expected from Lovelock's contention that

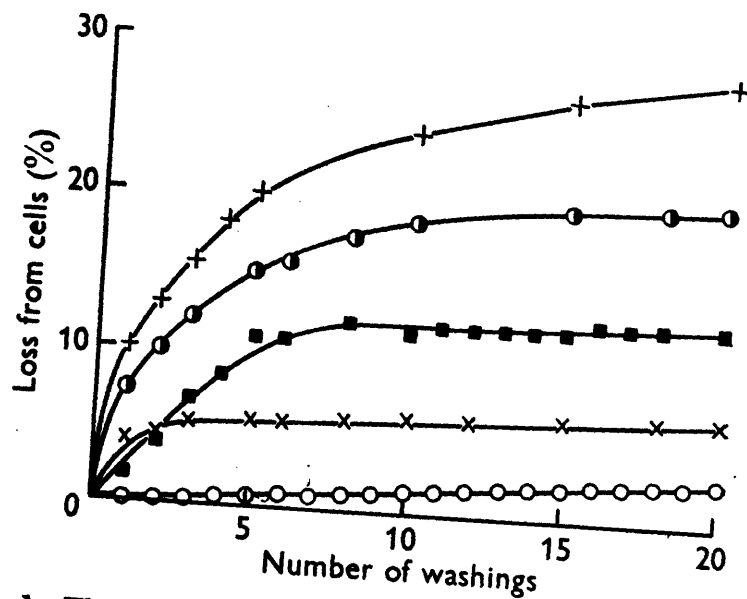


Fig. 1. The removal of components from the red cell by repeated washing. The cells were suspended in 0.16M-NaCl for 10 min. at 37°, separated by centrifuging and resuspended in fresh 0.16M-NaCl. This was repeated 20 times. +, Lipoprotein; ■, volume; ●, cholesterol; x, phospholipid; ○, haemoglobin.

Figure 5.1 Removal of Cell Membrane Components by Repeated Washings in Normal Saline (reproduced from reference [53]).

there is a superficial layer of membrane material that can be lost before appreciable hemolysis occurs. As an aside, it should be mentioned that for all experimental work done in this thesis, the red cells were washed three times prior to use. That there is such a superficial layer may be appreciated by referring to Figure 5.2 which is a scanning electron micrograph of an unwashed red cell. The so-called "shaggy-coat" is obvious at this 8000X magnification taken by Dr. T. Kuwabara, but much of it disappears with washing [54]. Technically, this coat as pictured in this figure may contain a significant amount of plasma protein in addition to the components specified by Lovelock, but the micrograph serves the purpose of visualizing a layer of material that is in a dynamic state of equilibrium with its environment--where the components of this layer are free to diffuse away from the membrane if appropriate driving forces are applied.

One such driving force that Lovelock chose to study was exposure of the cells to the neutral adsorbent alumina (Al_2O_3). Red cells were suspended in a solution of 0.16M NaCl and 500mg of alumina/ml of cells at 37°C. The transient loss of cell components is shown in Figure 5.3. The symbols are as before with the addition of lipid dry weight (●) to this figure. The 100 μ m diameter particles of alumina in the solution act as absorbers of the diffusing species and thereby effectively lower the respective chemical potentials in the suspending medium in comparison with a suspension containing NaCl alone. There appears to be a characteristic time of 1-3 minutes in which a large fraction of the mass transfer has occurred. After this characteristic



Figure 5.2 Electron Micrograph of the Erythrocyte "Shaggy Coat"
8000X (reproduced from reference [54]).

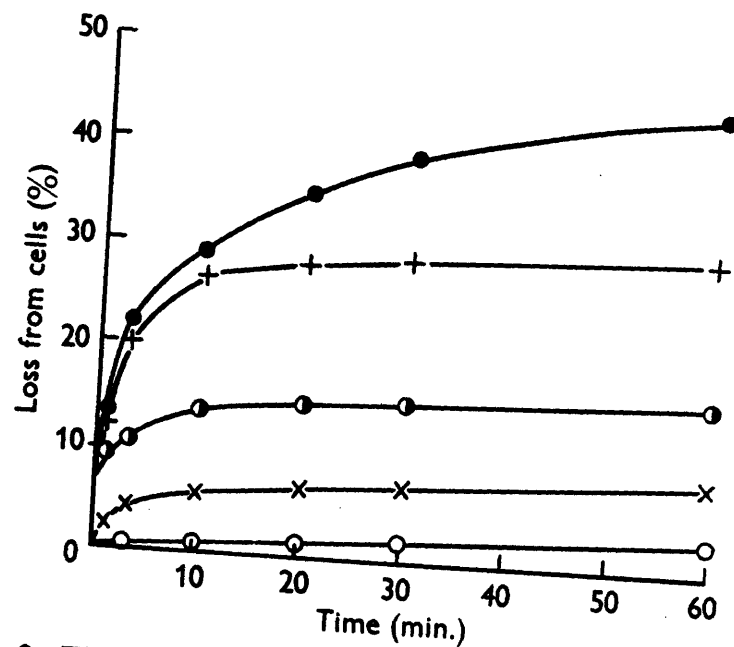


Fig. 2. The rate of removal of components from the red cell by exposure to alumina. Cells suspended in 0.16M. NaCl were exposed to powdered alumina (500 mg. Al_2O_3 /ml. of cells) at 37°. ●, Dry weight of lipids; +, lipoprotein; ⊙, cholesterol; ×, phospholipid; ○, haemoglobin.

Figure 5.3 Removal of Cell Membrane Components as a Function of Time as a Result of Exposure to Alumina (reproduced from reference [53]).

time, the rate of component loss matches the rate of hemoglobin loss (hemolysis). Note that after approximately 20 minutes the rates are almost identical for the different species but that the absolute level of loss is different for the different components. The finding that hemolysis itself is linear for this driving force is in agreement with the results of Morris [55] which are shown in Figure 5.4. This plot is similar to Lovelock's data of Figure 5.3, but what is most interesting about this figure is that the driving force for dissolving the membrane is exposure to hypertonic sodium chloride--exactly the same driving force used in the isothermal, osmotic perturbation kinetic experiments discussed in Chapter 4. Morris chose to monitor the transient response of cholesterol (Δ), phospholipid (\square), and hemoglobin (\circ) as a result of exposure to 1.2M NaCl (note that no data are accessible for times less than 5 minutes, one of the major shortcomings of the centrifugation, hemoglobin absorption measurement method of determining hemolysis.) The open symbols are for exposure at 37°C and the closed symbols are for exposure at 0°C. As with the case of alumina providing the stress, the cholesterol and phospholipid losses precede the loss of hemoglobin. In this instance there is a greater loss of phospholipid than cholesterol, while in the data for alumina-induced transients, there was a greater loss of cholesterol than phospholipid at any given time. This is undoubtedly a consequence of the fact that the driving potentials for mass transfer of the individual species are not the same for the two cases. There is no reason to believe an increase in ionic strength relative to isotonic will provide the identical effect as introduction of a neutral absorbent. The total amount of hemolysis taking place is very small, making good estimation difficult, but a

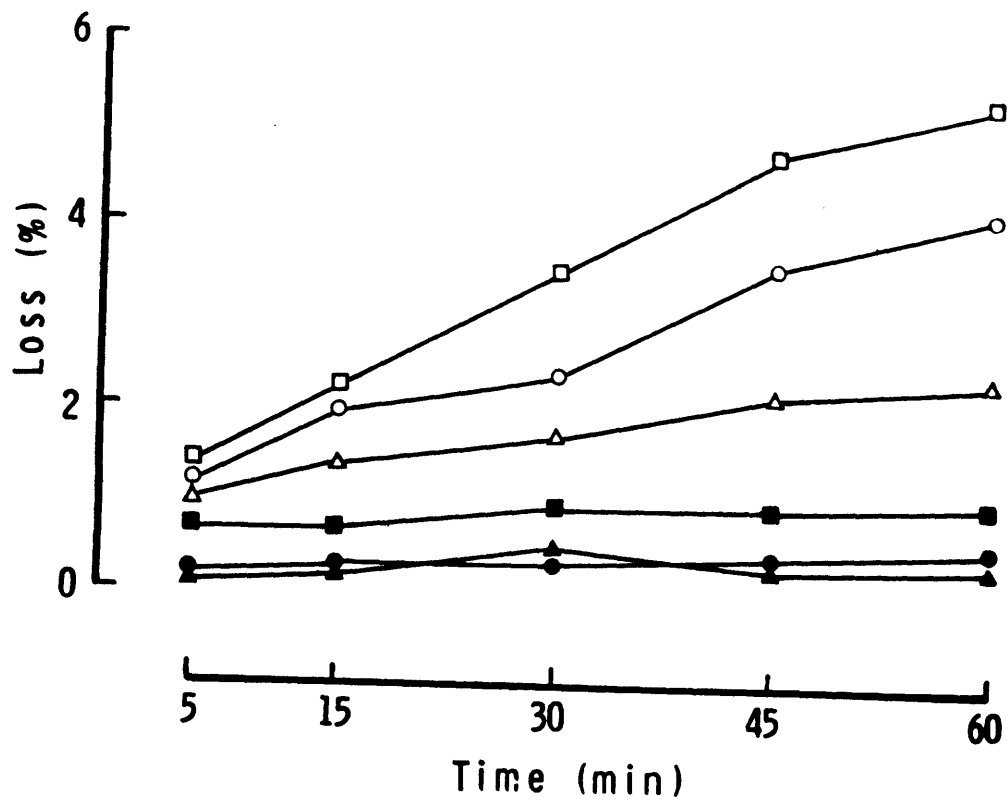


Figure 5.4 Removal of Cell Membrane Components as a Function of Time as a Result of Exposure to Hypertonic Sodium Chloride (reproduced from reference [55]).

linear relation between hemoglobin release and time is reasonable. This estimate compares favorably with Lovelock's data (Figure 5.3). Reducing the temperature from one isothermal set point at 37°C to another at 0°C clearly inhibits loss of membrane components and loss of hemoglobin. This result is in complete agreement with the data determined in Chapter 4 for this type of damage mode. Further discussion of the similarities between the results obtained in Chapter 4 and those of Lovelock and Morris will be postponed until the end of this chapter.

A Review of Basic Membrane Theory

The most widely accepted model for biological membranes is the fluid mosaic model [56]. This model suggests that the general membrane consists of a bilayer of lipid and associated protein. The lipids are composed of the triglycerides (neutral lipids), the phospholipids, cholesterol and cholesterol esters. The lipids are arranged so that the hydrophobic hydrocarbon tails sequester themselves within the bilayer leaflet and the hydrophilic regions such as the polar heads of the phospholipids extend outward into the external medium. This model of the membrane postulates two classes of proteins, the peripheral class which are proteins associated with the surface and the integral proteins which extend through the bilayer (see Figure 5.5). In general, there is free lateral diffusion of both proteins and lipids and the relative viscosity of this bilayer is between 100 and 1000 times that of water [57]. Most membranes appear to be asymmetric. For example, carbohydrates exist as glycoproteins only on the outside surface of the membrane and are presumed to be involved in antigen

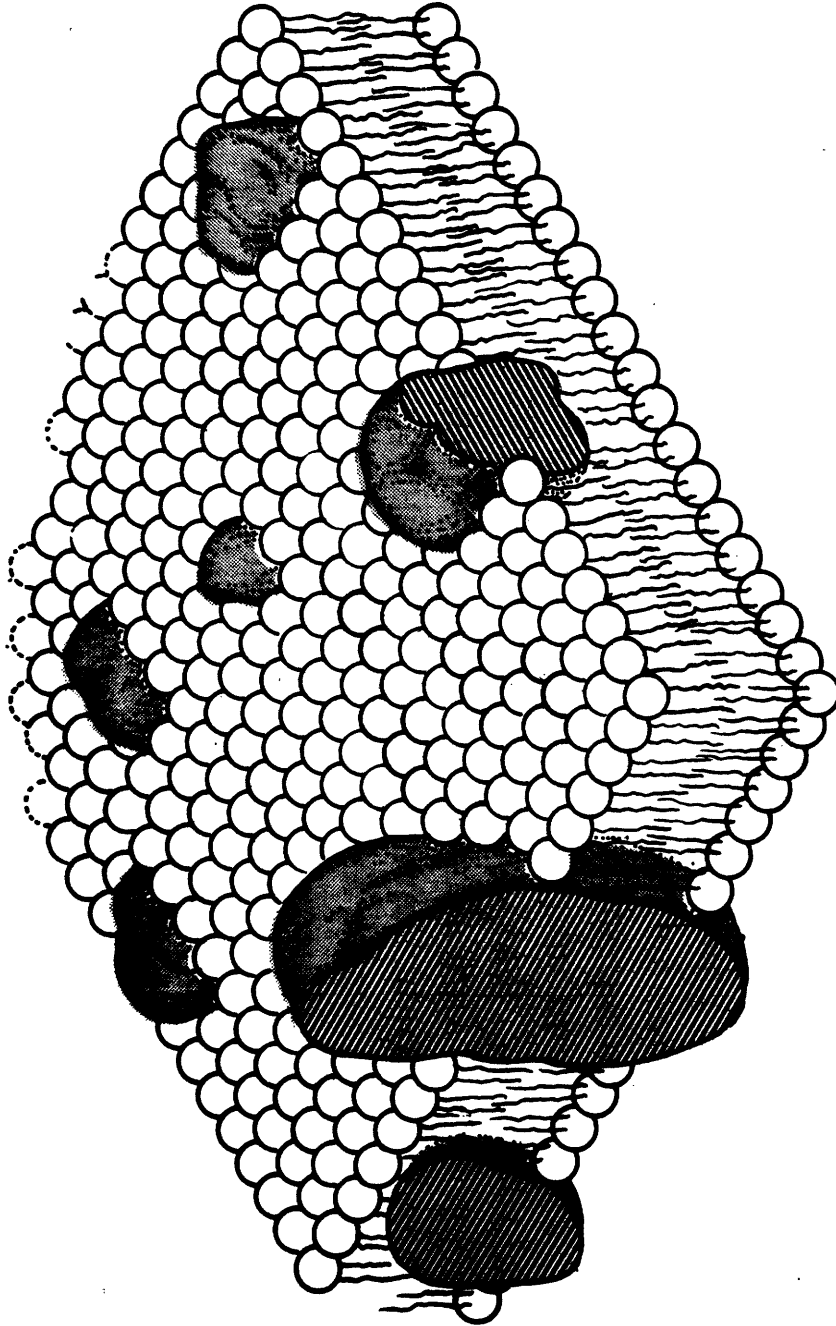


Figure 5.5 Schematic of the Fluid Mosaic Model of the Biological Membrane
(reproduced from reference [57]).

specificity, immune response, and self-cell recognition. The details specifying the factors responsible for membrane stability will be discussed in the next section involving the thermodynamic model. For now it is sufficient to assert that the bilayer stability is a direct result of the solubility of the lipid hydrocarbon chains in organic solvents (in this case the hydrophobic lipid tail region formed by the surrounding lipids) and the solubility of polar and charged regions in water (a polar solvent).

Sweeley and Dawson present a summary of the lipids of the human erythrocyte [58]. They assert that all cell lipid is associated with the membrane. Approximately 30% to 40% of the dry weight of the membrane is lipid. A breakdown of the lipid components present reveals that four major lipid classes account for 87% of the total lipid content. Cholesterol makes up 43% of the lipid present, phosphatidylcholine (lecithin) 16%, phosphatidylethanolamine 15%, and sphingomyelin 13%. The chemical structures of the four major lipid classes are shown in Figure 5.6, schematically inserted into a membrane to show their relative orientations. Of these four compounds, cholesterol is the only steroid. The other three are phospholipids. (Technically the sphingomyelin is best described as a sphingolipid due to the backbone structure to which the fatty acid is attached.) A good discussion including the classification and general properties of lipids and lipoproteins is set forth in reference [57]. A perusal of the membrane literature reveals a large number of factors capable of influencing the state of the membrane. In many cases the effects of each factor are measured by observations of a transition from an ordered state to disordered state or vice versa,

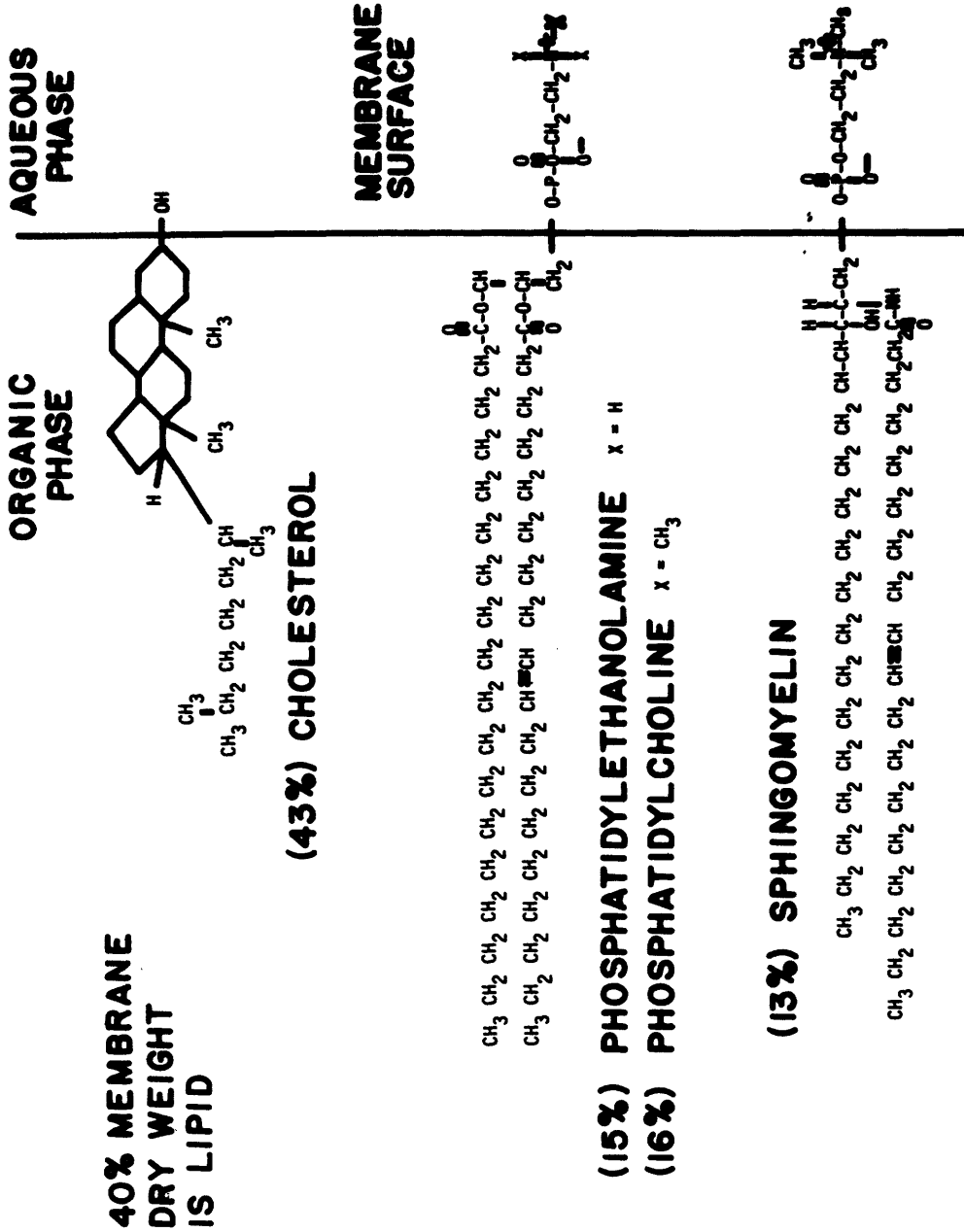


Figure 5.6 Chemical Structures and Orientations Relative to the Membrane Surface for the Four Most Abundant Lipid Types Found in the Human Erythrocyte Membrane.

for example shifts in phase change temperatures. The reader is referred to the literature for a discussion of each of the variables and its particular effect on the membrane: divalent cations [59,60], the degree of saturation of the lipid hydrocarbon chains [59], the length of the hydrocarbon chains [63], the type of polar head group [59,67] the addition of cholesterol [61], changes in pH [60], and the effect of mixtures of lipids in the membrane rather than pure lipids [59,62].

Derivation of the Gibbs-Duhem Equation for a Simplified Model of the Human Erythrocyte

The work in this section is intended to provide the means by which to identify the important thermodynamic properties of the membrane as well as the means to explore the consequences of changing any or all of these properties.

The thermodynamic system is identified in Figure 5.7. In the top left-hand corner of the figure a red cell is depicted with a typical characteristic diameter given as a guide to relative scale [64]. The actual system of interest lies within the outer cell membrane. This plasma membrane has been circled and expanded in the top right-hand part of the figure. The 80Å thickness of the membrane bilayer is a typical thickness [65] and this sketch could be considered a cross-sectional view of the fluid mosaic model shown in three dimensions in Figure 5.5. There is an axis of symmetry drawn in the figure which has been imposed as a simplifying assumption. The shaded portion of this sketch has been expanded once again in the

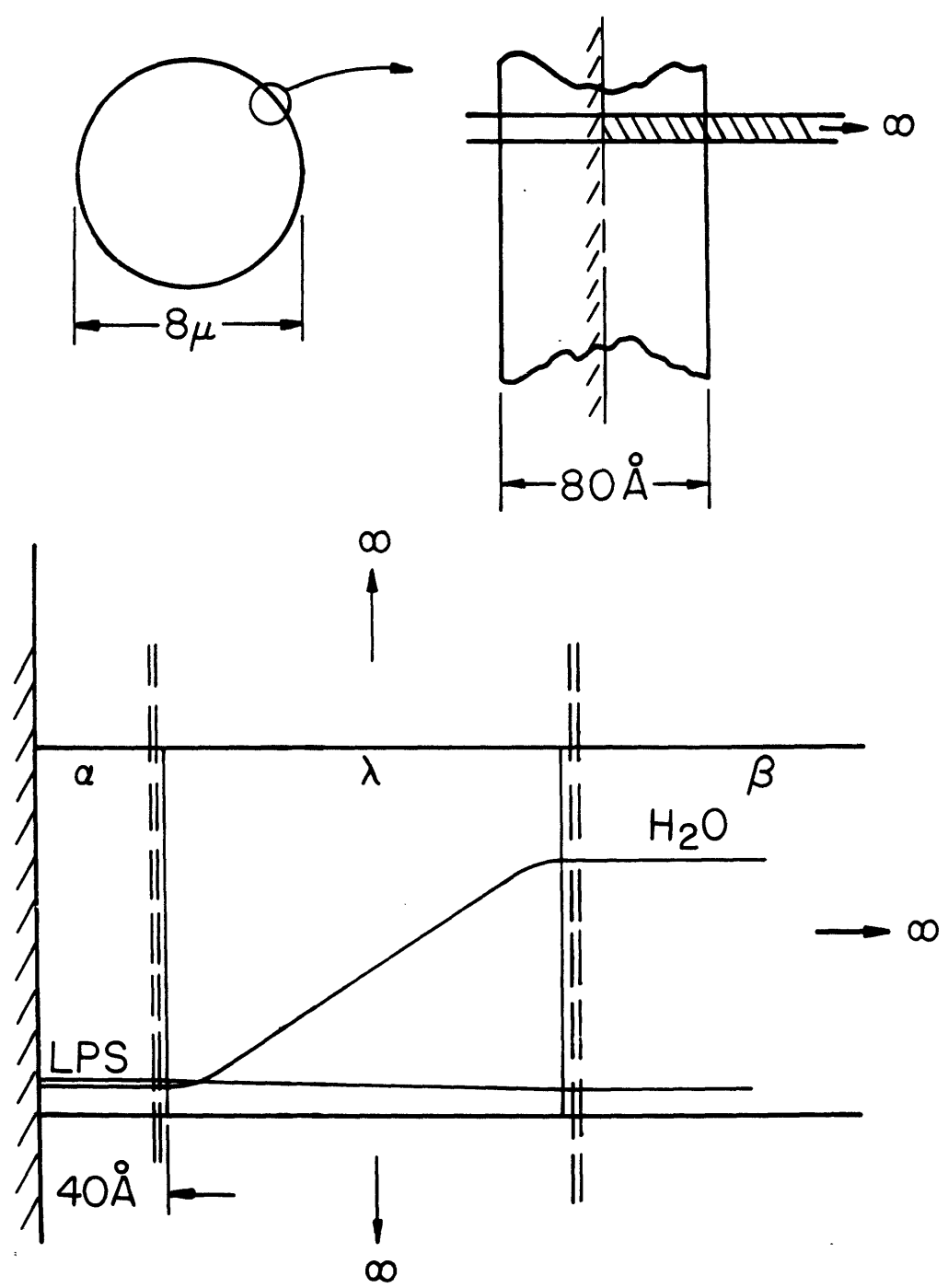


Figure 5.7 Schematic Defining the Thermodynamic System at the Erythrocyte Membrane Surface.

bottom drawing of Figure 5.7 which represents an enlargement of the region of interest from the central axis of symmetry, out through the three separate phases associated with the membrane to infinity. Two assumptions are now stated for the purposes of the analysis:

Assumption 1: The membrane is a thin film composed of a general organic phase with a plane of symmetry, surrounded on both sides by an aqueous phase (intracellular and extracellular compartments).

Assumption 2: One organic component of the membrane which will be designated LPS (for lipoprotein species) is free to pass from the organic phase (α) to the aqueous phase (β) and vice versa through the surface phase (λ). Water is also freely exchangeable.

The bottom sketch of Figure 5.7 shows a one dimensional model of one half of the symmetric membrane. Closest to the plane of symmetry is the organic phase α where the concentration of the organic molecules, wedged between the two aqueous phases, is greatest. With the simplifying assumption that only one general class of diffusible organic molecule (LPS) is of interest, the concentration of this molecule as a function of distance is shown schematically. The concentration is greatest within the membrane and diminishes to near zero value in the aqueous phase. The transition region wherein the concentrations of the respective membrane and aqueous phase species are changing with distance is denoted the surface phase λ . The bulk aqueous phase farthest to the right is called the β phase. The

concentration of water is very high in this region and diminishes to very low values within the membrane [66]. The surface phase λ is the thermodynamic system and the boundaries of this system are shown for the one-dimensional sketch at the bottom of Figure 5.7 by double dotted lines. Thus the thermodynamic system extends over the entire cell surface area and with the assumed membrane symmetry there are two identical systems, one on the inside surface of the cell and one on the outside surface.

The development of the Gibbs-Duhem equation for such a thermodynamic system including a surface phase was first accomplished by Gibbs and is reproduced in many texts [68,69]. This relation, which places constraints on the simultaneous variations in intensive properties of the system, is developed here for the case of the erythrocyte membrane model.

The fundamental equation for the open system in terms of temperature, pressure and mole numbers of the various species is the Gibbs form:

$$(5.1) \quad G = G(T, P, n_1, n_2, \dots, n_i)$$

The general differential form of this equation is:

$$(5.2) \quad dG = \left(\frac{\partial G}{\partial T}\right)_{P, n_i} dT + \left(\frac{\partial G}{\partial P}\right)_{T, n_i} dP + \sum_{i=1}^K \left(\frac{\partial G}{\partial n_i}\right)_{T, P, n_j} dn_i$$

where by definition:

$$(5.3) \quad S = - \left(\frac{\partial G}{\partial T}\right)_{P, n_i}$$

$$(5.4) \quad v = \left(\frac{\partial G}{\partial P} \right)_{T, n_i}$$

$$(5.5) \quad \mu_i = \left(\frac{\partial G}{\partial n_i} \right)_{T, P, n_j}$$

Therefore,

$$(5.6) \quad dG = - S dT + VdP + \sum_{i=1}^K \mu_i dn_i$$

This is sufficient thermodynamic information for the two bulk phases α and β but it is not enough to account for the surface phase λ , which is the present thermodynamic system. The creation of such an interface between two bulk phases involves an additional Gibbs free energy term. The differential amount of free energy involved in the creation of such a surface at constant temperature, pressure, and specie mole number is:

$$(5.7) \quad dG_s = \left(\frac{\partial G}{\partial A} \right)_{T, P, n_i} dA$$

where by definition

$$(5.8) \quad \gamma = \left(\frac{\partial G}{\partial A} \right)_{T, P, n_i}$$

is the free energy per unit area or as it is commonly called the surface tension. The surface phase is the unique feature of this system and this is where attention will be focused. The total differential equation for the Gibbs free energy of the surface phase λ , can be written

$$(5.9) \quad dG = - SdT + VdP + \sum_{i=1}^K \mu_i dn_i + \gamma dA$$

The Euler form of the Gibbs free energy is available in the literature [68] and can be written:

$$(5.10) \quad G = \sum_{i=1}^K \mu_i n_i + \gamma A$$

The complete differential of the free energy as expressed by this equation for the surface phase is

$$(5.11) \quad dG = \sum_{i=1}^K \mu_i dn_i + \sum_{i=1}^K n_i d\mu_i + \gamma dA + Ad\gamma$$

The differential change in free energy as expressed in equation 5.9 must be identical to that just derived. Therefore, eliminating like terms, the result is the Gibbs-Duhem equation:

$$(5.12) \quad \sum_{i=1}^K n_i d\mu_i + Ad\gamma = -SdT + VdP$$

or

$$(5.13) \quad d\gamma = -\left(\frac{S}{A}\right) dT + \left(\frac{V}{A}\right) dP - \sum_{i=1}^K \left(\frac{n_i}{A}\right) d\mu_i$$

Two more assumptions are made regarding the model system as well as the introduction of two definitions.

Assumption 3: The surface area of the film remains constant during any process.

Assumption 4: The system and its environment are isobaric for any process.

The surface entropy per unit area will be defined as:

$$(5.14) \quad \sigma = \left(\frac{S}{A} \right)$$

The number of moles of species i per unit area will be defined as:

$$(5.15) \quad \Gamma_i = \left(\frac{n_i}{A} \right)$$

With these assumptions and definitions, equation 5.13 can be written:

$$(5.16) \quad d\gamma = -\sigma dT - \sum_{i=1}^K \Gamma_i d\mu_i$$

Since there is a transition of the quantities S and n_i with respect to space through the surface phase, there is the possibility of some confusion as to the definitions of the thermodynamic properties within this phase. The following simple analysis will demonstrate that the properties of this phase should be predominantly those of water.

Within a highly compressed film, the effective diameter of the polar head group of the lecithin molecule is 8\AA [67]. An average lipid molecule possesses fatty acid chains of approximately fifteen to twenty carbon atoms long (see Figure 5.6). At an intercarbon bond length of 1.5\AA a reasonable estimate of the average lipid molecule length is 25\AA . A cube taken from one side of the membrane bilayer with an edge length of 25\AA would contain 9 lipid molecules ($25\text{\AA}/8\text{\AA} \approx 3$ molecules to a side) and the volume of the cube would be $1.56 \times 10^{-20} \text{ cm}^3$ for a maximum surface lipid concentration of

$$\begin{aligned}
 (5.17) \quad [C_{LPS}] &= \frac{(9 \text{ molecules}) (10^3 \frac{\text{cm}^3}{\ell})}{(1.56 \times 10^{-20} \text{cm}^3) (6.02 \times 10^{23} \frac{\text{molecules}}{\text{mole}})} \\
 &= 0.96\text{M}
 \end{aligned}$$

which is actually the bulk organic phase concentration. This corresponds quite well with a concentration of 1.6M calculated for the surface concentration of the strongly absorbed species lauric acid at the water-air interface [68]. Moving from the membrane surface out into the aqueous phase where $\Gamma_{LPS} \rightarrow 0$, the concentration of water is

$$\begin{aligned}
 (5.18) \quad [C_w] &= \frac{(10^3 \text{ cm}^3/\ell)}{18 \text{ cm}^3/\text{mole}} \\
 &= 55.6\text{M}
 \end{aligned}$$

Assuming the simple case of linearly varying concentrations for water and lipid through the surface phase the average concentration of lipid amounts to only 2% of the average water concentration. A first estimate of the thickness of the surface phase would be five to ten lipid molecular lengths, a distance large enough so that one would be able to reasonably detect gradients in the concentrations. This would be equivalent to a surface phase thickness of 125-250Å. This is in qualitative agreement with an estimate made in reference [68].

At the eutectic point for a simple sodium chloride-water system, the salt concentration is maximized and the sodium chloride mole fraction is 0.1587. This means that even for these maximum sodium chloride concentrations the ratio of the number of moles of water to the number of moles of salt in the surface phase will be 6.3 to 1.0.

The diameter of the hemoglobin molecule is 64\AA , which means that the maximum concentration of hemoglobin that could occur at the inner surface of the membrane would be

$$(5.19) \quad [\text{Hb}] = \frac{(10^3 \text{ cm}^3 / \ell)}{\frac{4}{3} \pi \left[\frac{(32 \times 10^{-8} \text{ cm})^3}{\text{molecule}} (6.02 \times 10^{23} \frac{\text{molecules}}{\text{mole}}) \right]}$$

$$= 1.21 \times 10^{-2} \text{ M}$$

It therefore appears that to a first approximation:

$$(5.21) \quad n_w > n_s \quad (\Gamma_w > \Gamma_s)$$

$$(5.22) \quad n_w \gg n_{\text{LPS}} \quad (\Gamma_w \gg \Gamma_{\text{LPS}})$$

$$(5.23) \quad n_w \gg n_{\text{Hb}} \quad (\Gamma_w \gg \Gamma_{\text{Hb}})$$

Thus, equation 5.16 can be reduced from

$$(5.24) \quad d\gamma = -\sigma dT - \Gamma_w d\mu_w - \Gamma_s d\mu_s - \Gamma_{\text{Hb}} d\mu_{\text{Hb}} - \Gamma_{\text{LPS}} d\mu_{\text{LPS}}$$

to

$$(5.25) \quad d\gamma = -\sigma dT - \Gamma_w d\mu_w$$

Similarly, the appropriate value of the surface phase entropy to a first approximation would be the entropy of water. The results of this analysis are convenient for two reasons. It simplifies the equation somewhat, but more importantly it allows the equilibrium surface energy of the film to be determined from changes in the water chemical potential. For all work in this thesis, cells were washed and resuspended in a solution containing only NaCl and

water. Lovelock measured equilibrium concentrations of lipids in such a solution of cells and saline at very low levels [34]. It is therefore assumed that the phase equilibrium of the simple NaCl-water binary solution is sufficient to specify the thermodynamic state of the extracellular medium of the cell suspension during freezing. Various thermodynamic models have also been developed to allow determination of the intracellular state of the cell [19,22,44].

For equilibrium freezing the intracellular and extracellular water chemical potentials are identical. The membrane is assumed to be in equilibrium with these solutions which means that the water chemical potential and temperature needed to determine the surface energy can be calculated from the known properties of the extracellular solution. The fact that damage from "solution effects" is the dominant mode of destruction at low cooling rates makes the assumption of equilibrium freezing a good one. Intracellular ice is not expected in erythrocytes for cooling rates less than $840^{\circ}\text{K}/\text{min}$ if there is no extracellular supercooling [16]; therefore, "low" rates for the erythrocyte would be those less than $840^{\circ}\text{K}/\text{min}$. For these rates the intracellular thermodynamic state of water does not differ appreciably from the extracellular equilibrium state [22,44].

One might expect that the surface energy of the membrane should be closely related to its stability with respect to a given set of environmental conditions. One might further suspect that if the environment were to be changed, which represents a perturbation to the membrane system, then the approach to the new equilibrium state

for the membrane should also be related to the surface energy. In the next section of this chapter, the Gibbs -Duhem equation, as an equilibrium relation, is included in a model for the kinetic process of hemolysis. The hemolysis process involves the non-equilibrium release of membrane components and the methods used for its analysis will be those of absolute rate theory.

The Postulated Kinetic Theory of Hemolysis

It is known that hemolysis kinetics are closely related to the loss of lipid material from the erythrocyte membrane [34,53,55]. In fact, it appears that after a superficial layer of material has been lost from the red cell membrane, the rate of the appearance of hemoglobin in the extracellular medium is quantitatively equal to the rate of the appearance of the membrane lipid components in the extracellular medium [53]. An analysis of the kinetics of lipid loss is therefore likely to produce the kinetic parameters of hemolysis as well.

Consider Figure 5.8 as a schematic view of one half of the membrane, i.e., one of the symmetric interfaces between an organic phase and an aqueous phase. The short horizontal lines with circles on the right-hand ends represent the lipid molecules embedded in the organic phase comprised of the fatty acid chains of the adjoining lipid molecules, the hydrophobic sections of the integral proteins, etc. A plot of the standard chemical potential per molecule for the lipoprotein diffusible species (LPS) is schematically superimposed on

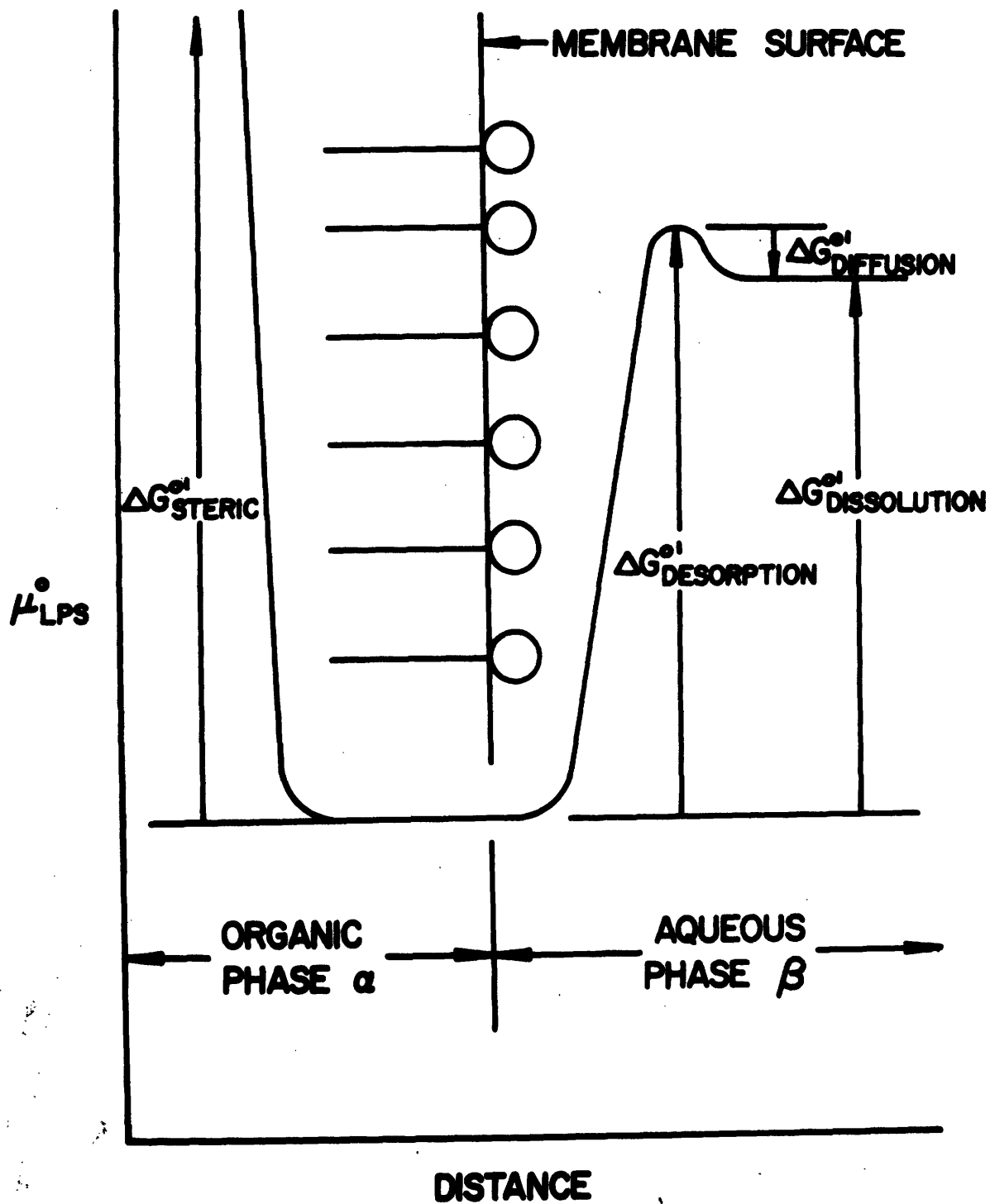


Figure 5.8 Free Energy of a Membrane Lipid Molecule as a Function of Distance from the Membrane Surface.

this figure as a function of distance from the membrane surface. The lipid molecules are in a stable configuration because they exist in a "free energy well". Lipid molecule movement to the left results in a very large increase of free energy ($\Delta G^{\circ}_{\text{steric}}$) due to steric interaction of the fatty acid chains of the lipid molecules [67]. Movement of the lipid to the right, into the aqueous phase also produces a net increase of free energy ($\Delta G^{\circ}_{\text{desorption}}$); as a result the lipid molecule tends to remain at the interface of the membrane surface. If the molecule has been moved far enough away from the surface, the surface no longer exerts influence on the molecule and a net decrease of free energy with respect to distance is seen ($\Delta G^{\circ}_{\text{diffusion}}$). In its stable position the lipid molecule is in a position of high lipid concentration as compared to the bulk aqueous phase.

For a case in which the lipid molecules in the membrane are in thermodynamic equilibrium with the lipid molecules of the same species in the extracellular medium, the temperature and pressure of the membrane and medium must be identical and the following condition must also be met for each species:

$$(5.26) \quad \mu_{\alpha} = \mu_{\beta}$$

where the subscript α refers to the organic phase and the subscript β refers to the aqueous phase. For the simplified erythrocyte membrane model, only one lipid specie is considered: The hypothetical lipoprotein species (LPS).

From the defining equations,

$$(5.27) \quad \mu_{\alpha} = \mu_{\alpha}^{\circ} + KT \ln a_{\alpha}$$

$$(5.28) \quad \mu_{\beta} = \mu_{\beta}^{\circ} + KT \ln a_{\beta}$$

the equilibrium distribution of the lipid molecules between the organic and aqueous phase is determined. The respective activities are used because they include non-ideal, non-dilute behavior. From the two equations above,

$$(5.29) \quad \frac{a_{\alpha}}{a_{\beta}} = \exp \left(\frac{\mu_{\beta}^{\circ} - \mu_{\alpha}^{\circ}}{KT} \right)$$

The quantity $(\mu_{\beta}^{\circ} - \mu_{\alpha}^{\circ})$ is an energy associated with the complete process of removing a lipid molecule from an initial state within the membrane to a final state in the bulk aqueous phase. It is therefore appropriate to designate this energy the Gibbs free energy of dissolution per molecule

$$(5.30) \quad \Delta G^{\circ'}_{\text{dissolution}} = (\mu_{\beta}^{\circ} - \mu_{\alpha}^{\circ})$$

Equation 5.28 is rewritten:

$$\frac{a_{\alpha}}{a_{\beta}} = \exp \left(\frac{\Delta G^{\circ'}_{\text{dissolution}}}{KT} \right)$$

Empirically it is known that $a_{\alpha} \gg a_{\beta}$, therefore $\Delta G^{\circ'}_{\text{dissolution}} > 0$ as shown in Figure 5.8. Since $\Delta G^{\circ'}_{\text{dissolution}} > 0$, there is a net barrier energy for removal of lipid molecules and work must be done on them to take them from the membrane. The free energies discussed here

are standard free energies corresponding to a standard state. A convenient standard state for the erythrocyte membrane corresponds to cells in normal saline at ambient temperature (25°C) and one atmosphere of pressure.

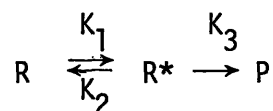
Consider now how this model could be used to explain some of the experimental observations of Lovelock. When fresh, washed red cells are suspended in isotonic sodium chloride at ambient temperature and one atmosphere of pressure, no hemolysis occurs (for times less than eight hours). The data of Lovelock suggest that for these washed cells placed in normal saline, a small amount of lipid diffuses from the cells to the medium and that this does not represent a destructive process since the cell has a superficial coating, much of which can be removed before hemolysis begins. For each of the lipid species that Lovelock studied, he recorded an equilibrium concentration of approximately 20 μ g/ml of lipid in the suspending medium. This material diffused from the cells quickly and reached the equilibrium state within two or three minutes. As Lovelock stated, these equilibrium concentrations did not appear to represent concentrations consistent with the interpretation that the solution was saturated with respect to these components [34]. Each time Lovelock placed the cells in fresh normal saline, the cells were introduced to an extracellular medium where $a_{\beta} = 0$ for the lipid. The dissolution energy may be very large for the average lipid molecule in a membrane [66], but it is not infinite and some lipid material must leave the membrane in order to establish the equilibrium condition for $\frac{a_{\alpha}}{a_{\beta}}$. The fact that the extracellular medium is not saturated with the lipid molecule

is a straightforward consequence of the existence of ΔG° ' dissolution. The diffusion process observed by Lovelock for the transport of lipid from the membrane to the suspending medium took two to three minutes. This time can be thought of as the characteristic diffusion time for the lipid molecules as they undergo the ΔG° ' diffusion part of the dissolution process, if it is assumed that diffusion is the rate-limiting step of the entire dissolution process.

The theory of absolute reaction rates as developed by H. Eyring in 1935 will be reviewed now for a simple, general unimolecular reaction and then the theory will be applied to the specific case of lipid loss from the erythrocyte membrane as a model for hemolysis.

Absolute reaction rate theory has been applied to many types of kinetic processes ranging from chemical reactions, to viscosity, diffusion and electrochemical phenomena [21,22,70]. The fundamental postulates of this theory are: (1) there is an energy variation in the transformation from reactants to products which involves the formation of an activated complex; (2) the reactants are always in equilibrium with the activated complex; and (3) the activated complex corresponds energetically to the top of the energy barrier separating the reactants and products.

A schematic of the free energy of the molecule with respect to the reaction coordinate is given in Figure 5.9. Suppose the reaction is unimolecular such that it can be expressed as:



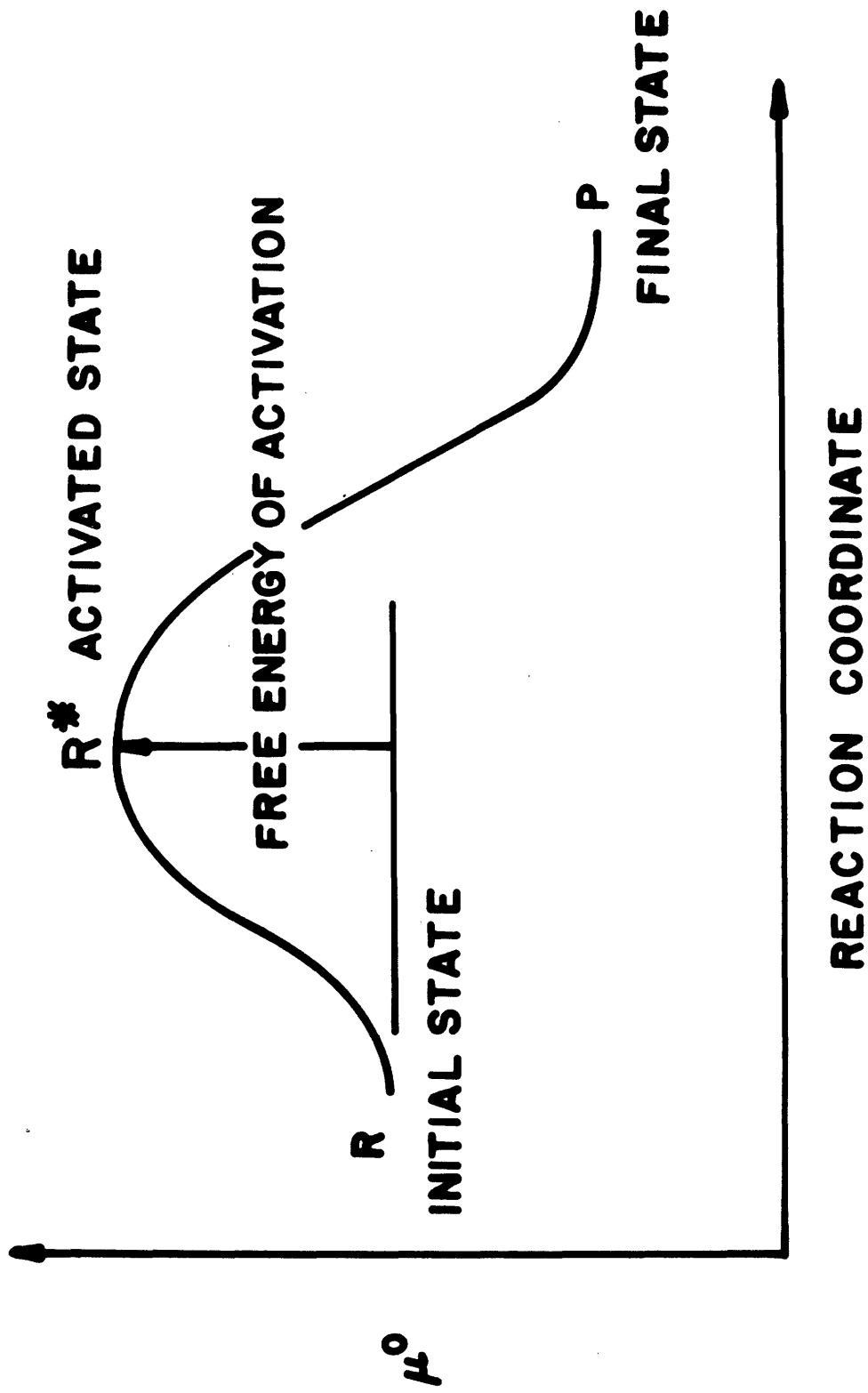


Figure 5.9 Absolute Rate Theory Interpretation of Molecular Free Energy as a Function of Reaction Coordinate.

where R is the reactant molecule, R* is the activated complex and P is the product. Further derivation of the details of this theory are based on the assumption that an equilibrium exists between R and R*, and that the reaction from the activated state R* to the product P is the rate-limiting step. Reference [71] points out these assumptions, and presents the mathematics to show that they are valid under the assumptions that the intermediate R* is present in small concentrations and in steady state concentrations, and that $k_2 \gg k_3$ i.e., that deactivation from the activated state is a much faster process than decomposition to the product. It can then be shown that

$$(5.29) \quad - \frac{d[R]}{dt} = k_3 \left(\frac{k_1}{k_2} \right) [R]$$

or

$$(5.30) \quad \text{rate} = k_3 \cdot K^* \cdot [R]$$

where

$$(5.31) \quad K^* = \frac{k_1}{k_2}$$

is the equilibrium constant for the molecules R and R*.

The form of the rate-limiting rate constant k_3 is usually derived by considering the activated complex R* to be a normal molecule R, with one vibration mode with respect to which it is unstable. If the frequency of this vibration is ν , then product P is formed at a rate of $\nu [R^*]$ or

$$(5.32) \quad k_3 = \nu$$

so that the overall rate of the reaction $R \rightarrow P$ is expressed either as

equation 5.29 or

$$(5.33) \quad \text{rate} = v \cdot K^* \cdot [R]$$

The concepts just reviewed will now be used to describe a model for hemolysis kinetics. Figure 5.10 which describes the entire lipid loss process, should be considered a summary of the information in Figures 5.8 and 5.9. The reactant molecule R for this system is an individual lipoprotein molecule which has been previously designated the hypothetical species LPS. The lipid molecules at the interface of the membrane are at a minimum free energy state as previously discussed.

The activated complex is a lipid molecule which has a free energy equal to the barrier desorption energy discussed in conjunction with Figure 5.9. In Figure 5.10 the activated molecule R* is shown removed from the bulk surface phase, where it is no longer entirely affected by the surface alone. A molecule in this state may either be reabsorbed into the membrane or it may diffuse away from the membrane. The molecules in states R and R* are assumed to be in equilibrium. Their relative concentrations are determined by the desorption free energy per molecule, ΔG° '_{desorption}.

The product molecule P in the dissolution reaction (assumed to be a pseudo-unimolecular reaction) is also a lipid molecule, but it is in its final state in which it is well-mixed in the saline solution and well away from the interface and its influence. The "decomposition" of the activated complex into a product has been

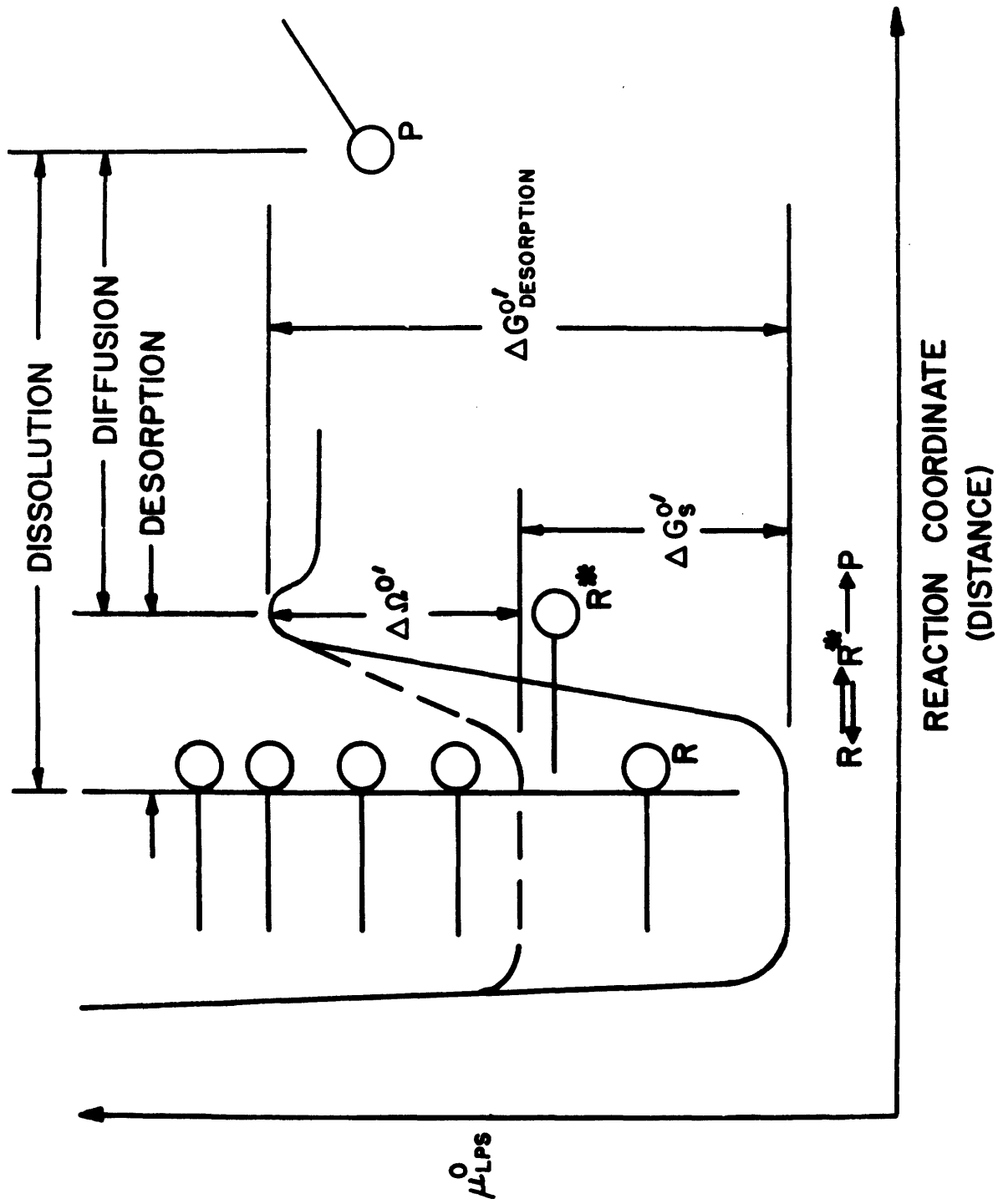


Figure 5.10 Absolute Rate Theory Interpretation of Membrane Dissolution Model.

modelled here as a diffusion process and is assumed to be rate-limiting. In all likelihood it is a more complex process which would involve among other factors, the mixing of the lipid into the bulk aqueous phase. The overall free energy profile for the process has been included in the diagram with each of the states, R, R*, and P identified corresponding to their respective free energy levels. The free energy diagram can be thought of as free energy versus reaction coordinate or equivalently, free energy versus distance. No attempt has been made to scale accurately either distance or energy.

According to absolute rate theory, the rate constant for lipid leaving the membrane would be

$$(5.34) \quad k = \nu K^*$$

As for all equilibrium constants, K^* can be expressed in terms of the difference in standard free energies between the reactants and, in this case the activated complex

$$(5.35) \quad \Delta G^{\circ'}_{\text{desorption}} = -KT \ln K^*$$

or

$$(5.36) \quad K^* = \exp \left[\frac{-(\Delta G^{\circ'}_{\text{desorption}})}{KT} \right]$$

The reaction rate for lipid removal is now formed,

$$(5.37) \quad \text{rate} = \nu K^* [R]$$

where the concentration of reacting molecules is actually the number of LPS molecules present at the membrane surface per unit area

$$(5.38) \quad [R] = \frac{n_{LPS}}{A} = \Gamma_{LPS}$$

Therefore substitution of equations 5.36 and 5.38 into equation 5.37 yields

$$(5.39) \quad \text{rate} = \Gamma_{LPS} \cdot v \cdot \exp \left[\frac{-(\Delta G^{\circ'}_{\text{desorption}})}{KT} \right]$$

Care must be taken in applying equation 5.39. In particular it must be determined whether factors external to the system can cause a modification in the value of $\Delta G^{\circ'}_{\text{desorption}}$. If such factors do cause changes in $\Delta G^{\circ'}_{\text{desorption}}$, then a suitable modification of equation 5.39 must be derived which will yield the correct, instantaneous value of the desorption free energy for the reaction of interest. Certainly in the general case external factors can modify the reaction rate by a change in the standard free energy [70].

It is known from Lovelock's data that increasingly concentrated sodium chloride solutions cause greater concentrations of cholesterol and phospholipid to appear in the extracellular medium after exposure for 10 minutes at 0°C [72]. For isothermal exposure of fresh cells (Γ_{LPS} and T are constants) the only change in rate equation 5.39 that could explain an increased rate of dissolution would be a decrease in the standard desorption free energy. If it is assumed that the increase in ionic strength is not acting as a catalyst (i.e., by lowering the energy of the activated complex) but rather as a means of increasing the free energy of the surface lipids, the correct value of the free energy of desorption would be that determined for cells in normal saline minus the amount by which the surface energy has been

increased $\Delta G_S^{\circ'}$ (see Figure 5.10). If the instantaneous free energy change for the desorption reaction $R \rightleftharpoons R^*$ is specified as

$$(5.40) \quad \Delta \Omega^{\circ'} = \Delta G^{\circ'}_{\text{desorption}} - \Delta G_S^{\circ'} \quad (\text{see Figure 5.10})$$

the rate of release of lipids is now correctly described as

$$(5.41) \quad \text{rate} = \Gamma_{\text{LPS}} \cdot v \cdot \exp \left[\frac{-(\Delta \Omega^{\circ'})}{KT} \right]$$

It is now assumed that the surface energy derived from the Gibbs-Duhem equation can be substituted for the factor $\Delta G_S^{\circ'}$

$$(5.42) \quad \Delta G_S^{\circ'} = \int_{G_S^{\circ'1}}^{G_S^{\circ'2}} dG_S^{\circ'}$$

State $G_S^{\circ'1}$ is associated with fresh cells in normal saline at ambient temperature (25°C) and one atmosphere. $G_S^{\circ'2}$ is the instantaneous value of the surface free energy. Since the surface area has been assumed constant for this process (Assumption 3), the change in surface Gibbs free energy can be stated

$$(5.43) \quad dG_S^{\circ'} = dG_S^{\circ} = Ad\gamma$$

This total free energy must be converted to a free energy per surface molecule. The surface energy per unit area (γ) was defined in equation for a surface phase with the properties of water. Therefore with this assumption, the correct number of surface molecules for reducing dG_S° to $dG_S^{\circ'}$ is n_w .

$$(5.44) \quad dG_S^{\circ'} = \frac{dG_S^{\circ}}{n_w} = \frac{Ad\gamma}{n_w}$$

By definition the quantity Γ is n/A ; hence the reaction rate for lipid loss would be

$$(5.45) \quad \text{rate} = \Gamma_{\text{LPS}} \cdot \nu \cdot \exp \left[\frac{-(G_{\text{desorption}}^{\circ}) - \int_{\gamma_0}^{\gamma} \frac{d\gamma}{\Gamma_w}}{KT} \right]$$

where from the Gibbs-Duhem equation

$$(5.25) \quad d\gamma = -\sigma dT - \Gamma_w d\mu_w$$

$$(\sigma > 0, \Gamma_w > 0)$$

and γ_0 is for fresh cells in normal saline at 25°C and one atmosphere.

Classical absolute rate theory derives the frequency factor ν in terms of translation of the activated complex through the transition state due to thermal motion, $h\nu = KT$. In the present case of a diffusion controlled process, the characteristic time is more appropriately $\tau = L^2/D$. The distance L is a characteristic diffusion distance and D is the diffusion coefficient for the lipid material through the extracellular medium. The overall dissolution process is therefore controlled by a process with a characteristic frequency ν , where

$$(5.46) \quad \nu = \frac{D}{L^2}$$

The rate expression is given as

$$(5.47) \quad -\frac{d\Gamma_{\text{LPS}}}{dt} = \Gamma_{\text{LPS}} \left(\frac{D}{L^2}\right) \exp\left(\frac{-\Delta G_{\text{desorption}}^{\circ}}{KT}\right) \exp\left(\frac{\int_{\gamma_0}^{\gamma} \frac{d\gamma}{\Gamma_w}}{KT}\right)$$

It can now be appreciated that the loss of lipid will appear to be a first order time response. The characteristic time of the reaction is L^2/D and the desorption energy parameters appearing as exponential terms are scaling factors that will determine the absolute magnitude of the amount of lipid that will leave the membrane per unit time;

however, these factors do not change the characteristic times involved.

As a final step in modelling the hemolysis process, the form of the hemolysis rate equation will be derived, making use of the rate equation for lipid loss.

The phenomenon of lipid loss is a continuous one once the cell membrane has been perturbed, yet the hemolysis process appears to be an all or none proposition [29,42]. The assumption that hemolysis is an all or none event is supported by the fact that microscopic observations of red cells after posthypertonic dilution [42], after freezing and thawing [73], and during and after exposure to hypertonic solutions [27,73] reveal that cells in these suspensions are essentially of two types, one with a very high refractive index and the other with a very low refractive index relative to water. This implies that the actual process of hemoglobin release is rapid with respect to any alterations in the membrane that may have preceded the event causing lysis. If it can be shown that the characteristic times associated with hemoglobin diffusing through the cell and then through the membrane are short compared with the release of lipid, then there is reason to believe that the hemolysis process can be modelled by a lipid diffusion rate-limiting process causing a critical state to be attained, followed by a very rapid release of hemoglobin. This model would account for observing only two cell types in suspension. The characteristic time for hemoglobin diffusion must be short on an absolute scale, as well as with respect to lipid diffusion, otherwise the transformation could be observed in real time which has not been done.

The diffusion coefficient of hemoglobin in water is $D = 6.90 \times 10^{-7} \text{ cm}^2/\text{sec}$ at 20°C [57]. The radius of the red cell at isotonic conditions is $4 \mu\text{m}$, hence an estimate of the characteristic time for the red cell to empty itself of hemoglobin once the critical lipid concentration is attained would be

$$(5.48) \quad \tau = L^2/D = \frac{(4 \times 10^{-4} \text{ cm})^2}{(6.90 \times 10^{-7} \text{ cm}^2/\text{sec})}$$

$$= 0.23 \text{ sec}$$

Similarly, the transit time for passage of a hemoglobin molecule through a distance typical of a membrane thickness (80 \AA), (assuming the same diffusion coefficient for hemoglobin in water) would be

$$(5.49) \quad \tau = \frac{(80 \times 10^{-8} \text{ cm})^2}{6.90 \times 10^{-7} \text{ cm}^2/\text{sec}}$$

$$= 9.3 \times 10^{-7} \text{ sec}$$

Admittedly, this value would be a low estimate since the diffusion constant would be much lower if the membrane were not assumed critically porous, i.e. containing aqueous filled cross-sectional areas with diameters greater than or equal to the diameter of the hemoglobin molecule. Even if this estimate were in error by as much as six orders of magnitude, these characteristic times are much shorter than the lipid diffusion times of several minutes observed by Lovelock [34,53].

It is therefore postulated that after perturbation, there is a

timewise first order decay of the surface concentration of lipid in accordance with equation 5.47. The membrane acts as an effective barrier to hemoglobin transmembrane flux until a well defined minimum surface concentration of lipid is reached. This concentration will be called Γ_{critical} . Once this condition is met at the membrane surface, then enough lipid has been lost such that a hemoglobin molecule can pass through the "free surface area" formed. Models similar to this have been formulated for passage of water through a membrane [74]. There is no evidence, electron micrographic or otherwise that there is preferential surface segregation of the lipid material in a red cell [75], and it is therefore assumed that, Γ , the instantaneous value of the surface lipid concentration, is valid over all of the surface area. This means that once Γ_{critical} is reached, hemolysis occurs over the entire surface area, a fact enhancing rapid release of hemoglobin. This rapid event can not occur until the critical condition of Γ has been realized at the membrane surface. Therefore the hemolysis characteristic time should be comparable to the diffusion time observed in the case of lipid release and the frequency factor in the hemolysis rate equation is

$$(5.46) \quad v = \left(\frac{D}{L^2} \right)$$

Figure 5.11 shows the mechanism hypothesized for hemolysis. At the top of the figure is the cell membrane depicted for isotonic conditions with integral and peripheral proteins.

In the middle is a situation in which the initial lipid concentration

INTRACELLULAR

EXTRACELLULAR

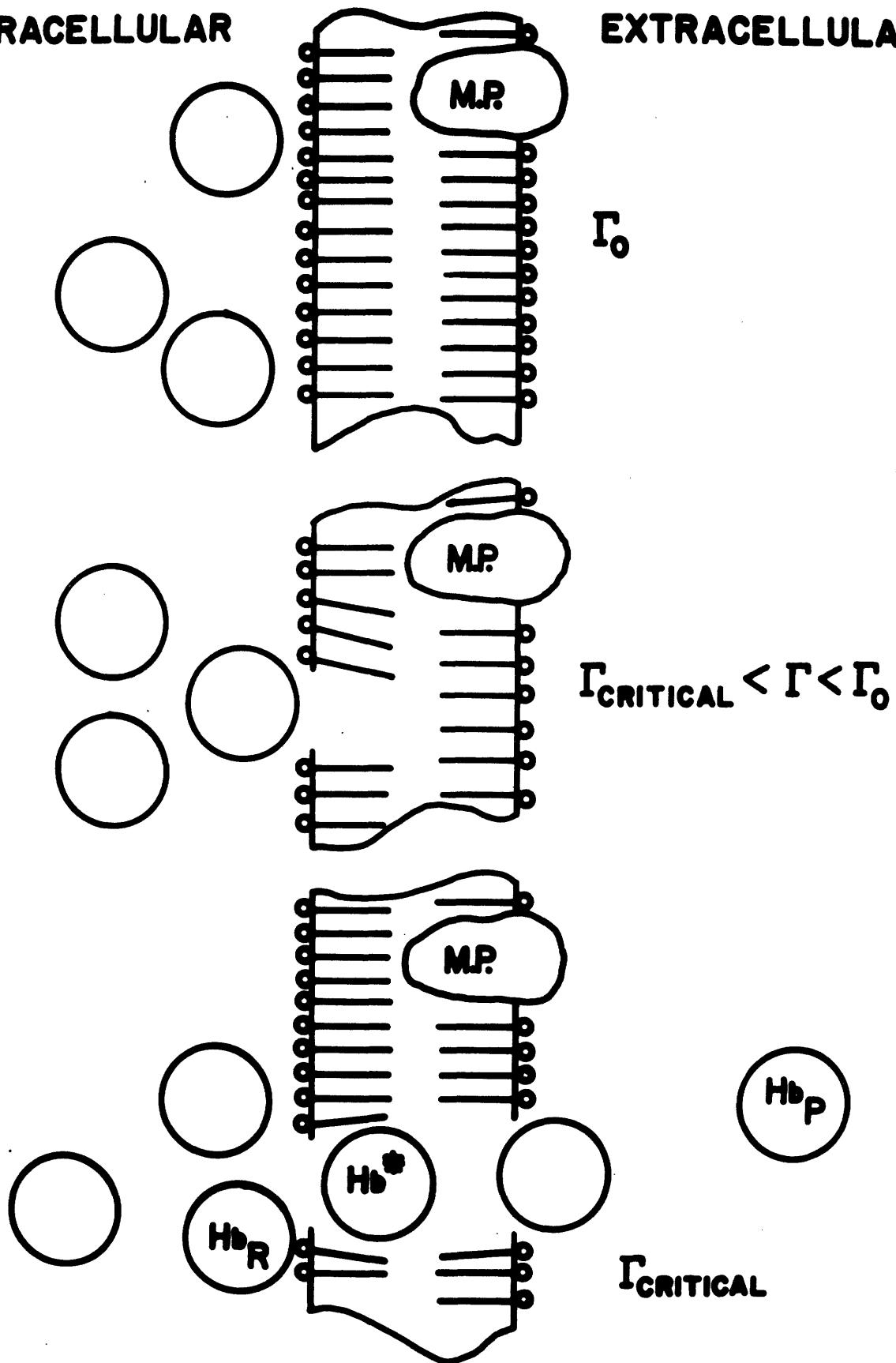
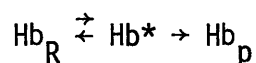


Figure 5.11 Schematic of the Hemolysis Process.

has decayed to a value intermediate between Γ_0 , the initial surface concentration and Γ_{critical} . The membrane is still an effective barrier. At the bottom is the case in which the critical minimum lipid concentration has been reached and hemoglobin rapidly diffuses out of the cell.

To obtain the full hemolysis reaction rate equation, an absolute rate approach is applied again. The intracellular hemoglobin molecules are the reactant molecules Hb_R , the molecules in the process of passing through the membrane are in the activated state Hb^* , and those in the extracellular medium are "product" molecules Hb_p . The reaction can be expressed as



and the reaction rate as

$$(5.50) \quad \frac{-d[\text{Hb}_R]}{dt} = [\text{Hb}_R] \cdot \nu \cdot \exp \left[\frac{-\Delta G_{\text{Hb}}^{\circ'}}{KT} \right]$$

where $\Delta G_{\text{Hb}}^{\circ'}$ is the activation free energy per molecule for passage of the hemoglobin molecule through the membrane.

When Γ_{critical} is reached, the reactant molecule Hb_R can be activated to a Hb^* molecule which is one within a "pore" created by the free surface area left when lipid diffuses away. The free energy associated with this activated molecule must be related to the free energy of dissolution of lipid. If the lipid were not diffusing away, the appearance of a hemoglobin molecule within the membrane would be very unlikely. The activation energy for passage of the hemoglobin

molecule through the membrane may be estimated by equating this energy to the amount of free energy needed to create the pore. A highly condensed black lipid film constituting an artificial membrane will have an effective polar group diameter of 8\AA for lecithin molecules [67]. The hemoglobin molecule, on the other hand has an effective diameter of 64\AA . The area ratio is therefore of the order

$$\left(\frac{64}{8}\right)^2 = 64$$

and since there is a bilayer, approximately 128 lipid molecules would have to be removed from the membrane to create a suitable "pore". This example is given to illustrate relative scales of the two types of molecules and to show why the energies of the activated hemoglobin molecule and the desorbing lipid should be related. To satisfy a general case without specifying the exact number of lipid molecules necessary to achieve hemoglobin activation, the number will be called m and the corresponding free energy for hemoglobin activation per molecule should be

$$(5.51) \quad \Delta G_{\text{Hb}}^{\circ'} = m \left[\Delta G_{\text{desorption}}^{\circ'} - \int_{\gamma_0}^{\gamma} \frac{d\gamma}{\Gamma_w} \right]$$

This interpretation retains the information in the term

$$(5.52) \quad \int_{\gamma_0}^{\gamma} \frac{d\gamma}{\Gamma_w}$$

which by way of the Gibbs-Duhem relation will link the changes in the surface energy to the hemolysis rate.

The concentration of Hb_R within the cell will be important in determining $[\text{Hb}^*]$ but $[\text{Hb}_R]$ does not change until the instant Γ_{critical} is achieved and therefore is not a variable.

The hemolysis rate equation is thus of the form

$$(5.53) \quad \frac{d(\%H)}{dt} = \Theta \left(\frac{D}{L^2} \right) \exp \left(\frac{-m \cdot \Delta G_{\text{desorption}}^{\circ'}}{KT} \right) \cdot \exp \left(\frac{-m \int_{T_0}^T \frac{\sigma}{\Gamma_w} dT}{KT} \right) \cdot \exp \left(\frac{-m \int_{\mu_w^0}^{\mu_w} d\mu_w}{KT} \right)$$

The Θ is included to modify the equation because the right-hand side of the equality was derived for the hemolysis of a single cell and the left side has been written as a percent hemolysis. Percent hemolysis is obviously based on the behavior of the entire red cell population which has experienced the perturbation. The meaning of the parameter Θ will be discussed below and in the next chapter.

It is well known that cell populations possess a distribution of properties. Examples for the red cell include surface area and volume distributions [64] and distributions of ion permeability [29]. It is therefore not unreasonable to assume that Γ_0 , the surface concentration of cell lipid before a perturbation is applied, would also have some distribution function; normal, gaussian or otherwise. Since the cells are all in the same suspending medium, the mechanism by which all of the cells could be in thermodynamic equilibrium with the same external concentration of lipid would be that there is a distribution of standard free energies of desorption within the population.

Figure 5.12 describes the consequences of accepting the hypothesis

ISOTHERMAL, OSMOTIC PERTURBATION

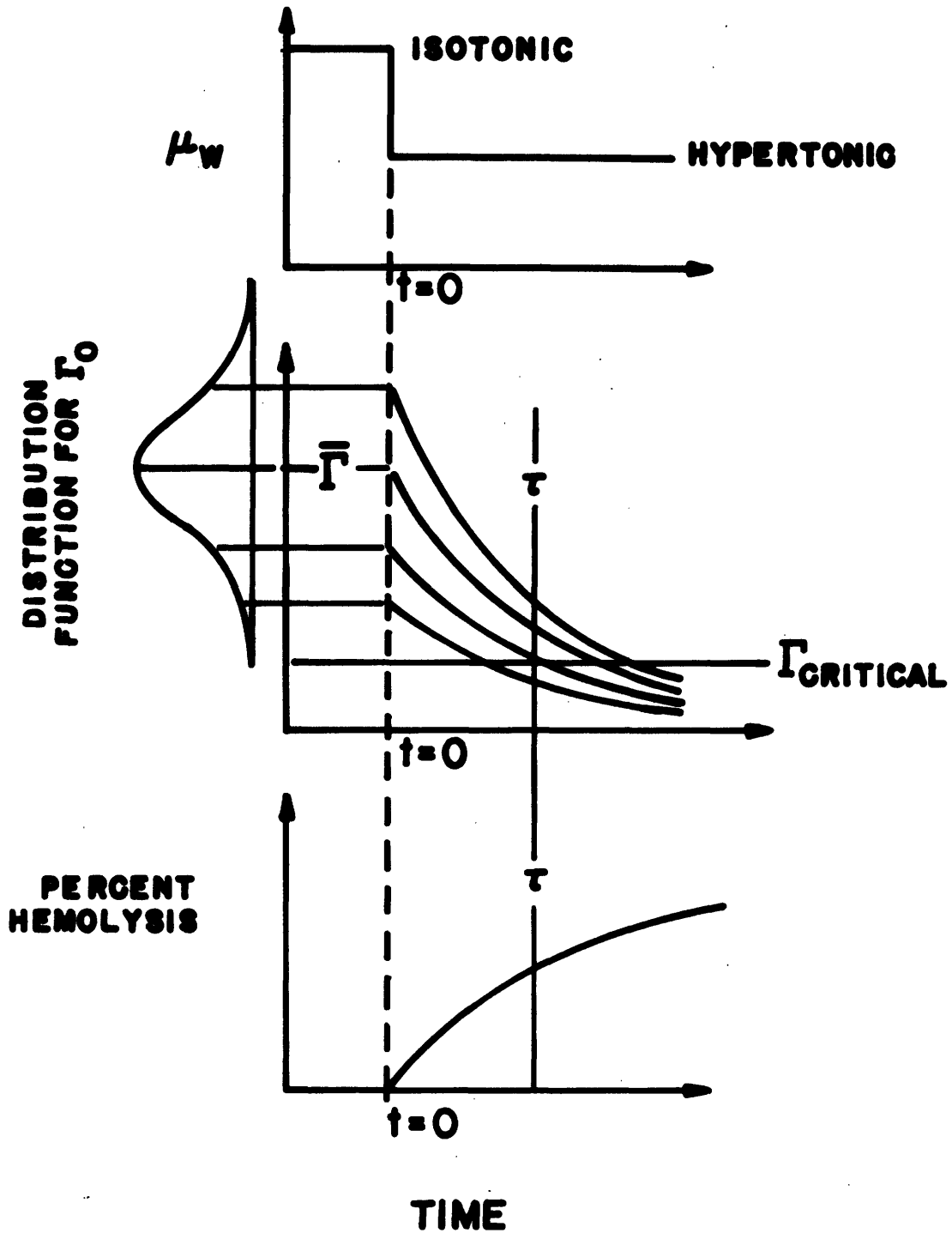


Figure 5.12 Schematic Transformation from the Rate of Loss of Lipid from an Individual Cell to the Percent Hemolysis for the Entire Cell Population.

that there is a distribution of standard free energies and therefore a distribution of initial lipid concentration, Γ_0 . The top part of this figure shows the step decrease of water activity of the extracellular solution when packed red cells in isotonic medium are injected into a hypertonic NaCl solution. The middle part of the figure shows the theoretical response of the cell population to such an isothermal, osmotic perturbation. The cell population has some distribution of initial lipid surface concentration Γ_0 , as shown schematically to the left of the ordinate. When the cells are injected into the hypertonic sodium chloride solution, the standard activation free energy of desorption is "instantaneously" lowered because the water chemical potential is changed in a quasi-stepwise fashion in the mixing chamber of the apparatus (see equations 5.47, 5.53). This causes a release of lipid as each cell approaches a new equilibrium value of Γ_{LPS} . As equation 5.47 predicts the decay of Γ to a lower level is a first order response and has a characteristic time $\tau = L^2/D$. The net result is that the cells are all responding with the same time constant but starting from different absolute levels. This means that some of the cells reach the critical concentration $\Gamma_{critical}$ very quickly, whereas others would require an exceedingly long period to reach this low level due to the decreasing magnitude of the derivative $\frac{d\Gamma}{dt}$ at longer times. As each cell in the population passes below the critical value of Γ , it hemolyzes. This means that the middle sketch for lipid loss in the population can be transformed to a hemolysis history as shown in the bottom sketch.

Calculation of the rate of hemolysis from the rate of lipid

loss in a strict mathematical fashion will not be attempted. Such an analysis would involve assuming a distribution function for the surface concentrations of lipid throughout the population and then performing a transformation by way of the model rate equation $\frac{d\Gamma}{dt}$ for determining the fraction of the total number of initial cells that had instantaneous Γ values less than or equal to Γ_{critical} . This fraction is equivalent to the fraction hemolyzed.

The parameter Θ should not modify the free energy nor the basic characteristic time. Rather, it is a parameter reflecting how far removed $\bar{\Gamma}_0$, the mean initial surface lipid concentration, is from the critical concentration Γ_{critical} . It would also take into account the distribution of $(\Gamma_0)_i$ about $\bar{\Gamma}_0$.

The data for isothermal, osmotic perturbation presented in Chapter 4 is linear for times of interest (less than one minute) which means from equation 5.53 that Θ has no time dependence within this same time domain.

It is therefore assumed that the hemolysis rate equation as shown in equation 5.53 is specific enough for present purposes. Significantly, the form of the hemolysis rate equation is identical to the lipid release rate equation with the introduction of the parameters Θ and m as the only differences.

Discussion and Conclusions

This chapter began with evidence suggesting that disturbances of various kinds in the red cell suspending medium can cause hemolysis. These disturbances can take the form of the presence of neutral absorbent addition to the medium, increased ionic strength and temperature drops. Hemolysis in these cases appears to be preceded by the loss of lipid material from the cell membrane. Some of the lipid is superficial in that it can be washed away without causing significant hemolysis.

The cell membrane is a dynamic structure consisting of a bilayer of lipid material with associated membrane proteins. The material within the membrane is dependent not only on its own characteristics but also on the state of its environment for determining whether the material remains within the membrane or is desorbed.

Kinetic models for lipid loss and hemolysis have been postulated based on absolute rate theory. The dissolution of lipid is comprised of two parts, a desorption of the molecule followed by the rate determining step of diffusion away from the membrane. A Gibbs-Duhem relation was derived for the surface phase of the membrane. Changes in the environment can affect the surface energy and hence the desorption energy of dissolution. These changes affect the amount and rate of lipid desorption but not the characteristic time.

In deriving the Gibbs-Duhem equation and using it in conjunction with the rate equations, the apparent coupling of thermal and osmotic

perturbation modes of damage is dissected to reveal the two factors responsible for each of these modes of damage. These terms can be separated as shown below

$$(5.54) \quad \text{rate} = C_2 \left(\frac{D}{L^2}\right) \exp\left(\frac{C_3(-G_{\text{desorption}}^{\circ})}{KT}\right) \exp\left(\frac{C_3 \int_{T_0}^T -\sigma/\Gamma_W dT}{KT}\right) \cdot \exp\left(\frac{C_3 \int_{\mu_W^{\circ}}^{\mu_W} -d\mu_W}{KT}\right)$$

(C_2 and C_3 are constants appropriate to lipid loss or hemolysis.)

This equation, then, represents a starting point for predicting the rates of lipid release and hemolysis for either uncoupled perturbation mode: isothermal, osmotic ($dT=0$) or iso-osmotic, thermal ($d\mu_W=0$). This single differential equation form is especially useful for the case of simultaneous variations in μ_W and T such as would occur for freezing and thawing.

For the first time a thermodynamic property has been identified as part of the driving force for lipid loss and hemolysis during temperature drops. The change in surface energy represented by the term $-(\sigma/\Gamma_W)dT$ shows that the surface entropy of the membrane is an important parameter determining the net rate of the reaction. There is therefore a thermodynamic driving force for thermal shock.

The Arrhenius form of the rate equation is applicable as was expected from the determination of rate equations for other biological

systems. The apparent activation energy derived experimentally for the hemolysis kinetics induced by isothermal, osmotic perturbation at 2.45m NaCl was 7.3Kcal/mole (see Chapter 4) between the temperatures of 273°K and 298°K. Lovelock obtained an apparent activation energy of 5.5Kcal/mole for the hemolysis kinetics induced by the presence of (2.0gm alumina)/(ml of cells) for temperatures between 278°K and 313°K [53]. Both of these energy values are well within the range expected of diffusion processes and much below the values associated with enzyme deactivation [75] and protein denaturation [39] (50-130Kcal/mole) (see appendix I for a tabulation of typical activation energies of various processes.)

It should be noted that lipid loss can result from two major types of perturbation even in the isothermal situation. Any perturbation is the introduction of a non-equilibrium condition. A perturbation favoring lipid release can occur by raising the surface energy of the lipids or by lowering the energy of the lipid in the bulk aqueous phase. In either case the characteristic time of the process will be the same unless $(\frac{D}{L^2})$ is altered. This is the reason it is not surprising that Lovelock noticed a time constant of approximately two or three minutes both in the release of lipid due to washing in lipid-less, fresh NaCl or by exposure to the neutral absorbent Al_2O_3 . A glance at the Chapter 4 results for the time dependence of hemolysis induced by isothermal osmotic perturbation shows a characteristic time of one to three minutes for a transition between a fast reaction rate and a slow rate. This result is expected from Figure 5.3 if the characteristic lipid release time is as determined by Lovelock. Probably, Lovelock's two experiments were examples of the two types of perturbation.

Insertion of cells into hypertonic NaCl causes a change in μ_w at the membrane surface resulting in an increase in surface energy. The presence of alumina on the other hand causes lipid to adsorb on the Al_2O_3 bead, effectively lowering the free energy of the lipid in the bulk aqueous phase. A final factor which might be applicable at times would be the presence of an agent capable of behaving as a catalyst. A catalyst reduces the barrier energy between the reactant and product but by definition does not change the equilibrium concentrations nor is it consumed during the reaction. Therefore, introducing a catalytic compound into the cell solution would not induce lipid release but would increase the rate of lipid release if a perturbation were imposed on the system.

In the next chapter a more detailed account of the consequences of this theoretical model is presented including quantitative comparisons of theory and experiment as further verification of the validity of the model.

Chapter 6

A Comparison of the Theoretical Consequences of the Thermodynamic Model with Experimental Data

In this chapter the differential equation for the hemolysis rate as derived from the theory presented in the last chapter will be applied to special cases representative of the two major freezing perturbation modes, osmotic and thermal shock, to determine whether the theoretical predictions from the model coincide with the experimental results obtained either in this thesis or in the literature.

The Isothermal, Osmotic Perturbation Mode

When cells are injected into various hypertonic sodium chloride solutions at $T=25^{\circ}\text{C}$, the general hemolysis rate equation

$$(5.53) \quad \frac{d(\%H)}{dt} = \Theta \left(\frac{D}{L^2} \right) \exp\left(\frac{-m \Delta G_{\text{desorption}}^{\circ'}}{KT} \right) \exp\left(\frac{-m \int_{T_0}^T \frac{\sigma}{\Gamma_W} dT}{KT} \right) \cdot \exp\left(\frac{-m \int_{\mu_W^0}^{\mu_W} d\mu_W}{KT} \right)$$

can be simplified to

$$(6.1) \quad \frac{d(\%H)}{dt} = C_2 \cdot \exp\left(\frac{-m \int_{\mu_W^0}^{\mu_W} d\mu_W}{KT} \right)$$

with

$$(6.2) \quad C_2 = \Theta \left(\frac{D}{L^2} \right) \exp\left(\frac{-m \Delta G_{\text{desorption}}^{\circ'}}{KT} \right) \exp\left(\frac{-m \int_{T_0}^T \frac{\sigma}{\Gamma_W} dT}{KT} \right)$$

The parameters Θ , D , L , m , and $\Delta G_{\text{desorption}}^{\circ'}$ are constants and $T=T_0=25^{\circ}\text{C}$ (T_0 is the reference state corresponding to $\Delta G_{\text{desorption}}^{\circ'}$ and this standard state was chosen to be $T_0=25^{\circ}\text{C}$, $P_0=1\text{ATM}$, for cells in normal saline.)

Since the water chemical potential per molecule is

$$(6.3) \quad \mu_W = \mu_W^\circ + KT \ln a_W$$

for isothermal conditions

$$(6.4) \quad d\mu_W = KT d(\ln a_W)$$

Therefore

$$(6.5) \quad \frac{d(\%H)}{dt} = C_2 \exp\left(\frac{-mKT \int_{a_W^\circ}^{a_W} d(\ln a_W)}{KT}\right)$$

$$= C_2 \exp(-m \ln(a_W/a_W^\circ))$$

For cells at the standard state in isotonic saline, $a_W^\circ = 0.995$ or to simplify, $a_W^\circ \simeq 1.0$ and

$$(6.6) \quad \frac{d(\%H)}{dt} = C_2 \exp(-m \cdot \ln a_W)$$

The isothermal, osmotic perturbation hemolysis rate data for 25°C, curve-fitted in Chapter 4 and given as equation 4.3 is

$$(4.3) \quad A = \frac{d(\%H)}{dt} = (9.078 \times 10^{-2}) \exp(-39.98 \cdot \ln a_W)$$

The forms obviously correspond very well. The fact that equation 4.3 was obtained from curve-fitting short-time kinetics for times less than or equal to one minute is probably a reflection of the fact that the transformation parameter Θ can be assumed independent of time within this region even though it accounts for many factors including $\bar{\Gamma}_o$, the distribution of Γ_o , $\Gamma_{critical}$ and the first order decay of Γ_{LPS} .

It is interesting to note that if the parameter m were equated numerically to the constant obtained experimentally in equation 4.3, the implication is that approximately 40 molecules of lipid ("lipoprotein species", LPS) must leave the membrane to allow a hemoglobin molecule to pass through the porous membrane during hemolysis. Assuming a highly condensed membrane, and complete loss of both sides of the bilayer, a rough estimate of the maximum number of molecules needed for hemolysis derived in the last chapter was 128 lipid molecules. The theoretical model does not predict that m should change, but the low temperature data for osmotic perturbation shown in Figure 4.11 yielded a curve-fitted value for m of 26.70. This suggests that the number of lipid molecules necessary to leave the membrane per hemoglobin molecule passing through has been reduced from 40 at 25°C to approximately 27 at 0°C. Experimentally the value of m remained constant for temperature variations between 0°C and -11°C. This may represent a change from a disordered to an ordered state for the membrane at approximately 0°C, thereby preventing further changes in m . The matter of phase changes within a red cell membrane is a controversial issue [55,77]. This subject of the number of molecules necessary to create a "pore" for hemoglobin flux arises again in dealing with thermal shock experiments which are discussed in the next section.

The Iso-osmotic, Thermal Perturbation Mode

Once again the analysis will begin with the general hemolysis rate equation which will be appropriately modified to match the specific conditions that occur during the thermal shock type of experiments.

In particular, it would be interesting to compare the dependence of thermal shock hemolysis on the initial temperature and the magnitude of the temperature drop. Lovelock performed this type of experiment holding constant the hypertonic solution concentration (1.0M NaCl), the exposure time prior to the temperature drop, and the cooling rate. His results were presented in Chapter 4 as Figure 4.13. The data of Morris et.al. as given in Figure 4.12 can be used to estimate the dependence of hemolysis on the concentration of sodium chloride during the exposure period prior to the temperature drop. The theoretical hemolysis rate equation will now be applied to simulate the situation for Morris' experiments and then for Lovelock's experiments.

Dependence of Thermal Shock Hemolysis on Exposure Concentration

Morris et.al. performed experiments in which the time of exposure to hypertonic sodium chloride was varied prior to subjecting the red cells to a temperature drop from +25°C to 0°C at 75°C/min. These data were presented as Figure 4.12, and one notices that these experiments were done at three concentrations: 1.0M, 1.2M, and 1.5M NaCl. For any exposure time chosen, the amount of damage produced is greater at the higher concentrations. Regardless of the concentration level, maximum damage occurs at an exposure time of five minutes. This suggests that the system behaves with a characteristic time response which is independent of the concentration; the concentration only determines the magnitude of the damage. The concept of a characteristic time is very much in keeping with the models developed

in the previous chapter. Therefore it is expected that the exposure time hemolysis data could be normalized with respect to $\%H_{\max}$ at five minutes and this would be a universal plot for the Morris series of experiments with the concentration dependence determining the absolute scale. The magnitudes of hemolysis are maximized at five minutes, so this exposure time is chosen for discussion since it will be easier to estimate accurate hemolysis data at this exposure time from Figure 4.12 to be used for comparison with theory.

The general hemolysis rate equation is repeated once again as the starting point of the analysis.

$$(5.53) \quad \frac{d(\%H)}{dt} = \Theta \left(\frac{D}{L^2} \right) \exp \left(\frac{-m \Delta G^{\circ'} \text{desorption}}{KT} \right) \exp \left(\frac{-m \int_{T_0}^T \frac{\sigma}{T_W} dT}{KT} \right) \cdot \exp \left(\frac{-m \int_{\mu_W^0}^{\mu_W} d\mu_W}{KT} \right)$$

Morris' experiments for exposure times of five minutes exceed the one minute limit where linearity of hemolysis versus time was observed for the osmotic perturbation experiments discussed in Chapter 4. Nevertheless, even if the temporal behavior is highly non-linear, it will be assumed that the behavior is reproducible from test to test so that temporal effects will not enter into a comparison of two thermal shock experiments if they are sampled after the same elapsed experimental time. For the same initial and final temperatures T_0 and T , the same exposure time, and the same cooling rate, the only factor determining the amount of damage after a given length of time

is μ_w because equation 5.53 can be written as

$$(6.7) \quad \%H = C_3 \cdot \exp\left(\frac{-m \int_{\mu_w^0}^{\mu_w} d\mu_w}{KT}\right)$$

exactly as in the osmotic perturbation experiment, but for a different value of C_3 because of the temperature change. As before, this can be simplified to

$$(6.8) \quad \%H = C_3 \exp(-m \ln a_w)$$

or equivalently

$$(6.9) \quad \%H = C_3 (a_w)^{-m}$$

where $a_w^0 \approx 1.0$ has been assumed again.

Estimates of Morris' data are

30% hemolysis at 1.0M ($a_w=0.9661$)

37% hemolysis at 1.2M ($a_w=0.9591$) and

50% hemolysis at 1.5M ($a_w=0.9482$).

A test fit of these data in the form

$$(6.10) \quad y = ax^b$$

yields values of C_3 and m in the hemolysis equation. The fitting program returns a correlation coefficient of $r=0.99$ and the values of the constants are

$$(6.11) \quad C_3=11.78$$

and

$$(6.12) \quad m=27.23$$

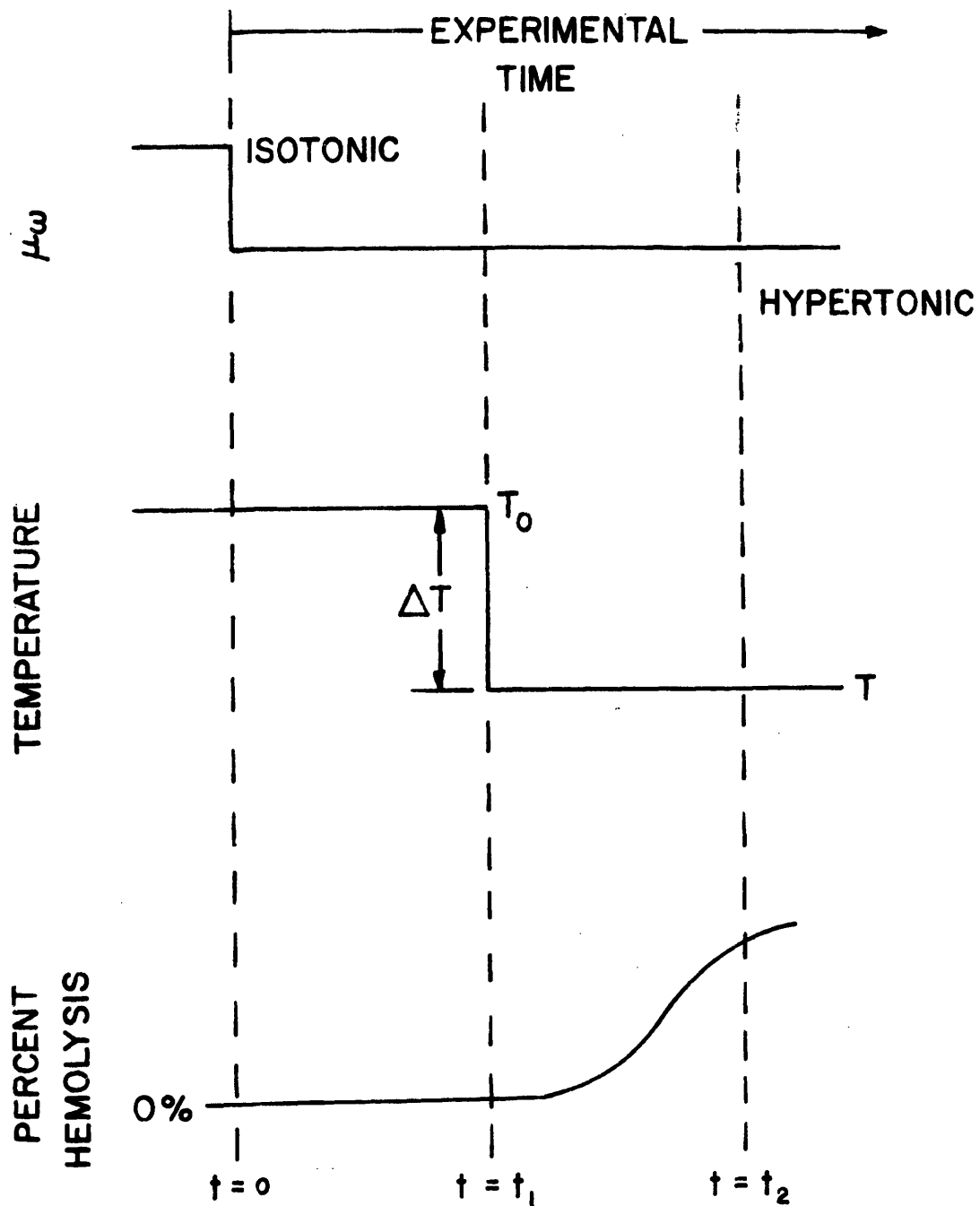
The high correlation coefficient means that the assumed form of the equation is a very good one, so the general hemolysis equation can predict concentration dependence both for osmotic perturbation and

when a hypertonic exposure is used for thermal perturbation experiments. The value of m , the apparent number of lipid molecules/hemoglobin molecule leaving the surface at hemolysis, is approximately 27. This number matches that obtained for osmotic perturbation alone at the low temperature range (262°K to 273°K) and suggests that the thermal shock hemolysis obtained by Morris would have occurred primarily at the lower temperatures close to 0°C rather than at the higher temperatures where m is larger. The results for the thermal shock kinetics obtained from the thesis apparatus and presented in Figures 4.15 and 4.16 reveal that thermal shock hemolysis does not occur at the higher temperatures; it is not apparent until the temperature has reached approximately +3°C.

Dependence of Thermal Shock Hemolysis on Initial Temperature and the Magnitude of the Temperature Drop

The results obtained by Lovelock revealing the effects of the initial exposure temperature and the magnitude of the temperature drop were based on the following experimental constraints: the exposure time prior to thermal shock was always five minutes, the hypertonic exposure concentration was always 1.0M NaCl and the cooling rate was rapid and invariant.

Consider Figure 6.1 to be a representative history of a thermal shock experiment. The top schematics show the thermal and μ_w histories, the bottom sketch the hemolysis history for the experiment. The thermal perturbation has been assumed instantaneous to simplify the situation,



$$\int_0^{\%H} d(\%H) = \int_0^{t_1} \left[\frac{d(\%H)}{dT} \right]_{T=T_0} dT + \int_{t_1}^{t_2} \left[\frac{d(\%H)}{dt} \right]_{T=T} dt$$

Figure 6.1 Water Chemical Potential, Temperature, and Hemolysis Histories for an Iso-osmotic, Thermal Perturbation Experiment.

because this assumption delineates only two time zones Δt_1 and Δt_2 instead of three which would be needed if the cooling rate were finite. In the first time segment $T = T_o$ and the situation is solely an osmotic perturbation experiment because

$$(6.13) \quad \int_{T_o}^{T_o} \frac{\sigma}{\Gamma_w} dT = 0$$

For a five minute exposure to these conditions (1.0M, 1.2M, 1.5M NaCl) there is negligible hemolysis (see Figure 4.2) and this is shown in the bottom sketch of Figure 6.1. Therefore the hemolysis equation will be evaluated at the final temperature T.

The hemolysis equation can be stated as

$$(6.14) \quad \%H = C_4 \cdot \exp\left(\frac{-m \int_{T_o}^T \frac{\sigma}{\Gamma_w} dT}{KT}\right)$$

for the hemolysis appearing at T as a result of the temperature drop, where

$$(6.15) \quad C_4 = \left(\frac{D}{L^2}\right) \exp(-m \ln a_w) \exp\left(\frac{-m \Delta G_{\text{desorption}}^{\circ}}{KT}\right) \cdot \left[\int_{t_1}^{t_2} \Theta(t) dt\right]$$

Once more $a_w^{\circ} \approx 1.0$ has been assumed, a_w corresponds to 1.0M NaCl, and a general form for the time behavior (here lumped in the Θ transformation parameter) has been assumed to be reproducible from one run to the next.

An estimate must now be made for the temperature dependence of the term (σ/Γ_w) so that the integral in the thermal shock hemolysis equation

can be evaluated. Recall that according to the definition of the red cell membrane surface as the thermodynamic system, the quantities γ and Γ_W were assigned values for a surface phase which is essentially water. Thus the properties of water are germane. Johansson and Eriksson [78] were able to determine the variation of the surface tension of water with respect to temperature. From the Gibbs-Duhem relation

$$(5.25) \quad d\gamma = -\sigma dT - \Gamma_W d\mu_W$$

and at constant water chemical potential

$$(6.16) \quad \sigma = -\frac{d\gamma}{dT}$$

which is the quantity measured by Johansson and Eriksson. A best fit for their data was

$$(6.17) \quad -\frac{\Delta\gamma}{\Delta T} = K_1 + K_2 \cdot t$$

where

$$K_1 = 0.1385 \pm 0.0011 \text{ dyne/cm } ^\circ\text{C}$$

$$K_2 = (8.90 \pm 0.46) \times 10^{-4} \text{ dyne/cm } (^\circ\text{C})^2$$

$$t = \text{degrees Celsius}$$

Equation 6.17 was used to convert to an absolute temperature fit. At $t = 10^\circ\text{C}$, $T = 283.15^\circ\text{K}$ and $\sigma = 0.1474$. At $t = 35^\circ\text{C}$, $T = 308.15^\circ\text{K}$ and $\sigma = 0.1697$, therefore

$$(6.18) \quad \sigma = (8.92 \times 10^{-4}) T - 0.1050$$

where T is in degrees Kelvin. The experimental curve shows no anomalies from $+5^\circ\text{C}$ to 40°C so it should be valid over the temperature region Lovelock used in his thermal shock experiments. It will be supposed that the form of the surface entropy per unit area at the membrane is

of the form

$$(6.19) \quad \sigma = aT - b$$

but the values of a and b obtained for pure water will not be imposed as constraints on the membrane system.

The general equation for thermal shock with this assumed form for the the surface entropy is

$$(6.20) \quad \%H = C_4 \exp \left(\frac{-m}{KT} \left\{ \int_{T_0}^T \frac{aTdT}{\Gamma_w} - \int_{T_0}^T \frac{b dT}{\Gamma_w} \right\} \right)$$

Assuming that Γ_w is independent of temperature and defining

$$(6.21) \quad \alpha = \frac{a \cdot m}{\Gamma_w K}$$

$$(6.22) \quad \beta = \frac{b \cdot m}{\Gamma_w K}$$

$$(6.23) \quad \Delta T = T_0 - T$$

and

$$(6.24) \quad \bar{T} = \frac{T_0 + T}{2}$$

the hemolysis equation is

$$(6.25) \quad \%H = C_4 \cdot \exp \left(\frac{-\beta \cdot \Delta T}{T} \right) \cdot \exp \left(\frac{\alpha \cdot \Delta T \cdot \bar{T}}{T} \right)$$

The magnitudes of ΔT are small as compared to the absolute temperature T. Typical values would be $\Delta T \leq 30^\circ\text{K}$ and $T \approx 250^\circ\text{K}$, which makes the assumption of $\left(\frac{\bar{T}}{T}\right) \approx 1.0$ a good approximation, especially

when T is large and ΔT small. For $(\frac{T}{T_0}) \approx 1.0$, equation 6.25 now contains a term which should be relatively independent of the absolute temperature. This term is

$$\exp (\alpha \Delta T)$$

The data from Lovelock's work for smaller values of ΔT , Figure 4.13, have been replotted as Figure 6.2 with $\log(\%H)$ as a function of ΔT for the three initial exposure temperatures of $T_0 = 273^\circ K$, $T_0 = 293^\circ K$, and $T_0 = 303^\circ K$. The results were curve-fitted in the form

$$(6.26) \quad \%H_{T_0, i} = \epsilon_i \exp (\eta_i \cdot \Delta T)$$

for $\%H \leq 20\%$. The three equations are

$$(6.27) \quad \%H_{303^\circ K} = (0.1184) \exp (0.277 \Delta T)$$

$$(6.28) \quad \%H_{293^\circ K} = (0.3964) \exp (0.262 \Delta T)$$

$$(6.29) \quad \%H_{273^\circ K} = (1.420) \exp (0.268 \Delta T)$$

It therefore appears that η is fairly constant and that a term such as

$$\exp (\alpha \cdot \Delta T)$$

does exist. A first approximation for α would be

$$(6.30) \quad \alpha = \bar{\eta} = 0.269$$

Suppose, at constant ΔT , the relative amount of hemolysis produced by starting from two different initial temperatures $T_{01} = 303^\circ K$ and $T_{02} = 273^\circ K$ are compared. The ratio of the two

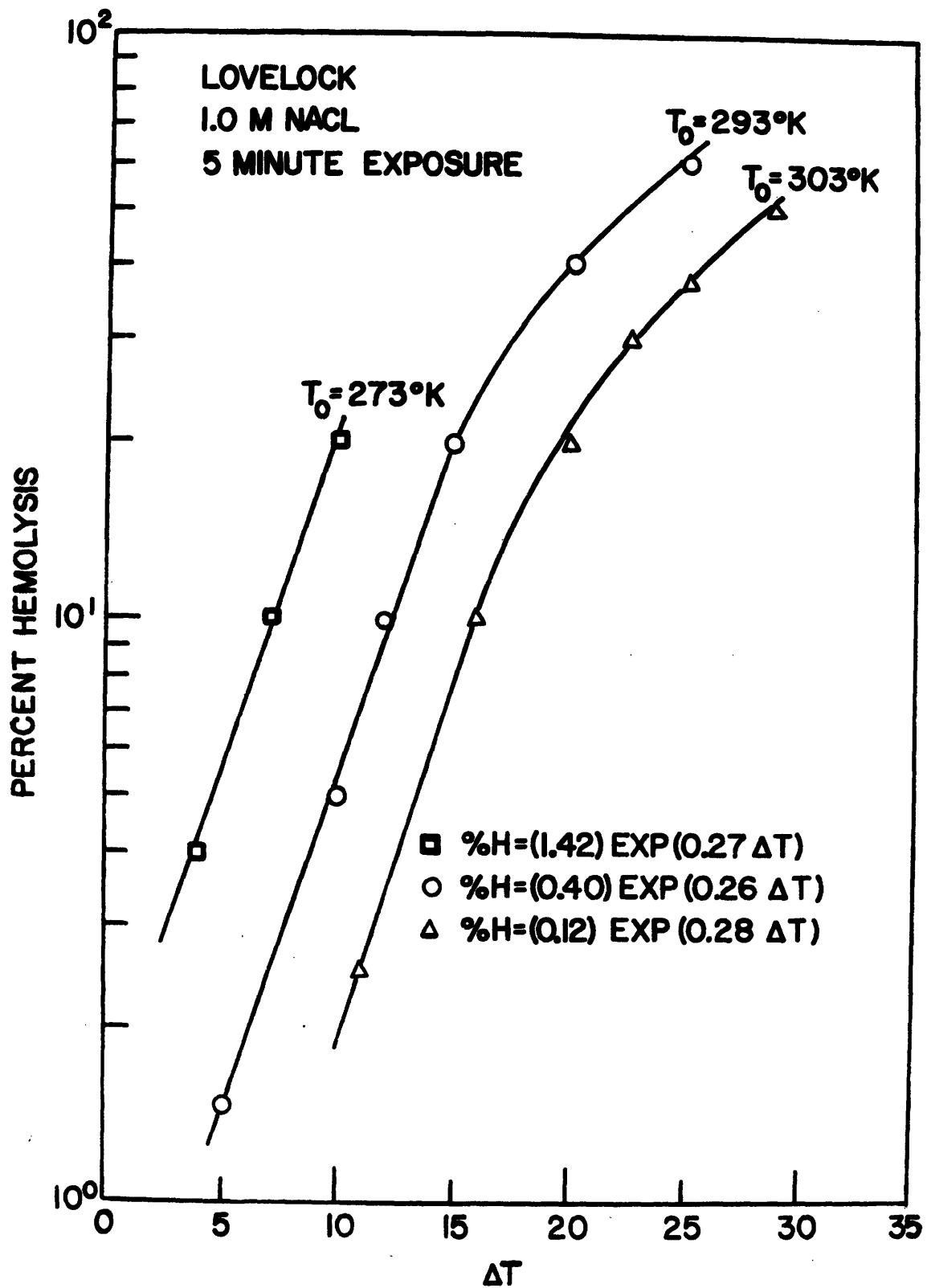


Figure 6.2 Thermal Shock Hemolysis as a Function of Initial Temperature and Magnitude of the Temperature Drop, Replotted and Curve-fitted (reproduced from reference [27]).

hemolysis cases, assuming α is a constant and

$$\left(\frac{\bar{T}}{\bar{T}}\right) \approx 1.0$$

is

$$(6.31) \quad \left(\frac{\%H_{T_{o1}}}{\%H_{T_{o2}}}\right)_{\Delta T} = \frac{\exp\left(\frac{-\beta \cdot \Delta T}{T_{o1} - \Delta T}\right)}{\exp\left(\frac{-\beta \cdot \Delta T}{T_{o2} - \Delta T}\right)} = \exp\left[-\beta \cdot \Delta T \left\{\frac{(T_{o2} - \Delta T) - (T_{o1} - \Delta T)}{(T_{o2} - \Delta T) \cdot (T_{o1} - \Delta T)}\right\}\right]$$

For $\Delta T = 10$, starting from initial temperatures of $T_{o2} = 303^\circ\text{K}$ and $T_{o1} = 273^\circ\text{K}$, Lovelock found $\%H_{T_{o1}} = 20$, and $\%H_{T_{o2}} = 2$ respectively.

Substituting these values into the equation above, a value of β is derived

$$(6.32) \quad \beta = -591.5$$

In the case of the experimentally determined values of a and b for the surface entropy of water

$$(6.33) \quad \left(\frac{b}{a}\right)_{\text{H}_2\text{O-He}} = \frac{0.1050}{8.92 \times 10^{-4}} = 117.71^\circ\text{K}$$

If the values $\alpha = 0.27$ and $\beta = -591.5$ are taken to be valid for thermal shock experiments, then

$$(6.34) \quad \frac{\beta}{\alpha} = \frac{\left(\frac{b \cdot m}{\bar{\Gamma}_w K}\right)}{\left(\frac{a \cdot m}{\bar{\Gamma}_w K}\right)} = \left(\frac{b}{a}\right)_{\text{thermal shock}} = \frac{-591.5}{0.27} = -2190.6^\circ\text{K}$$

Before proceeding further in discussing the meaning of the relative values of these ratios (b/a) for the cells in isotonic saline and cells undergoing thermal shock, some attention should be given to the significance of the magnitudes of the parameters α and β . For example, the numerical value of α can be used to derive a concentration of water within the surface phase. From equation 6.21 the surface concentration of water is

$$(6.21) \quad \Gamma_w = \frac{a \cdot m}{\alpha \cdot K}$$

where the value of a as given in equation 6.18 will be assumed to accurately describe water entropy temperature dependence whether the cells are in an isotonic medium or experiencing thermal shock. From the results of equation 6.12 and the thermal shock kinetic data shown in Figure 4.15, it would appear as if thermal shock hemolysis occurs at or near the minimum temperatures achieved and hence m is chosen to be 27. The surface concentration of water is derived,

$$(6.35) \quad \Gamma_w = \frac{(8.92 \times 10^{-4} \frac{\text{erg}}{\text{cm}^2 \cdot \text{K}^2}) 27}{(0.27 \text{ 1/}^\circ\text{K}) (1.38 \times 10^{-16} \frac{\text{erg}}{\text{K/molecule}})}$$

$$= 6.46 \times 10^{14} \text{ molecules/cm}^2$$

The value of the surface concentration of water at the interface of water and air saturated with water vapor at 20°C is given in reference [68] as

$$(6.36) \quad \Gamma_w = 1 \times 10^{15} \text{ molecules/cm}^2$$

This is based on the molecular size of the water and can be estimated by the formula

$$\begin{aligned}
 \Gamma_w &\sim (Mv)^{-2/3} \\
 (6.37) \quad &\sim \left[\frac{(6.02 \times 10^{23} \frac{\text{molecules}}{\text{mole}})}{(18 \text{ gm/mole})(1 \text{ cc/gm})} \right]^{2/3} \\
 &\sim 1.23 \times 10^{15} \text{ molecules/cm}^2
 \end{aligned}$$

The derived value of surface water concentration in equation 6.37 agrees to within a factor of two with the other estimates given above, which is an indication that the α value of 0.27 derived experimentally is meaningful.

In addition, the assumptions that the surface phase is primarily water and that a is the same for isotonic cells and thermally shocked cells, as well as the assumption that the hemolysis occurs at the lower temperatures can not be grossly inaccurate.

If the value of a is invariant from the isotonic to the thermal shock case, then equations 6.33 and 6.34 can be employed to reveal that

$$\begin{aligned}
 (6.38) \quad &\left[\frac{(b)_{\text{red cells thermal shock}}}{(b)_{\text{red cells in isotonic}}} \right] = \left[\frac{\left(\frac{b}{a}\right)_{\text{red cells thermal shock}}}{\left(\frac{b}{a}\right)_{\text{red cells in isotonic}}} \right] = \frac{-2190.4}{117.71} \\
 &= -18.61
 \end{aligned}$$

The temperature dependence of the entropy term is

$$(6.39) \quad \sigma_i = a_i T - b_i$$

whether the cell is in isotonic saline or experiencing thermal shock. The change in sign and increase in magnitude of b for cells subject to hypertonic conditions followed by a temperature drop, suggests that there must be a higher surface entropy associated with cells undergoing the temperature drop in hypertonic sodium chloride than there is associated with the surface entropy of red cells in isotonic saline. If this were true and the difference in entropy after a five minute exposure were a factor of 18 higher than for cells in isotonic saline, then red cells in isotonic saline should experience thermal shock damage that is significantly lower than for cells in 1.0M NaCl. In fact, there is no thermal shock damage found for red cells in isotonic saline as can be seen in Figure 3.2. It may be a general rule that thermal shock can not be produced in isotonic media for there is a lack of thermal shock damage to cells cooled under non-hypertonic conditions for bacteria as well as for red cells [11,79].

The difference between red cells in isotonic solutions and those in hypertonic solutions as viewed from the model for hemolysis kinetics presented in the last chapter, is that the cells in hypertonic solutions are experiencing a transient mass flux of lipid material away from the cell membrane in order to establish a new equilibrium condition between the membrane and its environment. The diffusion of lipid is an irreversible process and the instantaneous value of entropy generated within the membrane system as a result of lipid diffusion is

of interest. The production of entropy per unit volume can be calculated according to the equation given by Katchalsky and Curran [79] as:

$$(6.40) \quad \frac{\partial s}{\partial t} = - \text{Div } \vec{J}_s + \sigma$$

That is, the change of entropy per unit volume within the membrane surface phase per unit time is equal to the negative of the divergence of the entropy flux vector plus the amount of local generation within the volume. Relationships are given in the aforementioned reference for expressing the entropy flux and entropy generation parameters in terms of appropriate driving forces (in this case chemical potential gradients) and fluxes (mass fluxes).

An irreversible thermodynamic analysis therefore predicts that when a gradient in chemical potential is produced and a mass flux results, then local entropy will be generated and according to equation 6.40, unless the system entropy is transferred to the environment (i.e., $\text{Div } \vec{J}_s > 0$), the system entropy will be increasing with time. To carry the argument further, it is postulated that as lipid leaves the organic phase and enters the surface phase

$$\text{Div } \vec{J}_s < 0$$

(i.e., more entropy is entering the system than is transferred to the environment). Subsequently, the flux from the membrane diminishes, the chemical potential gradient may relax so that σ decreases while at the same time entropy is being transferred from the surface phase to the aqueous phase (i.e., $\text{Div } \vec{J}_s > 0$) which means the surface phase entropy per unit volume begins to decrease. If this were to be the case as the system relaxes by way of a mass flux, then at some point in time the entropy is maximized.

Recalling from the thermal shock hemolysis equation that the amount of damage due to this mode is proportional to

$$\exp\left(\frac{-m \int_{T_0}^T \sigma dT}{KT}\right)$$

the time corresponding to the maximization of σ would be the most dangerous period to subject the cells to a temperature drop. For minimum production of damage, either the cells must be taken through the temperature drop soon after the hypertonic exposure is first applied, or a suitable length of time must be allowed to pass so that the system can relax back to a state of chemical potential equilibrium,

$$(6.50) \quad \frac{\partial \mu_{LPS}}{\partial x} = 0$$

This effect could very likely be the cause of the minimum recovery obtained by Morris at exposure times of five minutes (Figure 4.12).

It should be noted that in returning cells to T_0 after they have been thermally shocked, the general hemolysis equation would predict lowering of the standard surface energy because

$$(6.51) \quad \left(-m \int_T^{T_0} \frac{\sigma}{\Gamma_w} dT\right) < 0$$

This tends to re-establish the higher activation energy for desorption which favors retention of lipid at the membrane. Of course if the cells are allowed to remain for long periods at the lower temperature T , then σ can relax back to a value comparable to σ^0 and the temperature change will produce very little change in the

surface energy. In either case (σ large or small), warming should produce no additional hemolysis. The experimental results of Lovelock show this to be true [52], warming back to the initial temperature produces no damage.

Chapter 7

A Technique for Computer Simulation of Freeze-Thaw Damage

Introduction

In Chapter 5 a thermodynamic model coupled with absolute rate theory yielded a general expression for the rate of hemolysis. This equation was further reduced in Chapter 6 to match the specific experimental constraints imposed for both major types of damage, osmotic perturbation and thermal perturbation. The qualitative agreement between theory and experiment is excellent and a quantitative comparison of arbitrary theoretical parameters (such as m) with the corresponding experimentally determined values has provided for a first-cut glimpse at quantitative detail for the physics of hemolysis at the membrane surface.

Specific experimental constraints were imposed as a part of the research work aimed at understanding osmotic shock and thermal shock in an attempt to delineate the separate effects of each. As viewed from the standpoint of the theoretical model, decoupling is not easily accomplished. This is especially true in the case of thermal shock where a mass flux of lipid from the membrane, induced by an osmotic stress, can produce a large amount of damage if the temperature drop occurs when the maximum surface entropy per unit area, σ_{\max} , is attained.

During the freezing process the constraints imposed on the membrane system are not the same as those used in the special cases of thermal and osmotic shock studies. In particular, heat and mass transfer are taking place simultaneously, which means that to predict correctly the total amount of damage by integrating the general rate equation,

$$\begin{aligned}
 \frac{d(\%H)}{dt} = & \left(\frac{D}{L^2}\right) \exp\left(\frac{-m \Delta G_{\text{desorption}}^{\circ'}}{KT}\right) \exp\left(\frac{-m \int_{T_0}^T \frac{\sigma}{\Gamma_w} dT}{KT}\right) \\
 (5.53) \quad & \exp\left(\frac{-m \int_{\mu_w^0}^{\mu_w} d\mu_w}{KT}\right)
 \end{aligned}$$

the instantaneous values of the surface entropy and chemical potentials must be known. As discussed in Chapter 5 during development of the thermodynamic model, a position within the membrane surface was chosen such that the change in surface free energy could be followed by the change in water chemical potential. The thermodynamic models for transmembrane water flux have shown that for cooling rates up to the range of 500-1000°K/min, the intracellular water is, to a good approximation, in equilibrium with the extracellular water because of rapid water transport [22, 44]. A closed form solution for water activity is therefore available for both sides of the membrane during these quasi-equilibrium freezing protocols:

$$\begin{aligned}
 \ln a_w = & 3.736 \times 10^3 \left(\frac{1}{T} - \frac{1}{T_0}\right) + 36.18 \cdot \ln \left(\frac{T}{T_0}\right) \\
 (7.1) \quad & + (0.1024) (T_0 - T) + (5.435 \times 10^{-5}) (T^2 - T_0^2)
 \end{aligned}$$

where $T_0 = 273.15^\circ\text{K}$ [22].

With a specified starting temperature and cooling rate $B = dT/dt$, the general rate equation can be numerically integrated for the freezing process down to a chosen minimum temperature, T_{\min} . At each time step, the temperature is known from the initial temperature and cooling rate. Once the temperature is known, the water activity is specified and a differential amount of damage can be calculated. By summing these

differentials, an integrated freezing damage can be obtained. The equation is similarly integrated at the chosen storage temperature T_{\min} for the simplified case for which T and a_w are fixed. Finally, the equation is integrated during the warming part of the protocol for a given warming rate W . In this manner, a prediction of the total amount of damage due to an arbitrarily specified protocol can be made. One is also able to separate out the relative amounts of damage accumulated during the three separate parts of the protocol:

$$(7.2) \quad \%H = \int_0^{\%H} d(\%H) = \int_{t_{\text{freeze}}} \frac{d(\%H)}{dt} dt + \int_{t_{\text{store}}} \frac{d(\%H)}{dt} dt + \int_{t_{\text{warm}}} \frac{d(\%H)}{dt} dt$$

Before presenting the computer simulation demonstrating the predictive use of the hemolysis rate equation, several important limitations of the equation must be brought to light.

These limitations are concerned with the temporal variations of two parameters in the general hemolysis rate equation. The first parameter is Θ , which was introduced to transform from the rate of lipid loss $\frac{d\Gamma_{\text{LPS}}}{dt}$ to the rate of hemolysis $\frac{d(\%H)}{dt}$. This parameter, based on a mean initial surface concentration $\bar{\Gamma}_0$ and a distribution function for the $(\Gamma_0)_i$ in the red cell population about $\bar{\Gamma}_0$, can be used to specify the total fraction of cells in the population that have reached Γ_{critical} and thus have hemolyzed. It is evident from matching the experimental hemolysis rate equation for osmotic perturbation (equation 5.53) and the general theoretical equation that for step changes in Γ_w , the Θ parameter is

time independent for periods up to one minute at 25°C, and longer for lower temperatures (see Figure 4.2). This time invariant behavior is apparently associated with the characteristic time necessary for the membrane to relax after the step change in Γ_w has been applied. If the change in Γ_w is not a step, but still rapid with respect to the characteristic diffusion relaxation time of the membrane (which for lipids release is on the order of 1-3 minutes), then the membrane will not be able to relax and it will not be able to distinguish between the step and the ramp change. For present purposes it will be assumed that θ is time independent for all rates of change of Γ_w away from Γ_w^0 . A detailed analysis of the transformation variable θ would define quantitative criteria on $\bar{\Gamma}_0$, $\Gamma_{critical}$, etc. for making this assumption.

The second parameter which could change with time is σ , the surface entropy per unit area. The analysis presented in the previous chapter suggested that the surface entropy could increase by a factor of 18 over the value for isotonic conditions when the cells had been exposed to 1.0M NaCl for 5 minutes. Thermal shock data have revealed a minimum recovery after a 5 minute exposure time prior to a temperature drop. A simple application of irreversible thermodynamics leads one to believe that this minimum recovery is associated with maximization of surface entropy at the time of the temperature drop. Until a more complete description of the σ time dependence is carried out, it is best to consider limiting cases in which σ is comparable to the isotonic value. This is equivalent to assuming that thermal shock is not a factor in freezing damage. There is no question that in neglecting this effect, the total damage is significantly underestimated. On the

other hand there are cases in which thermal shock is not important, and it is only for these cases that accurate predictions may be expected at the present time (see Figure 4.12).

Finally it should be stated once again that the model does not account for mechanical damage by the presence of ice, nor the dilution damage that might result from so-called posthypertonic hemolysis effects. Therefore the results to be presented will be designated as results for "limited damage" simulations.

Predicted "Limited Damage" Recovery for Various Cooling Rates
with a One Minute Storage Period

Figure 7.1 is representative of the thermal protocols which were simulated on the computer. To the left of the figure is a rapid freezing rate, a one minute storage period at the eutectic temperature of the binary sodium chloride-water solution, followed by a warming period. Several warming rates are shown to illustrate how the effect of warming rate can be studied after cooling at a single rate. The dotted protocols are for a slower cooling rate, to the one minute storage period at the eutectic temperature. The warming rates are again varied to study the effect of warming at this cooling rate. A complete scan of both cooling and warming rate effects is accomplished in this way. Note that the freezing protocol begins at a temperature of 273°K. Red cells in isotonic saline cooled from 298°K to 273°K suffer no damage, so this part of the protocol need not be introduced into the simulation. The general hemolysis rate equation assuming $\sigma = \sigma_{\text{isotonic}}$, can be written as

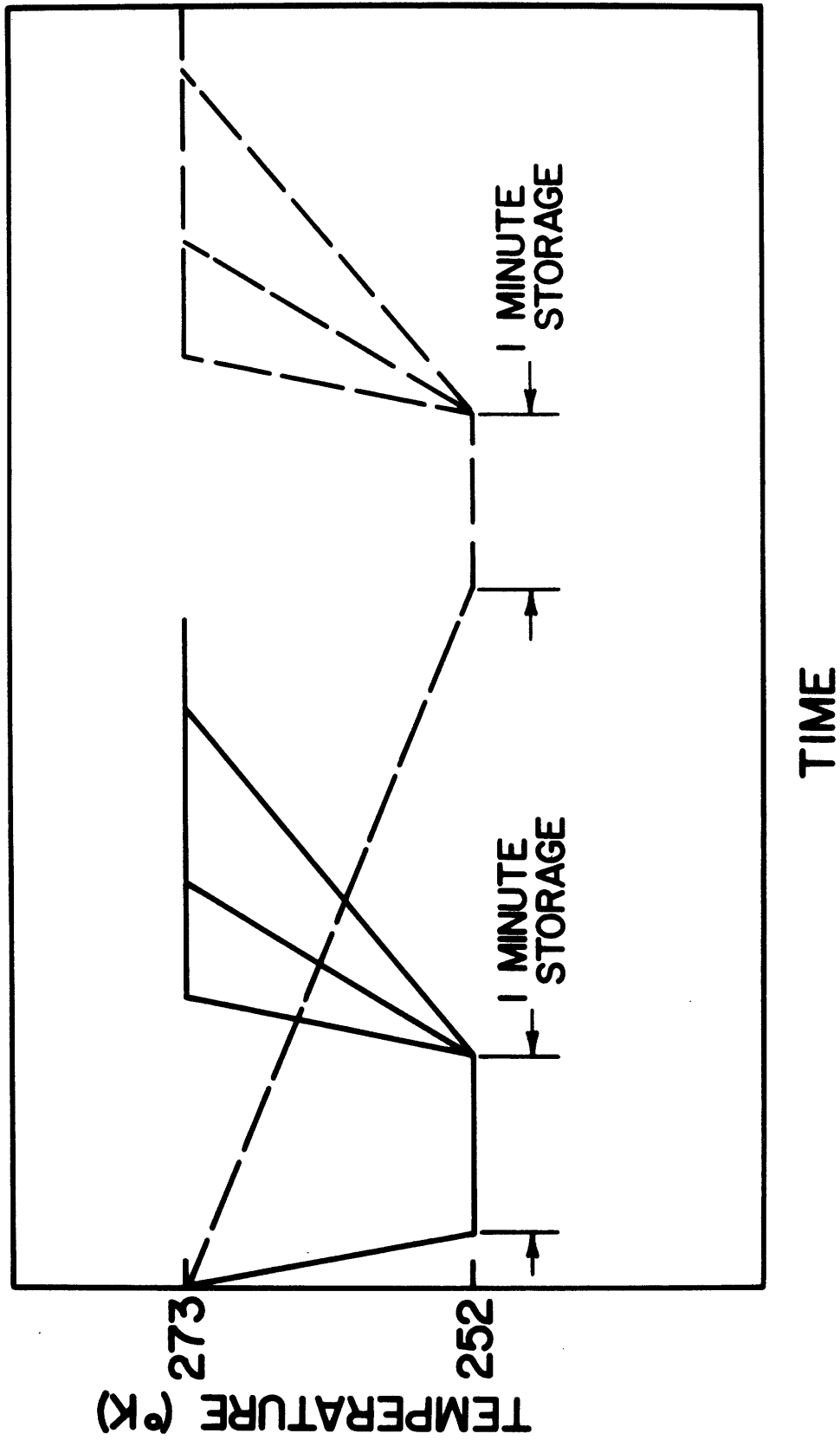


Figure 7.1 Examples of Freeze-Thaw Protocols Simulated on the Computer.

equation (4.4)

$$A = \frac{d(\%H)}{dt} = (9.115 \times 10^{-2}) \exp(-26.70 \ln a_w)$$

This equation was experimentally determined to hold for temperatures from 273°K down to 262°K. It is assumed that the lack of temperature dependence for this rate equation can be extended from 262°K to the eutectic temperature of 252°K. The storage period at the eutectic temperature is uniformly one minute. This short period should prevent nonlinearities in the rate equation due to time variations. The differential equation was numerically integrated on the Interdata Model 70 minicomputer of the M.I.T. Joint Computer Facility. The programs for this simulation and those to follow are in appendix J.

Figure 7.2 shows predicted red cell recovery percentage (100-%H) as a function of the log(cooling rate) for a variety of iso-warming rate (W) curves. The expected behavior for the so-called "solution effects" damage part of Mazur's dual damage theory of freezing injury [11] is clearly seen in these curves. Namely, the longer exposure times associated with slow cooling rates produces a great deal of osmotic damage. As the cooling rate increases, post freeze-thaw recovery also increases. This simulation predicts that for warming rates between +2°K/min and +1000°K/min, the most important range of cooling rates is approximately -1°K/min to -10°K/min. Diminishing returns are realized by increasing the rate another order of magnitude. Similar rate conclusions can be made for warming. Slow warming is detrimental. Increasing the warming rate from +1°K/min or +2°K/min to +10°K/min will significantly decrease the osmotic damage as modelled here for all cooling

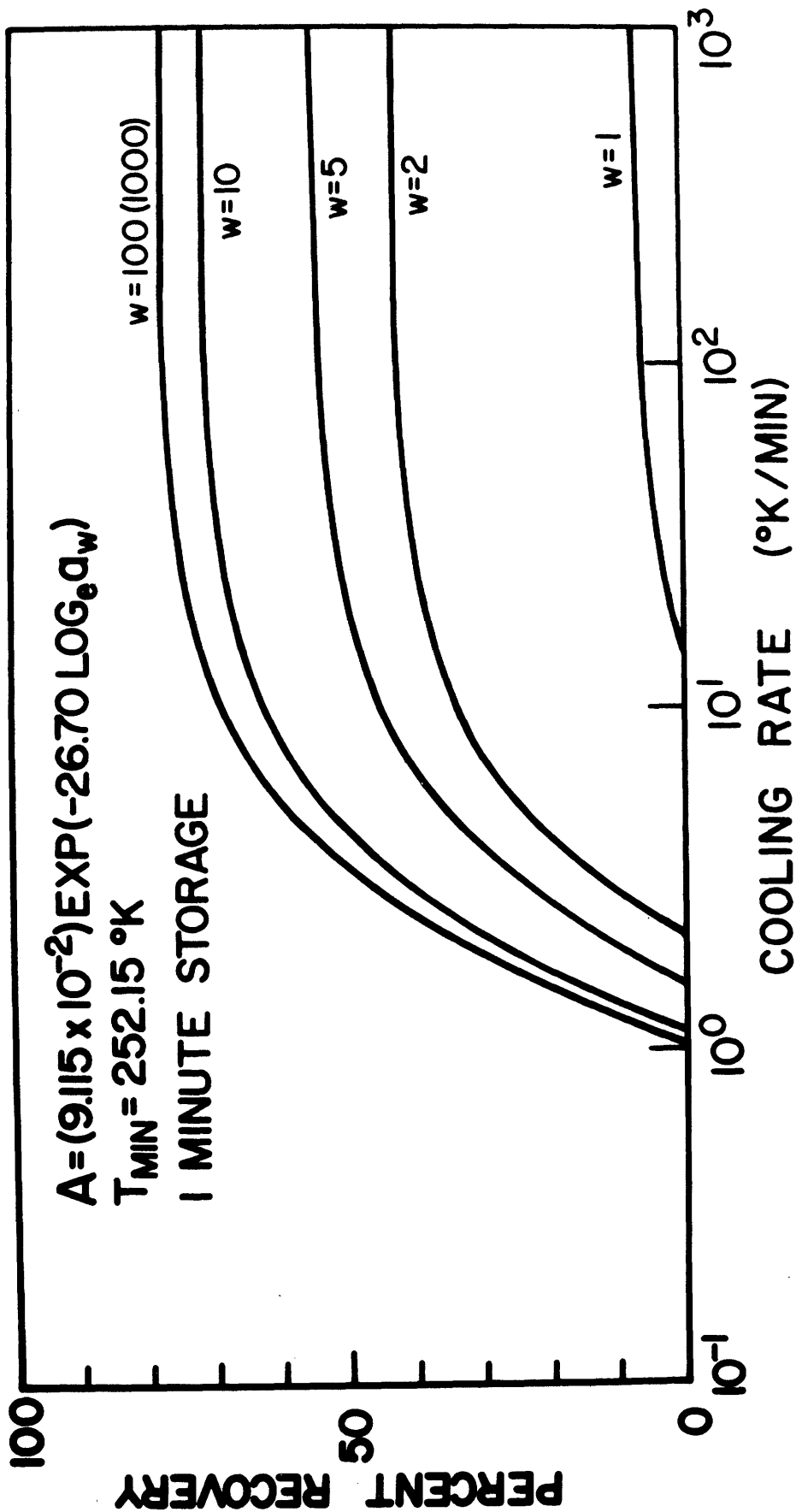


Figure 7.2 Predicted "Limited Damage" Percent Recovery for Erythrocytes as a Function of Cooling Rate for Various Constant Warming Rates.

rates. Increasing the warming rate to $+100^{\circ}\text{K}/\text{min}$ produces a marginal increase in recovery above a $+10^{\circ}\text{K}/\text{min}$ warming rate, whereas increasing the warming rate from $+100^{\circ}\text{K}/\text{min}$ to $+1000^{\circ}\text{K}/\text{min}$ produces a net increase in recovery of less than 1%.

Figure 7.3 contains some of the same information as Figure 7.2, but plotted to show the separate amounts of damage accumulated during the three parts of the thermal protocol for several cooling and warming rates. The left part of the figure shows accumulated damage as a function of temperature, as the temperature is reduced from 273°K to the eutectic temperature 252°K at cooling rates of $B = -1, -2, -5,$ and $-10^{\circ}\text{K}/\text{min}$. The freezing sequence is followed by a one minute storage during which the system is in an isothermal state at 252°K . The cells are then thawed from the eutectic temperature, back to 273°K at $+10^{\circ}\text{K}/\text{min}$. In one case the cells were thawed at $+1^{\circ}\text{K}/\text{min}$ (dotted line) for comparison with a thaw at $+10^{\circ}\text{K}/\text{min}$.

For cooling rates of $-1^{\circ}\text{K}/\text{min}$, the osmotic damage alone is enough to produce over 90% hemolysis by the time the eutectic temperature is reached. The remainder of the cells hemolyze before the one minute storage is over. Thawing plays no part in the outcome of these cells.

As the cooling rate is progressively increased, the amount of damage produced by the time the eutectic temperature is achieved is depressed considerably. Less than 10% hemolysis is expected at this temperature for cells cooled at $-10^{\circ}\text{K}/\text{min}$. All simulations show linearly increasing hemolysis during the storage because the system is isothermal and therefore a_w is constant. Since all storages were for

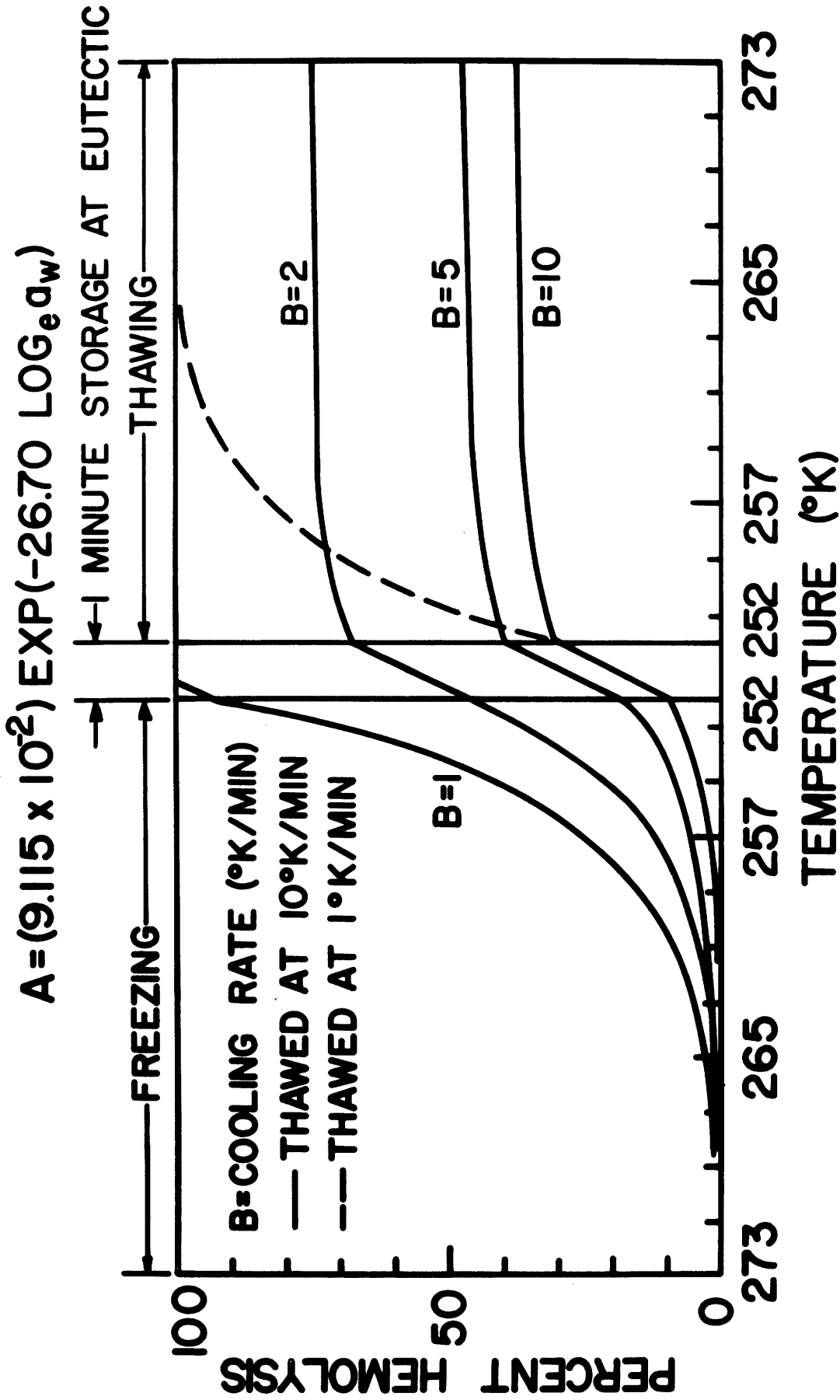


Figure 7.3 Predicted "Limited Damage" Percent Hemolysis as a Function of Temperature During Freezing, Storage, and Warming for Several Cooling and Warming Rates.

one minute, hemolysis during storage increased by a uniform amount of 21%. This is a significant amount of damage as compared to that during freezing at fast rates but relatively small when compared to cooling rates as low as $-1^{\circ}\text{K}/\text{min}$. For warming at $+10^{\circ}\text{K}/\text{min}$, the increase in damage during warming was approximately 7% hemolysis independent of the cooling rate. If a cell suspension cooled at $-10^{\circ}\text{K}/\text{min}$ and stored for one minute is thawed at $+1^{\circ}\text{K}/\text{min}$ (dotted line) instead of $+10^{\circ}\text{K}/\text{min}$, total hemolysis will result before the cells reach 265°K .

A Comparison of the "Limited Damage" Simulation with Experimental Freeze-Thaw Data for Erythrocytes

Ultimately, close agreement between simulated freeze-thaw damage and experimental data must rest on a model which includes all factors causing damage. The correct physio-chemical laws governing the inter-relationships between these factors must be determined and applied, and finally accurate quantitative data must be obtained to describe the relative importance of each factor.

The limited damage simulations performed on the computer have not included at least two known causes of freeze-thaw injury: posthypertonic hemolysis and thermal shock. No effort has been made to include post-hypertonic effects at present. Progress has been made in understanding the thermal shock phenomenon, but as discussed earlier, not enough is known about the variation of surface entropy with time to include it

in the computer model. It is therefore expected that the osmotic damage that has been modelled and quantified will produce a predicted damage that will be less than that obtained experimentally.

Figure 7.4 reveals that osmotic perturbation alone will not produce enough damage to match that found experimentally when cells are frozen at various rates. Percent recovery of the red cell population is plotted as a function of $\log(\text{cooling rate})$. The top curve is the computer simulation result for a one minute storage at the eutectic temperature of 252°K , followed by warming at $+100^{\circ}\text{K}/\text{min}$. As can be seen from Figure 7.2, this curve will not change much for variations in the warming rate between $+10^{\circ}\text{K}/\text{min}$ and $+1000^{\circ}\text{K}/\text{min}$ so it can be matched with experimental data taken over a wide range of warming rates. The curve at the bottom of the figure is a reproduction of that given by Morris et.al. in reference [81] for washed erythrocytes frozen in test tubes of unbuffered isotonic saline at 10% hematocrit. For these tests the test tubes were held at 1°C below the freezing point for 5 minutes. They were then seeded with a frozen normal saline solution and held at the same temperature for 5 minutes more. After this period, the test tubes were placed in various vessels which were cooled by liquid nitrogen and designed to achieve a variety of cooling rates. The temperatures of the test tubes were recorded with thermocouples and the rates were approximated by the time taken for the sample temperature to fall from -15°C to -60°C . After the sample temperature fell below -60°C the test tubes were plunged directly into liquid nitrogen. No storage time was given. Thawing was done by rapid agitation of the test tube in a bath at $+37^{\circ}\text{C}$ until the last crystal disappeared.

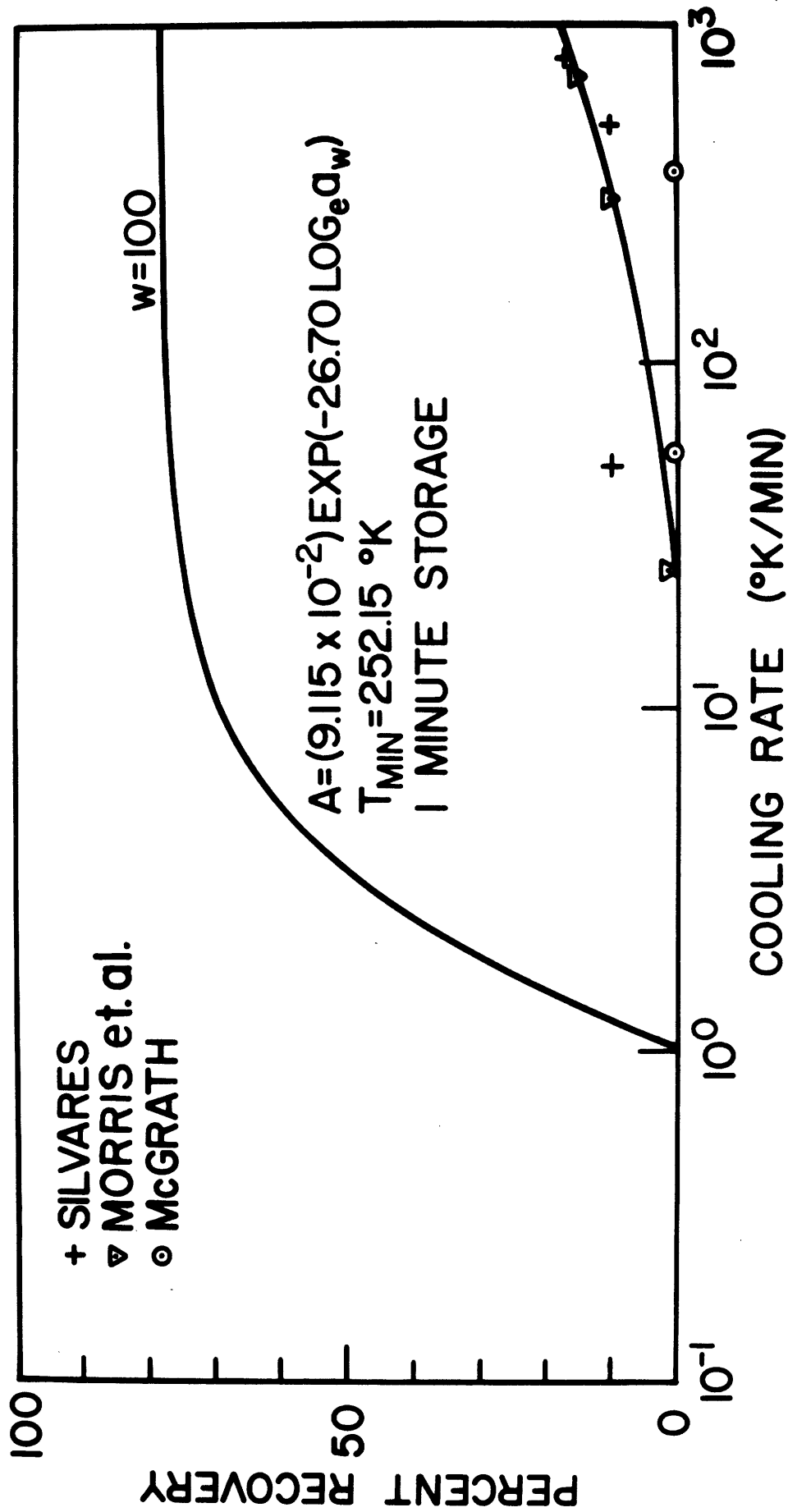


Figure 7.4 A Comparison of Predicted "Limited Damage" Percent Recovery and Experimentally Determined Percent Recovery as Functions of Cooling Rate.

Making a direct comparison between the simulation and thesis data has limited value, primarily because of the difference in storage temperatures and the lack of information on storage time and hemolysis kinetics below the eutectic temperature. Other experimental data are included which more nearly match the computer simulation thermal protocol. The data of Silvares (+) are for washed cells in normal saline and 0.04% ammonium hydroxide at 5% hematocrit. These cells were frozen and thawed at controlled rates on the cryomicroscope [44]. The cells were frozen at various rates to a minimum temperature of -40°C where they were held for one minute prior to warming at $+100^{\circ}\text{K}/\text{min}$. The author used the cryomicroscope to freeze and thaw washed red cells at rates of $-56^{\circ}\text{K}/\text{min}$ and $-420^{\circ}\text{K}/\text{min}$ where the suspensions were held for one minute at -21°C and -24°C respectively before warming at $+147^{\circ}\text{K}/\text{min}$. The cells were at 0.05% hematocrit and the same results were obtained for cells in unbuffered normal saline and cells suspended in saline phosphate buffered to a pH of 7.4.

The Morris data are for two experiments at each rate and a standard error less than 1.5% hemolysis. The Silvares and McGrath data are for single experiments at each datum point.

Although there is scatter in the experimental data, the data conclusively show that total freeze-thaw damage is significantly more destructive than osmotic perturbation damage alone.

This same conclusion is evident from Figure 7.5 which is a comparison between theory for a limited damage computer simulation and the experimental data of Lovelock [27]. This type of experiment is different from the

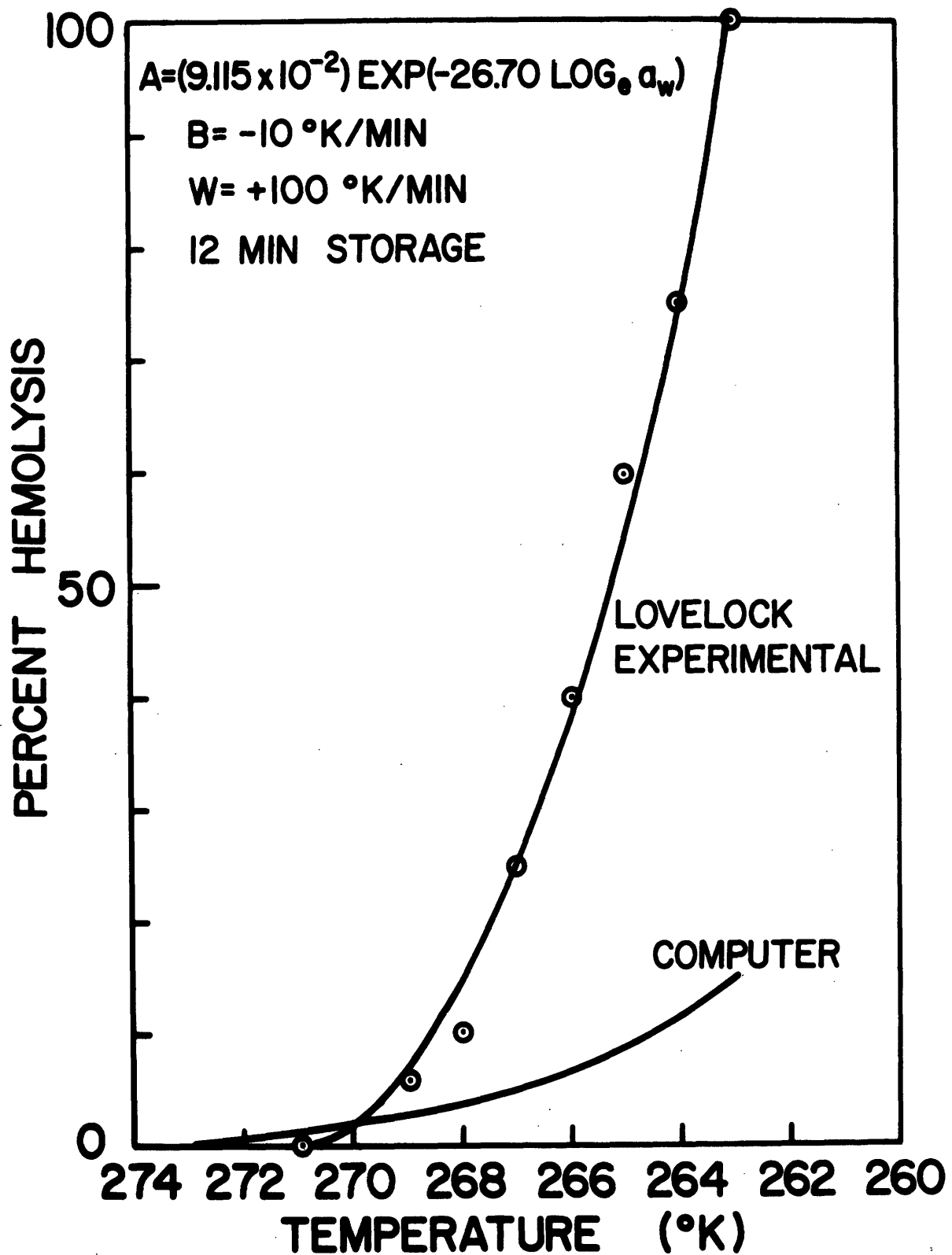


Figure 7.5 A Comparison of Predicted "Limited Damage" Percent Hemolysis and Experimentally Determined Percent Hemolysis as Functions of Storage Temperature.

freeze-thaw experiments just discussed, in that Lovelock was primarily interested in the effects of the storage temperature rather than the freezing or thawing rates.

Lovelock washed red cells in lightly buffered NaCl (NaCl 0.15M, Na_2HPO_4 0.005M, NaH_2PO_4 0.005M). The cells were then centrifuged and the supernatant removed. A sample consisting of 0.1 ml of packed cells was placed in a test tube immersed in a bath set at the desired storage temperature. After a two minute exposure to the bath temperature, 0.9 ml of normal saline, also at the bath temperature, was added to the cells and mixed. The cells were then at 10% hematocrit in a super-cooled solution of isotonic saline at the chosen bath temperature. The solution was then seeded by touching the surface with a capillary tube containing frozen normal saline. The temperature of the cell solution then rose to approximately -0.6°C , followed by a fall in temperature, to within 30% of the bath temperature by 20 seconds and to within 10% by 60 seconds. The suspension was left at the bath temperature for 12 minutes and then warmed by immersion for one minute in a water bath at $+42^\circ\text{C}$.

This technique would appear to be difficult to simulate on the computer because of the lack of control of cooling and warming rates, but the fact that the cells are held for 12 minutes at the storage temperature clearly predominates over a procedure involving freezing that takes place within approximately one minute and thawing that takes place in probably less time.

Therefore, estimates were made for the cooling and warming rates at $-10^{\circ}\text{K}/\text{min}$ and $+100^{\circ}\text{K}/\text{min}$, respectively. The hemolysis rate equation was then integrated down to the storage temperature, which is shown as the abscissa on Figure 7.5, integrated for a period of 12 minutes, and finally integrated for the thaw. The experimental results show negligible accumulated damage for storage temperatures as high as 270°K , but by the time the suspension reaches a storage temperature of 263°K , a 12 minute exposure followed by thawing produces complete destruction. The computer simulation produces the same qualitative trend but at a very much lower level. At storage temperatures of 263°K for 12 minutes, the simulation predicts only 15% hemolysis whereas the experiments show over six times that amount of damage. It should be noted that in these experiments no assumption need be made for the rate equation with respect to its validity over the temperature range covered. Hemolysis kinetic data were obtained down to 262°K .

Chapter 8

Discussion and Conclusions

Three major modes of freeze-thaw injury at sub-optimal cooling rates have been distinguished in the literature: 1) osmotic damage by exposure to hypertonic solutions, 2) thermal shock damage, and 3) posthypertonic exposure dilution damage. The first two of these effects have been studied in the present work. The initial motivation for this effort was a desire to produce experimental hemolysis data for each mode and to develop the methodology for quantitative estimates of the amount of damage produced by each of these two modes and the combination of the two for arbitrarily specified thermal and osmotic histories.

Hemolysis data does in fact exist for both damage modes of interest, but very little information has been previously available as to the rate at which hemolysis proceeds for given osmotic or thermal conditions. These rates and their respective temperature and concentration dependences are essential for numerically integrating the differential amount of damage produced as the red cell experiences exposure to varying temperatures and concentrations.

Although hemolysis data in the literature is not usually of a kinetic nature, the data have clearly demonstrated the fact that the thermal and osmotic modes of damage are coupled. For a complex process such as freezing, which involves simultaneous variations in temperature and concentration, quantitative prediction of total damage is impossible unless one has knowledge of the manner in which the two modes are coupled.

An experimental apparatus and technique have been developed which allow the determination of hemolysis on a real-time basis for a wide range of osmotic and thermal conditions. An advantage of this technique is the ability to retrieve hemolysis data with maximum dead times of 14 seconds, without the introduction of centrifuge artifacts. With the aid of the thermal control capabilities of the system, the osmotic perturbation mode of damage has been quite extensively studied for a series of isothermal cases. The hemolysis rate equation and its dependence on temperature and sodium chloride concentration have been well documented as a result. Preliminary experimental results were obtained for the kinetics of the thermal shock mode of red cell destruction. These experiments have demonstrated that the device is capable of producing data which are in agreement with data in the literature (at longer times where a quasi-steady state is achieved) and that in addition, previously inaccessible rate data are now easily obtained due to the improved time resolution of the present system compared with standard centrifugation techniques. Extensive experimental effort was not devoted to a complete description of the thermal shock kinetics. The limited results obtained indicate that the process as it is manifested kinetically is more complicated than the osmotic perturbation mode. This complexity is consistent with indications from the static thermal shock results available in the literature. These results show dependence on initial temperature, magnitude of the temperature drop, sodium chloride concentration, etc. Rather than produce a significant amount of thermal shock kinetic data at the present time, it was felt that this work could be sacrificed in favor of a theoretical investigation aimed at linking the thermal shock kinetics and osmotic shock kinetics once data for both are available.

Evidence in the literature suggests that hemolysis produced either by osmotic shock or thermal shock is accompanied by the loss of various membrane components. This evidence could be interpreted to mean that either mode results in destruction by the same basic process and that the process is membrane dissolution. Therefore, a thermodynamic system was defined at the membrane surface and a Gibbs-Duhem equation was derived for the membrane surface phase as an open system. It was shown that vicinal water plays a dominant role in the surface phase and that a reduction in the chemical potential of this water can cause an increase of energy of the molecules within this surface phase. Similarly, it was shown that a temperature drop could produce an increase in surface energy.

The release of membrane components is a non-equilibrium process and absolute rate theory has been applied in the derivation of a rate equation for the process. The dissolution process has been modelled as a desorption step requiring activation, followed by a diffusion process. An increase in surface energy causes a reduction in the desorption free energy of activation, hence the rate of lipid release can be enhanced when the water chemical potential is decreased or the temperature is dropped. This analysis has therefore produced the theoretical basis for explaining why both osmotic shock and thermal shock should be accompanied by membrane component loss and therefore why they are both essentially the same process--the raising of the surface energy which results in membrane dissolution. This thermodynamic treatment has identified, for the first time, the separate terms responsible for osmotic shock ($-\Gamma_i d\mu_i$) and thermal shock ($-\sigma dT$) membrane component loss.

It has been shown that the characteristic time for the rate of membrane component loss is associated with diffusion of the component away from the surface of the membrane. This time is long compared with diffusion times for hemoglobin to diffuse from the center of a red cell to the membrane and then across the membrane. Therefore the hemolysis rate has the same characteristic time as the rate of membrane component removal. The appropriate free energy associated with hemolysis appears to be related to the number of molecules of membrane component leaving the membrane. A simple estimate of this number was 128, based on a highly compressed film assumption and the loss of both sides of the membrane bilayer for hemolysis. The experimental hemolysis kinetic data were fit in a form consistent with that of the thermodynamic model and the apparent number of LPS molecules leaving the surface per molecule of hemoglobin passing through the membrane was 40 at 298°K and decreased to a value of 27 at temperatures of 273°K down to 262°K. The lower numbers are probably a reflection of the fact that the membrane is not so highly compressed as has been assumed [67,68] and that possibly only one side of the membrane need be lost before it is unstable enough to allow hemoglobin passage to the extracellular medium. The reason for the number of molecules to decrease with temperature and then remain insensitive to further temperature reductions below 273°K is unclear.

The general hemolysis rate equation that was developed is thus very closely tied to the rate equation for the loss of the membrane components. Perturbations produced in the extracellular medium in the form of temperature changes and water chemical potential variations, also occur at the surface phase. These variations affect the surface

energy and therefore the desorption energy and rate of hemolysis. The derived rate equation explicitly specifies the relationship between the driving forces for osmotic damage and thermal damage.

The hemolysis rate equation has been suitably reduced to match the experimental conditions during the osmotic shock tests and during the thermal shock tests. The general hemolysis rate equation predicts the form of the osmotic kinetics tests. It also predicts the correct form for the dependence of thermal shock hemolysis on exposure to various sodium chloride concentrations prior to the temperature drop. Curve-fitting experimental data from the literature suggests that 27 molecules of membrane component have been lost in this process which indicates hemolysis dissolution is taking place at the lower temperatures. This is substantiated by the thermal shock kinetic data presented in Chapter 4 (Figure 4.15). The hemolysis rate equation was also used to investigate theoretically the dependence of the thermal shock hemolysis on the initial exposure temperature and the magnitude of the temperature drop. The theory predicts the existence of an exponential term describing thermal shock hemolysis which is essentially independent of the absolute temperature, and dependent only on the magnitude of the temperature drop. This appears to be the case as judged by curve-fitting of experimental data from the literature. Once again, the constant returned from the curve-fitting program can be related to a physical parameter in the system and thereby used as a check on the validity of the model. In this instance the constant from the curve fit can be used to make an estimate of the surface concentration (molecules/area) for water at the membrane surface. The concentration agrees

well with an independent method of determining an approximate value for this surface property. The relative concentrations of water (estimated in this way) and LPS (estimated from compressed lecithin film data) agree well with effective characteristic lengths of the respective molecules at the surface (LPS, 8\AA diameter and water 1.5\AA). These relative sizes and concentrations show why the properties of the surface phase are well approximated by the properties of water. The initial temperature and ΔT dependence of the thermal shock hemolysis equation can also be manipulated to demonstrate that the surface entropy of the membrane must be greater for cells susceptible to thermal shock relative to those which are not (i.e., those in isotonic saline). The difference between those cells in isotonic and those in hypertonic sodium chloride solutions is that for the hypertonic case there is a mass flux occurring at the membrane surface. Simple irreversible thermodynamics states that the local entropy production is related to the mass flux and it is likely that membrane surface entropy will be maximized at some well-defined time after the mass flux has first been induced. This argument may explain why there is maximized hemolysis as a function of exposure time prior to the temperature drop for cells exposed to hypertonic sodium chloride.

All of these facts lead one to believe that the model can describe the rate at which hemolysis is expected not only for osmotic perturbation or thermal perturbation separately but also if they were to occur simultaneously for a process such as freezing. The major shortcomings of the model were pointed out in Chapter 7 when a technique for computer simulation of freeze-thaw damage was presented. The transition from the rate of loss of membrane components to the hemolysis rate

necessitated transformation from individual cell behavior to cell population behavior. Experimentally it would appear as if the transformation parameter Θ is time independent in certain time domains. For a more complete description of the hemolysis rate equation, Θ must be examined more rigorously in the sense of determining magnitude and time dependence. This is not the major shortcoming of the hemolysis rate equation at present because as long as one limits oneself to the time domain where $\Theta \neq \Theta(t)$, then this term can be lumped into an experimentally determined constant as can be seen in equation 5.53. The most serious problem in the use of the rate equation to predict freeze-thaw hemolysis from osmotic and thermal shock is that the time dependence of the surface entropy is as yet unspecified.

The osmotic perturbation mode of damage was not rate sensitive to temperature variations per se from 273°K to 262°K (and probably would not be down to 252°K). This effectively decouples the osmotic and thermal modes. However, the thermal perturbation mode of damage requires "pre-stressing" the membrane. For the iso-osmotic hypertonic, thermal shock experiments considered here, the "prestressing" is probably the production of entropy at the membrane surface by way of the inducement of a mass flux from the membrane. This means that thermal shock is not decoupled from osmotic effects and this complicates the problem considerably. However, it is not unlikely that a reasonable value of the surface phase volume-averaged entropy could be made for lipid loss into an infinite medium for temperature and concentration time-varying boundary conditions. This estimate would allow one to insert $\sigma = \sigma(t)$ into the hemolysis rate equation so that the instantaneous value of surface entropy would always be available for the $(-\sigma dT)$ calculation necessary to fully describe both

thermal and osmotic shock. The importance of the entropy term is suggested by the theoretical prediction of the initial temperature and ΔT dependence of hemolysis and comparison with experimental data. It is also evident from the computer simulations that osmotic perturbation alone is not enough to account for the total freeze-thaw damage seen experimentally.

Although the importance of rate in determining total damage has been recognized in the past, the hemolysis data for both osmotic and thermal shock have often been presented as if hemolysis were a thermodynamic state function. Figure 8.1 demonstrates two process paths by which red cells in isotonic saline at 298°K can be taken to a state in which the temperature has been reduced to 273°K and the concentration has been increased from 0.154M to 1.50M NaCl. In both cases the total time taken to proceed from state A to state C will be five minutes. Consider the path A→B→C. An instantaneous temperature drop at isotonic conditions produces no hemolysis. The cells are immediately transferred at 273°K to the hypertonic condition at C. After five minutes at 1.50M the total hemolysis at this temperature should be 1.85% as calculated from equation 4.4 (see Figure 5.4 for experimental verification). On the other hand, if the cells are instantaneously taken from A to B', a hypertonic state at 298°K, and remain at B' for five minutes, equation 4.3 predicts a total hemolysis of 3.70% after the five minute period. An "instantaneous" temperature drop from B' to C after the five minute exposure will produce hemolysis that can be estimated from Figure 4.14, for -100°K/min cooling, in excess of 60%. Even if this damage were to take five to ten minutes to appear, as suggested by the kinetic data of Figure 4.16, this amount of time added to the A→B→C process will produce a net damage of approximately 5-6% whereas the A→B'→C process has produced over 60% hemolysis.

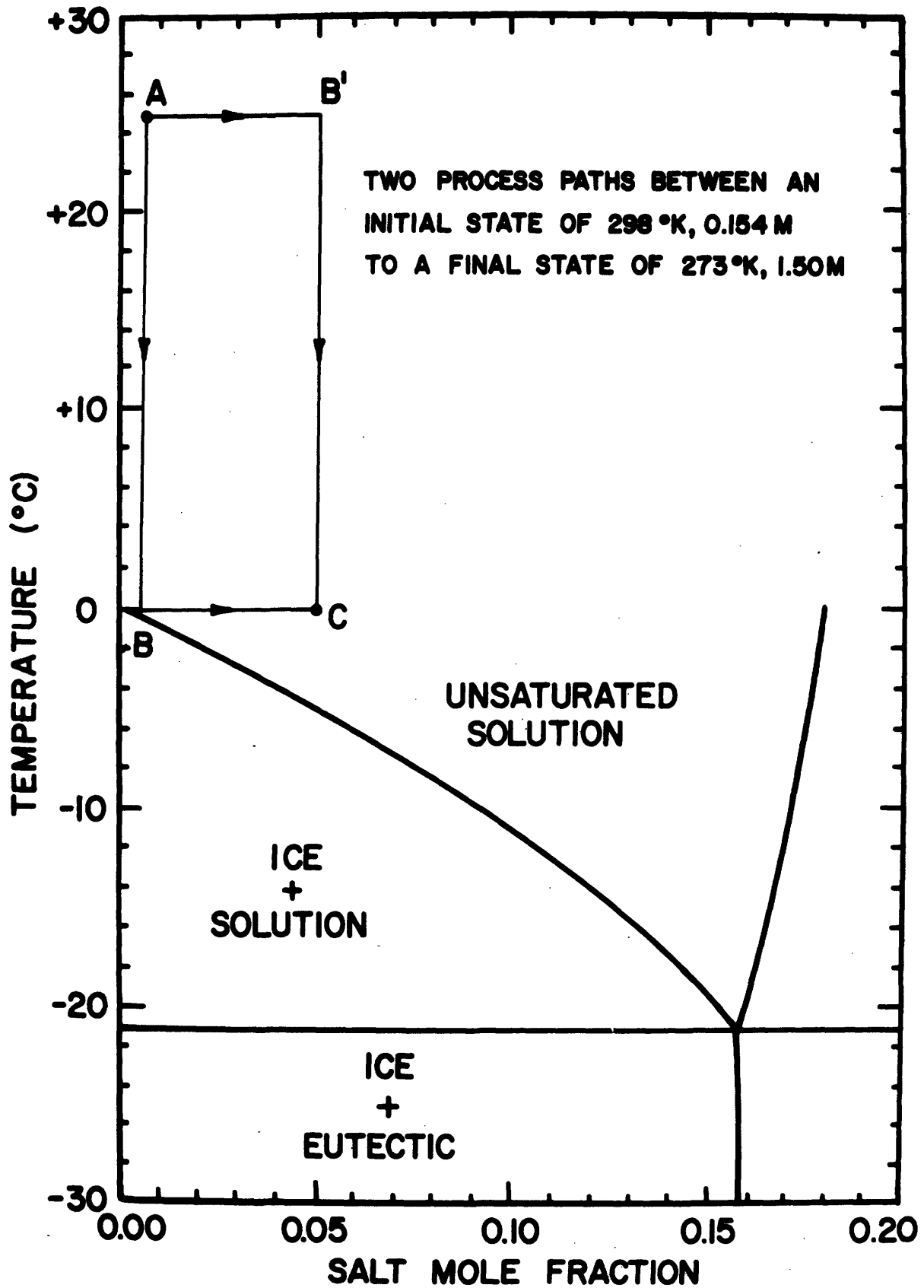


Figure 8.1 Two Process Paths for Altering the State of the Erythrocyte Suspending Medium from High Temperature and Low Concentration to Low Temperature and High Concentration.

The model biological system chosen in the present work was the human erythrocyte because hemolysis is a convenient measure of cellular destruction. The hemolysis rate equation developed in the present work would appear to have potential in the prediction of damage to cell types other than the human erythrocyte. For example, lipid material is lost from Karkhov wheat cells when they are plasmolyzed [81]. Effective use of the lipid (LPS) loss rate equation for the prediction of the damage rate for a given cell type would rest on the determination of a critical membrane state criteria, such as maximized surface pressure or minimum concentration at the surface. The apparatus, calibrated now to measure hemolysis in red cells may be able to measure accurately damage rates of other cell types. It would appear that light absorption and scattering is closely associated with the concentration of intracellular molecules. For example, in phase contrast microscopy, the internal contents of the cell can be measured by monitoring the index of refraction within the cell [82]. Figure 8.2 is a 35 mm photograph taken on the cryomicroscope, post freeze-thaw. The cells are HeLa S-3 cells and as judged by the method of fluorochromasia [18,83] the cell on the right is undamaged, whereas the one on the left has been irreversibly damaged. Presumably lipid material has left the membrane to the point that large and/or polar intracellular molecules such as the fluorescent dye molecule can leave. The reduction of intracellular concentration results in a marked difference in the contrasts of the two cells relative to the suspending medium. The contribution of the cell membranes themselves to the index of refraction is negligible, as judged by studies of the erythrocyte [64].

The apparatus is not only potentially capable of producing damage



Figure 8.2 Phase Contrast 35mm Photograph of HeLa Cells as seen Post Freeze-Thaw on the Cryomicroscope with Lack of Contrast for Damaged Cells (300X).

kinetic data for a variety of cell types, it is also a very straightforward procedure to recalibrate the instrument for experiments in which the cell suspension contains not only sodium chloride and water, but other compounds as well. Specifically, the instrument can be used to study the effects of existing and proposed cryophylactic agents (CPA) on the damage kinetics.

One of the interesting consequences of the model, with its assumed symmetry for the red cell membrane, is that lipid is released both external to the cell and internally. Since the lipid release process occurs over a long time with respect to the actual transfer of hemoglobin across the membrane, an increased concentration of lipid inside in a confined volume should be observed relative to the outside concentration of lipid which is diffusing into an "infinite" medium. The expected behavior of the cell would be a flux of water from the outside medium to the inside to reduce the increased osmolality of the intracellular volume. Nei has microscopically observed that for red cells "...instantaneous swelling of the cells was noted just before they hemolyzed." [35] It appears as if some cells are protected in this manner because the lipid lost to the intracellular space is not irreversibly lost as would be the case for transfer to the extracellular volume [84]. This is very interesting indeed from the viewpoint of cryophylactic agents, some of which are able to protect the cell without penetrating. A possible mechanism for such protection would be the prevention of lipid release to the extracellular medium, or at least the reduction of the rate of release of these components to a very low level. This could be accomplished either by a reduction of the surface energy or the extension of the characteristic time by altering the diffusion

coefficient. The release of lipid to the interior of the cell for such non-permeating CPA's is allowed but does not represent irreversible damage if the cell is properly warmed. The intracellular lipid content remains at a high concentration which favors return of the lipid to the membrane when the thermodynamic cycle is completed by warming, and the desorption-free energy is restored to its initial value. This effect of trapping the membrane components internally would be effective without a CPA also, and one might expect that if cooling has been slow where substantial lipid has been lost, then for optimum survival warming should also be slow to allow the reversible re-entry of the intracellular lipid back into the membrane.

The use of slow warming to obtain optimum survival from slowly cooled cells has been used to advantage for a number of cell types [9,13].

The effects of hemoglobin within the cell have not been accounted for in the sense of how this macromolecule might affect the assumption of symmetry made in the derivation of the thermodynamic model. This should be investigated, especially with reference to the internal release of lipid. Some consideration must be given to the added complexities of the general cell with its endoplasmic reticulum network of membraneous material and internal organelles. In particular, it should be decided whether the presence of these components significantly affects internal release of the plasma membrane components. Also, how do these internal membranes behave? Are they as sensitive to thermal and osmotic shock as the plasma membrane or are they protected by their internal position?

An unresolved difference in hemolysis kinetics at low temperatures was observed between the present results and results derived from the work of Lovelock. Lovelock reports static values of hemolysis after five minute exposures to various concentrations and sub-zero temperatures (see Figure 4.10). Since the hemolysis rate does not undergo transition to the slower rate until after approximately ten minutes or more have passed at these low temperatures (see Figure 4.7 and 4.9) and since the rate is linear, the static hemolysis value can be divided by the five minute exposure time to determine an effective rate. These derived kinetics are plotted as triangles in Figure 8.3 and a curve-fitted line is drawn through the data. Also shown are the two previous curves from Figure 4.11. The lower two curves of Figure 8.3 should coincide for identical kinetics for the temperature range 273°K to 262°K which was identical for the two sets of experiments. Both sets of data showed collapse of the kinetic data for temperatures between 273°K and 262°K but the Lovelock kinetics would produce less damage after any length of time at any concentration. The maximum discrepancy occurs at the extrapolated values for the eutectic concentration. The present data predict approximately three times the amount of damage as the Lovelock data at this maximum concentration. The curve-fitted Lovelock kinetic expression

$$(8.1) \quad \frac{d(\%H)}{dt} = A = (1.20 \times 10^{-1}) \exp(-20.13 \log_e a_w)$$

shows a difference in both the frequency factor and the activation energy as compared to the low temperature kinetic expression in equation (4.4).

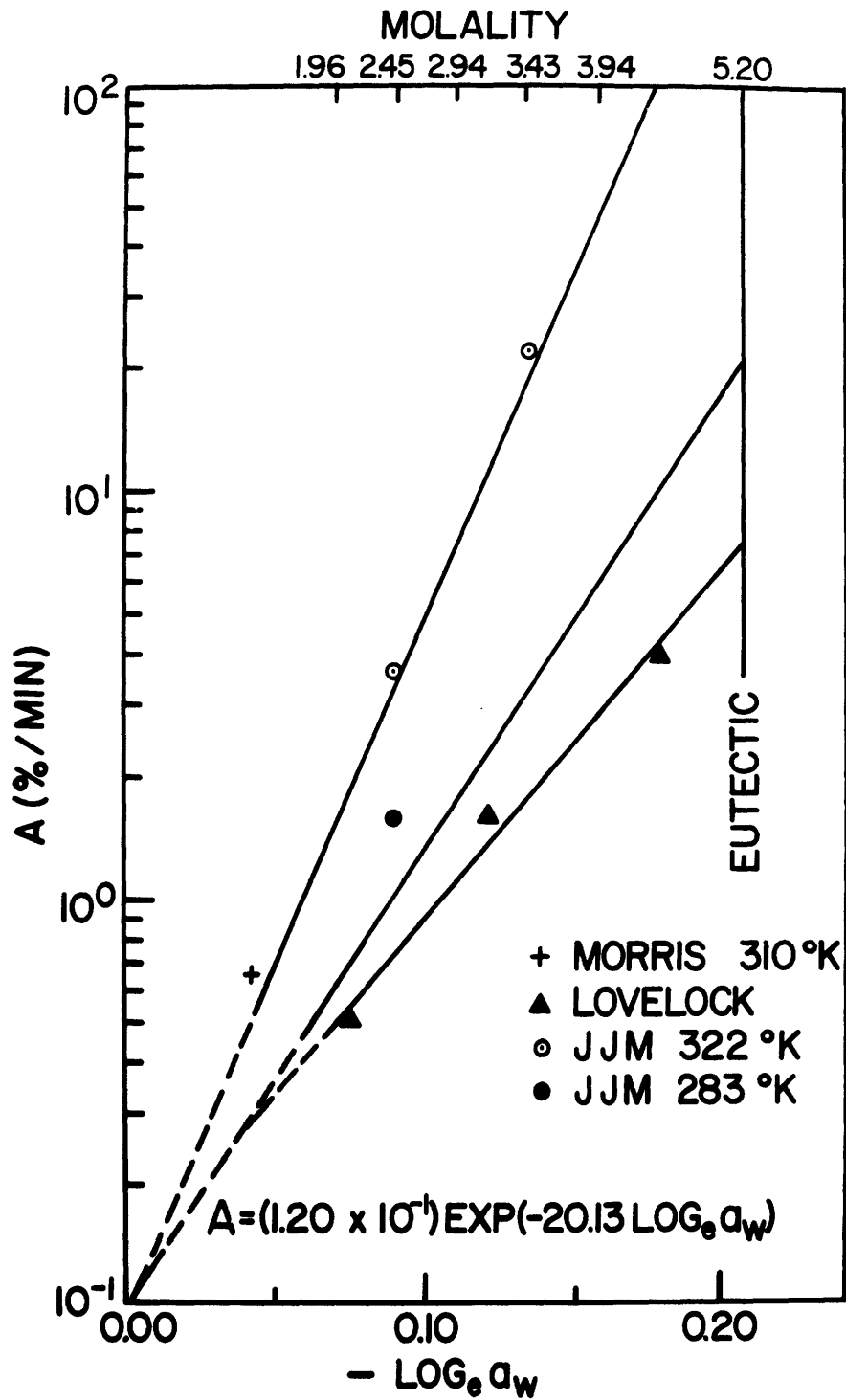


Figure 8.3 Rate of Hemolysis as a Function of $-\text{Log}_e(a_w)$ for Isothermal, Osmotic Perturbation Experiments: Derived Kinetics from Lovelock Data (reference [27]) Compared with Present Data.

$$(4.4) \quad \frac{d(\%H)}{dt} = A = (9.115 \times 10^{-2}) \exp(-26.70 \log_e a_w)$$

There appear to be two possible explanations for the difference. One would be that the present system is producing damage kinetics which include not only osmotic shock but also the effects of mechanical damage due to mixing. Another possibility is that the experimental conditions for the two determinations are significantly different. In particular, the Lovelock cells were in a lightly buffered saline solution which may account for the difference in activation energy. Secondly, the frequency factor, which theoretically is a function of the diffusion process, may be different for the two mixing processes.

Figure 8.3 also shows that kinetics derived from the Morris data (see Figure 5.4) are consistent with the high temperature kinetics obtained in the present work. The closed circle datum is at 283°K and was one of the data points used to evaluate the activation energy of 7.3 Kcal/mole (Figure 4.8). The two open circle data points show apparent collapse of rates at high temperatures but this is actually a misrepresentation. Reference to Figure 4.7 shows that at temperatures of 322°K the transition to the slower rate has occurred prior to one minute and the linear approximation of %H with time is not a good one. Table 4.1 also shows that for these temperatures the rate would be a function of time during the exposure time range of 0-1 minute.

The effect of phospholipids, cryophylactics and other agents on thermal shock have been studied [55], but no attention has been given to the problem of correlating why, for example, added chloesterol increases thermal shock damage and additional lecithin reduces thermal shock damage.

The theoretical model would predict that an agent capable of lowering the surface tension (γ) would be an agent that would have cryoprotective properties. Tests have shown that the CPA's glycerol, DMSO, sucrose, PVP, dextran, and HES are all surface active at low concentrations, i.e., they will lower the surface energy of water and hence could concentrate at the cell-solution interface and have the same effect [84]. Unfortunately, it appears as if the surface tension increases with increasing cryophylactic concentration in some ranges of concentration.

Further resolution of the factors included in the desorption energy term of the hemolysis rate equation may be realized by following the example of Davies and Rideal [68] who separate the desorption energy term into three parts: a term involving cohesive energy within the monomolecular layer, a term for the polar interaction of the lipid head groups and the polar nature of the solvent, and finally the electrostatic effects of ionized species adsorbing or desorbing onto a charged membrane.

Chapter 9

Suggestions For Future Research

Future contributions to the understanding of erythrocyte freeze-thaw damage at sub-optimal cooling rates can be made by both experimental and theoretical extensions of the present work.

The experimental apparatus has proven itself capable of producing thermal shock kinetic data. More data of this type should be taken to determine whether initial indications from the limited amount of thermal shock data presented in Chapter 4 are generally valid. For example, it should be determined whether or not the delay in the appearance of hemolysis following initial cooling is a general response for the thermal shock kinetics. Extensive thermal shock kinetic experimentation is not recommended at this time. Rather, this type of experimentation should be pursued in a limited way to check the accuracy or validity of assumptions made in the derivation of the rate equations.

A substantial effort should be made in developing a more detailed theoretical basis for understanding entropy generation at the membrane surface. The surface entropy of cells in isotonic saline at $T = 25^{\circ}\text{C}$ and $P = 1 \text{ atm}$ is apparently small enough so that no thermal shock results. In hypertonic saline a mass flux of lipid results in the local generation of entropy, which when added to the isotonic value is large enough at certain exposure times to produce substantial thermal shock damage. Starting with the lipid loss rate equation one could conceivably derive the flux and driving force terms necessary for generating an expression for surface entropy as a function of time. A parameter study could then be pursued and the theoretical results for the production of thermal shock hemolysis in a given situation could be checked against existing data or data obtained from the apparatus developed as a part of this thesis work.

The temporal variations in the membrane surface entropy must be determined before accurate predictions can be made for thermal shock damage alone or simulated freezing damage where both thermal shock and osmotic shock occur. An alternate approach which could prove to be valuable in the specific case of cells suspended in the binary sodium chloride-water system, would be to normalize the data which appears in Figure 4.12. This figure describes recovery percentage as a function of exposure time prior to the temperature drop. Curves at several sodium chloride concentrations look to be very similar and the hypothesis is that normalization of the amount of hemolysis after any length of exposure time with respect to the maximum amount of hemolysis (which occurs at five minutes for this system) will produce a unique curve of normalized hemolysis percentage as a function of exposure time for all hypertonic concentrations. The absolute magnitude of the reference hemolysis after a five minute exposure correlates well with sodium chloride concentration (equations 6.9,6.11, 6.12) which means that the normalized hemolysis variation with exposure time is probably a manifestation of the time wise-change in the surface entropy σ . This means that instantaneous surface entropy normalized with respect to isotonic conditions surface entropy should be derivable from the hemolysis rate equation (equation 5.53) and the normalized hemolysis curve derived above. If this procedure were to prove to be fruitful in describing existing data then, at least for this binary solution system, the thermal shock part of the freezing damage could be incorporated into the computer simulations. Although less fundamental than the first approach, this one could lead to results much more quickly. The normalized surface entropy as a function of time derived from the existing data for this system could also be used as a check on the theoretical development of the transient behavior of the surface entropy derived from

the irreversible thermodynamic analysis.

Analytical work should also be done to rigorously define the transformation parameter Θ to allow simulations of freezing to be made for the general case in which Θ is time varying. As noted in Chapter 5, Θ as judged by the results of the experimental data is not a function of time for the first minute after red cell exposure to hypertonic solution at 298°K. The analysis should reveal the relationships between the relevant parameters included in the parameter Θ . From information in the literature, from reasonable estimates and/or future experimental work it is likely that enough could be determined about $\bar{\Gamma}$, Γ_{critical} , D , L , and the distribution function for Γ , that a quantitative explanation could be given for the short time, time-invariant behavior of Θ . Agreement for specific cases such as this, then lends credence to the general transformation Θ expression from which it was derived. Therefore, the general transform could be made with confidence for cases in which time is varying.

If the time dependence of the parameters Θ and σ can be derived from fundamental approaches and verified experimentally then the hemolysis rate equation should be in a very general form which can be applied to red cells in many types of solutions, such as those including a cryophylactic agent. Once the Θ and σ time dependencies are determined, one is in an excellent position to estimate the consequences of changing from one solution to another, and in fact one can do so with the added advantage of having mechanistic insight as to how the changes occur and which are most important. With accurate information for the time dependence of Θ and σ , one is also able to derive the theoretical

cooling rate dependence of thermal shock hemolysis. As a result, it should be possible to understand why thermal shock damage is so weakly dependent on cooling rate.

The consequences of producing a hypertonic medium with sucrose rather than sodium chloride should be considered based on the hemolysis rate equation as a starting point. Thermal shock experiments for red cells in hypertonic sucrose rather than hypertonic sodium chloride do not reveal the five minute exposure time, maximized damage [30]. This indicates that the sucrose is not altering the membrane surface entropy nearly as much as the sodium chloride. This should be investigated.

In an effort to further generalize the present results, work should begin on accumulating information concerning the surface active properties of various agents at a water interface. It is known that cryophylatic agents lower the surface energy of the water interface and this is consistent with the conclusion one would arrive at if one started from the hemolysis rate equation and asked the question what would be one of the properties of an agent capable of protecting the cell. More needs to be known about how this surface energy reduction occurs for each of the agents and how the energy reduction changes with concentrations and temperature. Further work in this area might begin by following the example of Davies and Rideal [68] who discuss how the desorption energy can be altered by polar effects, ionic charge, etc.

The experimental apparatus should be recalibrated so that the optical subsystem would be capable of measuring hemolysis not only for red cells in a sodium chloride-water solution but also for red cells in

solutions such as sodium chloride-water-glycerol, sodium-chloride-water-DMSO, etc.

An improvement of the experimental apparatus thermal control system could be made by the inclusion of an integrator, rather than a simple proportional set point controller. This would make accurate and reproducible thermal shock experiments a routine matter.

For simulating freeze-thaw damage for protocols involving storage at low temperatures an analysis should be done on the possibility of tracking the thermodynamic state of the system below the eutectic point of the suspending medium.

If cells hemolyze during freezing and lipid is released to the external medium, as freezing occurs this lipid as a solute in the external medium becomes concentrated. The effect of this phenomenon should be studied as to how it may retard further lipid release and hence hemolysis.

It is possible that the posthypertonic hemolysis damage mechanism may be incorporated into the present model. Thermal shock and osmotic shock hemolysis have been modelled as the creation of "pores" large enough for hemoglobin to pass through the membrane. Prior to enlargement of the "pores" to the size of hemoglobin molecules a critical "pore" size could be reached for ionic solute transmembrane flux. If there is a critical maximum volume which the red cell can withstand upon return to an isotonic medium after exposure to a hypertonic solution then one can calculate how much solute has to enter the cell in order to cause dilution rupture. Based on rate equations similar to those for lipid

loss and hemolysis one would be able to calculate under what circumstances the cell would have allowed sufficient solute transport to be in danger of rupture upon dilution. Obviously these effects are more subtle than those producing gross transport of a molecule as large as hemoglobin, but there appear to be very strong similarities that could probably be used to advantage.

Although electron microscopy, either of the transmission or scanning type, may not yield much quantitative data, visualizations made for cells subjected to various stressful situations may help to boost confidence further in the present model. In particular, the hemolysis model postulated would predict identical modes of hemolysis for osmotic and thermal shock, i.e., the reduction of the surface concentration of cell components to a critical level. Cells that have been subjected to osmotic shock and damaged should therefore be morphologically quite similar to those cells damaged by thermal shock. Both of these types of damage should produce cells possessing significantly less surface mass than control cells in isotonic saline. Other electron micrographic evidence of interest would be the comparative morphological states of cells at minimum volume condition (where solute leakage occurs), cells damaged by posthypertonic dilution, and frozen-thawed cells for unprotected and protected conditions.

Finally, the thermodynamic model may be useful in the analytical study of thermal injury at the other thermal extreme, i.e., in hyperthermic conditions. Both HeLa cells and erythrocytes have been tested for thermal response at elevated temperatures [40,41]. Light microscopy reveals drastic membrane alterations in both cases and it is possible that the

present model could serve as a starting point for an analysis of these changes.

Appendix A

Increase in Optical Signal Due to Erythrocyte Sedimentation in a Finite Length Optical Chamber

Early attempts to monitor hemolysis kinetics on a stop-flow apparatus designed for reaction with characteristic times of 100msec-3 minutes [43] proved to be impossible since the characteristic hemolysis times of interest were typically longer than three minutes. At the longer times, the finite dimension of the optical chamber in the direction aligned with the gravitational field resulted in sedimentation of the red cells out of the optical path. The optical signal therefore increased, and this increase could not be distinguished from an increase in signal due to hemolysis.

Based on the dimensions of the system and the sedimentation velocity of the red cells a prediction was made as to when sedimentation should begin to be a problem. It is seen that the prediction matches experimental data from the apparatus.

Height of optical chamber = 0.250 cm

Optical path of diameter 0.193 cm centered on optical chamber

Therefore the distance from the top of the optical chamber to the topmost part of the optical light path would be the distance through which the cells must settle before the optical signal should increase.

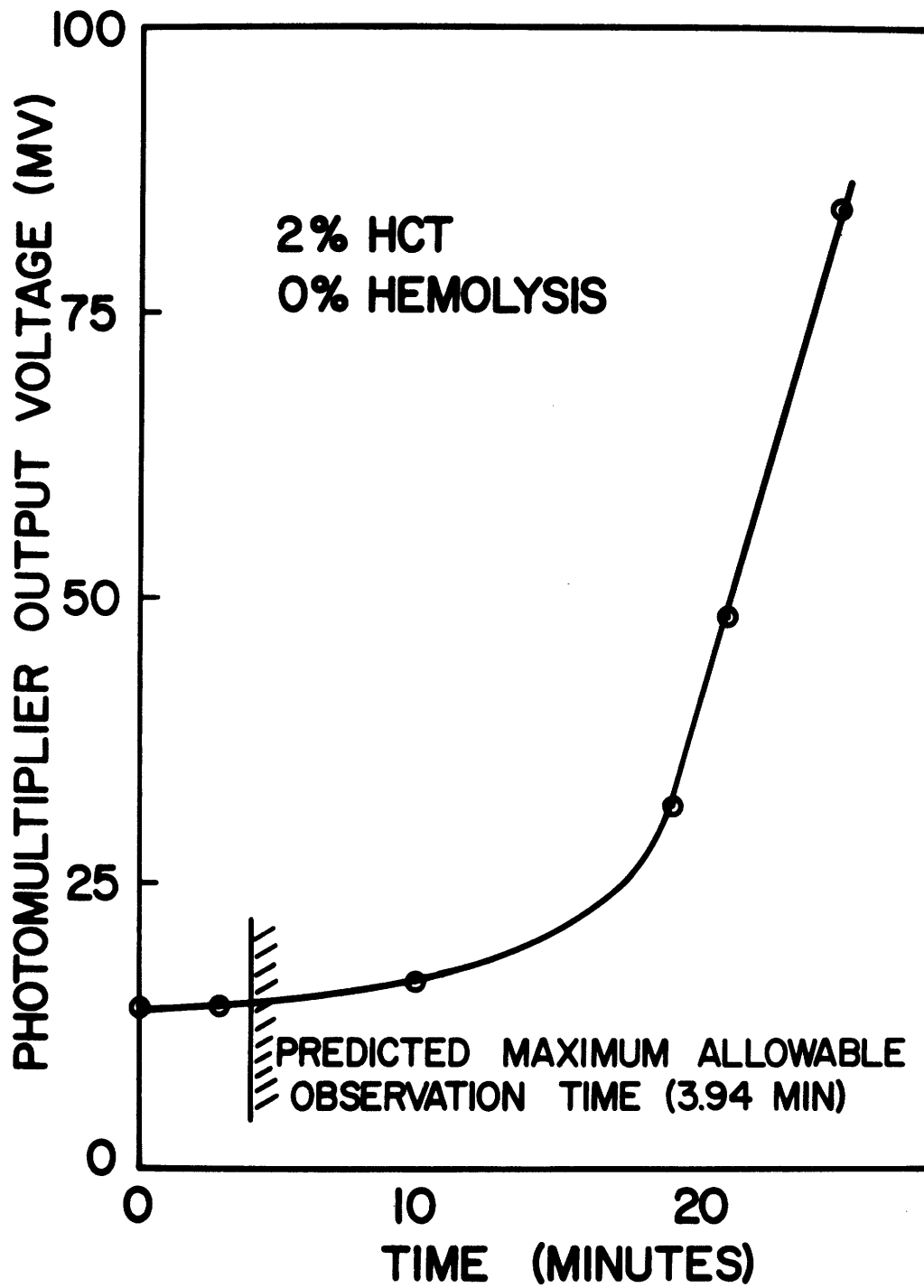
It has been experimentally shown that settling velocities for human erythrocytes can be accurately described at 2% hematocrit [45] by

$$u = 0.426 \text{ cm/hr}$$

This is a viscous flow situation so the velocity is essentially constant from time zero (see appendix F). Thus the characteristic time before depletion begins occurring within the light path is

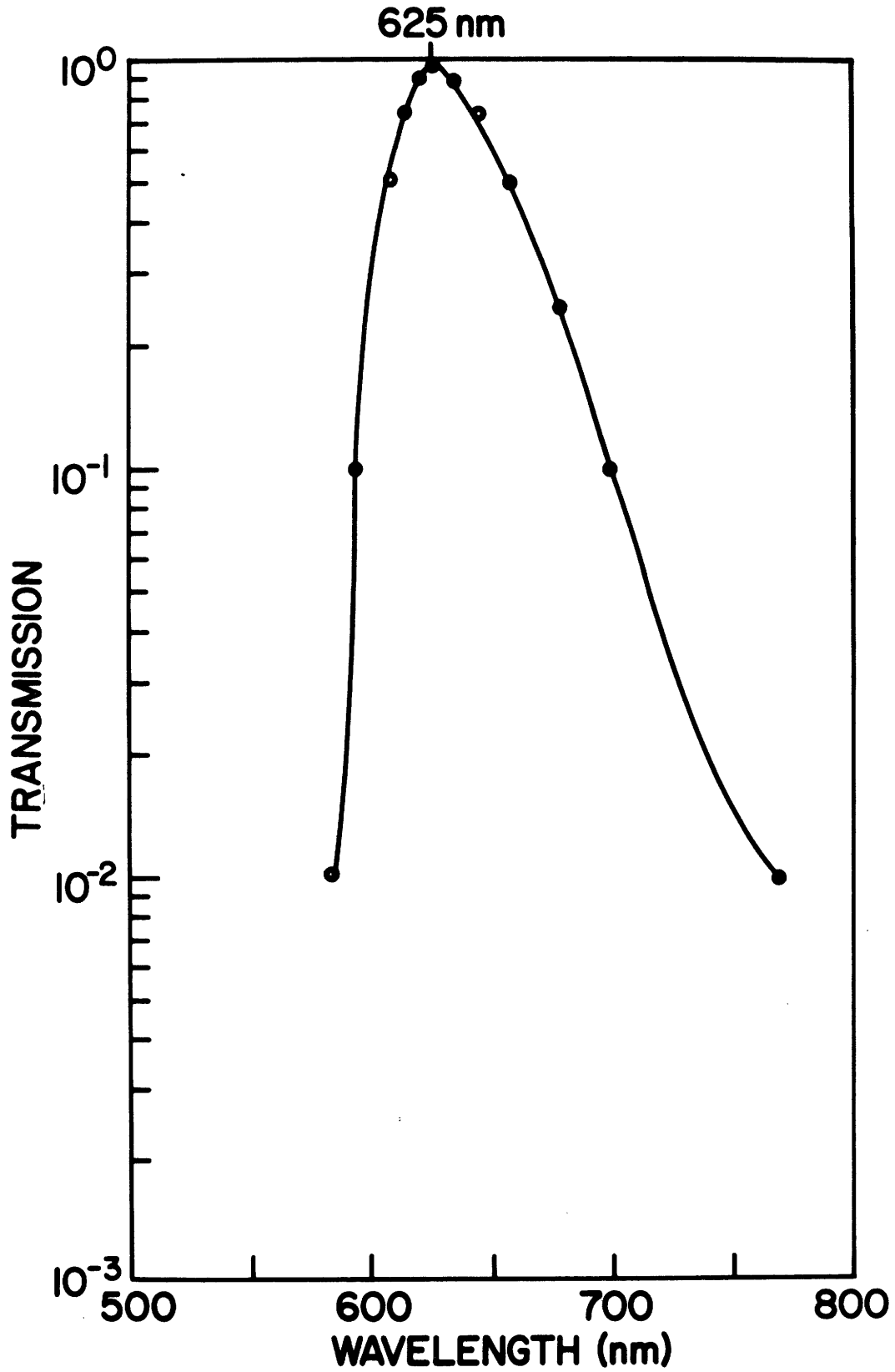
$$t = \frac{\delta}{u} = \frac{(0.125 - 0.097)\text{cm}}{0.426 \text{ cm/hr}} (60 \text{ min/hr})$$
$$= 3.94 \text{ min}$$

The figure that follows shows a steady optical signal, followed by a dramatic increase and the transition point agrees with the prediction.

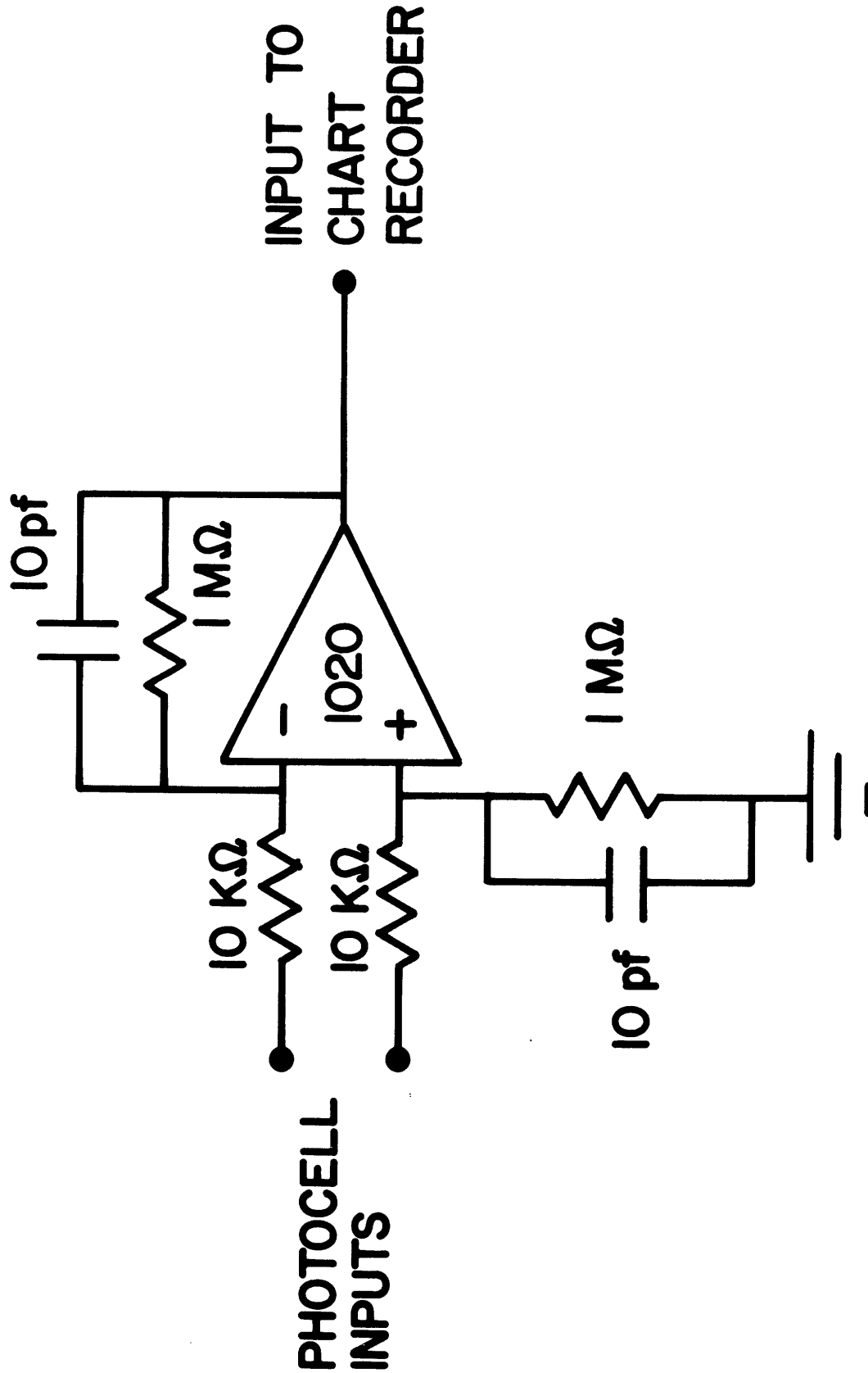


Appendix B

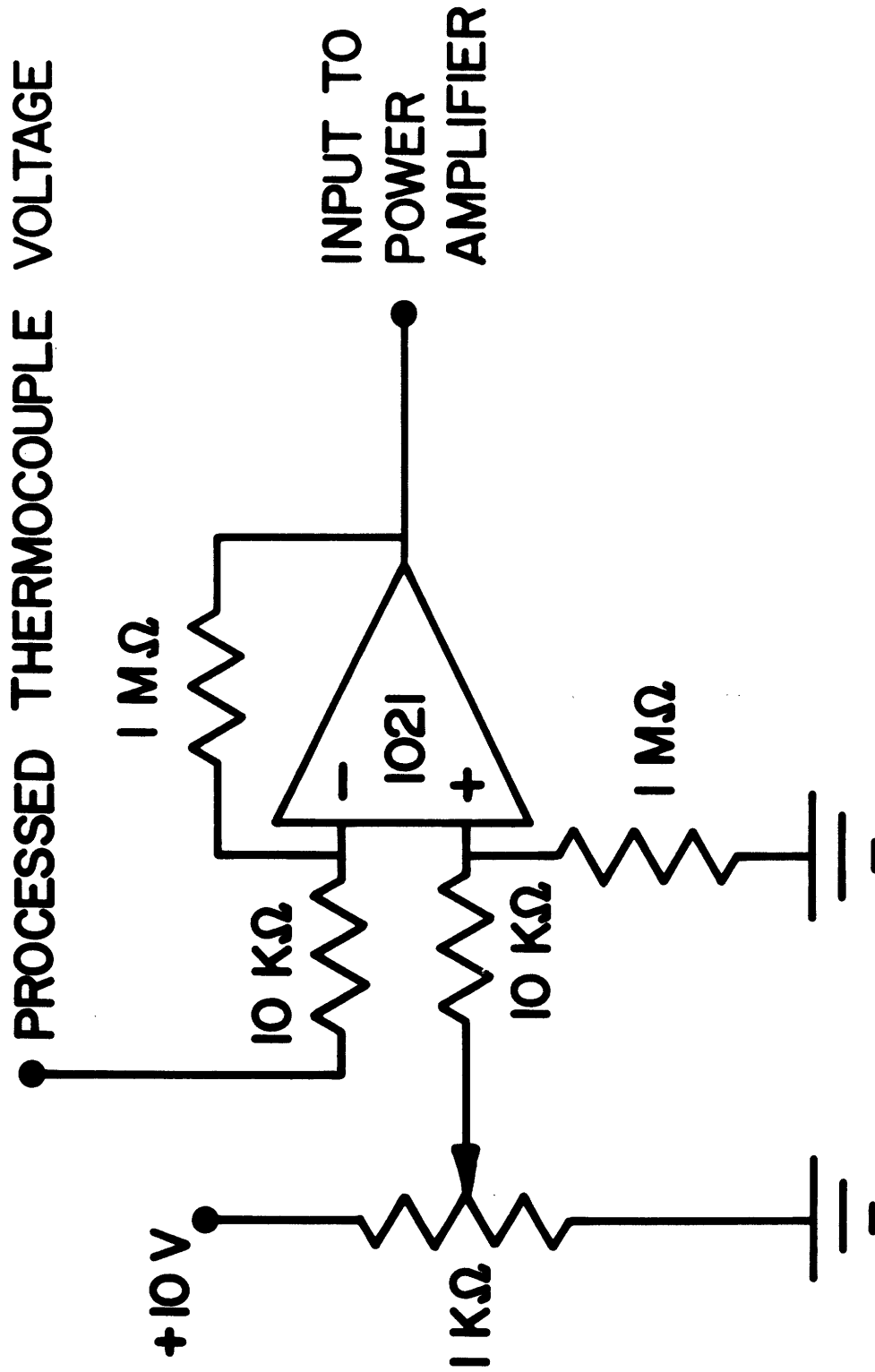
Optical Band Pass Filter Spectrum



1) Photocell Amplifier-Filter

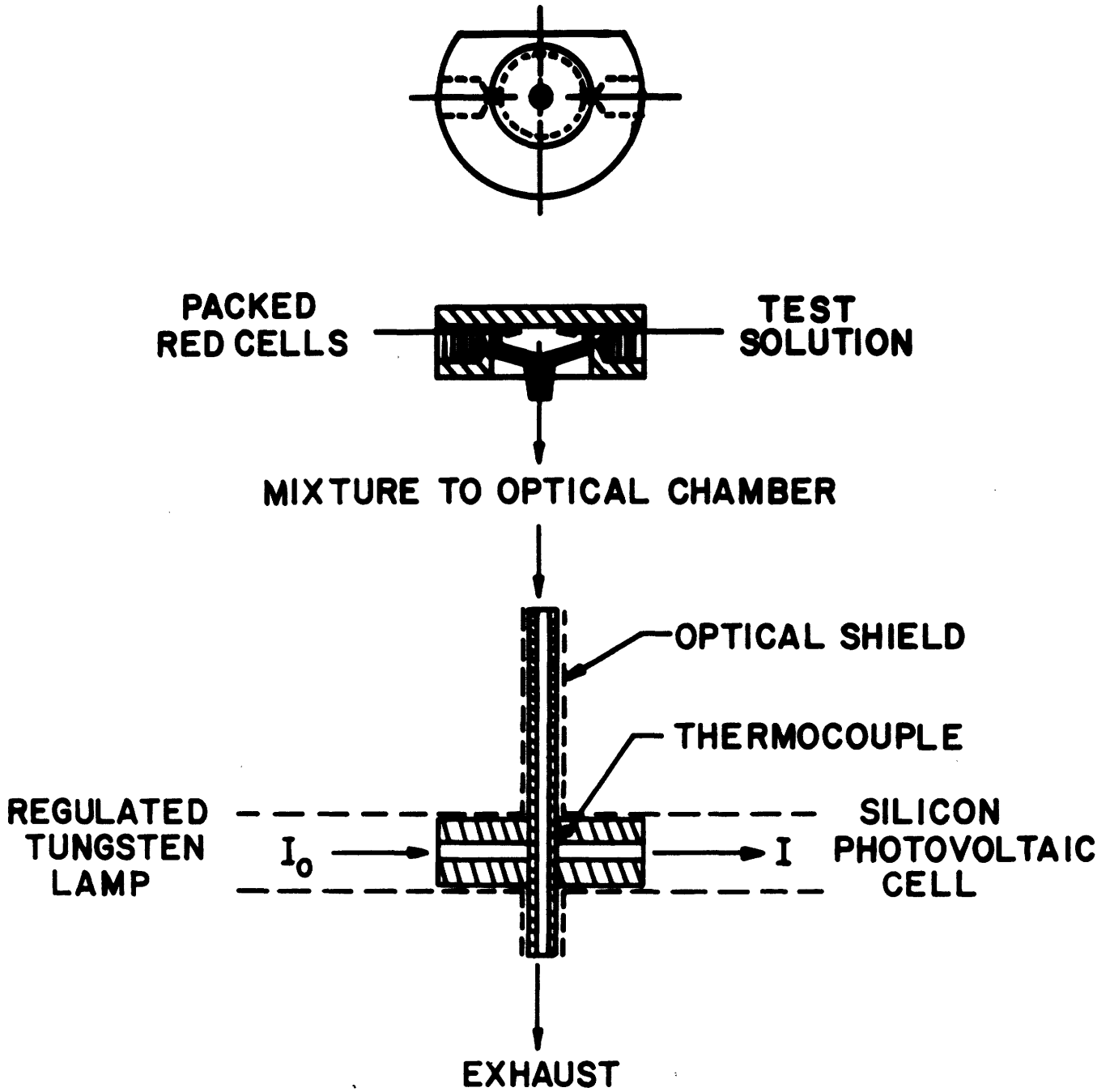


2) Temperature Set-Point Proportional Controller



Appendix D

Mixer Schematic



TO SCALE

┌───┐
1 INCH

Appendix E

Sensitivity of Optically Measured Percent Hemolysis to Variations in Delivered Hematocrit

The motivation for an analysis of this sort was a desire to understand how sensitive the optical subsystem would be to variations in injected hematocrits. Although during operation the absolute level of the photocell signal does not matter since the calibration of the system was done in terms of the normalized voltage ($\bar{V} = V_{\text{test}}/V_{0\%}$) and this calibration was found to be invariant for hematocrits between 4% and 10% (nominal). However, during the calibration procedure itself, the absolute values of the photocell voltages are important and it is at this stage that variations in the delivered hematocrit could influence the data for calibration.

The two expressions needed for the sensitivity determination are given below,

$$(E.1) \quad V' = \frac{V_{\text{test}}}{V_{\text{N.S.}}} = (3.36 \times 10^{-2}) (\text{Hematocrit})^{-1.56}$$

$$(E.2) \quad \% \text{ Hemolysis} = 24.313 \ln(\bar{V}) = 24.313 \ln\left(\frac{V_{\text{test}}}{V_{0\%}}\right)$$

Substituting (E.1) into (E.2)

$$\% \text{ Hemolysis} = 24.313 \ln \left[\frac{(V_{\text{N.S.}})(3.36 \times 10^{-2})(\% \text{Hct})^{-1.56}}{V_{0\%}} \right]$$

where %Hct has been substituted for "Hematocrit".

Assuming $V_{N.S.} = 8$ volts is a constant reference and $V_o\%$ is also constant then,

$$\% \text{ Hemolysis} = 24.313 \left\{ \ln \left[\frac{(V_{N.S.})(3.36 \times 10^{-2})}{V_o\%} \right] + \ln \left[(\% \text{ Hct})^{-1.56} \right] \right\}$$

From which

$$\begin{aligned} d(\% \text{ Hemolysis}) &= \frac{\partial(\% \text{ Hemolysis})}{\partial(\% \text{ Hct})} \cdot d(\% \text{ Hct}) \\ &= \frac{\partial}{\partial(\% \text{ Hct})} \left[-37.93 \ln(\% \text{ Hct}) \right] \cdot d(\% \text{ Hct}) \\ &= -\left(\frac{37.93}{\% \text{ Hct}} \right) \cdot d(\% \text{ Hct}) \end{aligned}$$

For the present experimental work nominal hematocrits were 4% and in most cases, due to non-complete "packedness" of the centrifuged cells the actual measured hematocrit was 2%. The measured hematocrit is the appropriate value since the relationship given above for V' as a function of hematocrit is for measured and not nominal hematocrit.

Experimentally measured deviations of the delivered hematocrit were 5% of the absolute value of 2%, or $d(\% \text{ Hct}) = 1 \times 10^{-3}$.

Therefore 5% variations in the delivered hematocrit would produce variations in the derived % Hemolysis:

$$\begin{aligned} d(\% \text{ Hemolysis}) &= -\left(\frac{37.93}{2} \right) (1 \times 10^{-3}) \\ &= -1.90\% \end{aligned}$$

The variation in absolute photocell voltage level associated with the 5% variation in delivered hematocrit at this 2% absolute level would be

$$\frac{V_1}{V_2} = \left(\frac{\% \text{ Hct}_1}{\% \text{ Hct}_2} \right)^{-1.56} = \left(\frac{2}{2.1} \right)^{-1.56}$$

$$\frac{V_1}{V_2} = 1.08$$

or an 8% change in the photocell voltage.

Appendix F

Red Cell Velocity Damping Estimate

For an erythrocyte sedimenting under the influence of gravity, one may equate the acceleration force to the gravitational force minus the viscous force and the buoyant force:

$$F_a = F_g - F_v - F_b$$

$$\rho \left(\frac{4}{3} \pi r^3 \right) \dot{u} = (\rho - \sigma) \left(\frac{4}{3} \pi r^3 \right) g - 6 \pi r \eta u$$

where ρ = erythrocyte density
 σ = suspension medium density
 r = erythrocyte radius
 u = erythrocyte velocity
 g = gravitational constant
 η = viscosity of suspension medium

The characteristic time of this system for damping out cell acceleration can be estimated from the homogeneous equation

$$\rho \left(\frac{4}{3} \pi r^3 \right) \dot{u} + 6 \pi r \eta u = 0$$

where the time constant for this first order system is

$$\tau = \frac{\rho \left(\frac{4}{3} \pi r^3 \right)}{6 \pi r \eta} = \frac{2 \rho r^2}{9 \eta}$$

$$\rho = 1.080 \text{ gm/cm}^3$$

$$r = 4.4 \times 10^{-4} \text{ cm}$$

$$\eta = 9.0 \times 10^{-3} \frac{\text{dyne} \cdot \text{sec}}{\text{cm}^2} = 9.0 \times 10^{-3} \text{ gm/cm-sec}$$

$$\tau = \frac{2(1.080 \text{ gm/cm}^3) (4.4 \times 10^{-4} \text{ cm})^2}{9(9.0 \times 10^{-3} \text{ gm/cm-sec})}$$

$$= 5.16 \times 10^{-6} \text{ sec}$$

The system is therefore highly damped and the erythrocyte should achieve its terminal velocity instantaneously with respect to hemolysis kinetics characteristic times.

Appendix G

Hemolysis Rate Curve-fits for Hypertonic Sodium Chloride
Exposure Times Greater Than Three Minutes at 298°K

<u>Concentration</u> (molality)	<u>Range of Exposure Times</u> (minutes)	<u>Curve-fit</u> (time in minutes)	<u>Correlation</u> <u>Coefficient</u>
1.00	60-800	$\%H=0.373(\text{time})^{0.508}$	0.99
1.96	3-10	$\%H=2.061(\text{time})^{0.326}$	0.98
2.45	3-9	$\%H=3.709(\text{time})^{0.318}$	0.99
2.94	3-11	$\%H=7.909(\text{time})^{0.213}$	0.99
3.43	3-7	$\%H=23.09(\text{time})^{0.205}$	0.99
3.92	3-6	$\%H=50.315(\text{time})^{0.061}$	0.99

Appendix H

Typical Resolution Capability of the Photocell For Percent Hemolysis Detection

A typical operating condition for hemolysis kinetics experiments would be 200mv, full scale. The strip chart paper is divided into 100 sub divisions and pen movement is easily detectable at one-half of one of these divisions. Therefore the resolved voltage reading is

$$V_{\text{resolved}} = \left(\frac{200\text{mv}}{100}\right) \times \frac{1}{2} = 1\text{mv}$$

Suppose that due to delivered hematocrit fluctuations, enough cells have been injected such that the zero percent hemolysis, minimum volume voltage ($V_0\%$) is 20mv. Then, by the reasoning above, the voltage could increase to 21mv before it would be easily discernible. The normalized voltage at this time would be,

$$\bar{V} = \frac{21\text{mv}}{20\text{mv}} = 1.05$$

which is translated to percent hemolysis by the calibration formula

$$\begin{aligned} \%H &= 24.313 \log_e(\bar{V}) \\ &= 1.19\% \end{aligned}$$

Appendix I

Tabulation of Typical Activation Energies in Biological Systems

<u>Process</u>	<u>Energy(Kcal/mole)</u>	<u>Reference</u>
1. Dissolution of cell membrane components	5.5	[53]
2. Diffusion through liquids and membranes, changes in viscosity, rigidity or tensile stress, and liquification	5-15	[39]
3. Diffusion of water through membranes	4-15	[22]
4. Lecithin-water phase transition	6-8	[59]
5. Hydrogen bond dissociation	7	[85]
6. Metabolic reactions both enzyme and non-enzyme catalyzed	10-50	[39]
7. Protein inactivation or denaturation	50-130	[39]

Appendix J

Computer Programs for Computer Freeze-Thaw Simulations, Figures 7.2 and 7.3

```

C     TOTAL TABULAR W AND B FORM
// JOB M70
// FOR
* LIST SOURCE
C     CHOOSE STARTING TEMPERATURE (K)
      TO= 273.15
C     CHOOSE COOLING RATE (K/MIN)
      DO 200 JS= 1,5
      B= 10.0**(JS-1)
C     CHOOSE WARMING RATE (K/MIN)
      DO 300 KS=1,5
      W= 10.0**(KS-1)
C     CHOOSE MINIMUM TEMPERATURE (K)
      TMIN= 252.15
C     CHOOSE HOLD PERIOD (MIN)
      TAUHLD= 1.0
C     CHOOSE INTEGRATION TIME STEP (MIN)
      DELTAU= 1.0/B
C     TIME IS INITIALIZED AND AMOUNT OF HEMOLYSIS
      TAU= 0.0
      TOTHMO= 0.0
      WRITE(5,100) TO,B,TMIN,TAUHLD,W,DELTAU
100  FORMAT(5X,'TO=',F7.3,2X,'B=',F9.3,2X,'TMIN=',F7.3,2X,'TAUHLD=',F5.
      13,2X,'W=',F9.3,2X,'DELTAU=',F6.3)
      WRITE(5,101)
101  FORMAT(//)
      WRITE(5,102)
102  FORMAT(20X,'THE FREEZING PROCESS')
C     FREEZING PORTION OF THE PROTOCOL
C     TRANSFORMATION FROM THE INDEPENDENT VARIABLE TO THE DEPENDENT
      CT= 0.0
10   CT= CT + 1.0
      T= TO-B*DELTAU*CT
C     WATER ACTIVITY CONSTANTS (RLL)
      CON1= 3.736*(10.0**3)
      CON2= 36.18
      CON3= 0.1024
      CON4= 5.435*(10.0**-5)
C     WATER ACTIVITY TEMPERATURE VARIABLES
      VAR1= (TO-T)/(TO*T)
      VAR2= ALOG(T/TO)
      VAR3= TO-T
      VAR4= (T**2)-(TO**2)
C     CALCULATION OF THE WATER ACTIVITY FOR EQUIL FREEZING
      RHS= CON1*VAR1 + CON2*VAR2 + CON3*VAR3 + CON4*VAR4
      XLNAW= RHS
C     HEMOLYSIS KINETIC PARAMETERS
      CON5= 9.115*(10.0**-2)
      CON6= 26.7
      DELHMO= CON5*EXP(-CON6*XLNAW)*DELTAU
C     TOTAL AMOUNT OF HEMOLYSIS IS INTEGRATED
      TOTHMO= TOTHMO + DELHMO
      WRITE(5,103) T,TOTHMO,TAU
103  FORMAT(5X,'TEMP=',F7.3,2X,'TOTAL % HEMOLYSIS=',F6.3,2X,'TOTAL TIME
      1 (MIN)=',F7.3)
C     INCREMENT TIME
      TAU= TAU + DELTAU
C     CHECK TO SFE IF STORAGE TEMPERATURE HAS BEEN REACHED
      IF (TMIN-T) 10,11,11
C     CALCULATE THE AMOUNT OF STORAGE DAMAGE

```



```

11 WRITE(5,101)
   WRITE(5,104)
104 FORMAT(20X,'THE STORAGE PERIOD')
   DELHMO= CON5*EXP(-CON6*XLNAW)*TAUHLD
C   INCREMENT TIME BY THE STORAGE TIME -TOTAL AMOUNT OF HFMOLYSIS
   TAU= TAU + TAUHLD
   TOTTHMO= TOTTHMO + DELHMO
   WRITE(5,103) TMIN,TOTTHMO,TAU
   WRITE(5,101)
   WRITE(5,105)
105 FORMAT(20X,'THE THAWING PROCESS')
   WRITE(5,103) T,TOTTHMO,TAU
C   WARMING PORTION OF THE PROTOCOL
C   CHOOSE INTEGRATION TIME STEP (MIN)
   DELTAU= 1.0/W
   CT= 0.0
12 CT= CT + 1.0
   T= TMIN + W*DELTAU*CT
   TAU= TAU + DELTAU
C   CALCULATION OF THE WATER ACTIVITY
   VAR1= (T0-T)/(T0*T)
   VAR2= ALOG(T/T0)
   VAR3= T0-T
   VAR4= (T**2)-(T0**2)
   RHS= CON1*VAR1 + CON2*VAR2 + CON3*VAR3 + CON4*VAR4
   XLNAW= RHS
C   CALCULATION OF DIFFERENTIAL AMOUNT OF HEMOLYSIS
   DELHMO= CON5*EXP(-CON6*XLNAW)*DELTAU
C   CALCULATE TOTAL AMOUNT OF HEMOLYSIS
   TOTTHMO= TOTTHMO + DELHMO
   WRITE(5,103) T,TOTTHMO,TAU
C   CHECK TO SEE IF INITIAL TEMPERATURE HAS BEEN REACHED
   IF (T-T0) 12,14,14
14 CONTINUE
300 CONTINUE
200 CONTINUE
   STOP
   END
// XEQ
// END

```

```

C      TRANSITION REGION 2<B<9
// JOB M70
// FOR
* LIST SOURCE
C      CHOOSE STARTING TEMPERATURE (K)
      T0= 273.15
C      CHOOSE COOLING RATE (K/MIN)
      B= 1.0
501 B= B + 1.0
      IF (B-10.0) 502,200,200
C      CHOOSE WARMING RATE (K/MIN)
502 CONTINUE
      W= 10.0
C      CHOOSE MINIMUM TEMPERATURE (K)
      TMIN= 252.15
C      CHOOSE HOLD PERIOD (MIN)
      TAUHLD= 1.0
C      CHOOSE INTEGRATION TIME STEP (MIN)
      DELTAU= 1.0/B
C      TIME IS INITIALIZED AND AMOUNT OF HEMOLYSIS
      TAU= 0.0
      TOTHMO= 0.0
      WRITE(5,100) T0,B,TMIN,TAUHLD,W,DELTAU
100  FORMAT(5X,'T0=',F7.3,2X,'B=',F9.3,2X,'TMIN=',F7.3,2X,'TAUHLD=',F5.
      13,2X,'W=',F9.3,2X,'DELTAU=',F6.3)
      WRITE(5,101)
101  FORMAT(//)
      WRITE(5,102)
102  FORMAT(20X,'THE FREEZING PROCESS')
C      FREEZING PORTION OF THE PROTOCOL
C      TRANSFORMATION FROM THE INDEPENDENT VARIABLE TO THE DEPENDENT
      CT= 0.0
10  CT= CT + 1.0
      T= T0-B*DELTAU*CT
C      WATER ACTIVITY CONSTANTS (RLL)
      CON1= 3.736*(10.0**3)
      CON2= 36.18
      CON3= 0.1024
      CON4= 5.435*(10.0**-5)
C      WATER ACTIVITY TEMPERATURE VARIABLES
      VAR1= (T0-T)/(T0*T)
      VAR2= ALOG(T/T0)
      VAR3= T0-T
      VAR4= (T**2)-(T0**2)
C      CALCULATION OF THE WATER ACTIVITY FOR EQUIL FREEZING
      RHS= CON1*VAR1 + CON2*VAR2 + CON3*VAR3 + CON4*VAR4
      XLNAW= RHS
C      HEMOLYSIS KINETIC PARAMETERS
      CON5= 9.115*(10.0**-2)
      CON6= 26.7
      DELHMO= CON5*EXP(-CON6*XLNAW)*DELTAU
C      TOTAL AMOUNT OF HEMOLYSIS IS INTEGRATED
      TOTHMO= TOTHMO + DELHMO
      WRITE(5,103) T,TOTHMO,TAU
103  FORMAT(5X,'TEMP=',F7.3,2X,'TOTAL % HEMOLYSIS=',F6.3,2X,'TOTAL TIME
      1 (MIN)=',F7.3)
C      INCREMENT TIME
      TAU= TAU + DELTAU
C      CHECK TO SEE IF STORAGE TEMPERATURE HAS BEEN REACHED
      IF (TMIN-T) 10,11,11

```

```

C    CALCULATE THE AMOUNT OF STORAGE DAMAGE
11  WRITE(5,101)
    WRITE(5,104)
104  FORMAT(20X,'THE STORAGE PERIOD:')
    DELHMO= CON5*EXP(-CON6*XLNAW)*TAUHLD
C    INCREMENT TIME BY THE STORAGE TIME -TOTAL AMOUNT OF HEMOLYSIS
    TAU= TAU + TAUHLD
    TOTHMO= TOTHMO + DELHMO
    WRITE(5,103) TMIN,TOTHMO,TAU
    WRITE(5,101)
    WRITE(5,105)
105  FORMAT(20X,'THE THAWING PROCESS')
    WRITE(5,103) T,TOTHMO,TAU
C    WARMING PORTION OF THE PROTOCOL
C    CHOOSE INTEGRATION TIME STEP (MIN)
    DELTAU= 1.0/W
    CT= 0.0
12  CT= CT + 1.0
    T= TMIN + W*DELTAU*CT
    TAU= TAU + DELTAU
C    CALCULATION OF THE WATER ACTIVITY
    VAR1= (T0-T)/(T0*T)
    VAR2= ALOG(T/T0)
    VAR3= T0-T
    VAR4= (T**2)-(T0**2)
    RHS= CON1*VAR1 + CON2*VAR2 + CON3*VAR3 + CON4*VAR4
    XLNAW= RHS
C    CALCULATION OF DIFFERENTIAL AMOUNT OF HEMOLYSIS
    DELHMO= CON5*EXP(-CON6*XLNAW)*DELTAU
C    CALCULATE TOTAL AMOUNT OF HEMOLYSIS
    TOTHMO= TOTHMO + DELHMO
    WRITE(5,103) T,TOTHMO,TAU
C    CHECK TO SEE IF INITIAL TEMPERATURE HAS BEEN REACHED
    IF (T-T0) 12,14,14
14  CONTINUE
    GO TO 501
200 CONTINUE
    STOP
    END
// XEQ
// END

```

Computer Program for Figure 7.5

```

C   LOVELOCK TMIN SIMULATION
// JOB M70
// FOR
* LIST SOURCE
C   CHOOSE STARTING TEMPERATURE (K)
    T0= 273.15
C   CHOOSE COOLING RATE (K/MIN)
    B= 10.0
C   CHOOSE WARMING RATE (K/MIN)
    W= 100.0
C   CHOOSE MINIMUM TEMPERATURE (K)
    TMIN= 262.15
    DO 201 JB= 1,10
    TMIN= TMIN + 1.0
C   CHOOSE HOLD PERIOD (MIN)
    TAUHLD= 12.0
C   CHOOSE INTEGRATION TIME STEP (MIN)
    DELTAU= 1.0/B
C   TIME IS INITIALIZED AND AMOUNT OF HEMOLYSIS
    TAU= 0.0
    TOTHMO= 0.0
    WRITE(5,100) T0,B,TMIN,TAUHLD,W,DELTAU
100  FORMAT(5X,'T0=',F7.3,2X,'B=',F9.3,2X,'TMIN=',F7.3,2X,'TAUHLD=',F5.
    13,2X,'W=',F9.3,2X,'DELTAU=',F6.3)
    WRITE(5,101)
101  FORMAT(//)
    WRITE(5,102)
102  FORMAT(20X,'THE FREEZING PROCESS')
C   FREEZING PORTION OF THE PROTOCOL
C   TRANSFORMATION FROM THE INDEPENDENT VARIABLE TO THE DEPENDENT
    CT= 0.0
    10  CT= CT + 1.0
    T= T0-B*DELTAU*CT
C   WATER ACTIVITY CONSTANTS (RLL)
    CON1= 3.736*(10.0**3)
    CON2= 36.18
    CON3= 0.1024
    CON4= 5.435*(10.0**5)
C   WATER ACTIVITY TEMPERATURE VARIABLES
    VAR1= (T0-T)/(T0*T)
    VAR2= ALOG(T/T0)
    VAR3= T0-T
    VAR4= (T**2)-(T0**2)
C   CALCULATION OF THE WATER ACTIVITY FOR EQUIL FREEZING
    RHS= CON1*VAR1 + CON2*VAR2 + CON3*VAR3 + CON4*VAR4
    XLNAW= RHS
C   HEMOLYSIS KINETIC PARAMETERS
    CON5= 9.115*(10.0**2)
    CON6= 26.7
    DELHMO= CON5*EXP(-CON6*XLNAW)*DELTAU
C   TOTAL AMOUNT OF HEMOLYSIS IS INTEGRATED
    TOTHMO= TOTHMO + DELHMO
    WRITE(5,103) T,TOTHMO,TAU
103  FORMAT(5X,'TEMP=',F7.3,2X,'TOTAL % HEMOLYSIS=',F6.3,2X,'TOTAL TIME
    1 (MIN)=',F7.3)
C   INCREMENT TIME
    TAU= TAU + DELTAU
C   CHECK TO SEE IF STORAGE TEMPERATURE HAS BEEN REACHED
    IF (TMIN-T) 10,11,11
C   CALCULATE THE AMOUNT OF STORAGE DAMAGE

```

```

11 WRITE(5,101)
   WRITE(5,104)
104 FORMAT(20X,'THE STORAGE PERIOD')
   DELHMO= CON5*EXP(-CON6*XLNAW)*TAUHLD
C   INCREMENT TIME BY THE STORAGE TIME -TOTAL AMOUNT OF HEMOLYSIS
   TAU= TAU + TAUHLD
   TOTTHMO= TOTTHMO + DELHMO
   WRITE(5,103) TMIN,TOTTHMO,TAU
   WRITE(5,101)
   WRITE(5,105)
105 FORMAT(20X,'THE THAWING PROCESS')
   WRITE(5,103) T,TOTTHMO,TAU
C   WARMING PORTION OF THE PROTOCOL
C   CHOOSE INTEGRATION TIME STEP (MIN)
   DELTAU= 1.0/W
   CT= 0.0
12  CT= CT + 1.0
   T= TMIN + W*DELTAU*CT
   TAU= TAU + DELTAU
C   CALCULATION OF THE WATER ACTIVITY
   VAR1= (T0-T)/(T0*T)
   VAR2= ALOG(T/T0)
   VAR3= T0-T
   VAR4= (T**2)-(T0**2)
   RHS= CON1*VAR1 + CON2*VAR2 + CON3*VAR3 + CON4*VAR4
   XLNAW= RHS
C   CALCULATION OF DIFFERENTIAL AMOUNT OF HEMOLYSIS
   DELHMO= CON5*EXP(-CON6*XLNAW)*DELTAU
C   CALCULATE TOTAL AMOUNT OF HEMOLYSIS
   TOTTHMO= TOTTHMO + DELHMO
   WRITE(5,103) T,TOTTHMO,TAU
C   CHECK TO SEE IF INITIAL TEMPERATURE HAS BEEN REACHED
   IF (T-T0) 12,14,14
14  CONTINUE
201 CONTINUE
   STOP
   END
// XEQ
// END

```

Appendix K

General Phase Diagram Information

1) Conversion from Molarity to Molality and vice versa

M = molarity

m = molality

$$m = \left(\frac{M}{1 - 0.0173M} \right)$$

$$M = \left(\frac{m}{1 + 0.0173m} \right)$$

where the maximum concentration to be expected in this sodium chloride-water system is the eutectic point:

$$[m] = 5.205m$$

$$[M] = 4.78M$$

2) HP-25 Program for Determination of Water Activity as a Function of Temperature (see reference [22]).

3.736×10^3	ST0 0
36.18	ST0 1
0.1024	ST0 2
5.435×10^{-5}	ST0 3
273.15	ST0 4
T	ST0 5
1.0	ST0 6

- | | | |
|-----------|-----------|---------------------|
| 1. RCL 6 | 14. RCL 5 | 27. X |
| 2. † | 15. † | 28. + |
| 3. RCL 5 | 16. RCL 4 | 29. RCL 5 |
| 4. ÷ | 17. ÷ | 30. gx ² |
| 5. † | 18. fln | 31. † |
| 6. RCL 6 | 19. RCL 1 | 32. RCL 4 |
| 7. † | 20. X | 33. gx ² |
| 8. RCL 4 | 21. + | 34. - |
| 9. ÷ | 22. † | 35. † |
| 10. - | 23. RCL 4 | 36. RCL 3 |
| 11. RCL 0 | 24. † | 37. X |
| 12. X | 25. RCL 5 | 38. + |
| 13. † | 26. RCL 2 | 39. GTO 00 |

- 3) Calculation of the activity of sodium chloride in the NaCl-H₂O system, including an HP-25 program to calculate the NaCl osmotic coefficient from the salt mole fraction.

The basic algorithm for this procedure is

$$\text{molarity} \rightarrow \text{molality} \rightarrow X_S \rightarrow \phi_S \rightarrow a_S$$

where

$$X_S = \frac{2n_S}{n_W + 2n_S}$$

n_S = number of moles of salt

n_W = number of moles of water

X_S = salt mole fraction

ϕ_S = salt osmotic coefficient

a_S = salt activity

and $\phi_S \ln X_S = \ln a_S$ or

$$a_S = X_S^\phi$$

The HP-25 program for the equation is:

$$\phi_s = \frac{1}{(39.965 X_s + 1.706)^3} + 2.57698 X_s + 0.79861$$

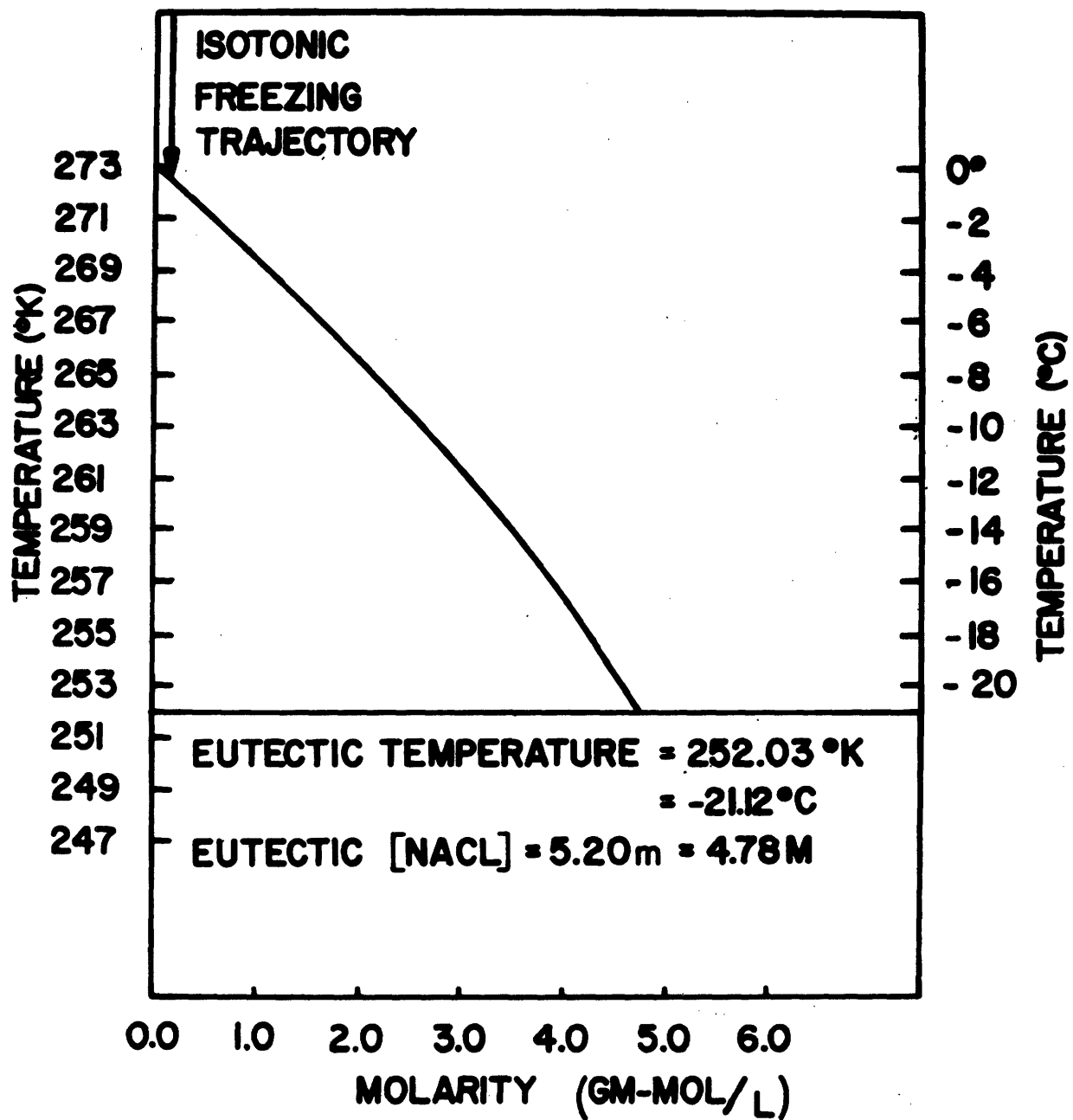
From ref. [44]

1.0	STO 0
3.0	STO 1
39.965	STO 2
1.706	STO 3
2.57698	STO 4
0.79861	STO 5
X_s	STO 6

1. RCL 2	9. $f y^x$	17. RCL 6
2. \uparrow	10. \uparrow	18. X
3. RCL 6	11. RCL 0	19. ENTER
4. X	12. $X \div Y$	20. RCL 5
5. RCL 3	13. \div	21. +
6. +	14. STO 7	22. RCL 7
7. ENTER	15. RCL 4	23. +
8. RCL 1	16. ENTER	24. GTO 00

4) References

- a) Sodium Chloride-Water Phase Diagram: °F vs Weight Percent Anhydrous NaCl, Saline Water Conversion Engineering Data Book, U.S. Department of the Interior, Office of Saline Water, November 1971.
- b) Sodium Chloride-Water Phase Diagram: °C vs Weight Percent Salt (to -80°C) from Cryobiology, Vol.13 No.5 1976
- c) Water Activity and Water Osmotic Coefficient as a Function of Molality of Sodium Chloride-Water Solution, Appendix 8.3, Table 1, p. 479, Electrolyte Solutions, by Robinson, R. and Stokes, R.



References

1. Polge, C., Smith, A.U. and Parkes, A., "Revival of Spermatozoa after Vitrification and Dehydration at Low Temperatures", Nature Vol. 164, 1949, p. 666.
2. Huggins, C.E., "Frozen Blood", Annals of Surgery, October 1964, pp. 643-649.
3. Sadleir, R.M.F.S., "Preservation of Mammalian Spermatozoa by Freezing", Laboratory Practice, Vol. 15, 1966, pp. 413-417.
4. Mueller, F.O., Casey, T.A., and Trevor-Roper, P.D., "Use of Deep-frozen Human Cornea in Full Thickness Grafts", British Medicine Journal, Vol. ii, 1964, pp. 473-475.
5. Lehr, H.B., Berggren, R.B., Lotke, P.A., and Coriell, L.L., "Permanent Survival of Preserved Skin Autografts", Surgery (St. Louis), Vol. 56, 1964, pp. 742-746.
6. Valeri, C.R., "Principles of Cryobiology-High Glycerol and Storage at -80°C and Low Glycerol and Storage at -150°C ", Red Cell Freezing, A Technical Workshop, Americana Hotel, Bal Harbour, Florida, November 11, 1973, pp. 1-30.
7. Huggins, C.E., Personal Communication, 1976.
8. Nusbacker, J., "The Clinical Use of Frozen Red Cells", Red Cell Freezing, A Technical Workshop, Americana Hotel, Bal Harbour, Florida, November 11, 1973, pp. 87-95.
9. Mazur, P., Leibo, S.P., Farrant, J., Chu, E.H.Y., Hanna, M.G., Smith, L.H., "Interactions of Cooling Rate, Warming Rate and Protective Additive on the Survival of Frozen Mammalian Cells", The Frozen Cell, J. and A. Churchill, London, 1970, pp. 69-88.
10. Mazur, P., "Causes of Injury in Frozen and Thawed Cells", Fed. Proc. Amer. Soc. Exp. Biol., Vol. 24, 1965, pp. 175-182.

11. Mazur, P., "Physical and Chemical Basis of Injury in Single-celled Micro-organisms Subjected to Freezing and Thawing", Cryobiology, ed. by H.T. Meryman, Academic Press, London, 1966, pp. 214-315.
12. Gupta, K.C., "The Mechanism of Cryohemolysis: By Direct Observation with the Cryomicroscope and the Electron Microscope", Cryobiology, Vol. 12, No. 4, 1975, pp. 417-426.
13. Buckman, R.L., McGrath J.J., Cravalho, E.G., Huggins, C.E., "HeLa Cell Survival as a Function of Constant Cooling Rate and Constant Warming Rate", unpublished data.
14. Leibo, S.P., McGrath, J.J., Cravalho, E.G., unpublished data.
15. Leibo, S.P., McGrath, J.J., Cravalho, E.G., "Microscopic Observation of Intracellular Ice Formation in Mouse Ova as a Function of Cooling Rate", submitted to Cryobiology, 1976.
16. Diller, K.R., "Intracellular Freezing: Effect of Extracellular Supercooling", Cryobiology, Vol 12, No. 5, 1975, pp. 480-485.
17. Rapatz, G., Sullivan, J., and Luyet, B., "Preservation of Erythrocytes in Blood Containing Various Cryoprotective Agents, Frozen at Various Rates and Brought to a Given Final Temperature", Cryobiology, Vol. 5, No. 1., 1968, pp. 18-25.
18. McGrath, J.J., Cravalho, E.G., Huggins, C.E., "An Experimental Comparison of Intracellular Ice Formation and Freeze-Thaw Survival of HeLa S-3 Cells", Cryobiology, Vol. 12, No. 6, 1975, pp. 540-550.
19. Mazur, P., "Kinetics of Water Loss from Cells at Subzero Temperatures and the Likelihood of Intracellular Freezing", Journal of General Physiology, Vol. 47, 1963, pp. 347-369.

20. Silvaes, O.M., Cravalho, E.G., Toscano, W.M., Huggins, C.E.,
"The Thermodynamics of Water Transport for Biological Cells During Freezing", ASME Paper No. 74-WA/Bio-2, presented at the ASME Winter Annual Meeting, New York, NY, November 17-22, 1974.
21. Toscano, W.M., Cravalho, E.G., Silvaes, O.M., Huggins, C.E.,
"The Thermodynamics of Intracellular Ice Nucleation in the Freezing of Erythrocytes", Journal of Heat Transfer, Trans., Trans. ASME, August 1975, pp. 326-332.
22. Levin, R.L., "Kinetics of Water Transport in Biomaterials During Freezing," Sc.D. Thesis, Department of Mechanical Engineering, M.I.T., February 1976.
23. Leibo, S.P., Farrant, J., Mazur, P., Hanna, M.G., Smith, L.H.,
"Effects of Freezing on Marrow Stem Cell Suspensions: Interactions of Cooling and Warming Rates in the Presence of PVP, Sucrose, or Glycerol", Cryobiology, Vol. 6, No. 4, 1970, pp. 315-332.
24. Lovelock, J.E., "The Mechanism of the Protective Action of Glycerol Against Haemolysis by Freezing and Thawing", Biochemica et Biophysica Acta, Vol. 11, 1953, pp. 28-36.
25. Meryman, H.T., "Review of Biological Freezing", Cryobiology, ed. by H.T. Meryman, Academic Press, London, 1966, pp. 1-114.
26. Cravalho, E.G., Huggins, C.E., Diller, K.R., Watson, W.W.,
"Blood Freezing to -272.29°C (-458.12°F)", presented at the 9th Annual Meeting, Society for Cryobiology, July 30-August 3, 1972, Washington, D.C.
27. Lovelock J.E., "The Haemolysis of Human Red Blood-Cells By Freezing and Thawing", Biochemica et Biophysica Acta, Vol. 10, 1953, pp. 414-426.

29. Zade-Oppen, A.M.M., "Posthypertonic Hemolysis in Sodium Chloride Systems," *Acta Physiol. Scand.*, Vol. 73, 1968, pp. 341-364.
30. Morris, G.J., Farrant, J., "Effects of Cooling Rate on Thermal Shock Hemolysis", *Cryobiology*, Vol. 10, No. 2, 1973, pp. 119-125.
31. Woolgar, A.E., Morris, G.J., "Some Combined Effects of Hypertonic Solutions and Changes in Temperature on Posthypertonic Hemolysis of Human Red Blood Cells", *Cryobiology*, Vol. 10, No. 1, 1973, pp. 82-86.
32. Daw, A., Farrant, J., Morris, G.J., "Membrane Leakage of Solutes After Thermal Shock or Freezing", *Cryobiology*, Vol. 10, No. 2, 1973, pp. 126-133.
33. Farrant, J., Woolgar, A.E., "Human Red Cells Under Hypertonic Conditions: A Model System for Investigating Freezing Damage: 1. Sodium Chloride", *Cryobiology*, Vol. 9, No. 1, 1972, pp. 9-15.
34. Lovelock, J.E., "Physical Instability and Thermal Shock in Red Cells", *Nature* (London), Vol. 173, 1954, pp. 659-661.
35. Nei, T., "Mechanism of Hemolysis of Erythrocytes by Freezing at Near-Zero Temperatures. I. Microscopic Observation of Hemolyzing Erythrocytes during the Freezing and Thawing Process", *Cryobiology*, Vol. 4, No. 3, 1960, pp. 153-156.
36. Brandts, J.F., Fu, J., Nordin, J.H., "The Low Temperature Denaturation of Chymotrypsinogen in Aqueous Solution and in Frozen Aqueous Solution", *The Frozen Cell*, Churchill 1970, pp. 189-212.
37. Tappel, A.L., "Effects of Low Temperatures and Freezing on Enzymes and Enzyme Systems", *Cryobiology*, ed. by H.T. Meryman, Academic Press, 1966, pp. 163-177.

38. Damjanovic, V., "Selective Thermal Effects on Freeze-Dried Biological Materials", Cryobiology, Vol. 12, 1975, pp. 169-174.
39. Henriques, F.C., Jr., "Studies of Thermal Injury, Part V: The Predictability and the Significance of Thermally Induced Rate Processes Leading to Irreversible Epidermal Injury", Arch. Pathol., Vol. 43, 1947, pp. 489-502.
40. Asimacopoulos, P.J., McGrath, J.J., Cravalho, E.G., "The Thermal Sensitivity of the Human Fibroblast HeLa S-3 as a Model for Thermal Insult to the Neointima of a Nuclear-Fueled, Blood-Cooled, Left Ventricular Circulatory Assist Device", 1975 Advances in Bioengineering, Winter Annual Meeting, ASME, Nov. 30-Dec. 5, 1975.
41. Lloyd, J.R., Mueller, J.R., Waugh, R.E., "On In Vitro Thermal Damage to Erythrocytes", presented at the ASME Winter Annual Meeting, Detroit, Michigan, Nov. 11-15, 1973.
42. Mazur, P., Leibo, S.P., Miller, R.H., "Permeability of the Bovine Red Cell to Glycerol in Hyperosmotic Solutions at Various Temperatures", J. Mem. Biol., Vol. 15, 1974, pp. 107-136.
43. Papanek, T.H., "An Apparatus to Measure Red Cell Permeability at Low Temperature", S.M.M.E. Thesis, Dept. of Mechanical Engineering, M.I.T., May 1975.
44. Silveiras, O.M., "A Thermodynamic Model of Water and Ion Transport Across Cell Membranes During Freezing and Thawing: The Human Erythrocyte", Ph.D. Thesis, Dept. of Mechanical Engineering, M.I.T., October 1974.
45. Kermack, W.O., McKendrick, A.G., and Ponder, E., "XV. The Stability of Suspensions. III. The Velocities of Sedimentation and of Cataphoresis of Suspensions in a Viscous Fluid", Proc. Roy. Soc.

- Edinburgh, Vol. 49, 1929, pp. 170-197.
46. Keshaviak, P., Blackshear, P.L., Forestrom, R., "Red Cell Destruction in Regions of Accelerated Flow", 1975 Advances In Bioengineering, Winter Annual Meeting, ASME, Nov. 30-Dec.5, 1975.
 47. Diller, K.R., "A Microscopic Investigation of Intracellular Ice Formation in Frozen Human Erythrocytes", Sc.D. Thesis, Dept. of Mechanical Engineering, M.I.T., June 1972.
 48. Ushiyama, M., "Volumetric Changes in Sacchromyces Cerevisiae during Freezing at Constant Cooling Velocities", S.B. and S.M. Thesis, Dept of Mechanical Engineering, M.I.T., 1972.
 49. Masouredis, S.P., "Clinical Use of Erythrocyte Preparations", Chapter 166, Hematology, ed. by Williams, W.J., Beutler, E., Erlev, A.J., Rundles, R.W., McGraw Hill 1972, p. 1320.
 50. Soderstrom, N., "Hemolysis by Hypertonic Solutions of Neutral Salts", Acta Physiol. Scand., Vol. 7, 1944, pp. 56-68.
 51. Papanek, T., Personal communication, 1976.
 52. Lovelock, J.E., "Haemolysis by Thermal Shock", Brit. J. Haematol., Vol. 1, 1955, pp. 117-129.
 53. Lovelock J.E., "The Physical Instability of Human Red Blood Cells", Biochem. J., Vol. 60, 1955, pp. 692-696.
 54. Weinstein, R.S., "Electron Microscopy of Surfaces of Red Cell Membranes", Chapter 2 of Red Cell Membrane Structure and Function ed. by Jamieson, G. and Greenwalt, T., J.B. Lippincott, 1969, pp. 36-82.
 55. Morris, G.J., "Lipid Loss and Haemolysis by Thermal Shock: Lack of Correlation", Cryobiology, Vol. 12, No. 3, 1975, pp. 192-201.
 56. Singer, S.J., and Nicolson, G.L., "The Fluid Mosaic Model of the Structure of Cell Membranes", Science, Vol. 175, 1972, pp. 720-731.
 57. Lehninger, A.L., Chapter 11: Lipids, Lipoproteins, and Membranes, Biochemistry, Worth Publishers Inc., Second Edition, 1975, pp.279-308.

58. Sweeley, C., Dawson, G., "Lipids of the Erythrocyte", Chapter 8 of Red Cell Membrane Structure and Function, ed. by Jamieson, G., and Greenwalt, T., J. B. Lippincott, 1969, pp. 172-227.
59. Chapman, D., Urbina, J., Keogh, K.M. "Biomembrane Phase Transitions, Studies of Lipid-Water Systems Using Differential Scanning Calorimetry", J. Biol. Chem., Vol. 249, No. 8, 1974, pp. 2512-2521.
60. Trauble, H., and Eibl, H. "Electrostatic Effects on Lipid Phase Transition: Membrane Structure and Ionic Environment", Proc. Natl. Acad. Sci., Vol. 71, No. 1, 1974, pp. 214-219.
61. Vanderkooi, J., Fishkoff, S., Chance, B., Cooper, R., "Fluorescent Probe Analysis of the Lipid Architecture of Natural and Experimental Cholesterol-Rich Membranes", Biochemistry, Vol, 13, No. 8, pp. 1589-1595.
62. McElhaney, R., "The Effect of Alterations in the Physical State of the Membrane Lipids on the Ability of *Acholeplasma laidlawii* B to Grow at Various Temperatures", J. Mol. Biol., Vol. 84, 1974, pp. 145-157.
63. Chapman, D., Biological Membranes, ed. by D. Chapman, Vol. 1, Academic Press 1968, New York.
64. Evans, E., and Fung, Y.C., "Improved Measurements of the Erythrocyte Geometry", Microvasc. Res. Vol. 4, 1972, pp. 335-347.
65. Vander, A., Sherman, J., Luciano, D., Chapter 2, "Movement of Molecules Across Cell Membranes", Human Physiology: The Mechanism of Body Function, McGraw-Hill 1970, pp. 35-61.
66. Tien, H.L., "The Bifacial Tension of BLM", Bilayer Lipid Membranes: Theory and Practice, Marcel Dekker Inc. New York pp. 34-35.
67. Haydon, D., "Properties of Lipid Bilayers at a Water-Water Interface", Proceedings of the Symposium entitled: Lipid Monolayer and Bilayer Models and Cellular Membranes, conducted by the

- American Oil Chemists' Society at its 58th Annual Spring Meeting, New Orleans, Louisiana, May 7-10, 1967.
68. Davies, J., and Rideal, E., Chapter 4, "Adsorption at Liquid Interfaces, The Gibbs Equation", Interfacial Phenomena, Academic Press, New York 1963, pp. 196-197.
 69. Castellan, G., Chapter 18 "Surface Phenomena", Physical Chemistry, 2nd Ed. Addison-Wesley, 1971, pp. 429-432.
 70. Glasstone, S., Laidler, K., Eyring, H., The Theory of Rate Processes, McGraw-Hill, New York, 1941.
 71. Frost, A. and Pearson, R., Kinetics and Mechanism, 2nd Ed. John Wiley and Sons, New York, 1961.
 72. Lovelock, J., "The Denaturization of Lipid-Protein Complexes as a Cause of Damage by Freezing", Proc. Roy. Soc. Ses. B., Vol. 147, 1957, pp. 427-433.
 73. McGrath, J.J., unpublished data.
 74. Trauble, H., "The Movement of Molecules Across Lipid Membranes: A Molecular Theory", J. Membrane Biology, Vol. 4, 1971, pp. 193-208.
 75. Lyons, J., "Phase Transitions and Control of Cellular Metabolism at Low Temperatures:", Cryobiology, Vol. 9, No. 5, 1972, pp. 341-350.
 76. Zimer, G. and Schirmer, H., "Viscosity Changes of Erythrocyte Membrane and Membrane Lipids at Transition Temperatures", Biochem. et Biophys. Acta, Vol. 345, 1974, pp. 314-320.
 77. Johansson, K. and Eriksson, J., "Determination of dy/dT for Water by Means of a Differential Technique", Journal of Colloid and Interface Science, Vol. 40, No. 3, 1972, pp. 398-405.

78. Postgate, J., and Hunter, J., "On the Survival of Frozen Bacteria", J. Gen. Microbiol., Vol. 26, 1961, pp. 367-378.
79. Katchalsky, A., and Curran, P., Nonequilibrium Thermodynamics in Biophysics. Harvard University Press, Cambridge, Mass., 1967.
80. Morris, G., and Farrant, J., "Interactions of Cooling Rate and Protective Additive on the Survival of Washed Human Erythrocytes Frozen to -196°C ", Cryobiology, Vol. 9, No. 3, 1972, pp. 173-181.
81. Williams, R., Hope, H., Willemot, C., "Membrane Collapse as a Cause of Osmotic Injury and its Reversibility in a Hardy Wheat", Cryobiology, Vol. 12, No. 6, 1975, p. 554, (abstract).
82. Barer, R., Joseph S., "Refractometry of Living Cells, Part I. Basic Principles", Quart. J. Micr. Sci., Vol. 95, 1954, pp. 399-423.
83. Rotman, B., and Papermaster, B., "Membrane Properties of Living Mammalian Cells as Studied by Enzymatic Hydrolysis of Fluorogenic Esters", Proc. Natl. Acad. Sci., U. S., Vol. 55, 1966, pp. 134-141.
84. Williams, R., Harris, D., "The Surface Active Properties of Cryo-protective Agents", Cryobiology, Vol. 12, No. 6, 1975, p. 586, (abstract).
85. Mahan, B., University Chemistry, Addison-Wesley, Reading, Mass., 1967, p. 464.
86. Ealing Catalog, The Ealing Corporation, 22 Pleasant Street, South Natick, Massachusetts, Optical Components, pp. 84-85.

Acknowledgements

I would like to thank the members of my thesis committee, Professor Cravalho, Dr. Essig, Dr. Huggins and Professor Mikic for their assistance and congeniality throughout this effort. It would be a pleasure to interact with them and learn from them in the future.

A special thanks must go to my thesis advisor, Ernie Cravalho. His most appreciated skills from my standpoint were his uncanny ability to teach and inspire, all the while flavoring his approach with patent informality.

I feel fortunate in having had the opportunity to be associated with Dr. Charles Huggins, Director of the Massachusetts General Hospital Blood Bank for the past five years. He courteously made available the fresh blood and the resources of his laboratory for the experimental part of this thesis. Working with Dr. Huggins and his staff has been invaluable in gaining a fuller appreciation for the practical problems of frozen blood banking.

I would like to thank the members of the Cryogenic Engineering Laboratory for their contributions in making my M.I.T. experience an enjoyable one. I appreciated Professor J.L. Smith readily offering his advice and encouragement at all times. Thanks to Karl Benner and Bob Gertsen for their technical support and the good times in the shop. During my stay in this lab, I also grew to appreciate the value of effective administrative assistance and I'd like to thank Rachel Levin

for her aid. Former and present graduate students within the lab have added to the work which appears in this thesis by way of discussing the problems encountered: Dr. Otavio de Mattos Silves, Dr. Ronald Levin, Mike O'Callaghan, Tom Papanek, and Dr. N. Albert Moussa. Josie Stein certainly deserves credit for her hemolysis kinetics experiments which produced data that was valuable both in establishing a calibration technique for the present apparatus and for checking preliminary data obtained from the apparatus.

My thanks to Sharon Joyner and Susan Smith for their efforts which appear as the illustrations in this thesis. Jack Darnell of the Massachusetts General Hospital Blood Bank as well as Maury Cosman and Mike O'Callaghan were especially helpful in the last frantic days when they helped transform the finished drawings into slides and mounted figure prints.

My thanks to Beverly Harris and Betty Larsen for their friendly secretarial aid and especially to Diane Hickman who transformed the original scribbled manuscript of this thesis into the final product which appears between these two covers.

Finally the author would like to express his appreciation to the Mechanical Engineering Department of M.I.T. for financial support in the form of a research assistantship and to the National Institute of General Medical Sciences for the fellowship which made my graduate education possible.

Biographical Sketch

The author was graduated from Catalina High School in Tucson, Arizona in June, 1967. He attended Stanford University and received the Bachelor of Science degree in Mechanical Engineering, graduating cum laude in June 1971. He received his Master of Science degree in Mechanical Engineering from the Massachusetts Institute of Technology in January, 1974. The title of the Masters thesis was "The Dynamics of Freezing and Thawing Mammalian Cells: The HeLa Cell." While at M.I.T. as a graduate student, the author was supported for his first two and one half years by a research assistantship. For the remainder of his tenure, he held a National Institutes of General Medical Sciences Fellowship. He is a member of The Society for Cryobiology, A.S.M.E., and Sigma Xi. His publications are listed below:

1. McGrath, J.J., Cravalho, E.G., Diller, K.R., Huggins, C.E., "Response of HeLa Cells to Freezing and Thawing at Constant Cooling Rates", Cryobiology, Vol. 10, No. 6, 1973, p. 528 (abstract)
2. McGrath, J.J., Toscano, W.M., Buckman, R.L., Cravalho, E.G., Huggins, C.E., "Nucleation Temperatures for Intracellular Ice Formation in HeLa Cells", Cryobiology, Vol. 11, No. 6, 1974, p. 548 (abstract)
3. McGrath, J.J., Cravalho, E.G., Huggins, C.E., "HeLa Cell Freezing Injury: Intracellular Ice Formation and Survival as a Function of Cooling Velocity", Cryobiology, Vol. 11, No. 6, 1974, p. 549, (abstract)
4. Leibo, S.P., McGrath, J.J., Cravalho, E.G., "Microscopic Observation of Intracellular Ice Formation in Mouse Ova as a Function of Cooling Rate," Cryobiology, Vol. 12, No. 6, 1975, p. 579 (abstract)

5. McGrath, J.J., Cravalho, E.G., Huggins, C.E., "An Experimental Comparison of Intracellular Ice Formation and Freeze-Thaw Survival of HeLa S-3 Cells", Cryobiology, Vol. 12, No. 6, 1975, pp. 540-550.
6. Asimacopoulos, P.J., McGrath, J.J., Cravalho, E.G., "The Thermal Sensitivity of the Human Fibroblast HeLa S-3 as a Model for Thermal Insult to the Neointima of a Nuclear-Fueled, Blood-Cooled, Left Ventricular Circulatory Assist Device", 1975 Advances in Bioengineering, Winter Annual Meeting, A.S.M.E., November 30-December 5, 1975, pp. 28-31.
7. Cravalho, E.G., McGrath, J.J., Toscano, W.M., "Utilization of Refrigeration Available from Regasification of LNG for the Desalination of Water", Presented at the Sixth International Cryogenic Engineering Conference, May 11-14, 1976, Grenoble, France.
8. Leibo, S.P., McGrath, J.J., Cravalho, E.G., "Microscopic Observation of Intracellular Ice Formation In Mouse Ova as a Function of Cooling Rate", submitted to Cryobiology, 1976
9. Moussa, N.A., Asimacopoulos, P.J., McGrath, J.J., Cravalho, E.G., "Kinetics of Thermal Injury in Cells", to be published in the Journal of Biomechanical Engineering, A.S.M.E., 1977
10. Cravalho, E.G., McGrath, J.J., Toscano, W.M., "Thermodynamic Analysis of the Regasification of LNG for the Desalination of Sea Water", submitted to Cryogenics, 1976.
11. McGrath, J.J., Cravalho, E.G., Huggins, C.E., "Hemolysis of Human Erythrocytes in Hypertonic Sodium Chloride Solutions at Subphysiological Temperatures", Cryobiology, Vol. 13, No. 6, 1976, p. 651, (abstract)
12. McGrath, J.J., and Cravalho, E.G., "The Total Hemispherical Emittance of Silicon-Carbide Coated Reinforced Carbon Composites

in the Temperature Range 100°K to 450°K and a Critique of the Calorimetric Experimental System", submitted for presentation at the AIAA 12th Thermophysics Conference, June 27-29, 1977, Albuquerque, New Mexico.